SOUTHWEST RESEARCH INSTITUTE
Post Office Drawer 28510, 8500 Culebra Road
San Antonio, Texas 78284

BELLOWS FLOW-INDUCED VIBRATIONS AND PRESSURE LOSS

by
C. R. Gerlach
E. C. Schroeder
R. L. Bass, III
J. L. Holster

FINAL REPORT
Contract No. NAS8-21133
Control No. DCN 1-7-52-20017 (IF)
SwRI Project No. 02-2119

Prepared for
National Aeronautics and Space Administration
George C. Marshall Space Flight Center
Marshall Space Flight Center, Alabama 35812

April 13, 1973

Approved:

H. Norman Abramson
Technical Vice President

ABSTRACT

Results are presented from a theoretical and experimental investigation of ducting and ducting components used in space vehicle feed systems. A definition of a bellow flow excitation mechanism is presented, a simple method for predicting failure or fatigue characteristics of a bellow is developed, the effects of internal cryogenic flow are predicted, and a computer program is presented to allow quick computation of bellows mode frequencies, lock in ranges, and stress indicator values. In addition, feed systems acoustic resonance effects, bellows liner designs, bellows pressure loss characteristics, elbow pressure loss characteristics and external damping devices are discussed.

TABLE OF CONTENTS

TABLE OF CONTENTS (Cont'd) -

LIST OF ILLUSTRATIONS

List of Illustrations (Cont'd) -

List of Illustrations (Cont'd) -

List of Illustrations (Cont'd) -

[redacted]

List of Illustrations (Cont'd) -

List of Illustrations (Cont'd) -

List of Illustrations (Concluded) -

List of Illustrations (Cont'd) -

List of Illustrations (Cont'd) -

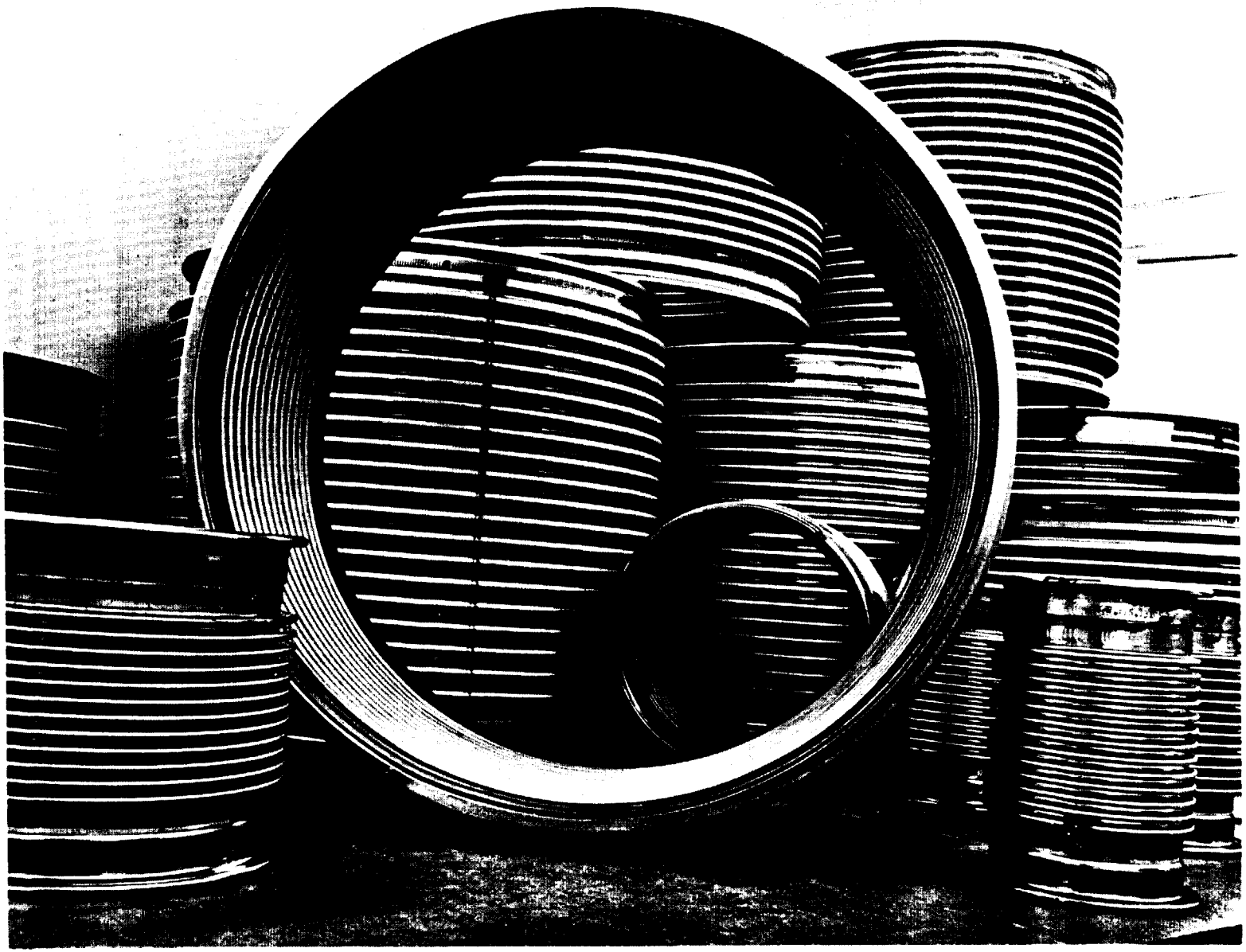

FRONTISPIECE

I. INTRODUCTION

This report describes all work which has been performed by the Southwest Research Institute under Contract NAS8-21133, "Study of Minimum Pressure Loss in High Velocity Duct Systems". This study was performed for the George C. Marshall Space Flight Center of the National Aeronautics and Space Administration and administered technically by the Astronautics Laboratory with Mr. R. H. Veitch serving as Technical Manager and Mr. H. Bandgren as Alternate Technical Manager.

The general objective of this study was to perform a theoretical and experimental investigation of ducting and ducting components to minimize pressure drop, surge pressures and vibration levels and, thus, to generally improve flow conditions of gases and liquids in space vehicle feed systems. Because of NASA needs, much emphasis was placed on the study of bellows flow-induced vibrations.

Summary of Results

A number of significant findings have been made throughout this study and are discussed in detail in this report; these are summarized below:

(a) Definition of Bellow Flow Excitation Mechanism - The fluid-elastic mechanism causing bellows flow excitation (vortex shedding) has been observed and described. Analytical models have been developed to allow a designer to predict when flow excitation may occur, and to estimate the severity of the bellows vibrations.

(b) Fatigue Prediction - A simple method of predicting the failure or fatigue characteristics of a bellows has been developed and verified experimentally for a broad range of bellows sizes.

(c) Bellows with Cryogenic Flow - The differences in flow excitation for bellows with internal cryogenic flow, as compared with non-cryogenic fluid flows, has been studied and the effects defined.

(d) Computer Program - A computer program has been developed to allow quick computation of bellows mode frequencies, lock-in ranges and Stress Indicator values.

(e) Acoustic Resonance - The occurence of an acoustic resonance for internal gas flows has been quantified and may be predicted by the method defined herein. The computer program also calculates the acoustic resonance condition.

(f) Bellows Liner Design - A limited amount of information is presented to aid in the design of a conventional bellows liner which suppresses flow-induced vibrations.

(g) Bellows Pressure Loss - All available data has been compiled which gives bellows pressure loss for various convolution geometries, various sizes, and various flow media. Existing bellows pressure loss correlation methods have been reviewed, and while none are completely adequate, one is recommended for future use.

(h) Elbow Pressure Loss - A new elbow design has been discovered which results in a significant reduction in pressure loss, as confirmed by tests.

(i) External Damping Devices - Various bellows external damping devices have been tried as a means of suppressing bellows flow-induced vibrations. The results of these tests are presented to guide the designer in achieving vibration suppression by this means.

II. INTRODUCTION TO BELLOWS FLOW-INDUCED VIBRATIONS AND DESIGN PROCEDURE

II. 1 Introduction

The occurrence of flow-induced vibrations of metal bellows contained in fluid ducting systems has, for some time, been a problem in industry and in particular, for aerospace applications. There are known instances where flow-induced vibrations of bellows have resulted in fatigue failures which forced the premature shutdown of some critical fluid systems. The most common methods for correcting unsuccessful bellows installations have been either to install a liner inside the component, where possible, or to use multiple plys or thicknesses of metal when constructing the bellows. Unfortunately, increasing the number of metal plys has not always cured the flow-induced vibration problem, and the use of a bellow's liner generally leads to an increase in component weight and cost. A major obstacle in the past has been that the flow mechanism which causes bellows vibration has not been described or understood so that flow induced failures could be anticipated. From the standpoint of the designer, a desirable goal is to have available an analytical procedure which allows a prediction of critical fluid flow ranges for a given bellows configuration and, further, which gives a method for estimating stress levels resulting from the flow excitation in these critical ranges.

This section of the report gives an overall summary of the bellows flow-induced vibration problem and a short description of the design or stress calculation procedure. Further details of the bellows flow-induced vibration problem are given in subsequent sections of this report.

II. 2 Bellows Flow Excitation Mechanism

Typical Bellows Excitation Example and Flow Visualization Results

The phenomena of flow excitation of an actual bellows is illustrated by the "classic" results shown in Figure 1. These results are typical of those obtained from the large number of bellows tests conducted over the period of this investigation. Each test bellows was instrumented to allow flow-induced strain to be monitored. For each test bellows it was generally found that as the fluid velocity was slowly increased, starting from zero flow, successive longitudinal accordian vibration modes were excited.

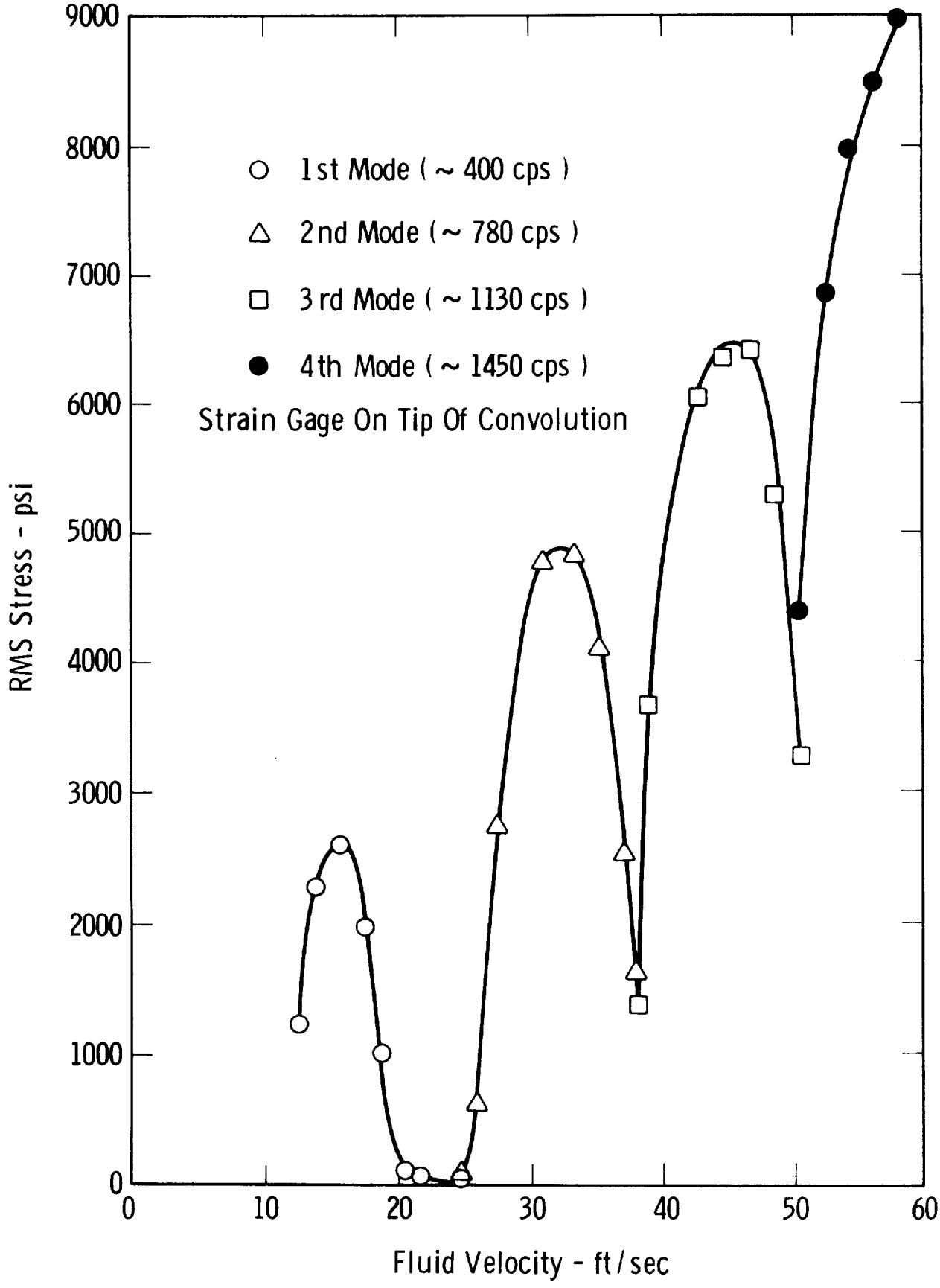

Figure 1. Bellows Stress As A Function Of Flow Rate For Four Flow Excited Modes Of Vibration - PN 08046

Figure 1 shows typical strain data and Figure 2 illustrates the longitudinal vibration modes observed. As may be seen, each vibration mode was excited over some fluid velocity range with the peak excitation occurring near the center of this range.

Analysis of preliminary test results obtained from this program led to the conclusion that vortex shedding from the convolution tips was the source of fluid excitation. Calculation of a Strouhal number

$$S = \frac{f\sigma}{V} \qquad (1)$$

based on the convolution width σ (see Figure 3) was carried out; here f is the bellows frequency and V the mean fluid velocity. The results, shown typically by Figure 3, revealed that the value of S generally varied over a range from about 0.1 to 0.25 with a value at peak flow-induced response of about 0.18, very much like the vortex shedding excitation of an elastically restrained cylinder.

Stimulated by these original flow-induced vibration results, a flow visualization experiment was set up to verify the vortex shedding hypothesis. Based on the results of the flow visualization experiments, there is undisputable evidence that excitation of bellows longitudinal modes is a result of a dynamic coupling between the bellows structure and a fluid vortex generation and shedding process. In every sense, the phenomena is a fluid-elastic instability (References 1-5), since a mutual interaction or coupling occurs between the dynamics of the bellows (the elastic system) and the nonsteady flow near and between the convolutions (the dynamic fluid system). Many factors have an influence on this coupling phenomena, including the convolution geometry, the flow conditions, and possible local cavitation or acoustic resonances.

For flow through a convoluted section of bellows, with the convolutions fixed to prevent vibration, a steady turbulent flow exists throughout the bellows, as illustrated in Figure 4. This is a physical picture formulated from our own flow visualization experiments, and from the information reported by Haugen and Dhanak (6), and Townes and Sabersky (7). Each convolution, in general, experiences an internal eddying flow because of momentum transfer from the free stream. Energy is transferred into each convolution in a mixing zone or shear layer. The number and size of the steady vortices which exist in the convolutions are a function of the convolution geometry. Very shallow convolutions may contain only one vortex, while two or more may exist in deep convolutions.

The physical picture described above is valid only with no convolution motion or vibration. When the bellows is flow excited, the physical

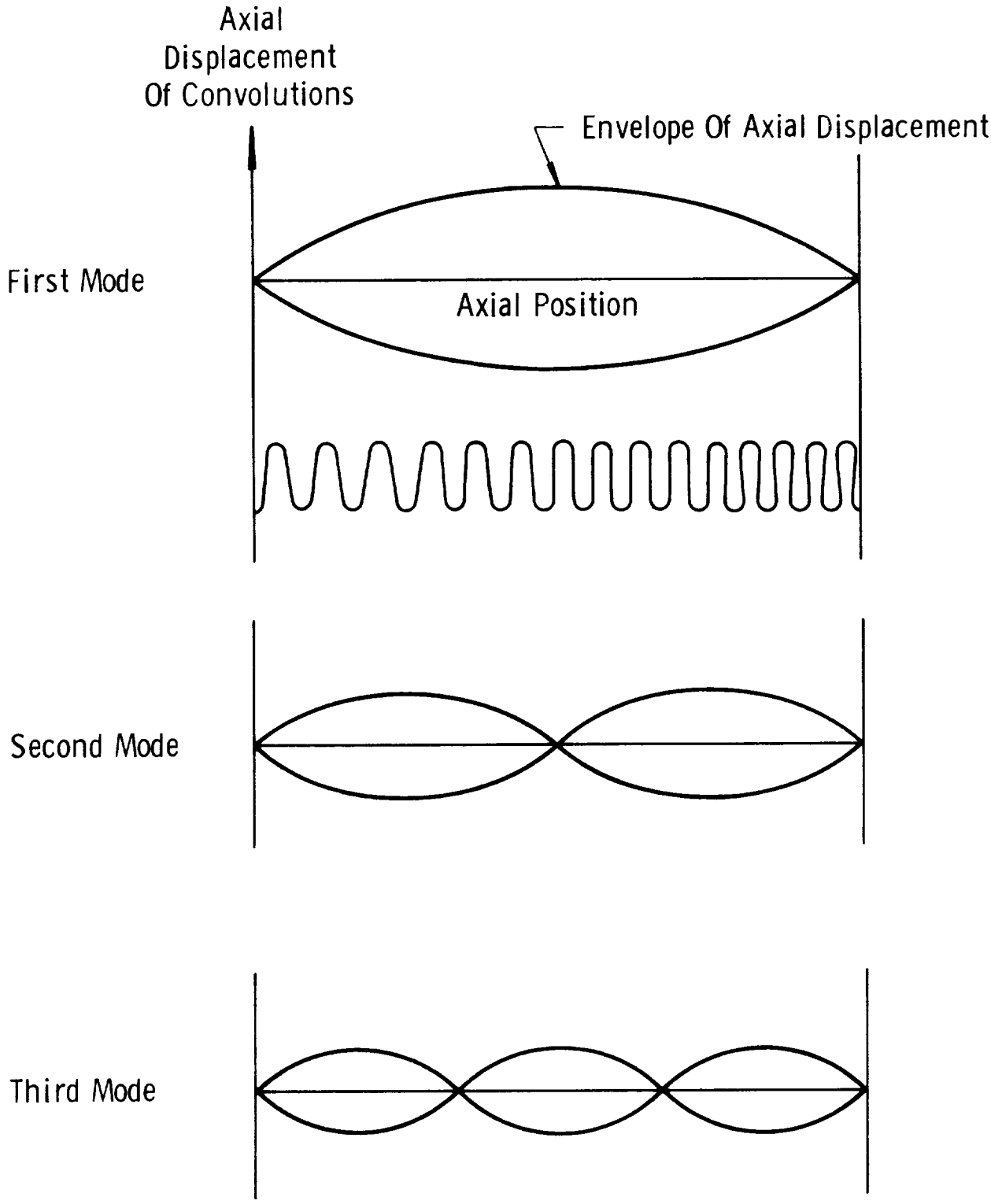

Figure 2. Observed Bellows Longitudinal Vibration Mode Shapes

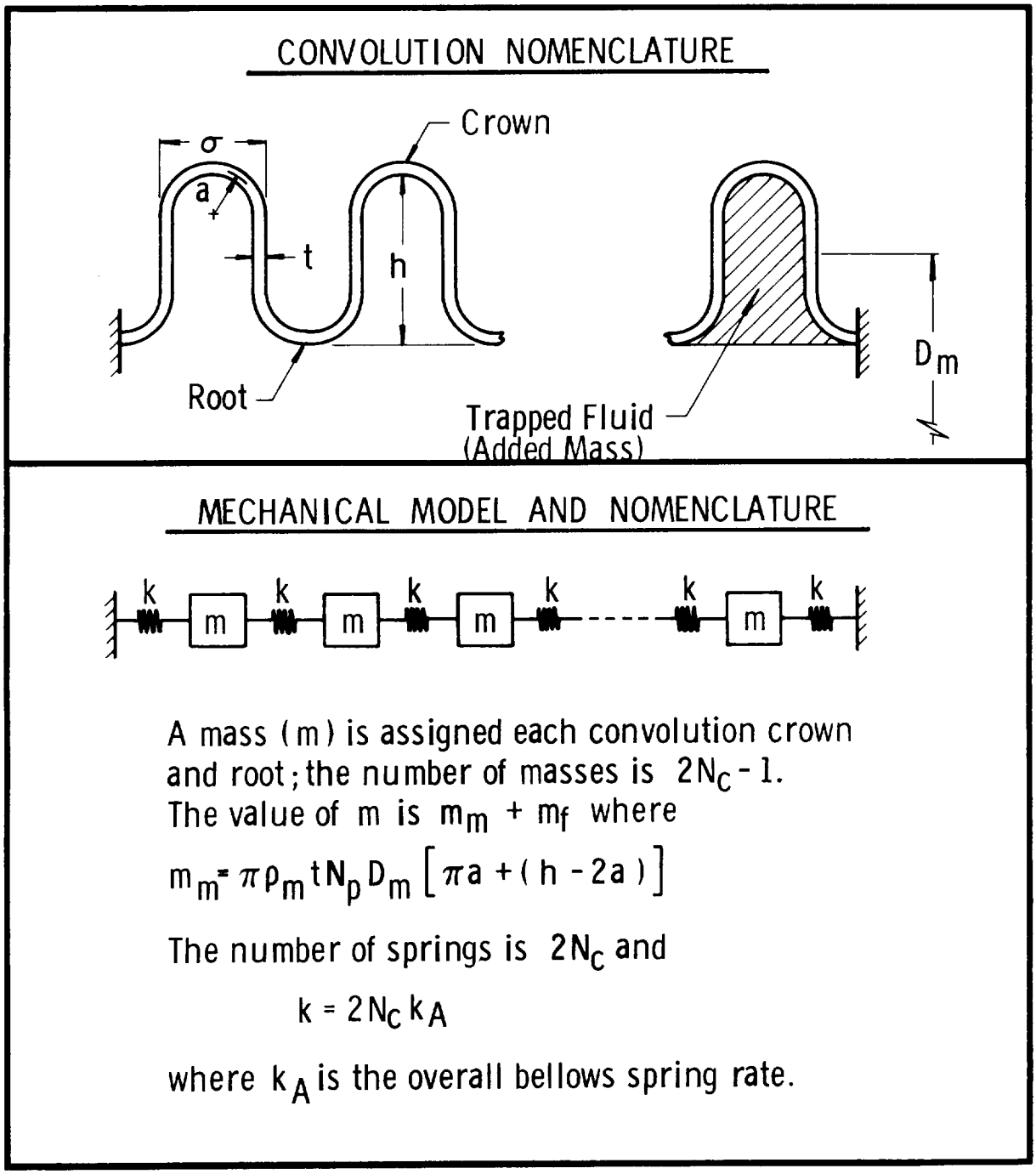

Figure 3. Convolution Nomenclature and Mechanical Vibration Model

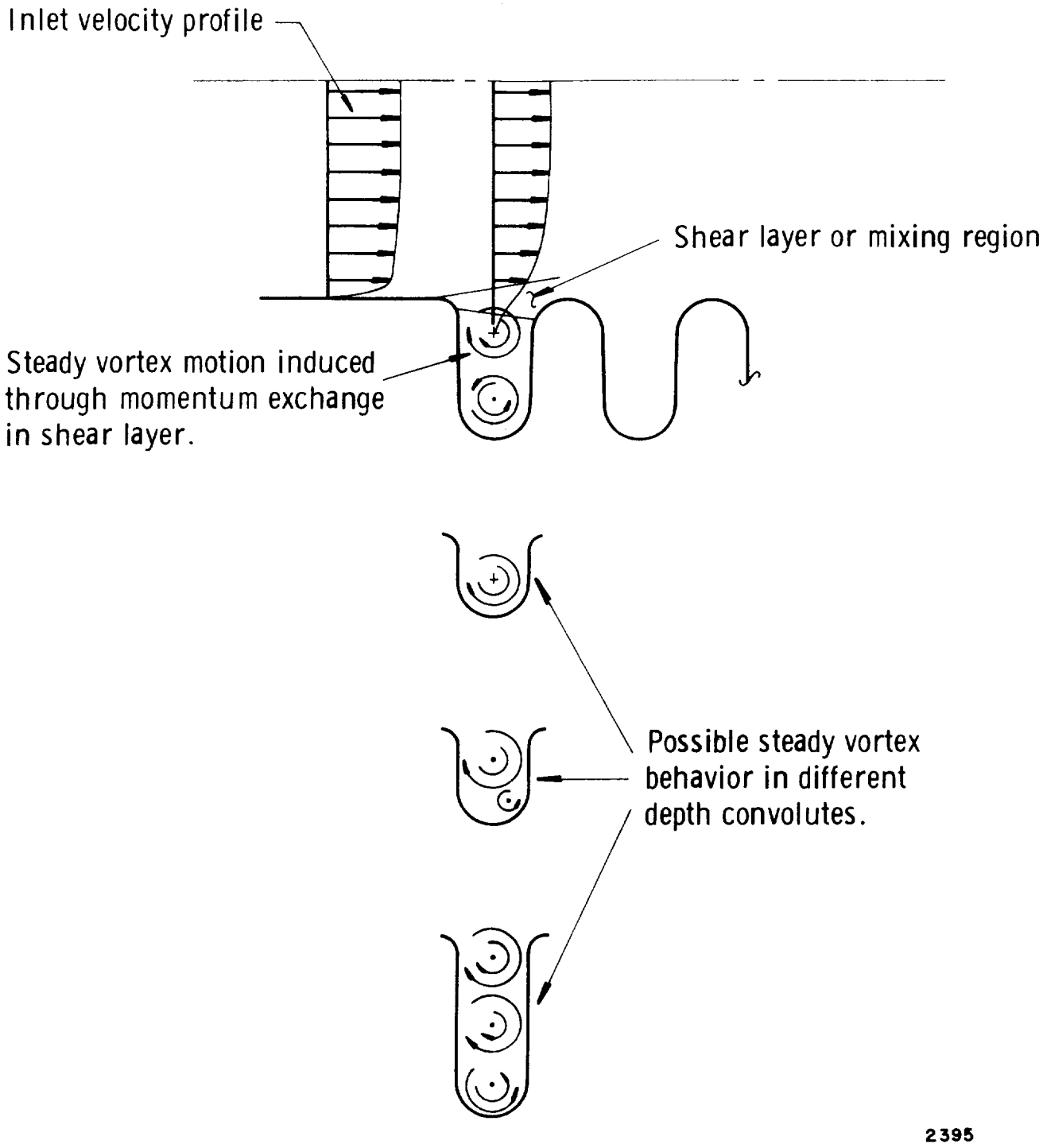

Figure 4. Fluid Flow Behavior With Stationary Convolutions

picture of internal flow described above is no longer valid, in general. For this case, a large-scale periodic vortex formation and shedding process occurs which has been visualized with an apparatus shown in Figure 5. The apparatus consists of a two-dimensional clear plastic channel containing a short section of convoluted metal which is placed so that the convolution tips are exposed to the fluid flow, as in an actual bellows. When water is passed through the channel at the proper velocity, the segment is flow excited; this vibration may be viewed with the aid of a strobe light. By injecting ink upstream from the convoluted segment the vortex shedding process is easily visualized.

Both still and moving pictures of the vortex shedding have been made; Figure 6 shows several of the still pictures which were taken at random times. The presence of a vortex pattern is evident in each picture. The movie, of course, shows the interaction of the fluid motion and the segment much more clearly than do the still pictures.

Figure 7 shows the sequence of fluid and convolution events which have been observed in a frame-by-frame examination of the motion picture. Note, first of all, that the mode of vibration of the segment is one where each convolution moves out-of-phase with the adjacent convolution(s). This corresponds to the highest longitudinal bellows mode. The vortex shedding process on the vibrating segment, as shown by Figure 7, occurs as follows: In Position I, a large vortex (c) has formed between the convolutions 1 and 2, and is being "pushed" out into the fluid stream by the pinching action of these two convolutions. A large, well-formed vortex (a) is moving across the tip convolution 3; the origin of this vortex will be made clear in the description of other events. Finally, a small vortex (b) is beginning to form on the downstream side of convolution 2. In Position II, vortex (c) has been pinched from between convolutions 1 and 2, and has now moved out into the fluid stream, and will soon "detach" from convolution 1 to be swept downstream. Vortex (b), which is forming on the downstream side of convolution 2, is gaining in strength. Vortex (a), which in Position I was beginning to move over the tip of convolution 3, is now further downstream. In Position III, the space between convolutions 1 and 2 is opening up, hence fluid is being drawn in, and vortex (d) is beginning to form on the downstream side of convolution 1. Vortex (c) has been swept over the top of convolution 2, with the timing being about right to reinforce vortex (b), which is being pinched from between convolutions 2 and 3; the combined vortex is labeled (b + c). In Position IV, vortex (d) has gained in strength as it forms on the downstream side of convolution 1. Vortex (b + c) is being pinched out from between convolutions 2 and 3, and will begin to propagate downstream. Finally, Position V is the same as Position I, so the cycle is complete. Note that vortex (a) in Position I was a combination of two vortices, as is vortex (b + c) in Position V.

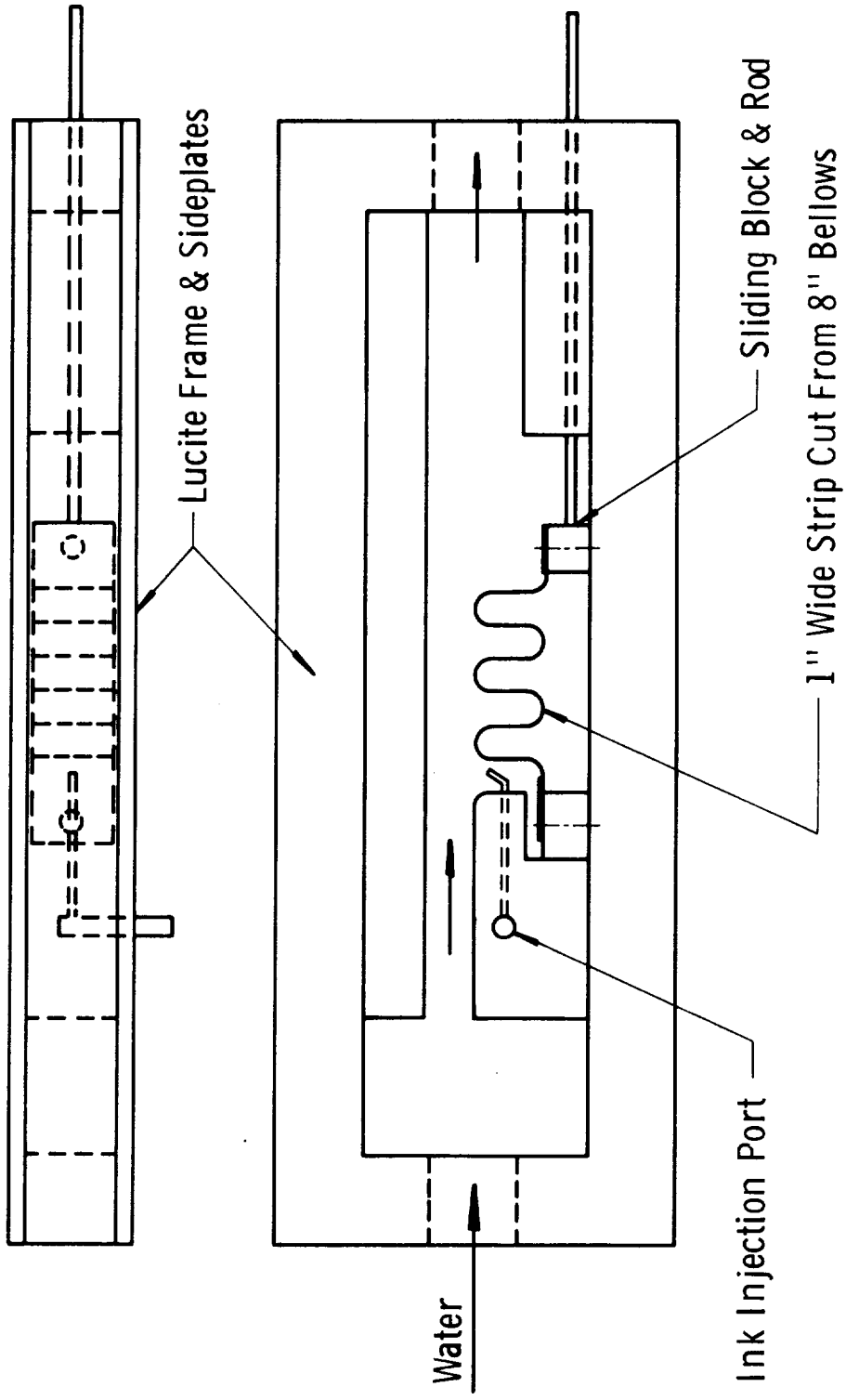

Figure 5. Two Dimensional Bellows Flow Visualization Model

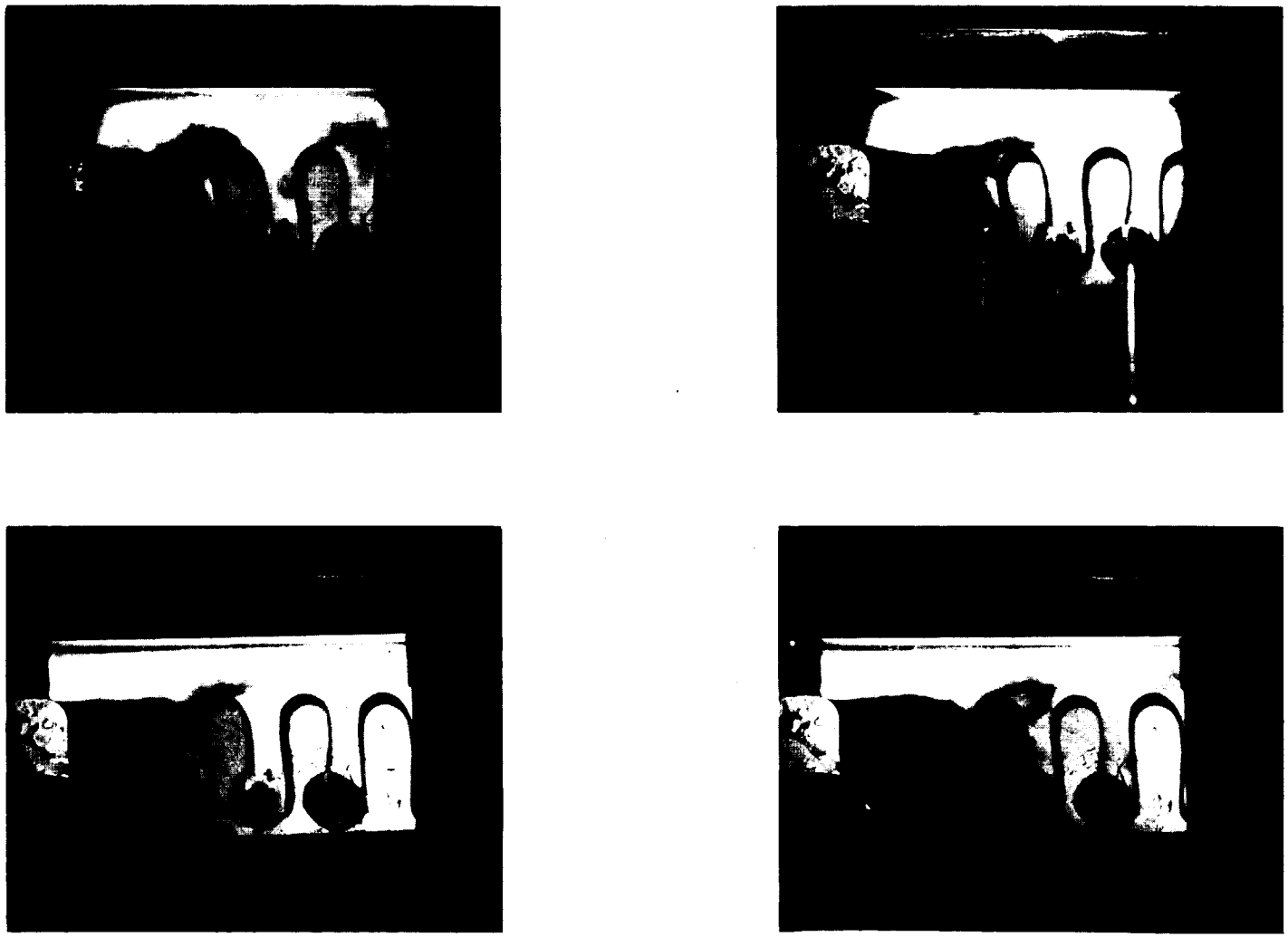

FIGURE 6. SERIES OF PHOTOGRAPHS SHOWING VORTEX SHEDDING FROM TWO-DIMENSIONAL CONVOLUTED METAL SEGMENT

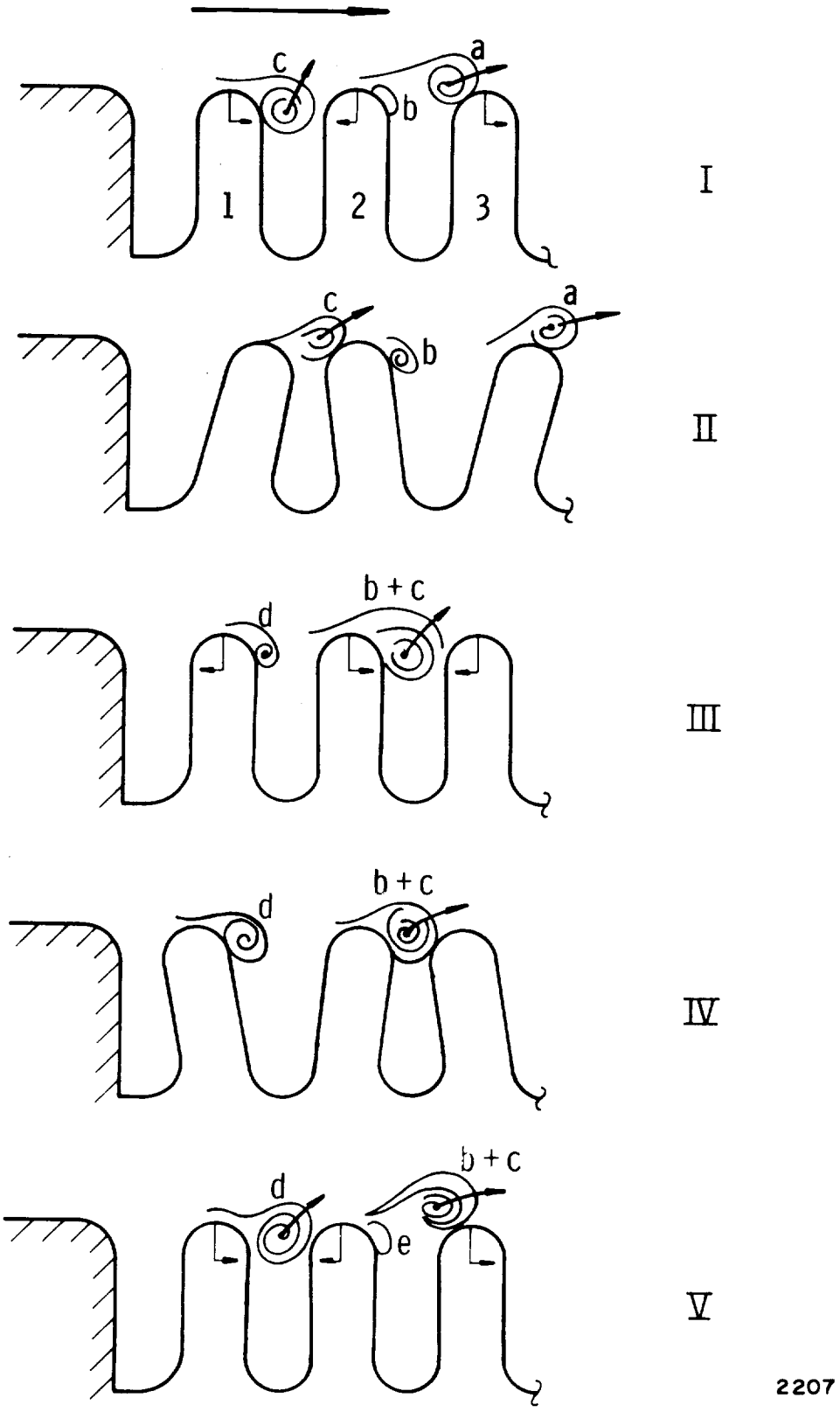

Figure 7. Sequence Of Coupled Fluid - Convolution Events Observed With Two-Dimensional Bellows Flow Visualization Model

It must be emphasized that the series of fluid events described in the foregoing are probably not exactly descriptive of all bellows modes excited. The main difference likely seen from a comparison with other situations, would be that the phasing of vortices propagating downstream would not always be correct, with respect to a vortex forming at a point downstream, to give a reinforcement condition, as shown in the above discussion. We have some experimental evidence suggesting that there might be optimum convolution geometries, for a given mode of vibration, which yield relative peak excitation amplitudes. This might be caused by a vortex reinforcement phenomena.

It has been shown in the foregoing that two different fluid flow regimes exist; one occurs when the convolutions are constrained and, consequently, no organized large scale vortex shedding is observed, only a steady-state turbulent situation. The other flow regime occurs when the convolutions are vibrating as a result of flow excitation; here a large scale vortex formation and shedding process does exist. Therefore the bellows flow excitation can be described as a mutual or coupled instability between the bellows structure and the fluid vortex shedding process. One cannot exist without the other.

The primary condition which must be satisfied for this coupling to occur is that the bellows structural frequency and the ideal vortex shedding frequency be equal, or about equal within certain limits. This limit of vortex-structure coupling can be called a "lock-in" range, and it can exist over a rather broad velocity range.

II. 3 Prediction of Flow-Excitation Lock-In Range

The purpose of this section is to discuss how the occurrence of the vortex shedding and bellows structure coupling can be predicted. Basically, this involves calculating the ideal vortex shedding frequency and the bellows vibration mode frequencies, and then comparing the two. Also, some allowance must be made for the fact that a "lock-in" range exists.

Vortex Shedding Frequency

For a given bellows, having some particular convolution geometry and structural mode frequencies, there are certain optimum fluid velocities which result in a maximum amplitude bellows excitation of each mode (see again Figure 1). It is at these velocities that the vortex shedding process is best able to feed energy from the fluid stream into the vibration process. In other words, the vibration frequency and fluid velocity conditions are

"optimum" from a vortex shedding standpoint. It has been found that the use of a Strouhal number is an excellent means of correlating the vibration frequency, fluid velocity and geometry under these optimum conditions, as is true for any vibration phenomena involving vortex shedding.

In general terms, a Strouhal number is a dimensionless quality of the form

$$S = f \ell / V \qquad (1)$$

where f is a frequency, ℓ is a length quantity, and V a fluid velocity. For the case of bellows flow-induced vibrations, the only problem in using this correlation parameter is in selecting a satisfactory length quantity. Referring back to the discussion of the vortex formation and shedding process illustrated in Figures 6 and 7, it would seem that two length quantities may be primarily involved; these are the convolution pitch and the convolution tip width σ. While neither of these quantities has been found entirely satisfactory, that is neither gives a precisely constant value of S for all conditions, we have chosen to use σ in making Strouhal number calculations.

Based on a composite of all test data, a single curve of Strouhal number (based on tip width σ) as a function of the ratio of pitch to tip width (λ / σ) has been prepared and is valid for a general case. This curve is shown in Figure 8; also shown are dotted curves defining the limits of the lock-in range. Using this data, it is possible to calculate the fluid velocity V at which a given bellows longitudinal vibration mode (defined by a frequency value) will most likely be excited and, also, to estimate the total lock-in range of a given mode. To make this calculation it is necessary to know three quantities; namely, the pitch λ, the convolution tip width σ and the mode frequency f_m. The value of this critical velocity is, then

$$V = \frac{f_m \sigma}{S_\sigma}$$

where S_σ is obtained from Figure 8.

Bellows Structural Frequencies

In order to calculate the fluid velocity range(s) over which bellows excitation will occur by the procedure described in the foregoing section, it is necessary to know the frequencies of all bellows modes which may be

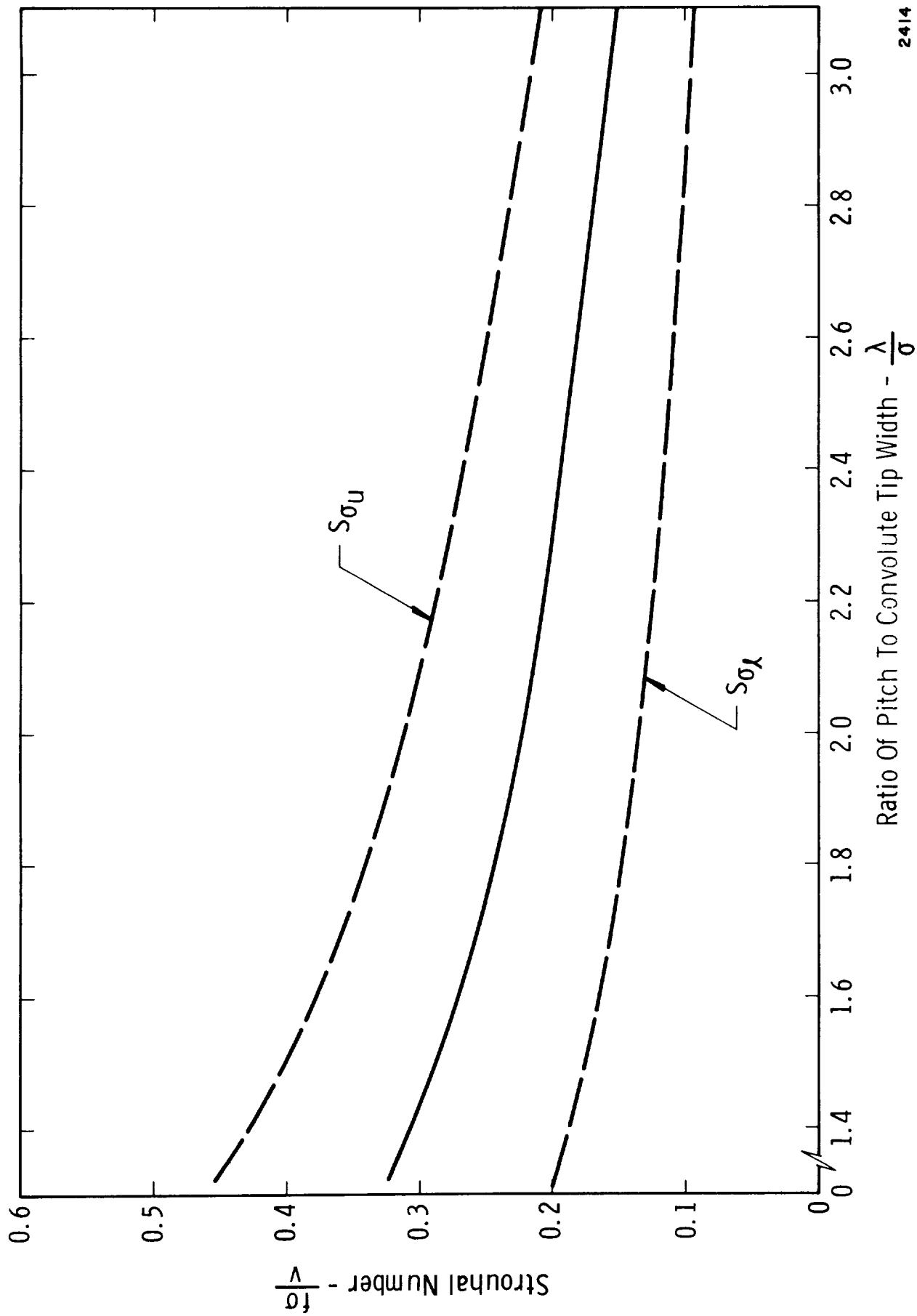

Figure 8. Composite Of All Strouhal Number Correlation Data

flow excited. Therefore, some method must be used to calculate these frequencies. A method, based on an analogous mechanical model, has been developed and will be discussed below. Because the structural bellows modes cannot be considered independent of fluid loading, this influence is discussed also.

It has been determined from experiments that three different kinds of structural modes can be flow excited, these are; axisymmetric longitudinal or accordian modes, longitudinal antisymmetric or cocking modes, and local convolution bending modes. These different kinds of bellows modes are illustrated in Figure 9. The longitudinal modes (both symmetric and antisymmetric) involve vibrations where there is longitudinal motion of the roots and/or crowns of the convolutions. The higher order local bending modes will involve no longitudinal motion of roots and crowns, only local flexural distortion of the convolutions.

During the course of this study, the mechanical model shown in Figure 3 has been found to yield adequate predictions of the longitudinal symmetric mode frequencies of a free bellows, if the overall spring rate is accurately known. The model consists of $(2N_c - 1)$ elemental masses m and $2N_c$ elemental springs k connected alternately in series, giving an $N = 2N_c - 1$ degree-of-freedom system; N_c is the number of bellows convolutions. Each elemental mass represents one-half of the mass of metal contained in each bellows convolution plus some fluid added mass, and k represents the spring rate of one-half of a convolution. A tabulation of dimensionless frequencies obtained for this model up to 25 degrees of freedom is shown in Table I; the normalizing frequency is

$$f_o = \frac{1}{2\pi} \left(\frac{k}{m} \right)^{1/2}$$

For use in the mechanical model, the values of the elemental spring rate k and the elemental metal mass m_m may be estimated by the following procedure. The value of k is defined in terms of the overall bellows spring rate K_A as

$$k = 2N_c K_A$$

where K_A is known either from a spring rate test or from some analytical calculation. The value of the elemental metal mass m_m is equal to one-half of the mass of one complete convolution and may be satisfactorily approximated by the expression

$$m_m = \pi \rho_m t N_p D_m \left[\pi a + (h - 2a) \right]$$

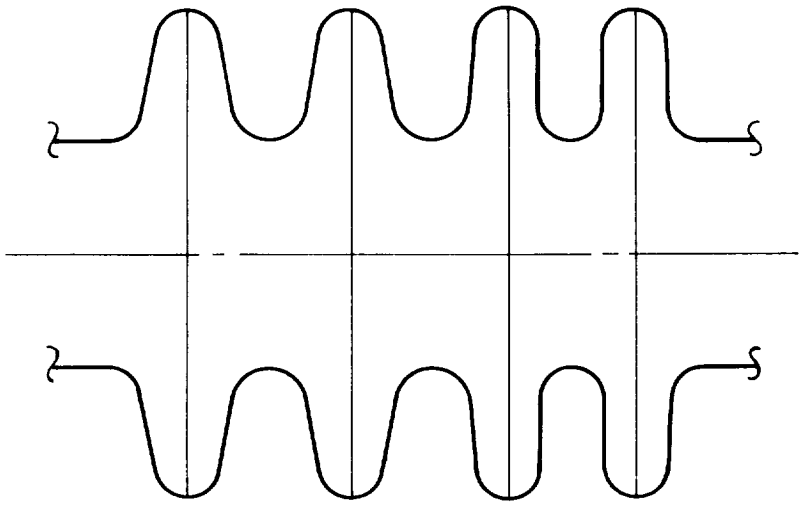

Axisymmetric
Longitudinal Modes

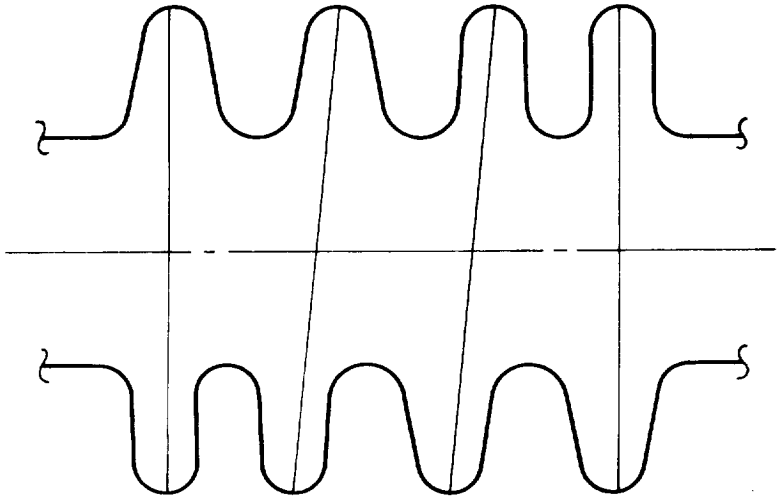

Nonsymmetric
Longitudinal (Cocking)
Modes

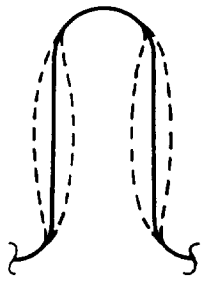

Higher Order
Local Convolute
Bending Mode

2396

Figure 9 . Kinds Of Bellows Modes

MODEL NUMBER N = 2i$_c$ - 1 \ MODE NUMBER	1	2	3	4	5	6	7	8	9	10	11	12	13	14	15	16	17	18	19	20	21	22	23	24	25
1	1.414																								
2	1.000	1.732																							
3	0.765	1.414	1.845																						
4	0.620	1.175	1.620	1.900																					
5	0.520	1.000	1.414	1.732	1.930																				
6	0.445	0.868	1.247	1.564	1.802	1.950																			
7	0.390	0.765	1.111	1.414	1.663	1.848	1.962																		
8	0.347	0.684	1.000	1.286	1.532	1.732	1.879	1.970																	
9	0.314	0.618	0.908	1.176	1.414	1.618	1.782	1.902	1.975																
10	0.285	0.563	0.831	1.082	1.310	1.511	1.682	1.819	1.919	1.980															
11	0.264	0.518	0.765	1.000	1.217	1.414	1.587	1.732	1.848	1.932	1.983														
12	0.245	0.479	0.709	0.929	1.136	1.326	1.497	1.646	1.771	1.870	1.942	1.985													
13	0.226	0.445	0.661	0.868	1.064	1.247	1.414	1.563	1.693	1.802	1.888	1.950	1.987												
14	0.213	0.416	0.618	0.814	1.000	1.176	1.338	1.486	1.618	1.732	1.827	1.902	1.956	1.988											
15	0.199	0.390	0.583	0.765	0.942	1.111	1.269	1.414	1.546	1.663	1.764	1.848	1.913	1.962	1.990										
16	0.185	0.367	0.547	0.722	0.891	1.052	1.205	1.347	1.478	1.596	1.700	1.790	1.864	1.923	1.965	1.991									
17	0.174	0.347	0.518	0.684	0.845	1.000	1.147	1.285	1.414	1.532	1.638	1.732	1.812	1.879	1.931	1.969	1.992								
18	0.165	0.329	0.491	0.649	0.803	0.952	1.093	1.228	1.354	1.471	1.578	1.674	1.758	1.831	1.891	1.938	1.972	1.993							
19	0.157	0.313	0.467	0.618	0.765	0.908	1.044	1.175	1.298	1.414	1.520	1.618	1.705	1.782	1.847	1.902	1.944	1.975	1.993						
20	0.149	0.298	0.445	0.590	0.731	0.868	1.000	1.126	1.246	1.360	1.466	1.563	1.652	1.732	1.801	1.861	1.911	1.949	1.977	1.994					
21	0.142	0.285	0.425	0.563	0.699	0.831	0.958	1.081	1.198	1.309	1.414	1.511	1.601	1.682	1.755	1.819	1.873	1.918	1.954	1.979	1.994				
22	0.136	0.272	0.407	0.540	0.670	0.797	0.920	1.039	1.153	1.262	1.365	1.461	1.551	1.633	1.708	1.775	1.834	1.884	1.925	1.958	1.981	1.995			
23	0.131	0.262	0.390	0.518	0.643	0.765	0.885	1.000	1.111	1.217	1.318	1.414	1.503	1.586	1.662	1.732	1.793	1.847	1.893	1.931	1.961	1.982	1.995		
24	0.126	0.251	0.375	0.497	0.618	0.736	0.852	0.964	1.071	1.175	1.274	1.369	1.457	1.541	1.618	1.688	1.753	1.809	1.859	1.902	1.937	1.964	1.984	1.996	
25	0.121	0.241	0.361	0.479	0.595	0.709	0.821	0.929	1.034	1.136	1.233	1.326	1.414	1.497	1.574	1.645	1.711	1.770	1.823	1.870	1.909	1.941	1.967	1.985	1.996

Table I - Dimensionless Frequencies For Bellows Mechanical Model

where (see Figure 3)

M_m = mass density of bellows metal

t = thickness per ply of metal

N_p = number of bellows plys

D_m = mean diameter of bellows convolution, $D_m = (D_i + D_o)/2$.

a = mean radius of convolution

h = convolute height

The frequencies obtained using the information given above are for the symmetric longitudinal modes only. An analysis has been made to determine the cocking mode frequencies and the results show that these new modes are always within the frequency limits of the symmetric longitudinal modes. Therefore, a calculation of the range of symmetric longitudinal modes can be considered to include any cocking modes which may occur. Cocking modes have been observed only for bellows with quite deep convolutions, and will probably not occur in most instances.

The higher order local bending mode shown in Figure 10 may be modeled with the mechanical analog shown in the same figure.

Fluid Loading Effects

The previous discussion concerning calculation of structural bellows mode frequencies made no mention of possible fluid loading effects. The presence of the fluid can, however, cause some changes in the structural frequencies and even add more degrees of freedom to the system (increase the number of possible modes).

When a bellows is being excited by a flowing fluid, two basic classes of forces are present; namely, active forces which are vortex shedding derived, and passive fluid forces which are present regardless of the excitation source. For the idealized case of an incompressible fluid, only two types of passive fluid forces are possible and these give rise to an added-mass and damping influence; they result because the fluid must be moved in and out from between the convolutions and, to some extent, back and forth longitudinally as the bellows vibrates. If only added-mass and damping effects are introduced, the number of degrees of freedom of the bellows (that is, the number of possible vibration modes) does not necessarily change. One exception to this are in-phase

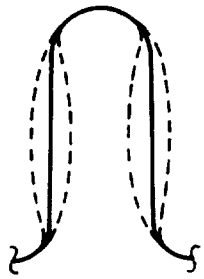

Illustration Of First Local Convolute Bending Mode

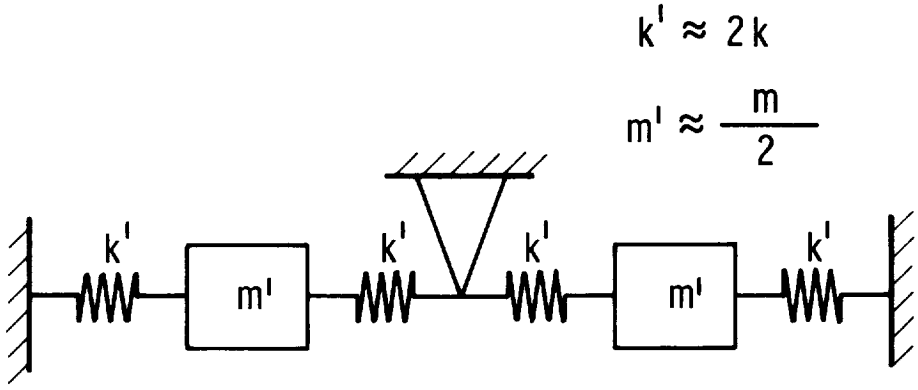

Approximate Mechanical Model Of First Local Bending Mode

2397

Figure 10. Only Observed Higher Order Mode

and out-of-phase flex hose modes to be discussed later.

For a compressible fluid, the complexity of the situation is greatly increased, because the bellows' vibrations may couple with various system acoustic modes. Generally, this increases the number of degrees of freedom, or the number of possible vibration modes of the bellows. For the present, only incompressible fluid loading effects will be considered in regard to coupled bellows-fluid mode frequency calculations. Further, because the fluid damping is small enough to give a very small change in the system resonant frequencies, it will be disregarded in all frequency calculations. Later, however, damping will be shown to be of great importance in calculating bellows flow-induced stress levels.

For the first few modes of a free bellows (more precisely, where the mode number N is small with respect to the number of convolutions N_c), it has been determined by comparing calculated with observed frequencies that the fluid added mass is adequately represented by setting it equal to the total amount of fluid trapped between adjacent convolutions; see Figure 3. Physically this makes sense since the first few modes involve a gross back-and-forth motion of adjacent convolutions with the trapped fluid carried along with the convolutions. This means, then, that each elemental mass of the mechanical model must include one-half of the mass of fluid trapped between two adjacent convolutions, or approximately

$$m_f = \frac{\pi}{2} \rho_f D_m h (2a - tN_p)$$

with, now, the elemental model mass becoming

$$m = m_f + m_m$$

where the value of m_m is the metal mass discussed previously. In the above expressions, ρ_f is the fluid mass density; other symbols were defined previously.

For the higher modes of a free bellows, it is not adequate to consider the fluid added mass as being simply that amount of fluid trapped between convolutions. The fluid behavior for the higher modes is rather more of a "squeezing in-and-out" type of motion. This acceleration of the fluid out of and back into the convolutions results in alternating pressure forces which may be interpreted as an added-mass effect with respect to the bellows vibrations. This added mass is analytically estimated to be

$$m_f = \frac{\pi D_m \rho_f h^3}{3\delta}$$

where δ is the gap width between adjacent convolutions as shown in Figure 2.

Flex Hose Modes

The difference between the convolution vibrations of a flexible hose and a free bellows is that the allowed modes are limited by the wire braid covering. In most cases this covering clamps tightly around the bellows when the hose is pressurized, preventing longitudinal motion of the convolution crowns. Except for special instances where not all convolutions crowns are in contact with the wire braid, it is believed that the only purely structural longitudinal mode which can exist is the one shown in Figure 11(a). Because of fluid added-mass effects, however, two coupled fluid-structural longitudinal modes appear possible, and these are shown in Figure 11(b) and (c). Note that both of the coupled fluid structural modes are possible for the single allowed structural mode.

The primary difference between the two coupled fluid-structural modes shown in (b) and (c) of Figure 11 is the fluid mass loading involved. For the case in Figure 11(b), the in-phase mode, the fluid-added mass corresponds to a portion of fluid contained between adjacent convolutions. This quantity of mass accounts for the fact that fluid is accelerated back and forth with the convolutions as they vibrate in the in-phase mode. For the out-of-phase mode, the fluid added mass does not correspond to some real quantity of fluid, but is an apparent mass which results from the fluid being accelerated in and out from between the convolutions as discussed in the foregoing for the free bellows.

Estimating Flow Excitation Range

The foregoing discussions have described how the conditions for bellows excitation can be correlated with a Strouhal number, and, further, how the modal frequencies of a bellows can be calculated. The purpose of this section is to summarize how this information can be used to predict possible bellows flow-excitation ranges.

As we have seen, a given bellows will have a number of structural modes which may be flow excited. These modes may be defined in terms of a number of modal frequencies denoted by

$$f_{m1},\ f_{m2},\ f_{m3} \cdots\ f_{mn}$$

Here f_{m1} denotes the first or lowest modal frequency and f_{mn} denotes the highest. For the case of a free bellows, f_{m1} will represent the first longitudinal mode and f_{mn} will denote the convolute bulging mode;

the total number of modes will depend on the number of convolutions. For a flex hose, there are, so far as we presently known, only three possible modes; these are the in-phase and out-of-phase longitudinal modes shown in Figure 11, and the convolution bulging mode shown in Figure 9.

Each of the bellows modes may experience flow excitation over a fluid velocity range defined by

$$V = \frac{f_m \sigma}{S_{\sigma u}}$$

$$V_u = \frac{f_m \sigma}{S_\sigma}$$

and the optimum or most severe excitation will occur at a velocity equal to

$$V = \frac{f_m \sigma}{S_\sigma}$$

In the above equations, we have

f_m	=	a bellows mode frequency
$S_{\sigma u}$	=	upper limit Strouhal number
S_σ	=	lower limit Strouhal number
S_σ	=	optimum Strouhal number
V	=	velocity at lower limit of lock-in range
V_u	=	velocity at upper limit of lock-in range
σ	=	convolution tip width

Because of the lock-in range phenomena, and the closeness of successive bellows modes, it is best to assume that flow excitation can occur continuously over a velocity range from the minimum velocity for the lowest mode to the maximum velocity for the highest mode. Therefore, if f_{ml} and f_{mn} are the lowest and the highest mode frequencies, the extreme possible limit of flow excitation is defined by the limiting velocities

$$V = f_{ml}\sigma/S_{\sigma u}$$

$$V_u = f_{mn}\sigma/S_\sigma$$

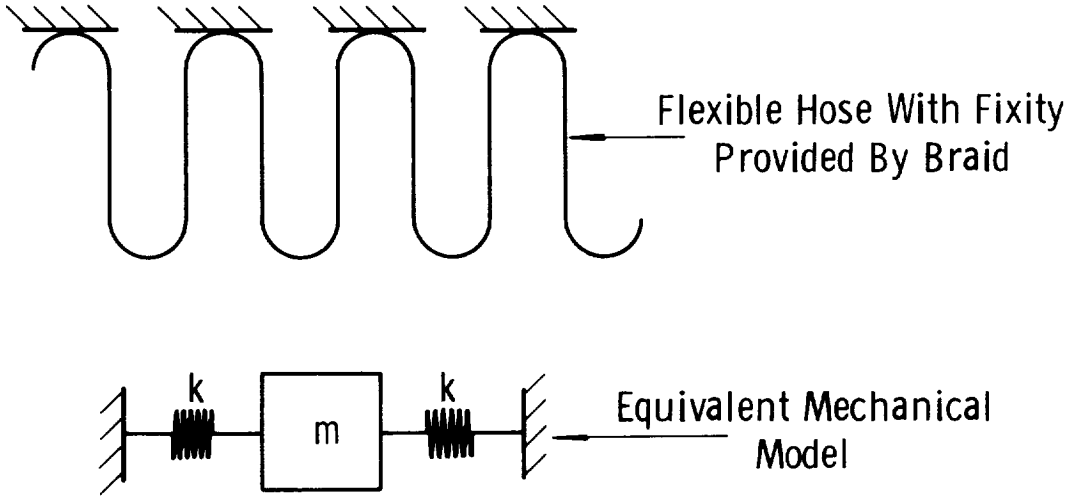

(a) Structural Mode For Flexible Hose

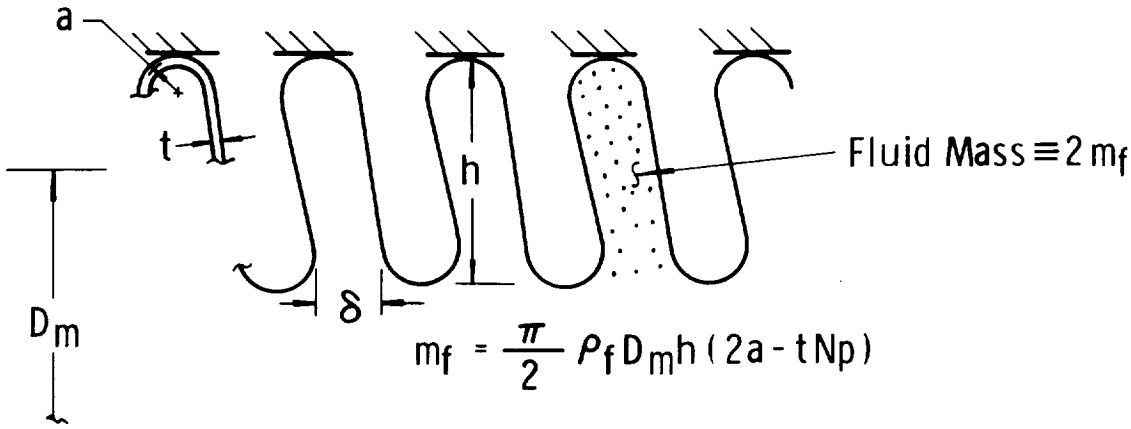

(b) In-Phase Mode

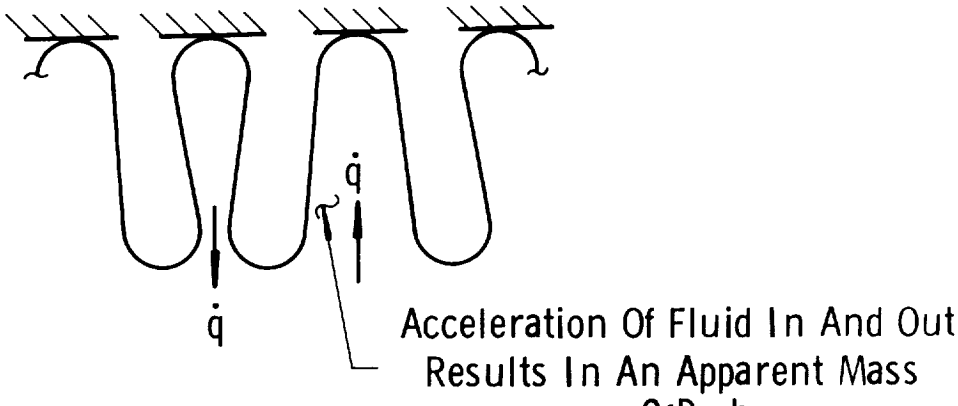

(c) Out-of-Phase Mode

2003

Figure 11. Summary of Flexible Hose Longitudinal Vibration Modes

II. 4 Bellows Flow-Induced Vibration Model

A calculated coincidence of the coupled bellows-liquid frequencies and the vortex shedding frequency only indicates a possible flow excitation problem, but does not guarantee that the bellows will vibrate, or indicate the severity of vibration. A desirable design goal is to be able to accurately predict anticipated stress levels for a given bellows and given flow conditions.

Figure 12 illustrates a physical model of the fluid and structural behavior for bellows flow excitation. The process of periodic vortex formation and shedding produces periodic pressures on the convolutions. The amplitude of this alternating pressure is proportional to the free-stream stagnation pressure ($^1/_2\ \rho_f\ V^2$). So far as the bellows structure is concerned, this alternating pressure produces a net force which may be considered applied at the tip of each convolution. The amplitude of this force is assumed to be of the form

$$F = C_F A_P (^1/_2\ \rho_f\ V^2) \qquad (1)$$

where C_F is a vortex force coefficient (a dimensionless coefficient) and A_P is the projected convolutes height area over which the pressure acts (the fluctuating pressure producing the force).

If the frequency of the vortex shedding coincides with a bellows longitudinal mode frequency, then a resonance may occur and the bellows convolutions will experience a vibratory displacement of the form

$$x = \frac{C_m F Q}{K_A} \qquad (2)$$

In the above equation, C_m is a dimensionless factor dependent on the bellows mode of vibration (mode factor), F is the vortex shedding force defined in equation (1), K_A is the bellows overall spring rate, and Q is the dynamic amplification factor (damping). This convolution vibratory displacement x will cause a corresponding stress whose magnitude is dependent on the convolution geometry.

Accepting this simple physical model of bellows flow excitation, the problem of calculating resultant stress levels reduces to one of obtaining a knowledge of the various "factors" illustrated in Figure 12. The primary factors are: C_F, a vortex force coefficient; C_m, a vibration mode factor; Q, a dynamic amplification factor; and C_s, a geometric stress factor. Other factors may also be introduced to account for various unique situations. For example, when an elbow is located upstream of a bellows, higher-than-normal stress levels may occur for a given flow

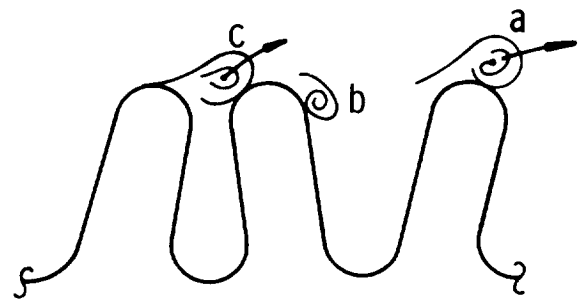

Vortex Shedding From Convolutions

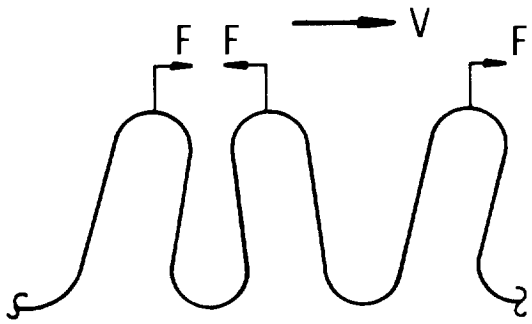

Vortex Force

$$F = C_F C_E A_p \left(\frac{1}{2} \rho V^2 \right)$$

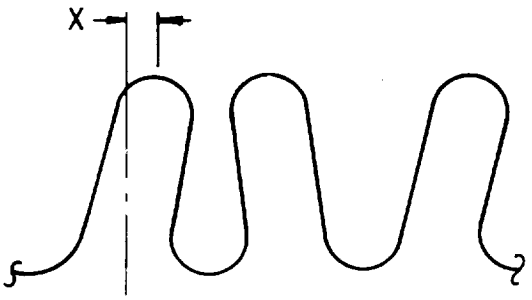

Convolution Displacement

$$x = \frac{C_m F Q}{k_A}$$

The resultant stress is

$$\text{Stress} = \frac{C_S E t x}{h^2}$$

In the above equations

C_F = vortex force coefficient
C_E = elbow factor
C_m = vibration mode factor
Q = dynamic amplification (damping)
C_S = geometric stress factor

2331

Figure 12. Illustration Of Stress Resulting From Vortex Force

velocity. If an acoustic resonance exists, this can change the picture, also. The objective of the next several sections is to summarize results of studies of these various factors.

Bellows Mode Factor

Using the force coefficient information obtained with a single convolution test model, along with an equivalent bellows mechanical model concept, flow-induced vibration amplitudes were predicted. This was accomplished by assinging a vortex force at each convolute tip, and then calculating the forced amplitude of the mechanical model. Comparing the resultant vibration amplitudes with observed values showed the preliminary predictions to be high by a factor equal to the number of convolutions involved in each "half wavelength" of bellows vibration. This suggested that there was only one effective vortex force per mode number of the vibration. Further detailed comparison of calculated and observed vibrations of bellows confirmed this idea. Also, reexamination of the visualized vortex shedding activity (illustrated in Figure 6) and reconsideration of the pressure forces involved, showed how this must happen.

Figure 13 depicts the action of a bellows with several convolutions vibrating in the first longitudinal mode. As shown, the vortex shedding causes fluctuating pressure forces on each side of each convolution. Because of the phasing of these pressure forces, however, only one effective vortex force exists per mode number of vibration. The first mode has one effective force point, the second mode, two, etc. Each of these effective forces is exerted at the central convolution of each mode half wavelength, or at the point(s) of maximum displacement of each mode.

Using the one-force-per-half-wave length concept illustrated in Figure 13, the analytical derivation of a value for the mode factor C_m, which relates displacement and force during a resonant condition, was undertaken. As shown in Section III, the resultant bellows mode factor is of the form

$$C_m = \frac{1}{8N}\left[\frac{N}{N_c} + \sin\left(\frac{\pi}{2}\,\frac{N}{N_c}\right)\right] \qquad (3)$$

and refers to the maximum relative displacement point (maximum stress point) along the bellows. Thus, from equations (2) and (3), it is evident that the bellows convolute maximum relative vibratory displacement is

$$X_{mr} = \frac{FQ}{8NK_A}\left[\frac{N}{N_c} + \sin\left(\frac{\pi}{2}\,\frac{N}{N_c}\right)\right] \qquad (4)$$

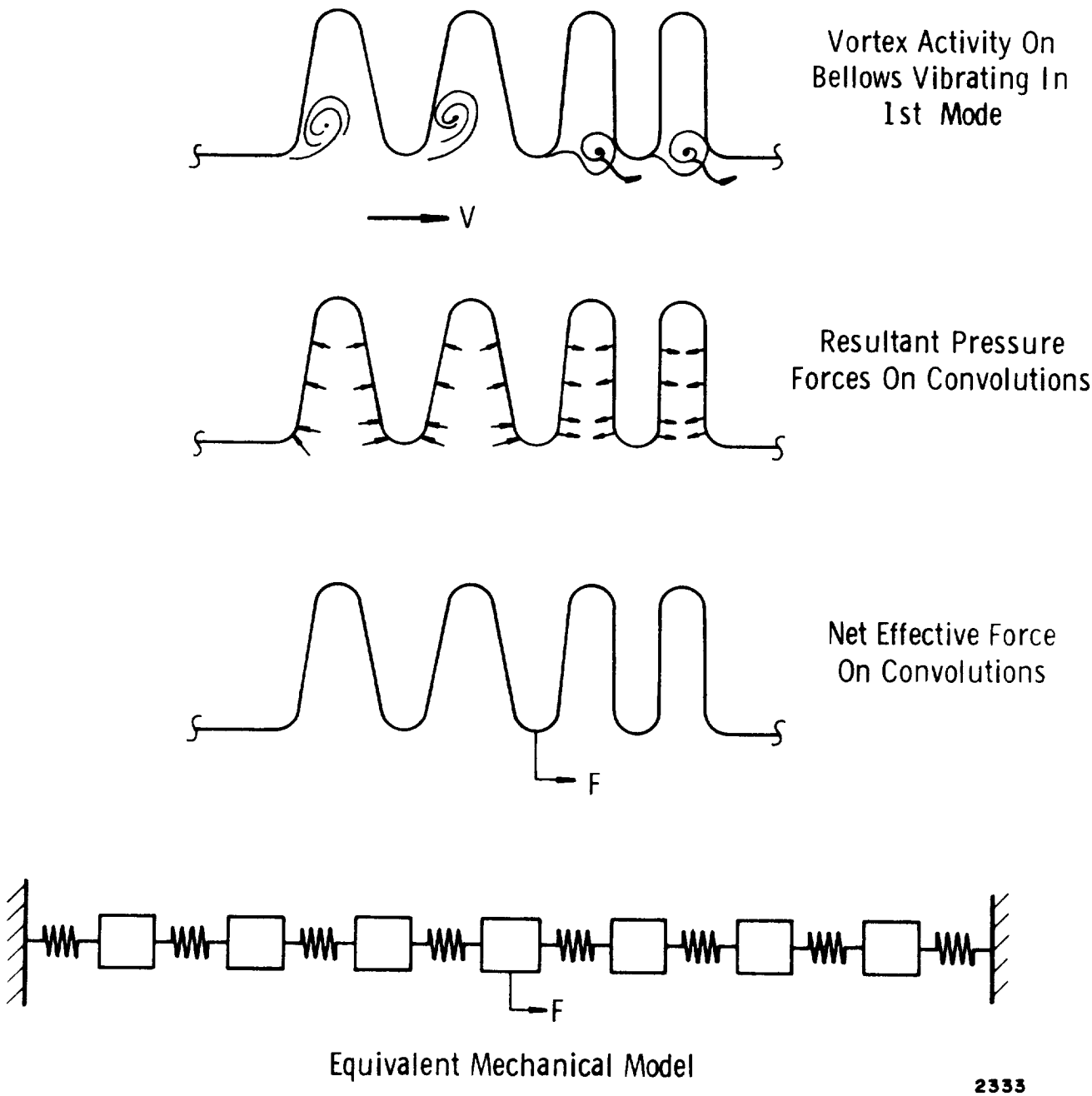

Figure 13. Effective Vortex Force On Bellows Vibrating In The First Longitudinal Mode

In equation (4), F is the amplitude of the vortex shedding force applied as illustrated in Figure 13; N is the vibration mode number (1, 2), and N_c is the total number of convolutes.

Bellows Damping

Because the value of damping is so important in the prediction of bellows flow-induced vibration amplitudes, a large number of mechanical vibration tests were conducted from which Q values could be obtained for typical conditions. These tests, and detail results are discussed in Section III.

Based on the test damping data and other flow results, a damping model was formulated, and is presented in Figure 14 and Table II. To reflect the change of Q with strain level, the factor

$$\frac{C_F C_E P_d}{N_p} \left(\frac{h}{t}\right)^2$$

called the "Bellows Operational Parameter," is employed as the independent variable. To account for different internal media, the effect of the number of plies, the bellows stiffness, and the mode number, the data in Figure 14 are shown as a number of application curves of Q versus the bellows operational parameter. Table II defines the use of each application curve.

Force Coefficient

Values for the vortex force coefficient have been obtained entirely from experiments. The effect of convolute geometry and bellows size have been examined in some detail as discussed in Section III. Figure 15 shows a model of the C_F (force coefficient) data resulting from all tests.

The C_F model shown here, because of the complexity of the flow-induced vibration problem is not always accurate for all bellows geometries, vibration modes and flow conditions. The data, however, represents a starting point for the analysis of a given bellows, and calculation of the Stress Indicator. Section III more fully discusses the force coefficient.

Acoustical Resonance

All previous discussion has related primarily to the flow-excitation of bellows with internal liquid flow. Tests conducted with internal gas flows reveal that a similar vortex shedding excitation can occur, but there is an added effect which is likely. It has been determined that when the vortex shedding frequencies become high enough, a radial acoustic resonance can

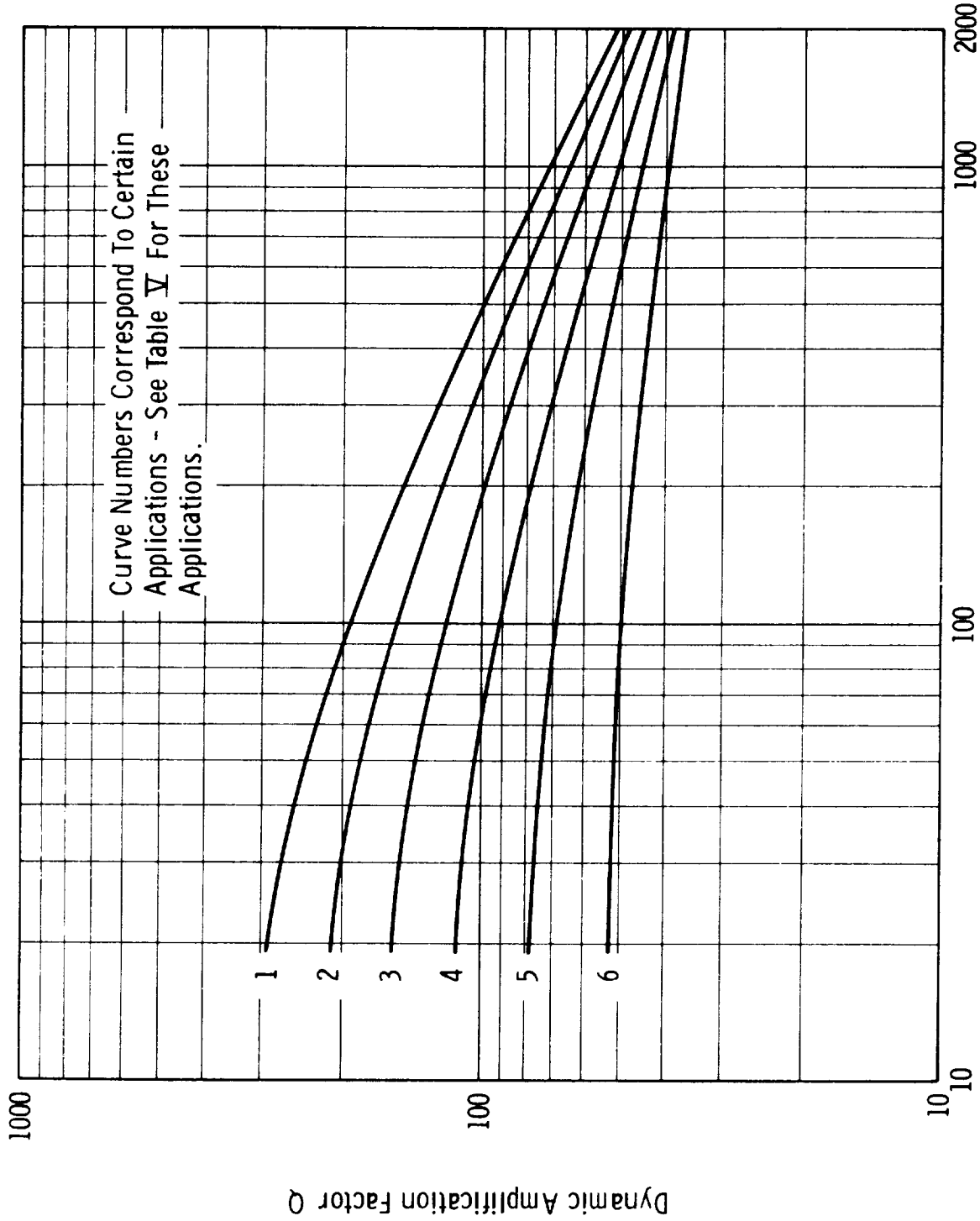

Figure 14. Dynamic Amplification Factors For Various Bellows Applications

Specific Spring Rate (see Note 1)	Number Plies	Internal Media (see Note 2)	Curve No.
all ranges	1	low pressure gases	1
over 2000 lb/in^2	1	high pressure gases, light liquids	1
over 2000	1	water, dense liquids	2
under 2000	1	high pressure gases, light liquids	2
under 2000	1	water, dense liquids	3
over 3000	2	all	3
2000-3000	2	all pressure gases	4
under 2000	2	all pressure gases	5
2000-3000	2	all liquids	5
under 2000	2	all liquids	6
over 3000	3	all	4
2000-3000	3	all	5
under 2000	3	all pressure gases	5
under 2000	3	all liquids	6

Use of Table - To use table, first calculate bellows specific spring rate, then look up application curve number corresponding to this specific spring rate, number of plies, and internal media.

Note 1: The specific spring rate is here defined as

$$S.S.R. = \frac{K_A N_c}{D_m N_p}$$

or is the spring rate per convolute, per ply, per unit of diameter.

Note 2: Low pressure gases will be defined here as being those gases below 150 psia. Light liquids will be defined as having a density, relative to water, of less than 0.2.

TABLE II

Applications Information for Use with Q Values
Data in Figure 14

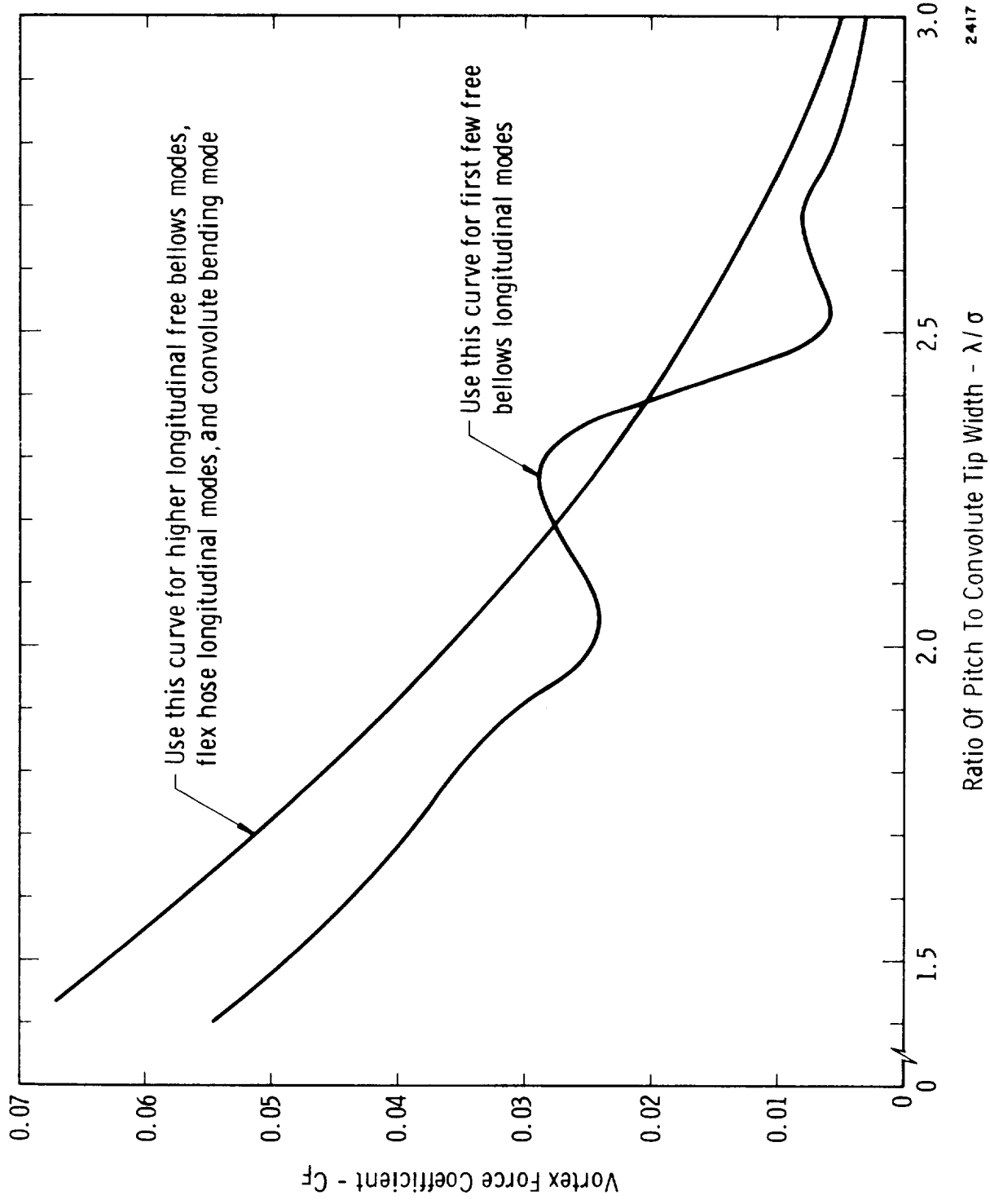

Figure 15. Summary Of Bellows Vortex Force Coefficient Experimental Data

be excited within the bellows. The effect of this resonance is to greatly amplify the convolute vibratory stresses. This effect must be anticipated and allowed for in any calculation of bellows flow-induced stresses where a gas is the internal flow media. Section V of the report is devoted entirely to this subject.

Effect of Heat Transfer - Cryogenic Fluids

Heat transfer effects as well as vortex, acoustic, geometric and cavitation influences must sometimes be considered in examining the flow-induced vibrations of bellows. The consequences of heat transfer in the case of cryogenic flow in bellows are of particular interest since large temperature differences exist between the flowing liquid and the bellows environment which could lead to a phase change near the inside bellows wall. Vapor formation will result in a "killing off" of the vortex shedding, and a change in the bellows flow response. Even low rates of heat transfer, which do not produce large scale boiling, may raise the vapor pressure near the wall so cavitation can occur and suppress the flow induced vibration. In addition to vapor effects on the flow induced vibration, frost buildup and liquid condensation on the outside bellows surface will affect the heating rate and add damping to the bellows structure, thus influencing its operating characteristics. Another question regarding bellows operation is the change in the bellows characteristics at extremely low temperatures in contrast to conditions tested in air and water at near ambient conditions.

The entire problem of heat transfer effects on the bellows response is considered in detail in Section IV of this report.

II. 5 Summary of Design Analysis Procedure

The procedure for analyzing a given bellows design to assure freedom from a flow-induced vibration failure consists of several distinct steps which are listed below.

Step 1* - Calculate the natural frequencies for all modes of the bellows or flex hose.

Step 2* - Determine the lock-in or critical velocity range for each possible mode of vibration

Step 3* - Calculate the Stress-Indicator for each mode at the critical point. For this step the possible

---

* Note: Step 1, Step 2 and Step 3 may be performed using the computer program discussed in Appendix A.

effects of heat transfer and radial acoustic resonance should be included.

Step 4 - Determine the potential for failure of the bellows using the Stress Indicator versus Cycles-to-Failure correlation plot.

Step 5 - For those bellows determined to be marginally safe from Step 4, perform a more thorough analysis of the critical modes by the procedure outlined below, and further discussed in Section III. A redesign and reanalysis is definitely required for those cases determined unsafe from Step 5.

The following discussion briefly outlines the procedures required for each step listed above.

Step 1 - Calculation of Natural Frequencies

As we have seen, a given bellows will have a number of structural modes which may be flow excited. These modes may be defined in terms of a number of modal frequencies denoted by

$$f_{m1},\ f_{m2},\ f_{m3} \cdots\ f_{mn}$$

Here f_{m1} denotes the first or lowest modal frequency and f_{mn} denotes the highest. For the case of a free bellows, f_{m1} will represent the first longitudinal mode and f_{mn} will devote the convolute bulging mode; the total number of modes will depend on the number of convolutions. For a flex hose, there are, so far as we presently know, only three possible modes; these are the in-phase and out-of-phase longitudinal modes shown in Figure 11, and the convolution bulging mode shown in Figure 10. Tables III and IV summarize the frequency calculation procedure for free bellows and flex hose.

The calculation of the modal frequencies may be conveniently performed, if desired, by the computer program described in Appendix A.

Step 2 - Modal Lock-In Range

Each of the bellows modes may experience flow excitation over a fluid velocity range from a lower value V to an upper value V_u defined as

$$V = \frac{f_m \sigma}{S_{\sigma u}}$$

$$V_u = \frac{f_m \sigma}{S_\sigma}$$

Step A - Consider the hose convoluted structure representable by the mass-spring model shown in Figure 11.

Step B - Calculate the elemental spring rate value k from the expression

$$k = 2K_A$$

where K_A is the overall spring rate of one complete convolution. The value of K_A may be determined by a method given in Appendix A or from a force-deflection test.

Step C - Calculate the elemental metal mass m from the expression

$$m_m = \pi \rho_m t\, N_p\, D_m\, [\pi a + (h-2a)]$$

Step D - Calculate the in-phase mode and out-of-phase longitudinal mode fluid masses from

$$m_f = \frac{\pi}{2}\, \rho_f D_m h\, (2a - tN_p) \Big\} \quad \text{in-phase mode}$$

$$m_f = \frac{\pi D_m \rho_f h^3}{3\delta} \Big\} \quad \text{out-of-phase mode.}$$

Step E - Calculate the in-phase and out-of-phase longitudinal frequencies from

$$f = \frac{1}{2\pi} \sqrt{\frac{2k}{m}}$$

where

$$m = m_m + m_f$$

Step F - Calculate the first bending mode frequency from the information in Figure 10, or

$$f = \frac{1}{2\pi} \sqrt{\frac{2k'}{m'}} = \frac{1}{2\pi} \sqrt{\frac{8k}{m}}$$

where

$$k' = 2k$$

and

$$m' = \frac{m}{2} = \frac{m_m + m_f}{2}$$

For the value of m_f use

$$m_f = \pi D_m \rho_f h^3 / 3\delta$$

TABLE IV - SUMMARY OF FLEX HOSE FREQUENCY CALCULATION PROCEDURE

Step A - Consider the bellows structure representable by the lumped mass-spring mechanical model shown in Figure 3.

Step B - Calculate the elemental spring rate value k from the expression

$$k = 2N_c K_A$$

where K_A is the overall spring rate determined from a method given in Appendix A or from a force-deflection test.

Step C - Calculate the elemental metal mass m_m from Equation (4) or

$$m_m = \pi \rho_m t \, Np \, D_m [\pi a + (h-2a)]$$

Step D - Calculate the fluid added mass m_f, for the first few longitudinal modes (N values) and for the higher longitudinal modes as

$$m_f = \frac{\pi}{2} \rho_f D_m h (2a - tN_p) \Big\} \quad \text{First few N values}$$

and

$$m_f = \frac{\pi D_m \rho_f h^3}{3\delta} \Big\} \quad \text{Higher N values}$$

Step E - Calculate the reference frequency f_o from the expression

$$f_o = \frac{1}{2\pi} \sqrt{\frac{k}{m}}$$

where

$$m = m_m + m_f$$

Step F - Look up proper dimensionless frequencies in Table I (corresponding to given N_c value) and then calculate the true mode frequencies by multiplying by the reference frequency. This gives all of the longitudinal mode frequencies.

Step G - Calculate the first bending mode frequency from the information in Figure 10, or

$$f = \frac{1}{2\pi} \sqrt{\frac{2k'}{m'}} = \frac{1}{2\pi} \sqrt{\frac{8k}{m}}$$

where

$$k' = 2k$$

and

$$m' = m/2 = \frac{m_m + m_f}{2}$$

For the value of m_f use

$$m_f = \pi D_m \rho_f h^3 / 3\delta$$

TABLE III - SUMMARY OF FREE BELLOWS FREQUENCY CALCULATION PROCEDURE (ASSUMED INCOMPRESSIBLE FLUID)

where the Strouhal number limits are shown in Figure 8. The critical ranges of velocity must be calculated in Step 2.

The range of possible bellows flow excitation may be predicted as follows:

(a) Calculate the lowest and highest bellows mode frequencies, f_{m1} and f_{mn}. The procedure for doing this is summarized in Tables III and IV.

(b) Calculate the limits of fluid velocity corresponding to these two frequencies. This is done with the equations above and with the values of the Strouhal numbers $S_{\sigma\ell}$ and $S_{\sigma u}$ obtained from Figure 8.

(c) Compare this flow excitation fluid velocity range with the known operating range of the bellows. If an overlap of these ranges exists, then excitation may occur.

A graphical method of predicting bellows excitations ranges is illustrated in Figure 16. This method involves preparing a plot of frequency versus fluid velocity which contains both the bellows mode frequency information and the possible vortex shedding frequency limits. The upper and lower bellows frequencies are represented by horizontal lines on the plot (constant frequency lines), as shown in Figure 16. Also, lines of constant slope which pass through the origin are drawn in to represent the vortex frequency limits (as a function of velocity), defined by the expressions

$$f = \frac{S_\sigma \; V}{\sigma}$$

and

$$f_u = \frac{S_{\sigma u} V}{\sigma}$$

The range of possible flow excitation is clearly seen from this plot.

The computer program discussed in Appendix A may be used to rapidly predict the critical velocity ranges for each bellows mode.

Step 3 - Stress-Indicator

A quick method for estimating the dynamic flow-induced stress level for a given bellows installation has been developed. This method consists of calculating a "Stress-Indicator" which is a number roughly

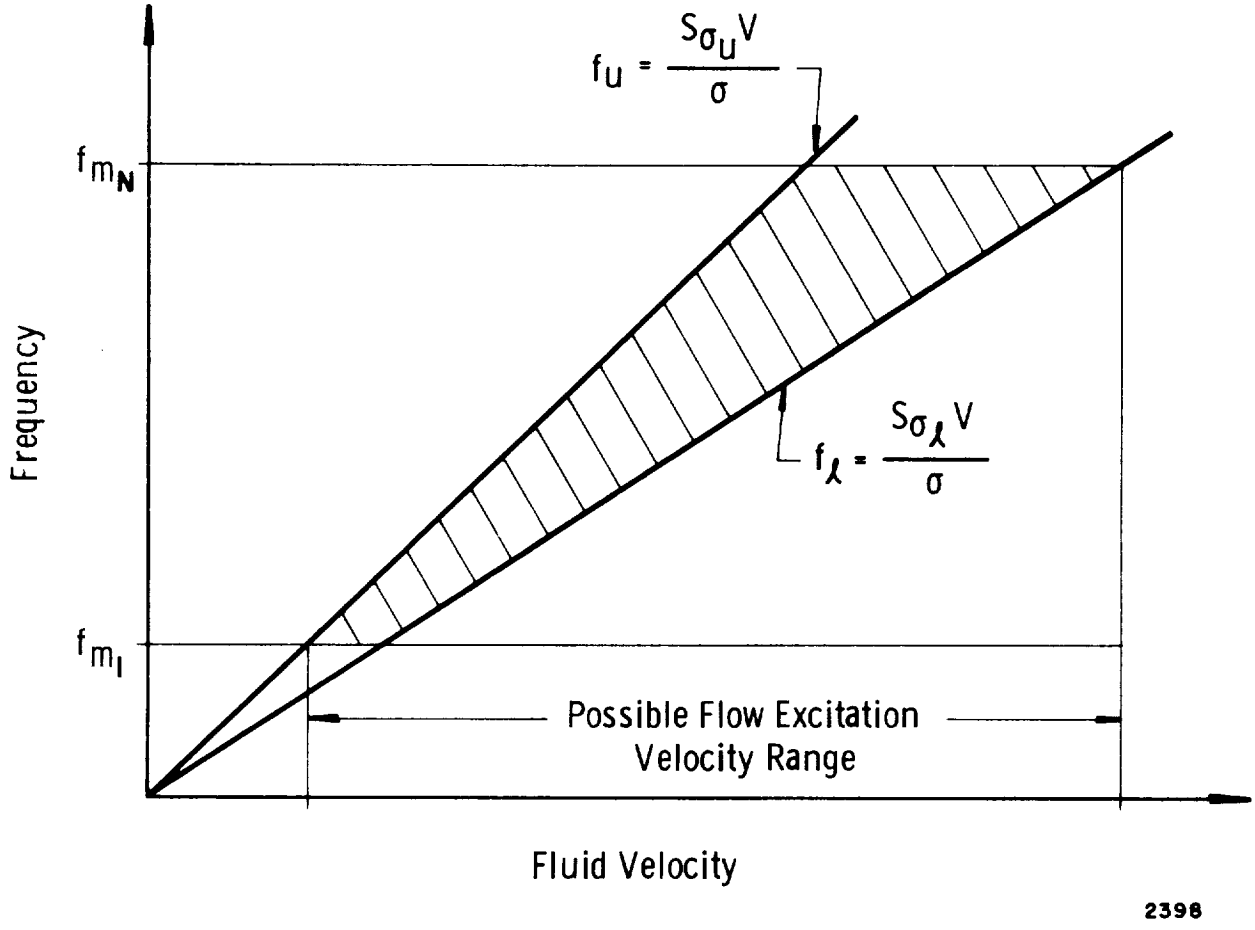

Figure 16. Frequency versus Velocity Plot To Illustrate Bellows Flow Excitation Region

proportional to stress and apparently valid for judging the relative severity of bellows vibrations.

The basic equations which describe flow-induced stress, as given previously are

$$F = C_F A_p (1/2 \rho V^2) = C_F A_p p_d \tag{5}$$

$$x = \frac{C_m F Q}{K_A} \tag{6}$$

and

$$\text{Stress} = \frac{C_s E t x}{h^2} \tag{7}$$

The objective of the "Stress-Indicator" approach is to combine these expressions in a simple form so as to give a single expression for stress which contains only readily-known bellows dimensional data, or parameters, and flow variables. Therefore, we will assume the following:

(a) A_p can be approximated by

$$A_p \approx \pi D_m h$$

(b) C_F is known from Figure 15

(c) C_m can be approximated by

$$C_m \approx \frac{1}{4N_c}$$

(d) K_A can be approximated by

$$K_A \approx D_m E (N_p/N_c) (t/h)^3$$

(e) Q can be found from Figure 14.

(f) The factor C_s is approximately constant for all bellows.

Based on these assumptions, Equations (5), (6), and (7) may be combined to give

$$\text{Stress} = \pi C_s \left(\frac{C_F Q}{N_p}\right) \left(\frac{h}{t}\right)^2 (1/2 \rho V^2) \tag{8}$$

Since C_s has been assumed constant, we can extract a quantity from Equation (8) which is approximately proportional to flow-induced stress for all bellows; this quantity is

$$\text{Stress Indicator} = \left(\frac{C_F Q}{N_p}\right)\left(\frac{h}{t}\right)^2 (1/2\ \rho V^2) = \left(\frac{C_F Q}{N_p}\right)\left(\frac{h}{t}\right)^2 p_d \qquad (9)$$

To find values for the Stress-Indicator for each critical velocity, it is first necessary to find C_F and Q values from Figures 14 and 15.

The Stress Indicator value may be hand calculated by the procedure outlined above, or the computer program presented in Appendix A may be directly used to calculate S.I. values.

Step 4 - Failure Potential

The Stress Indicator value, as previously discussed, represents an indication of the dynamic or flow-induced stress level within the convolutes. When this stress level is of sufficient magnitude, fatigue failures of the convolutes may be expected. To permit prediction of bellows flow-induced fatigue, a correlation of the S.I. value with the number of cycles-to-failure for a large number of bellows specimens has been generated, as discussed in Section III. This correlation is presented in graphical form in Figure 17. Step 4 of the analysis and design procedure involves predicting the life of a given bellows by use of the information contained in Figure 17, and a knowledge of the modal frequency for a given operating condition.

As an example, suppose a certain bellows having a critical modal frequency of 1000 cps had a calculated S.I. value of 40,000 psi. From Figure 17 we see that this bellows is not safe beyond about 2.5×10^5 cycles. Based on this we can readily predict the safe life to be limited to

$$\text{time} = \frac{2.5 \times 10^5}{10^3} = 250 \text{ seconds.}$$

It should be emphasized here that the use of the Stress Indicator approach, utilizing the method defined above gives a conservative answer as to the failure potential of a bellows. In fact, some bellows which fall in the marginal or random zone of Figure 17 may actually be failure-free. Step 5 provides a closer look at these bellows.

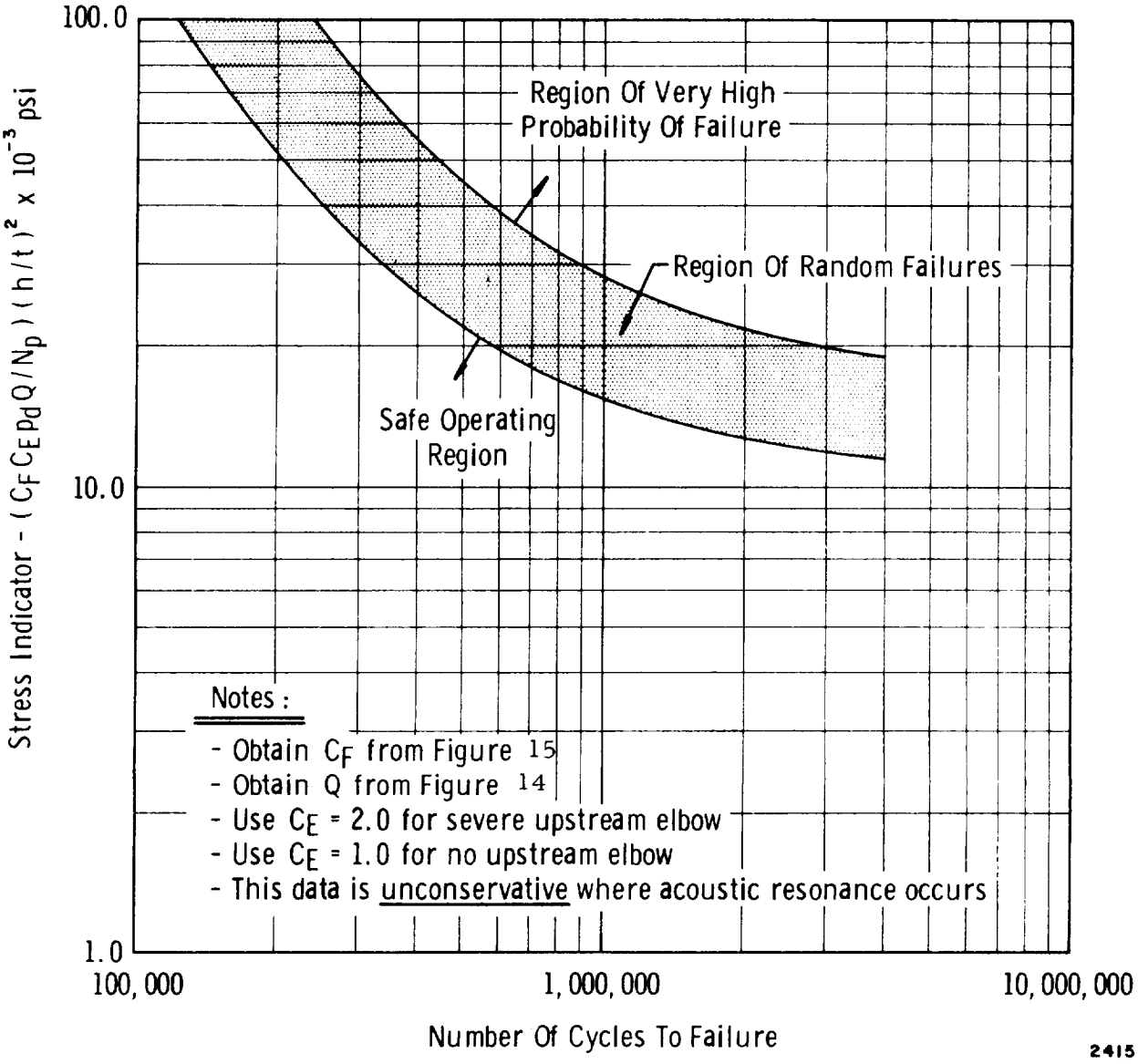

Figure 17. Preliminary Bellows Fatique Life Data

Step 5 - Closer Look and Redesign

Those bellows determined unsafe from Step 4 should definitely be further examined by a more refined analysis. The quantities C_F and Q presented in Figures 14 and 15 are conservative. As discussed in Section III. the product of these two, that is $C_F Q$, has been correlated for a large range of bellows geometries and flow conditions to give an improved model. Figure 18 shows a model of this correlation. Here $C_F Q$ is plotted as a function of the parameter

$$\frac{(\frac{1}{2} \rho V^2) A_p}{N K_A N_c \sigma} \left(\frac{h}{\delta}\right)$$

The correlation is branched, that is one curve is valid for the lower order modes defined by the condition

$$N < N_c \quad \text{(lower order modes)}$$

and another curve is valid for the higher order modes defined by the condition

$$N \geq N_c$$

To use the data of Figure 18, one simply calculates the independent parameter based on the bellows operating condition and geometry, and then obtains the corresponding value for the quantity $C_F Q$. This value for $C_F Q$ is then used to calculate a new Stress Indicator value. The new Stress Indicator is then reintroduced into the data of Figure 17, and any bellows falling in the safe zone is definitely safe, while those falling in the random zone or above will fail.

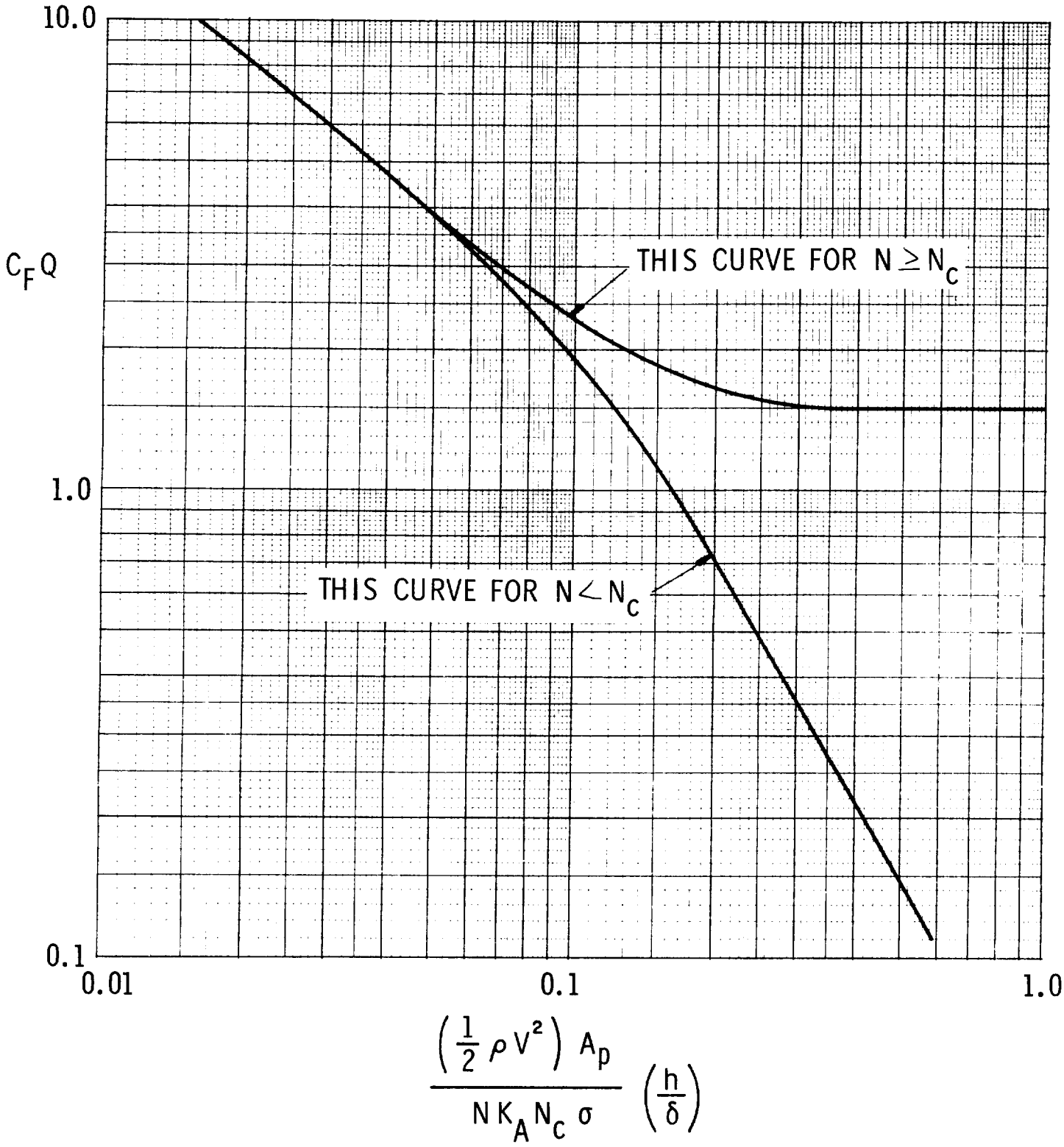

Figure 18. Correlation of $C_F Q$ with A Bellows Parameter Involving Operational and Geometric Parameters

III. BELLOWS FLOW-INDUCED VIBRATIONS WITH LIQUIDS

III. 1 Introduction

A search of the open literature, conducted at the start of the project, revealed that no previous work had been reported on flow excitation of bellows. In fact, the only discussions found in the literature which deal with the related problem of mechanically excited vibration characteristics of bellows are those of Daniels (10) and Lytle (11). A study of unpublished reports from the aerospace industry, however, revealed that bellows flow-induced fatigue failures had been observed for a variety of conditions, including liquid and gas flow, single- and multiple-ply bellows, and both free and wire braid-covered items.

The study described in this report has resulted in a rather detailed examination of several phases of the bellows flow-induced vibration problem. The initial two years of the program were devoted to a detailed study of the mechanism of flow excitation, resulting in a formulation of the model summarized in Section II, and presented also in Reference 1. The initial studies were made using rather small bellows (1.5 to 2.0 inches I.D.) and with water as the predominant test fluid.

Following this initial investigation with water, the program was expanded to verify the model initially generated (Section II) to accomplish the following:

(1) Verify the Strouhal number correlation for a range of bellows sizes and geometries.

(2) Verify the force coefficient model as a function of size and geometry.

(3) Develop additional failure data to verify the Stress Indicator versus Cycles-to-Failure correlation for a range of bellows geometry.

The remainder of this section describes results of the above studies.

III. 2 Strouhal Number Correlation

For a given bellows, having some particular convolution geometry and structural mode frequencies, there are certain optimum fluid velocities which result in a maximum amplitude bellows excitation of each mode.

It is at these velocities that the vortex shedding process is best able to feed energy from the fluid stream into the vibration process. In other words, the vibration frequency and fluid velocity conditions are "optimum" from a vortex shedding standpoint. It has been found that the use of a Strouhal number is an excellent means of correlating the vibration frequency, fluid velocity and geometry under these optimum conditions, as is true for any vibration phenomena involving vortex shedding.

In general terms, a Strouhal number is a dimensionless quality of the form

$$S = f \ell / V$$

where f is a frequency, ℓ is a length quantity, and V a fluid velocity. For the case of bellows flow-induced vibrations, the only problem in using this correlation parameter was in selecting a satisfactory length quantity.

Figures 19 and 20 show example data, which was originally presented in Reference 1, of the Strouhal number calculated at the optimum flow excitation condition for two different bellows. The pitch of these bellows were changed by stretching and compressing them from their original configuration. Strouhal number values based on both the tip width σ and the pitch λ have been plotted. Based on a composite of all initial test data, a single curve of Strouhal number (based on tip width σ) as a function of the ratio of pitch to tip width (λ/σ) was prepared and originally presented in Reference 1. This Strouhal correlation model, shown by the curves in Figure 21, was originally based on test data obtained with bellows in the 1.5 to 2.0 inch I.D. size range. As part of the more recent studies to validate this model for large bellows, data was obtained from a number of bellows with internal diameters of 3 inch, 6 inch and 14 inch.

Table V presents geometric and test results for the 3 inch bellows, while Table VI gives similar results for the 6 inch and 14 inch bellows. In each case, the Strouhal number was calculated for the observed peak strain point for a given mode of vibration. All of these new data points have been plotted in Figure 21. As may be seen, the results from these larger bellows agree very well with the original model, since the Strouhal number for peak excitation falls well within the range for lock-in indicated. We have concluded from these results that the original Strouhal number correlation is valid.

III.3 Bellows Forced Vibration Model

A physical model of bellows flow excitation was outlined in Section II.4 and illustrated in Figure 12. In this model, the vortex force is assumed to be of the form

$$F = C_F A_p \left(\frac{1}{2} \rho_f V^2 \right) \qquad (10)$$

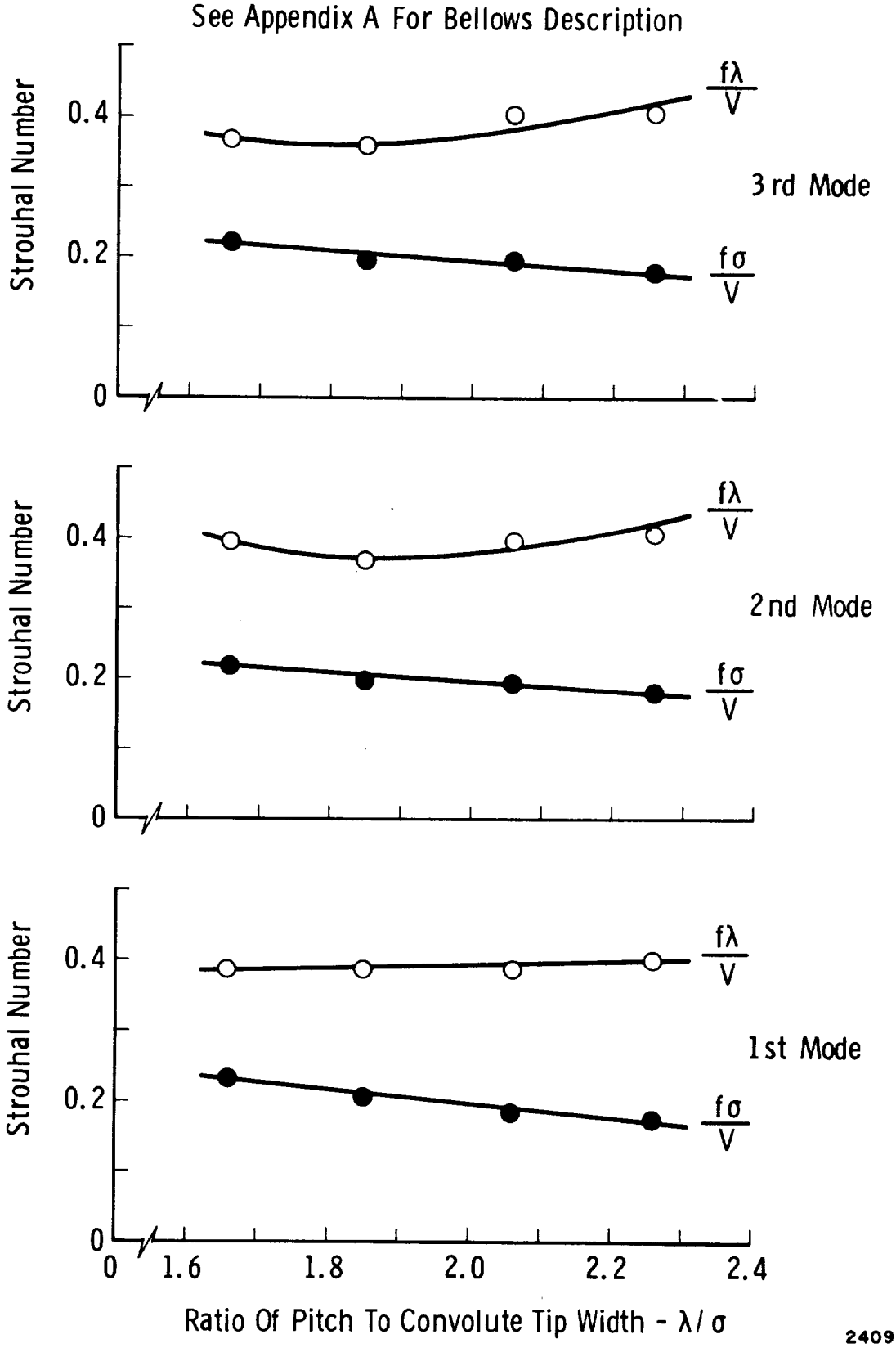

Figure 19. Strouhal-Number Correlation For Bellow #113

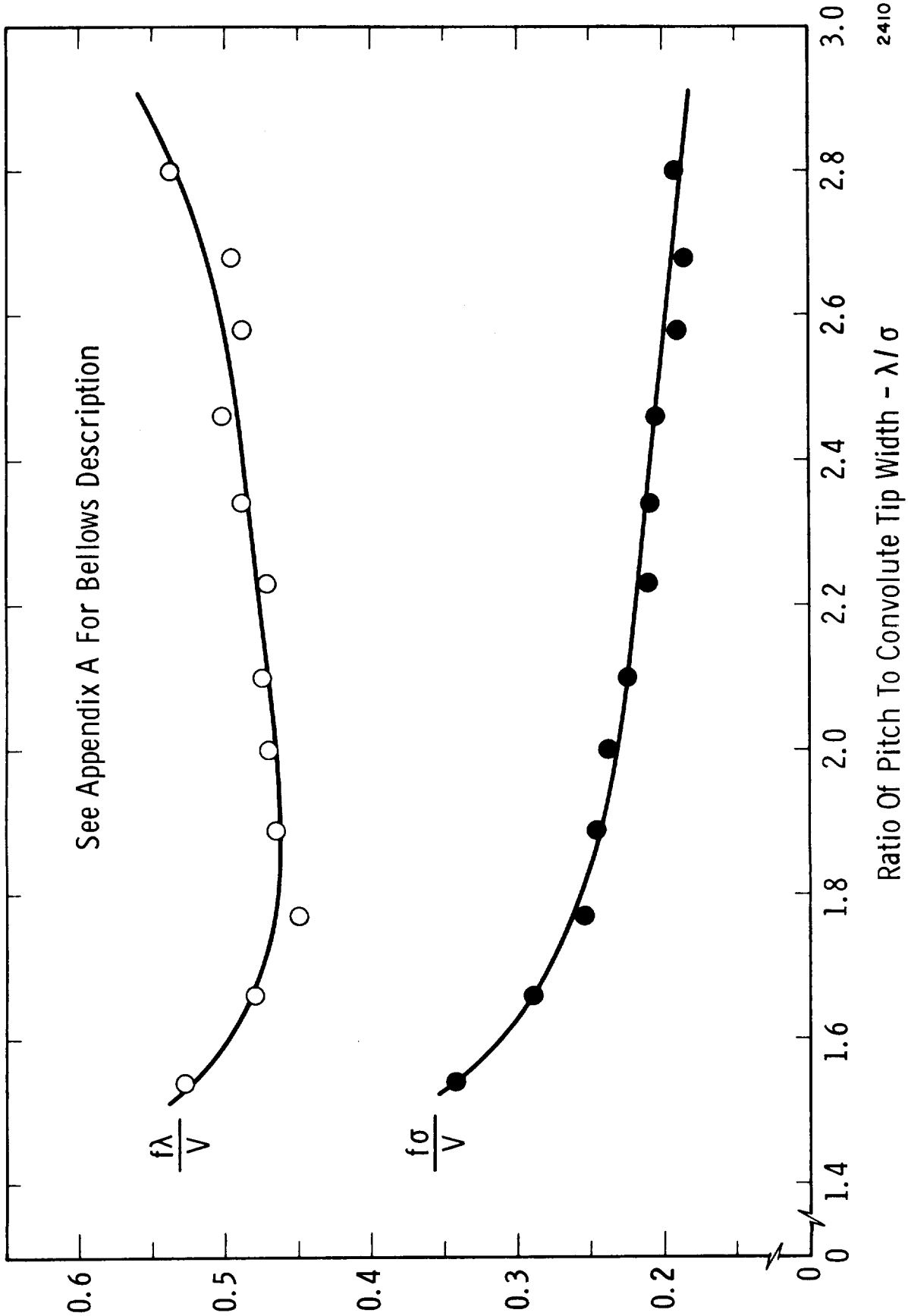

Figure 20. Strouhal Number Correlation For Bellows #105 (first mode)

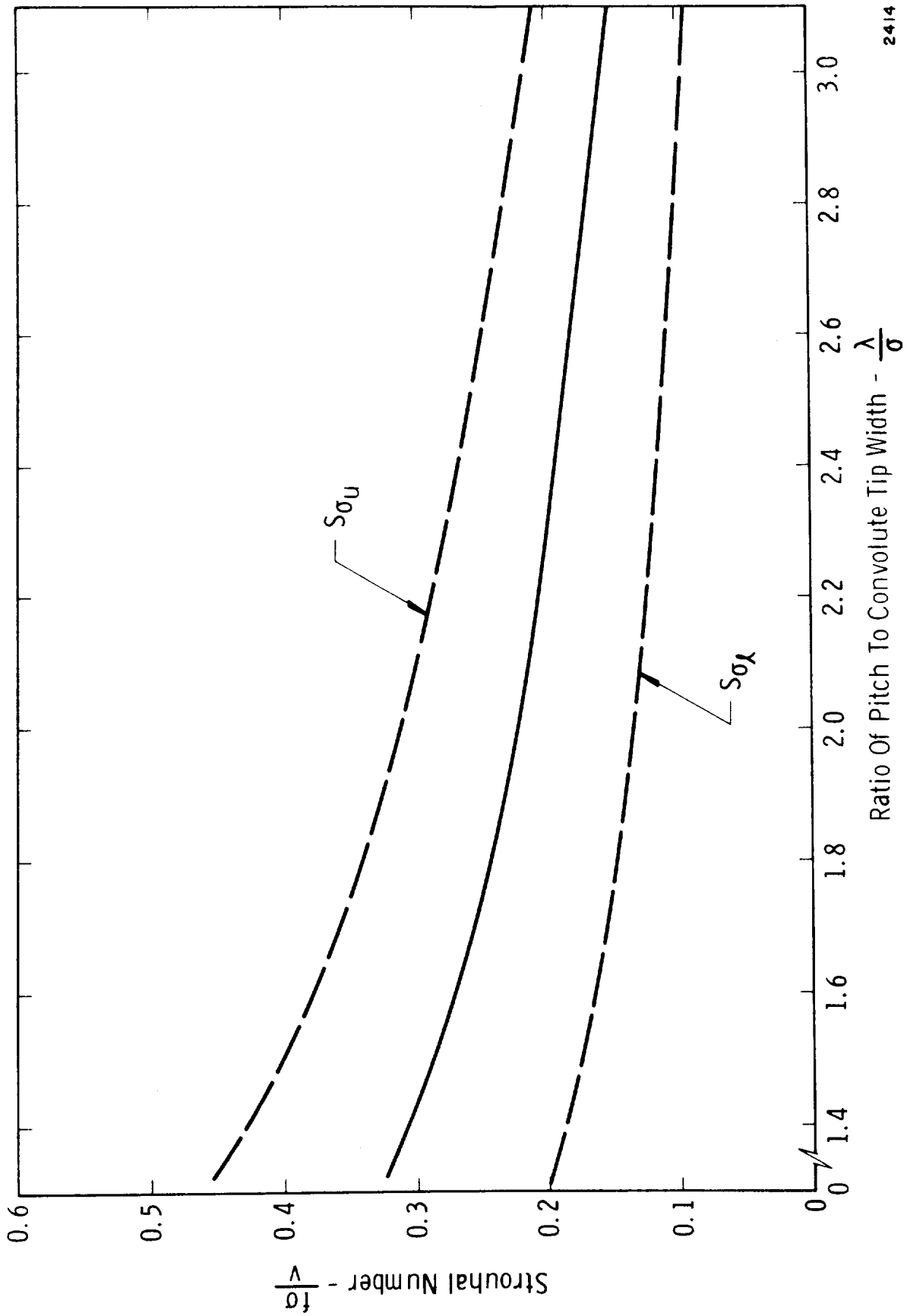

Figure 21. Composite Of All Strouhal Number Correlation Data

TABLE V. STROUHAL CORRELATION FOR 3-INCH TEST BELLOWS

Bellows #	σ	λ/σ	Ve	f	N	$\frac{f\sigma}{V}$
2	.150	1.57	22.3	430	1	.241
			40.8	830	2	.254
			56.0	1220	3	.271
3	.12	1.97	7.0	140	3	.200
			9.0	185	4	.205
			12.5	235	5	.187
5	.125	1.89	9.4	175	1	.194
			17.7	340	2	.201
			26.6	500	3	.195
			34.6	640	4	.193
			50.8	990	6	.185
			55.5	990	6	.185
8	.12	1.92	14.2	250	1	.176
			27.8	500	2	.180
			40.8	725	3	.178
10	.135	1.75	5.0	100		.225
			9.5	190		.225
			15.0	265		.200
14	.135	1.63	5.0	80	1	.180
			10.0	175	2	.197
			14.6	260	3	.200
			20.0	330	4	.186
			24.0	400	5	.188
			28.0	455	6	.183
	.135	1.72	10.0	180	2	.202
			15.8	270	3	.193
			20.5	345	4	.189
			26.0	415	5	.180
			32.	485	6	.171

TABLE VI. STROUHAL CORRELATION FOR 6-INCH & 14-INCH TEST BELLOWS

Bellows #1	Di (inches)	σ (inches)	λ/σ	Ve (fps)	f (Hz)	N	$\frac{f\sigma}{V}$
SwRI-D #3	6	.12	1.87	7.5	155	1	.207
				11	236	2C	.215
				16	293	2	.183
				17.5	323	2C	.185
				20	418	3	.209
				26.5	528	4	.200
				34.5	626	5	.182
SwRI-E	6	.12	1.87	7.5	146	1	.195
				10.0	214	2C	.214
				16	282	2	.176
				18.5	315	2C	.170
				21.5	403	3	.188
				23	430	4C	.187
				26	509	4	.196
				33	605	5	.183
SwRI-F	6	.12	1.87	9	167	1	.186
				13	261	2C	.200
				17	318	2	.187
				17+	330	2C	.183
				24.5	449	3	.183
				33.5	574	4	.172
SwRI-G #4	6	.16	1.81	12.5	180	1	.192
				16	270	2C	.225
				22.5	346	2	.205
				27.5	494	3	.239
				34.5	530	C	.205
				41.5	630	4	.202
				50.5	746	5	.197
SwRI-H #3	14	.24	1.87	10.2	92	1	.180
				12.5	130	2C	.208
				20.5	180	2	.176
				27.5	256	3	.186
				37.0	325	4	.176
				45.0	387	5	.172

The resultant bellows vibratory displacement, as illustrated in Figure 12, is assumed to be of the form

$$X = \frac{C_m F Q}{K_A} \tag{11}$$

and the vibratory peak stress in the bellows convolute is assumed to be given by

$$\text{Stress} = \frac{C_s E t X}{h^2} \tag{12}$$

This model contains several factors which must either be analytically modeled or determined from experiments. These factors are

C_F = vortex force coefficient

C_E = elbow factor

C_m = vibration mode factor

Q = dynamic amplification factor

C_s = geometric stress factor

C_{AR} = acoustic resonance factor

The factors C_m and C_s may be analytically modeled, but the rest must be modeled from experimental data. The discussion which follows describes the models developed for each factor except C_{AR} which is discussed in Section V of this report.

III. 3. 1 Initial Studies of Vortex Force Coefficient

The initial study of the nature and magnitude of the vortex shedding force was undertaken with a special single convolution test model which is illustrated in Figure 22. A bellows convolution is simulated in this test model by a flexible ring which is geometrically quite similar to a convolution. The ring was constructed from steel and had a coating of lead on the flexible web section to provide sufficient damping to prevent early fatigue failure during actual testing; this happened with the first several rings which were constructed without added damping. The test ring or simulated convolution is clamped in a special housing between a pair of exciter coils; also, a displacement probe is built into the apparatus to allow ring vibration amplitudes to be monitored.

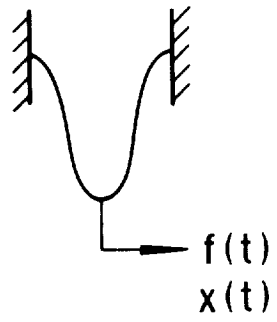

SINGLE BELLOWS CONVOLUTION

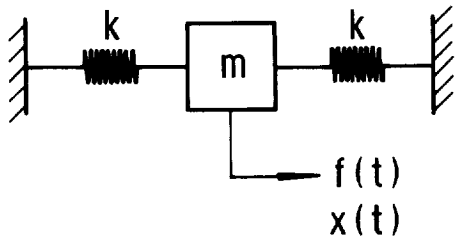

MECHANICAL MODEL OF CONVOLUTION

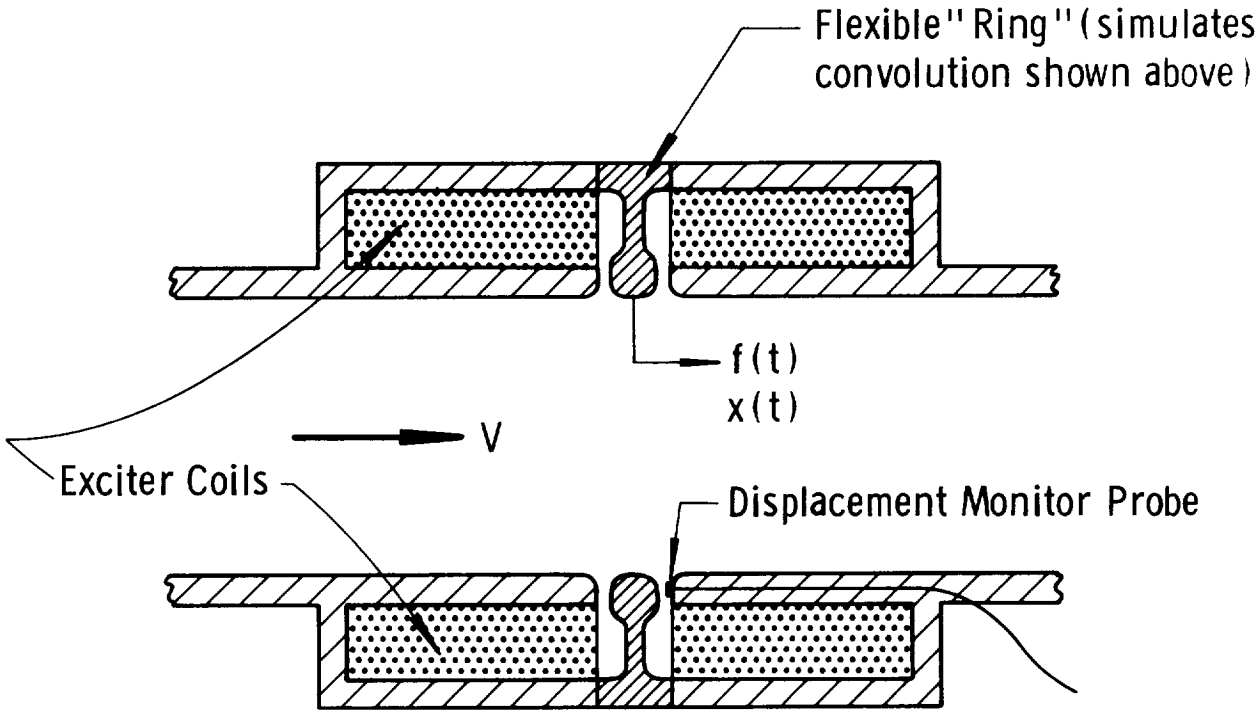

1868

CONVOLUTION VIBRATION TEST MODEL

Figure 22. Diagram Of Convolution Vibration Test Model And Equivalent Bellows And Mechanical Model Representations

With this apparatus the following types of tests have been performed: (a) frequency response of the ring in air with excitation provided by the coils; (b) frequency response of the ring in water with excitation provided by the coils; and (c) response of the ring as a result of flow excitation with internal water flow. Also, a calibration of static force versus deflection was made for the ring. From these tests and the force-deflection calibration, several kinds of information were obtained. The forced vibration test in air gave essentially the ring-only natural frequency and damping (neglecting air loading). The forced vibration test in water allowed the water-added-mass and water damping to be calculated. Also, Figures 23 and 24 show typical test data obtained by monitoring ring amplitude as a function of frequency for a constant coil current amplitude (constant coil force amplitude) for the forced vibration test in water. Note the increase in peak amplitude as the flow velocity is increased. The greatest ring vibration amplitude will occur when the velocity is such that the ideal vortex shedding frequency corresponds to the ring critical frequency.

Finally, the flow-induced vibration data allowed an effective vortex force coefficient to be obtained over the lock-in range. This effective vortex coefficient was reduced from the ring flow-induced vibration data in the following manner:

(a) The vibration amplitude (as a function of fluid velocity) was converted to an apparent force through the use of the force-deflection calibration.

(b) This apparent force was converted to a true vortex force by dividing by the Q value reduced from the forced vibration test data (in water).

(c) This true force was converted to a force coefficient through the use of Equation (10).

Vortex coefficient data was obtained in this manner for two different convolution geometries and the results are shown in Figure 25. Notice the great reduction in the force coefficient as the convolution pitch is "opened up".

III. 3. 2 Vibrations of Real Bellows

Bellows Mode Factor

Having available the results of the experiments with the single convolution test model, discussed in the previous section, the next logical step was to use this force coefficient information, along with the equivalent mechanical model concept, to predict flow-induced vibration amplitudes

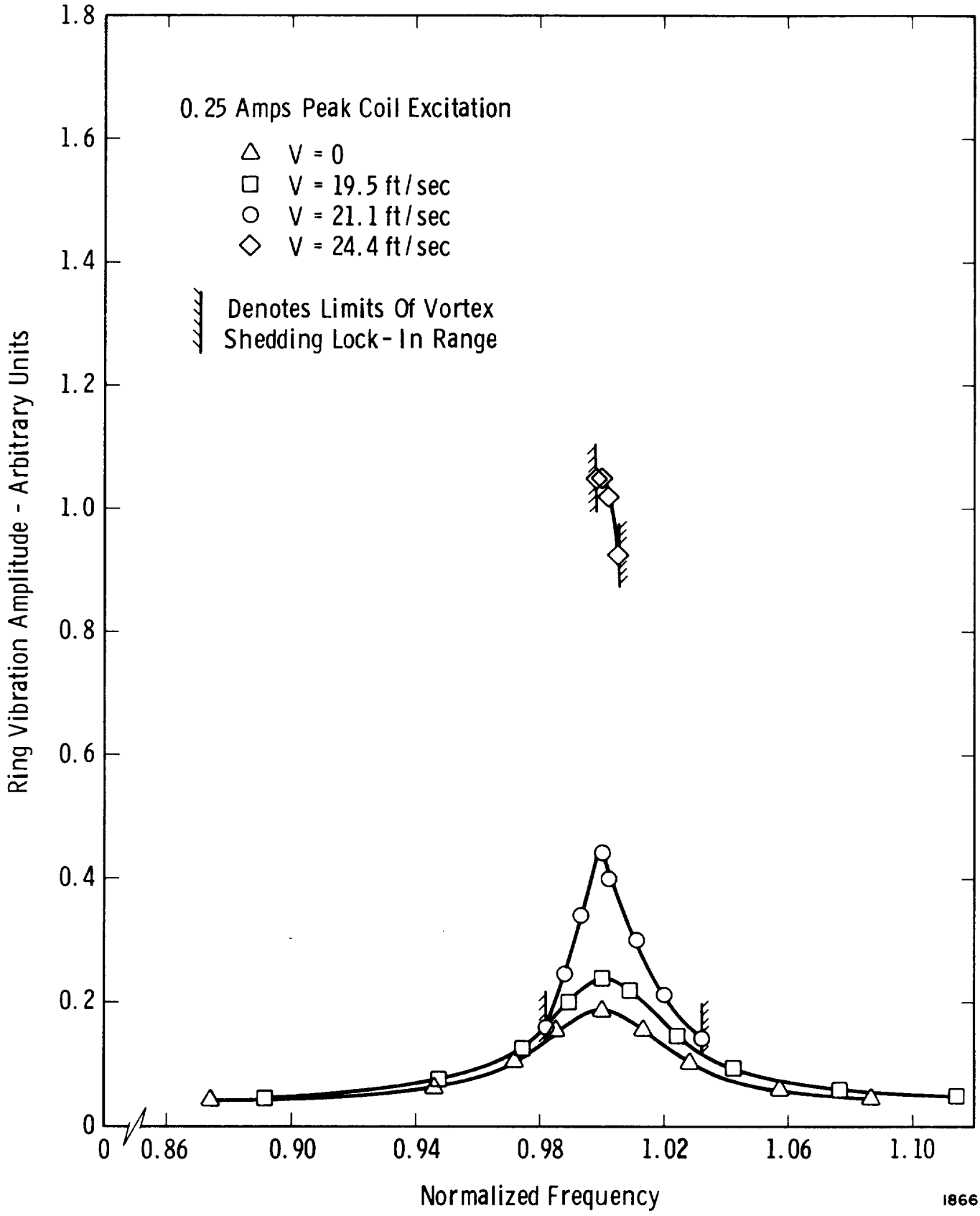

Figure 23. Typical Forced Response Data From Vibrating Ring Test Model - Constant Coil Excitation Current (0.25) - Variable Flow Velocity

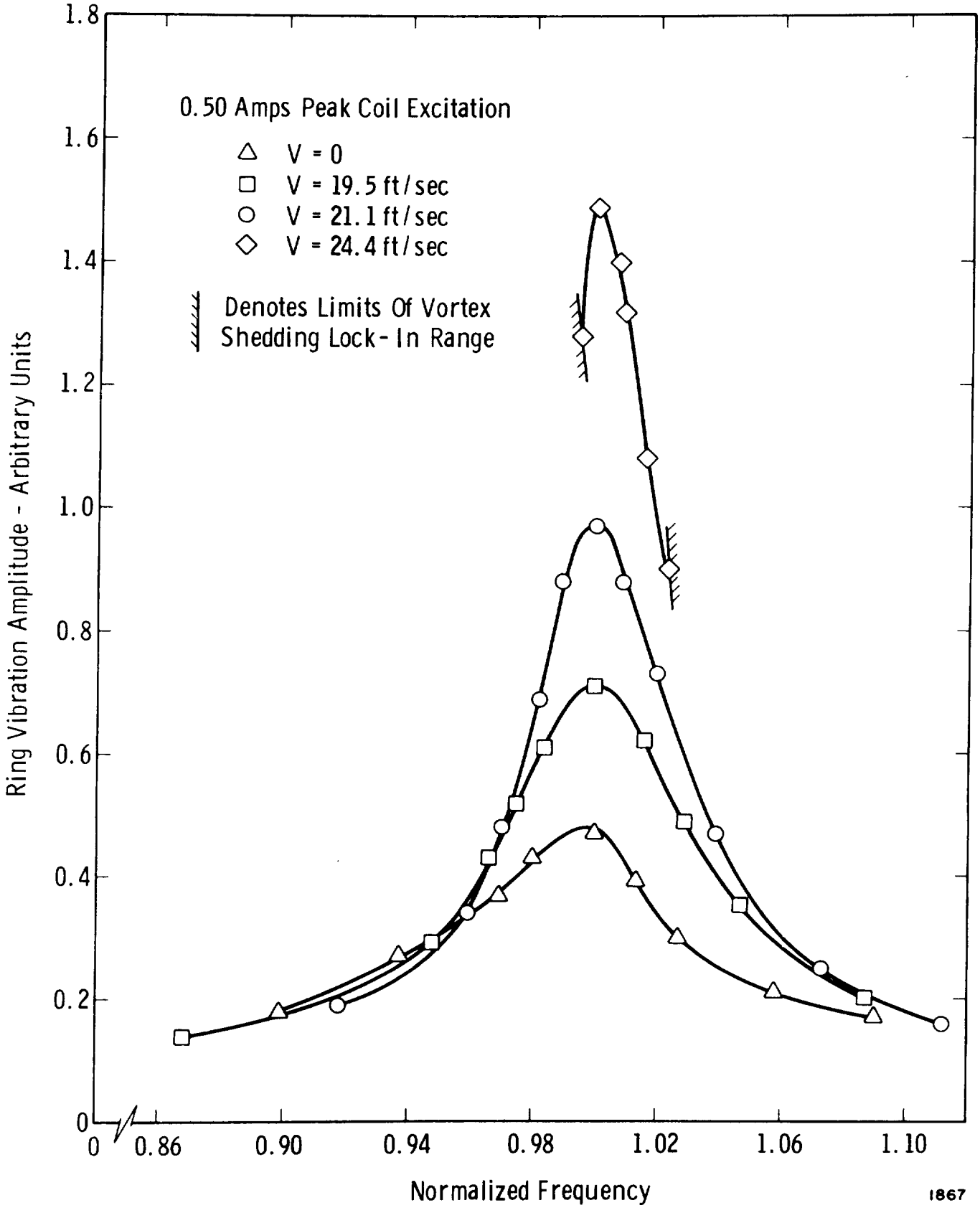

Figure 24. Typical Forced Response Data From Vibrating Ring Test Model - Constant Coil Excitation Current (0.50) - Variable Flow Velocity

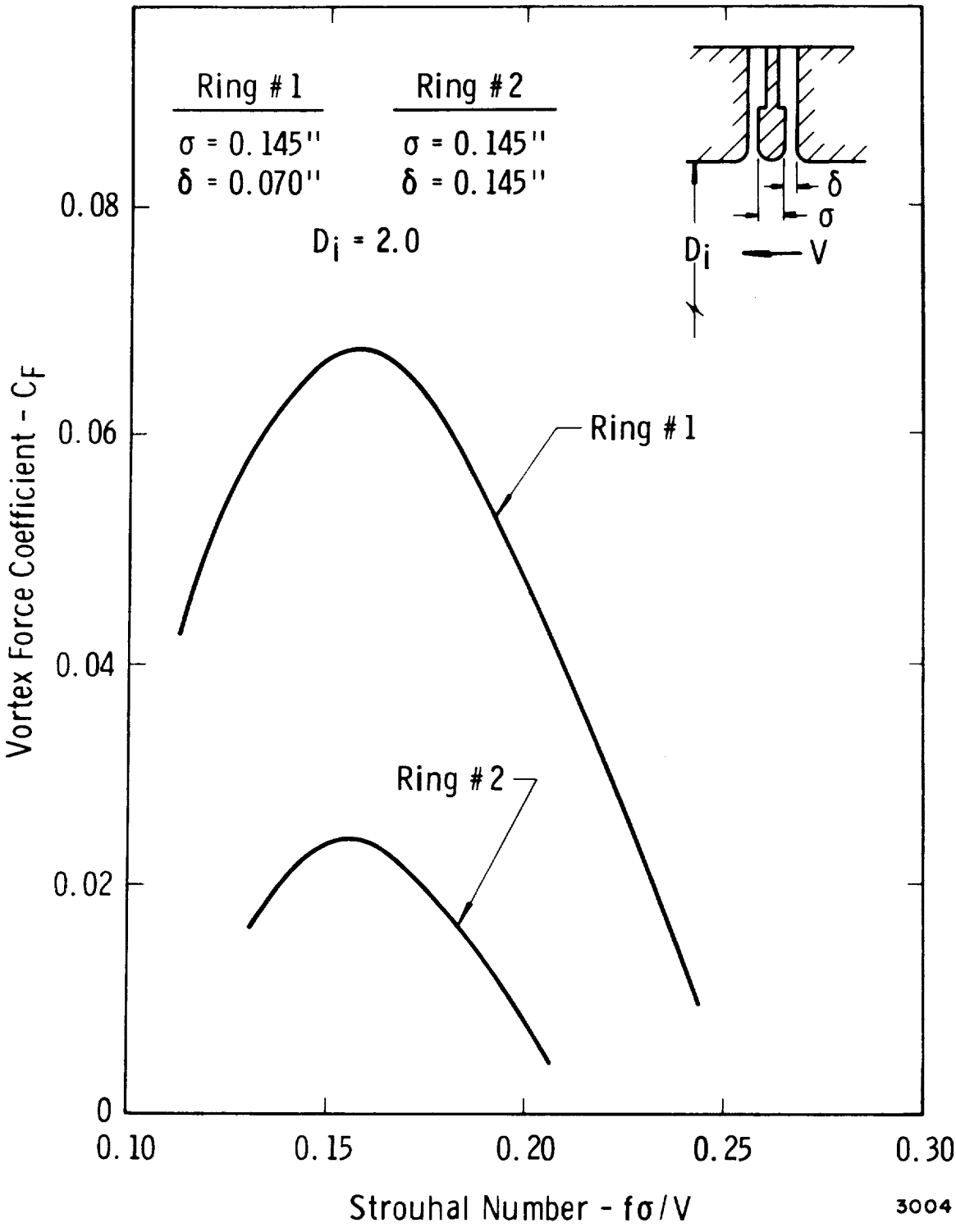

Figure 25. Vortex Shedding Force Coefficients From Tests Of Two Simulated Convolution Geometries

of real bellows. This was done by assigning one force per mass point*, as shown in Figure 26, and then calculating the forced amplitude of the mechanical model. Comparing the resultant vibration amplitudes with observed values showed the predictions to be high by a factor about equal to the number of convolutions involved in each "half wavelength" of bellows vibration. This suggested, therefore, that there was only one effective vortex force per mode number of the vibration. Further detailed comparison of calculated and observed vibrations of bellows confirmed this idea. Also, reexamination of the visualized vortex shedding activity (illustrated typically in Figure 7) and reconsideration of the pressure forces involved, showed how this must happen.

Figure 13 depicted the action of a bellows with several convolutions vibrating in the first longitudinal mode. As shown, the vortex shedding causes fluctuating pressure forces on each side of each convolution. Because of the phasing of these pressure forces, however, only one effective vortex force exists per mode number of vibration. The first mode has one effective force point, the second mode, two, etc. Each of these effective forces is exerted at the central convolution of each mode half wavelength, or at the point(s) of maximum displacement of each mode.

Using the one-force-per-half wavelength concept illustrated in Figure 13, we can now proceed with the derivation of a value for the mode factor C_m which relates displacement and force during a resonant condition. The following assumptions will be made:

(a) The shape of the longitudinal bellows modes is intermediate between a linear and a sinusoidal form. This is a very good assumption as comparison of the exact mode shapes with this approximation has shown.

(b) The maximum deflection for a given mode is equal to the static deflection times Q, the dynamic amplification factor.

(c) The maximum stress point for a given vibration mode occurs at the convolution with the maximum relative displacement; this is the end convolution for each half-wave mode shape, in general.

The first assumption noted above implies that the mode shape is of the form illustrated in Figure 27, or over the first quarter wavelength

---

* By assigning one force per mass point, where each mass point represented one-half of a convolution, it was necessary to take each force equal to one-half of the force in Equation (10).

All forces are of the form $f_n = f_0 \sin(\omega t + \Phi_n)$
where ρ depends on mode of vibration

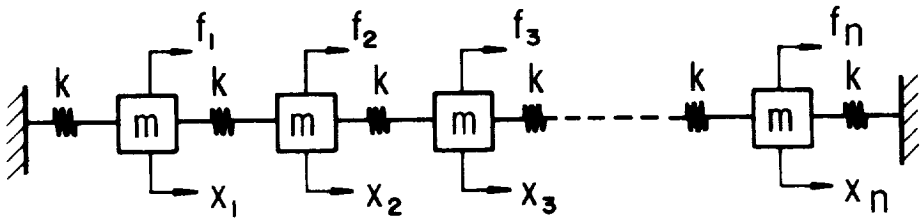

Figure 26. Mechanical Model With One Force Per Mass Point - All Forces Are Of Equal Magnitude

$$x = \frac{x_o}{2} \left[\left(\frac{N}{\ell} \right) y + \sin \left(\frac{N\pi y}{\ell} \right) \right] \tag{13}$$

where x denotes the axial absolute displacement of a given point along the bellows defined by the axial position coordinate y; N is the mode number.

The second assumption given above, when considered in light of the one-force-per-half-wavelength concept, implies that the maximum absolute displacement x_o (see Figure 27) is

$$x_o = \frac{FQ}{4Nk_A} \tag{14}$$

where F is the amplitude of the vortex shedding force applied as was illustrated in Figure 13. Again, Q is the dynamic amplification factor and K_A is the overall bellows spring rate.

From the third assumption given above, the point of maximum relative displacement x_{mr} for a given bellows, and a given mode of vibration, occurs at a point where $y = \ell/2N_c$. Therefore, from Equation (13),

$$x_{mr} = \frac{x_o}{2} \left[\frac{N}{N_c} + \sin \left(\frac{\pi}{2} \frac{N}{N_c} \right) \right] \tag{15}$$

Combining Equations (14) and (15) yields

$$x_{mr} = \frac{FQ}{8\,NK_A} \left[\frac{N}{N_c} + \sin \left(\frac{\pi}{2} \frac{N}{N_c} \right) \right] \tag{16}$$

and comparison with Equation (11) shows that the "mode factor C_m" defined in Equation (11), or

$$x = \frac{C_m FQ}{K_A} \tag{17}$$

now becomes

$$C_m = \frac{1}{8N} \left[\frac{N}{N_c} + \sin \left(\frac{\pi}{2} \frac{N}{N_c} \right) \right] \tag{18}$$

and refers to the maximum relative displacement point (maximum stress point) along the bellows.

At this stage, we are about in a position to estimate bellows flow-induced vibration amplitudes using Equations (10), (17) and (18), plus

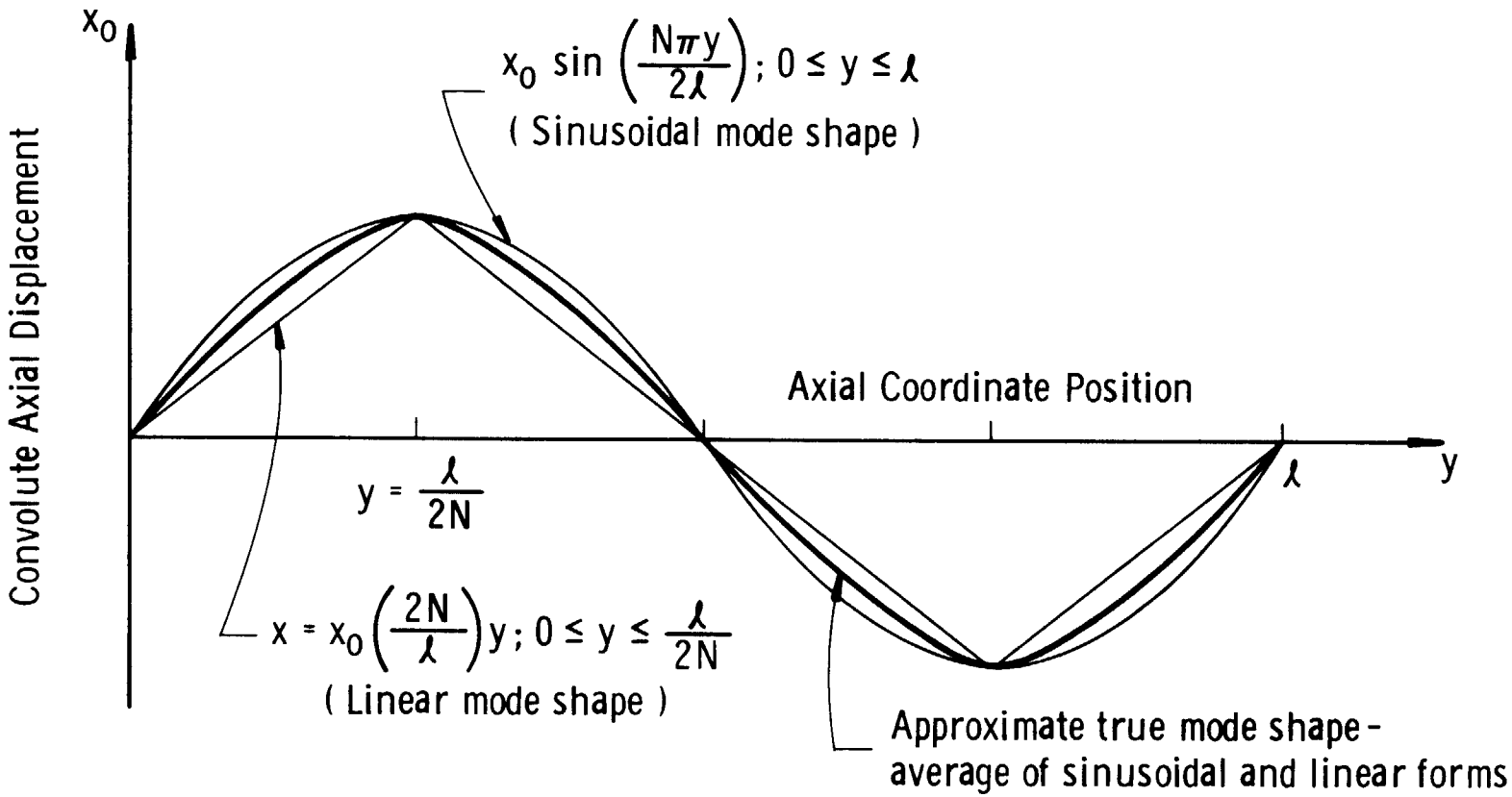

Figure 27. Illustration Of Approximate True Bellows Mode Shapes

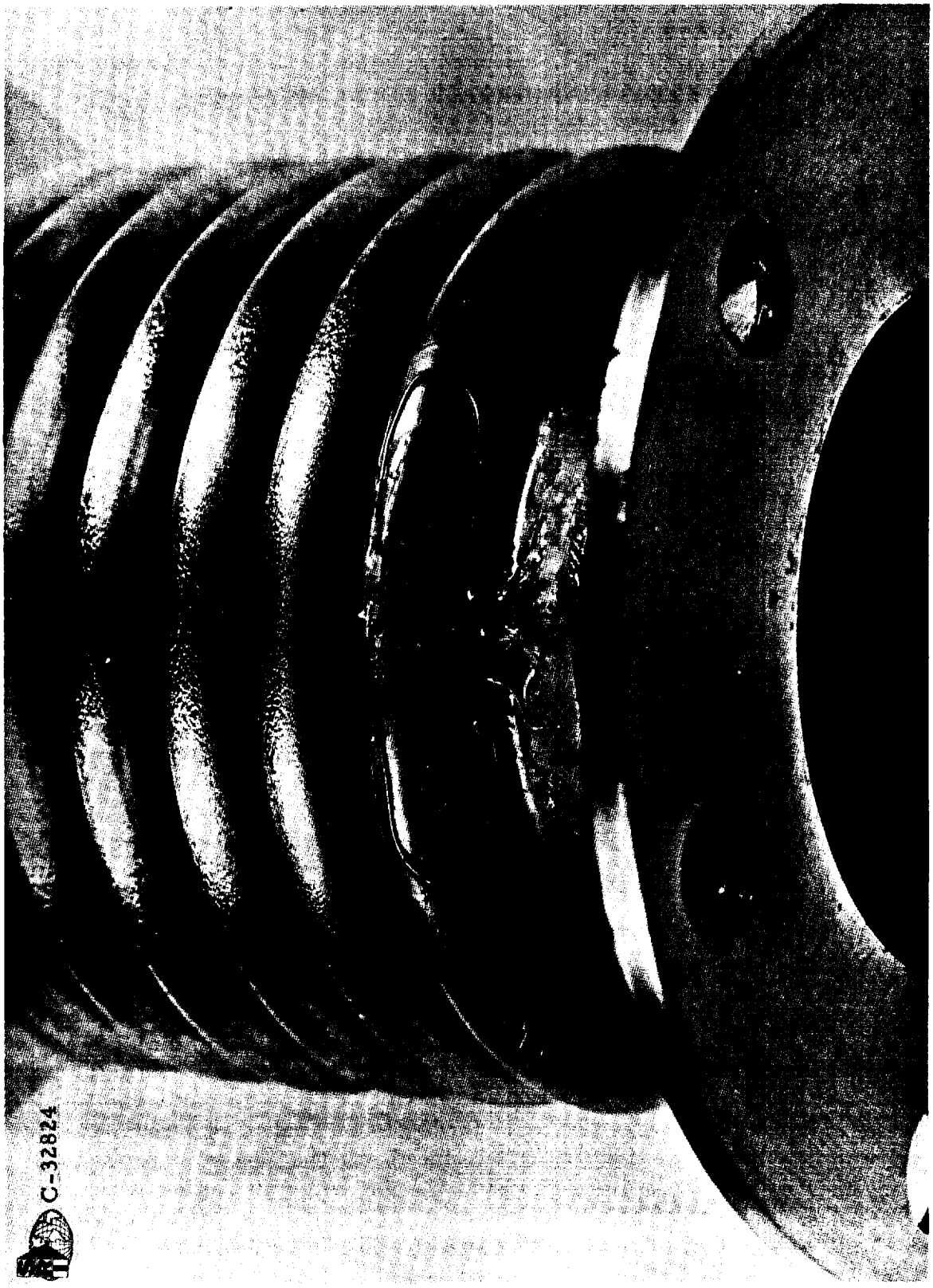

Figure 28. Typical Strain Gage Installation

the data from Figure 25. We still need, however, values of Q, the amplification factor. A comprehensive discussion of bellows damping and the resultant Q values will be delayed until a later section of this report; for the present we will assume the damping values are known.

Initial Test Data for Real Bellows

The analysis method described in the foregoing was initially used to correlate data from a number of flow-induced vibration tests of bellows in the 1.5 to 2.0 size range. These tests were conducted in the following manner:

(a) Strain gages were installed on the tips of the end convolutions of all test bellows. On all bellows, one strain gage was oriented to monitor longitudinal strain and, on a few bellows, a gage to monitor circumferential strain was also installed.

(b) Each test bellows was subjected to a static load test, during which both deflection and strain were monitored. This allowed force-deflection and force-strain curves to be plotted for each bellows.

(c) Each bellows type was subjected to a mechanical vibration test (to be discussed later) and the damping was determined.

(d) Each test bellows was installed in the water-flow system, and flow-induced stress levels were monitored as a function of flow velocity.

(e) This data was finally correlated with the analysis described earlier.

The following discussion describes these various steps, and the results, in more detail.

A typical strain gage installation on a bellows is shown in Figure 28. For most cases 1/32-inch gages were used, while some 1/64-inch gages were installed on those bellows with small width convolutions. Actual gage installation was straightforward, however, particular care was needed in lead installation to prevent fatigue. It was found that very small lead wire worked best (say about 0.005-0.010 inch) and that the best procedure was to glue the wires down along the sides of the end convolution with rubber cement. The amount of cement used was kept to a minimum to ensure that the damping of the bellows was not significantly increased.

Following strain gage installation, each bellows was tested to obtain force-deflection and strain-deflection curves. The reasons for doing this were twofold; first, it was desirable to have experimental spring rate values to allow more accurate mode frequency calculations and, second, by having a strain-deflection "calibration" along with the spring rate value, the flow-induced strain amplitudes could be directly interpreted as vortex shedding forces after suitable data reduction to account for the dynamic amplification, and mode factor. By this procedure, errors inherent in trying to analytically relate strain (or stress), and vibration amplitudes and forces, were eliminated. This allowed a more realistic judgment of the validity of the bellows flow-induced vibration analysis presented earlier in this report. Some typical force-deflection and strain-deflection data are shown in Figures 29 and 30.*

The next step in the bellows test procedure was to subject one bellows of each particular type to mechanical vibration and thereby obtain a forced response plot for various conditions (various internal media, various internal pressures, different peak strain levels, etc.). This mechanical vibration test procedure will be discussed in much more detail in a later section. The important point here is to realize that the result of these tests was a tabulation of Q values for each bellows for the various test conditions.

The final step in testing each bellows was to mount it in the water flow loop and monitor vibratory strain levels as a function of internal fluid velocity. Figures 31, 32 and 33 illustrate typical flow-induced strain data for three different bellows types with a 1.5 inch internal diameter. In Figure 31, data for three supposedly identical test bellows is given, however, variations in vibration characteristics are readily evident. The main reason for this difference in the vibration characteristics is that the force-deflection and strain-deflection calibrations of these supposedly identical bellows were quite dissimilar, also. As will be shown, however, correlation of the apparently dissimilar data in Figure 31 for "identical" bellows using the flow-induced vibration analysis discussed earlier gives very consistent results.

This correlation for all data was carried out in the following manner:

(a) The peak flow-induced strain data, as exemplified by the data in Figures 31, 32 and 33, was converted to equivalent maximum relative convolution displacement (x_{mr}) values. The equation giving this conversion is

* Appendix B gives dimensional data for all bellows used throughout the study; refer to this appendix for data on numbered bellows in all figures.

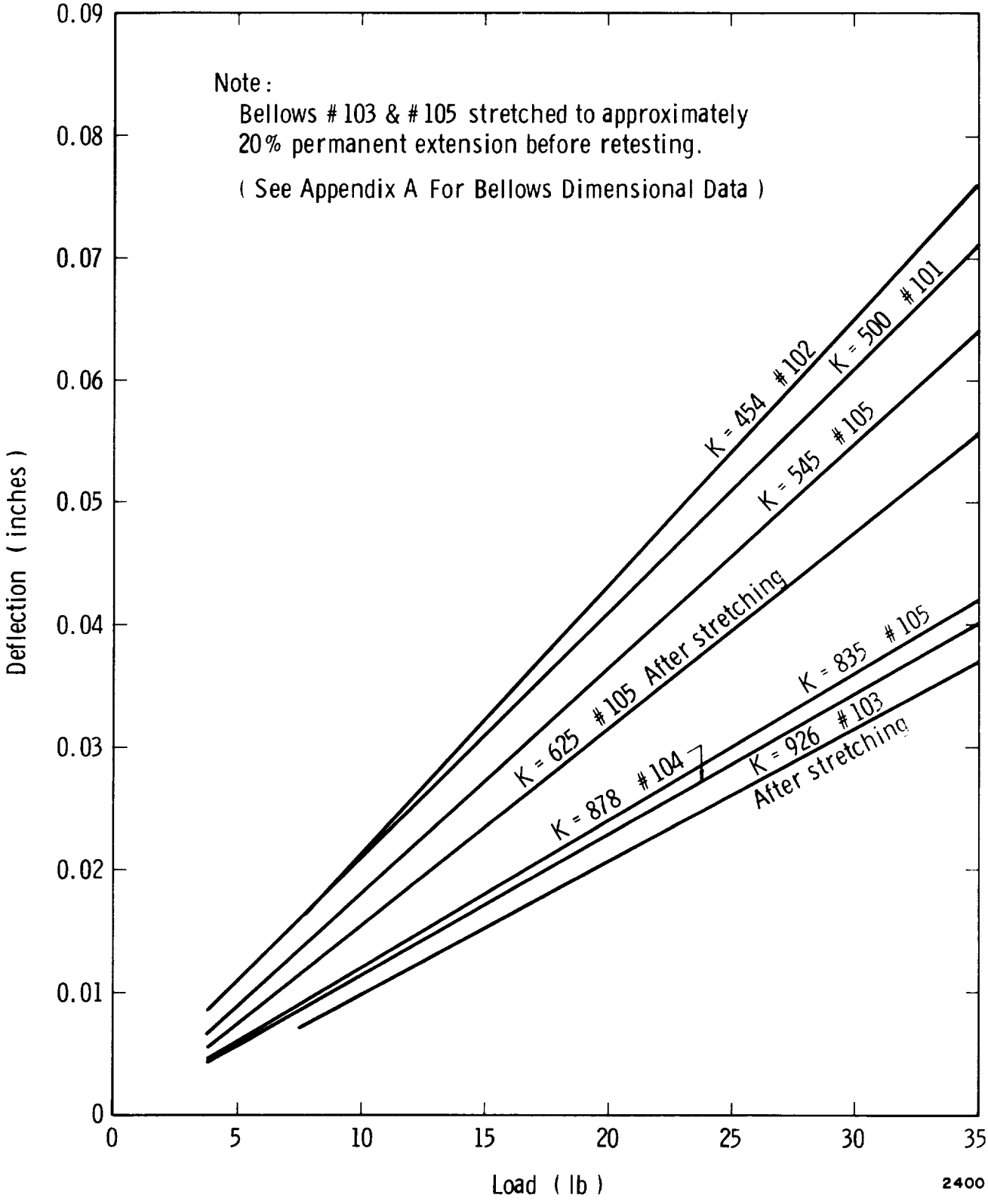

Figure 29. Typical Load - Deflection Data For Test Bellows

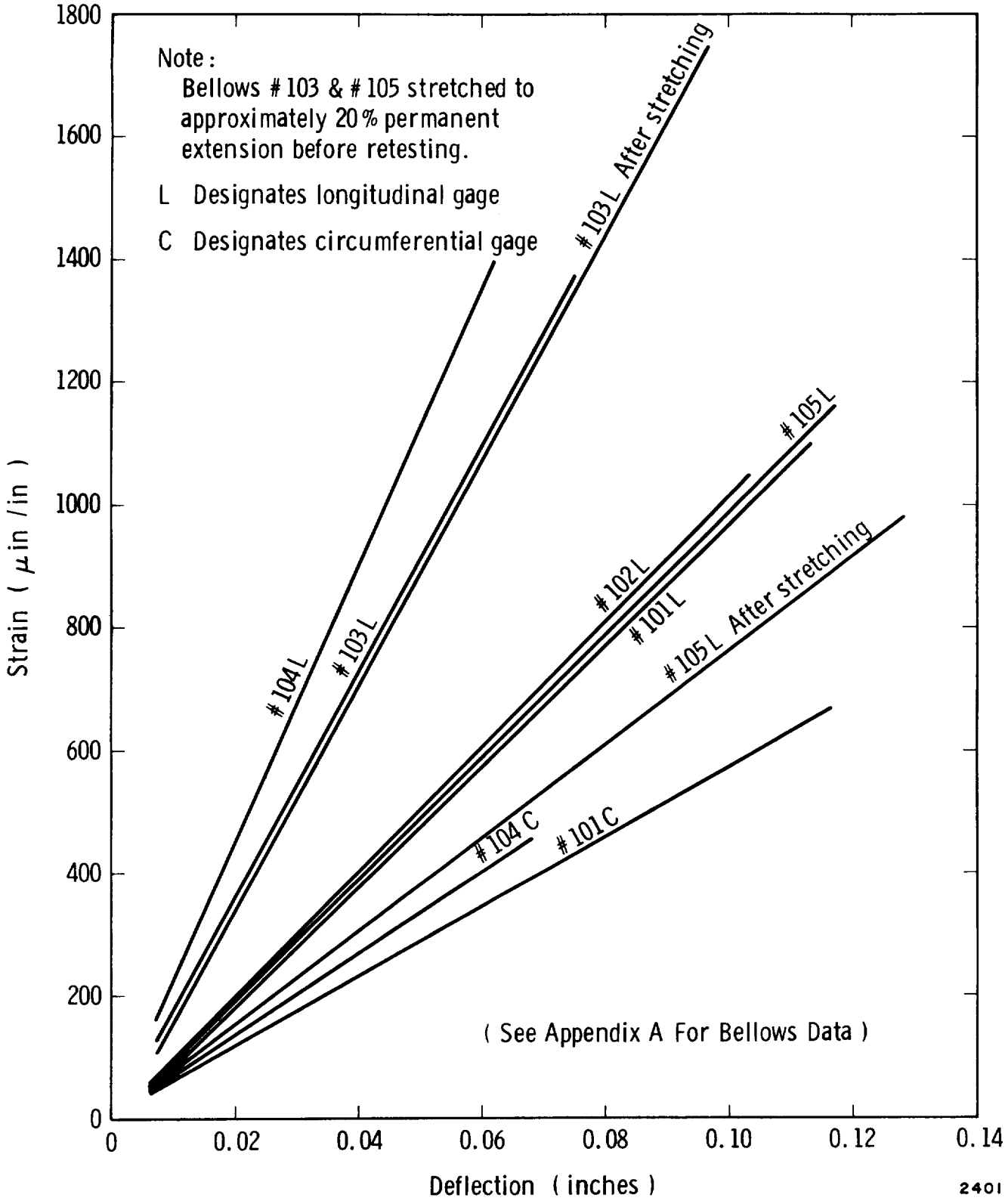

Figure 30. Typical Strain - Deflection Data For Test Bellows

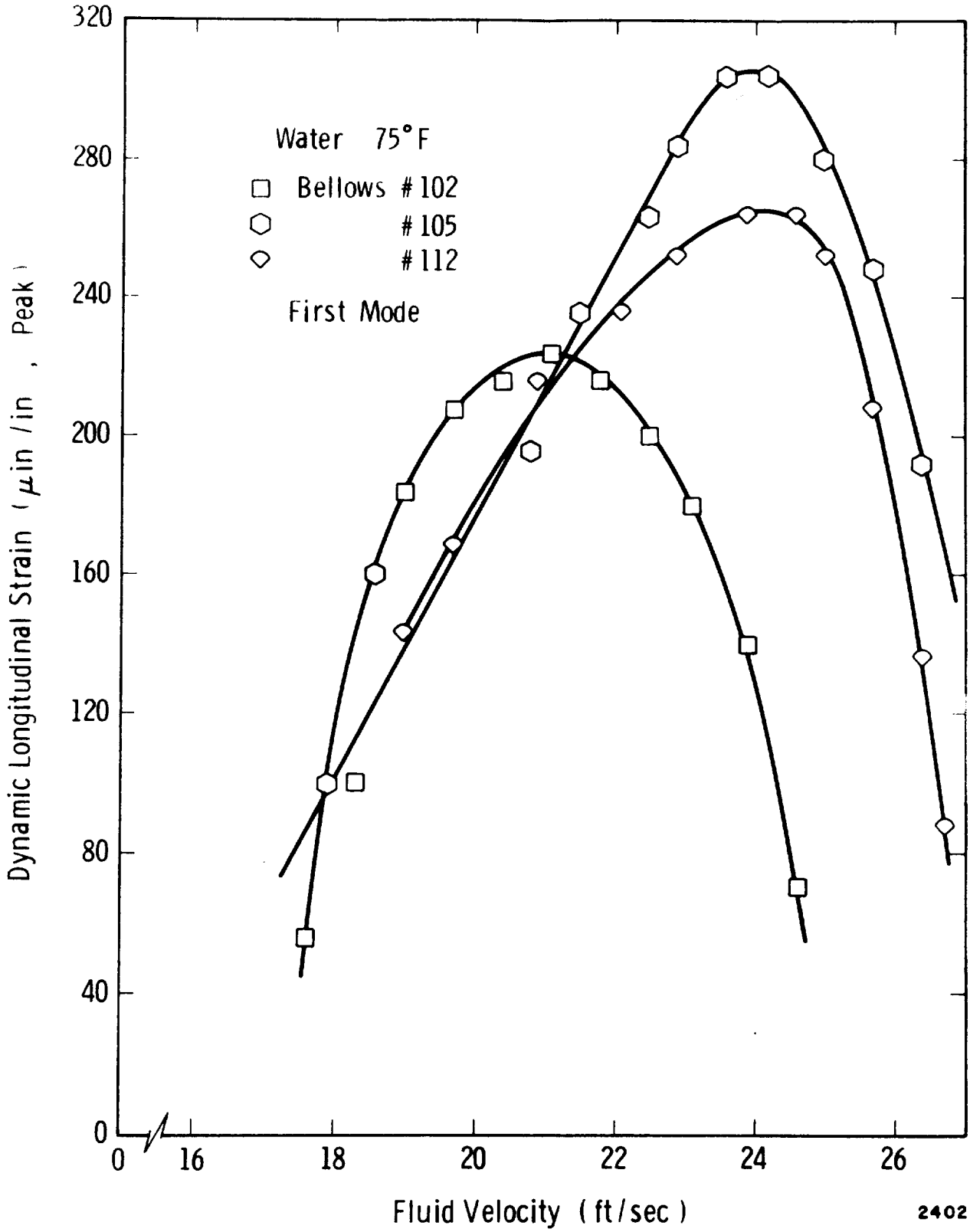

Figure 31. Peak Flow-Induced Strain For Three Supposedly Identical Test Bellows

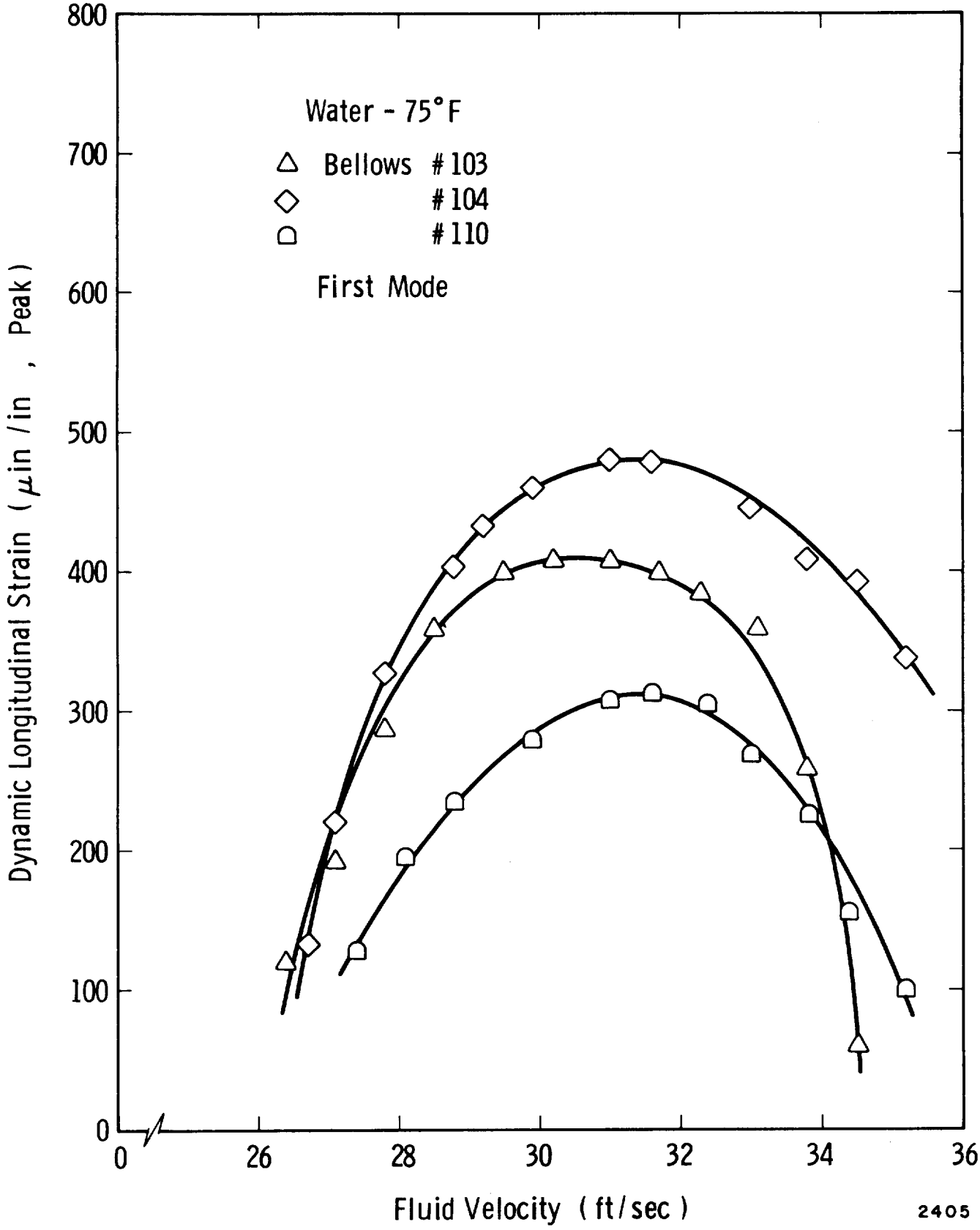

Figure 32. Peak Flow - Induced Strain Of Three Test Bellows

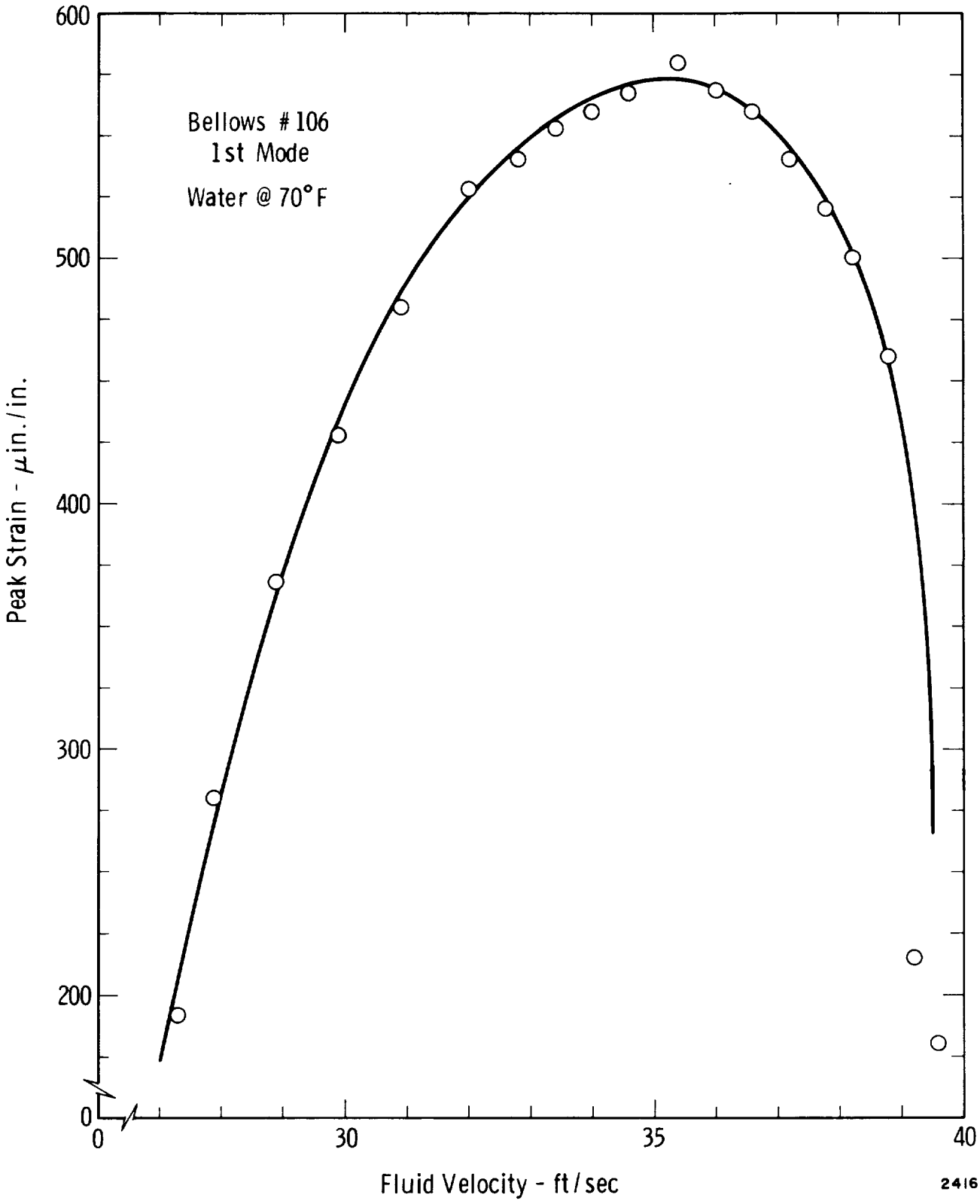

Figure 33. Peak Flow - Induced Strain As A Function Of Fluid Velocity For Bellows #106

$$x_{mr} = \frac{S}{2\,N_c}\,(dS/dx)^{-1} \qquad (19)$$

where S is the measured peak strain and dS/dx is the slope of the overall bellows strain-deflection curve (see Figure 30).

(b) Next, these maximum relative displacement values were used to calculate the quantity FQ from Equation (16), or

$$FQ = \frac{8\,NK_A\,x_{mr}}{\left[\frac{N}{N_c} + \sin\left(\frac{\pi}{2}\,\frac{N}{N_c}\right)\right]} \qquad (20)$$

Here, F is the peak vortex shedding force and Q is the dynamic amplification factor.

(c) From the results of the bellows damping study (to be discussed in a later section) the value of Q was known from the conditions of the test, therefore, the vortex force F was readily found from the results of (b) above.

(d) Finally, the value of vortex shedding force F was used to calculate an effective vortex force coefficient C_F from Equation (10), or

$$C_F = \frac{F}{(1/2\,\rho V^2)\,(A_p)} \qquad (21)$$

where

$$A_p = \pi\,(D_i h + h^2)$$

Figures 34 and 35 show the result of this data reduction process as applied to the flow-induced strain data of Figures 31 and 32. The independent variable in Figures 34 and 35 is the Strouhal number based on convolution tip width. Note how much better the data for the supposedly identical bellows is correlated when reduced to the form shown in Figure 34 than it was in Figure 31.

The flow-induced strain data from all of the initial 1.5 inch and 2.0 inch test bellows was reduced to the form shown in Figures 34 and 35. Because of differences in the convolution geometry, the peak C_F values varied somewhat from item to item. In general, the greater the ratio of

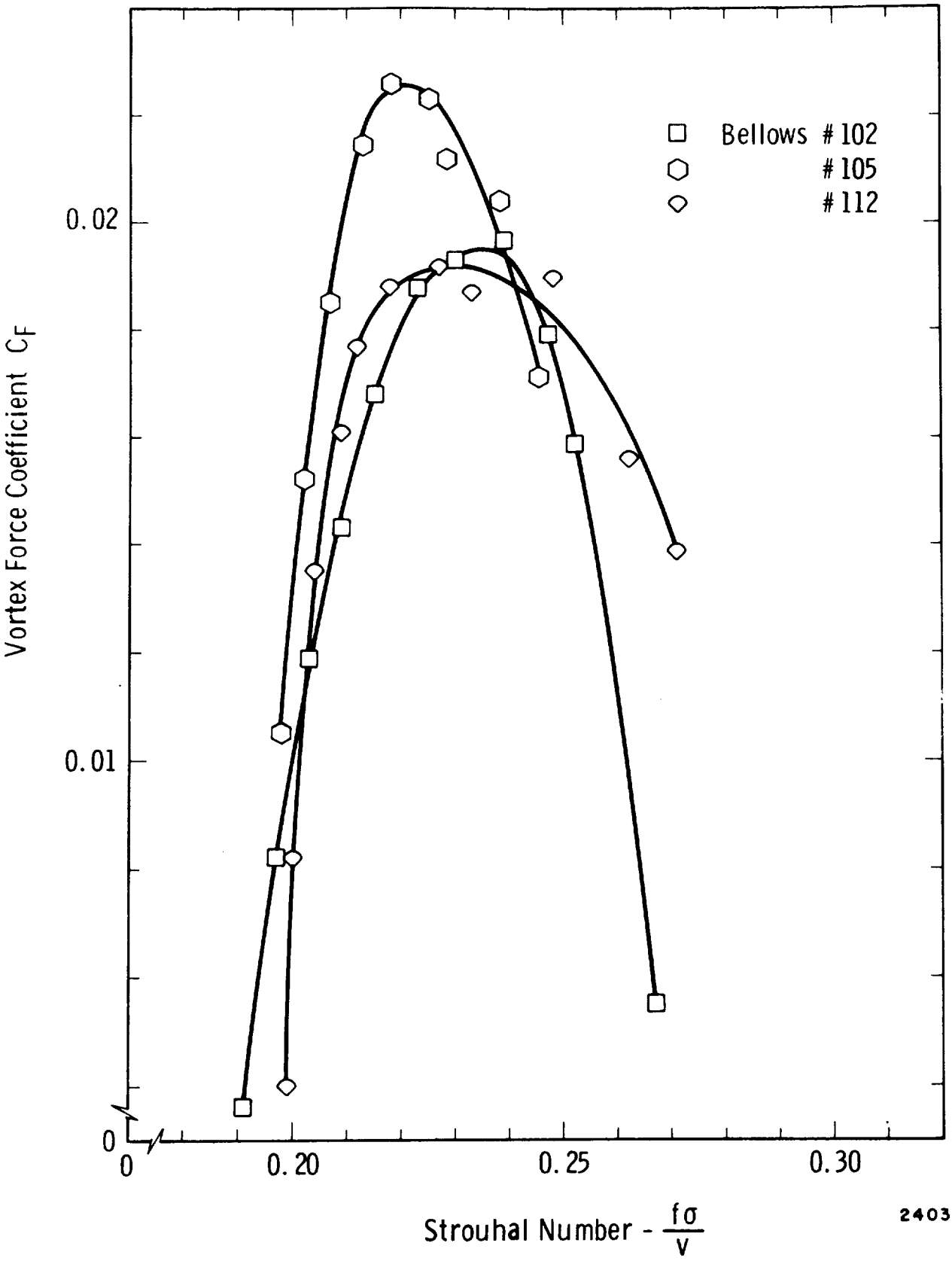

Figure 34. Force Coefficient Data Reduced From Strain Data Of Figure 29

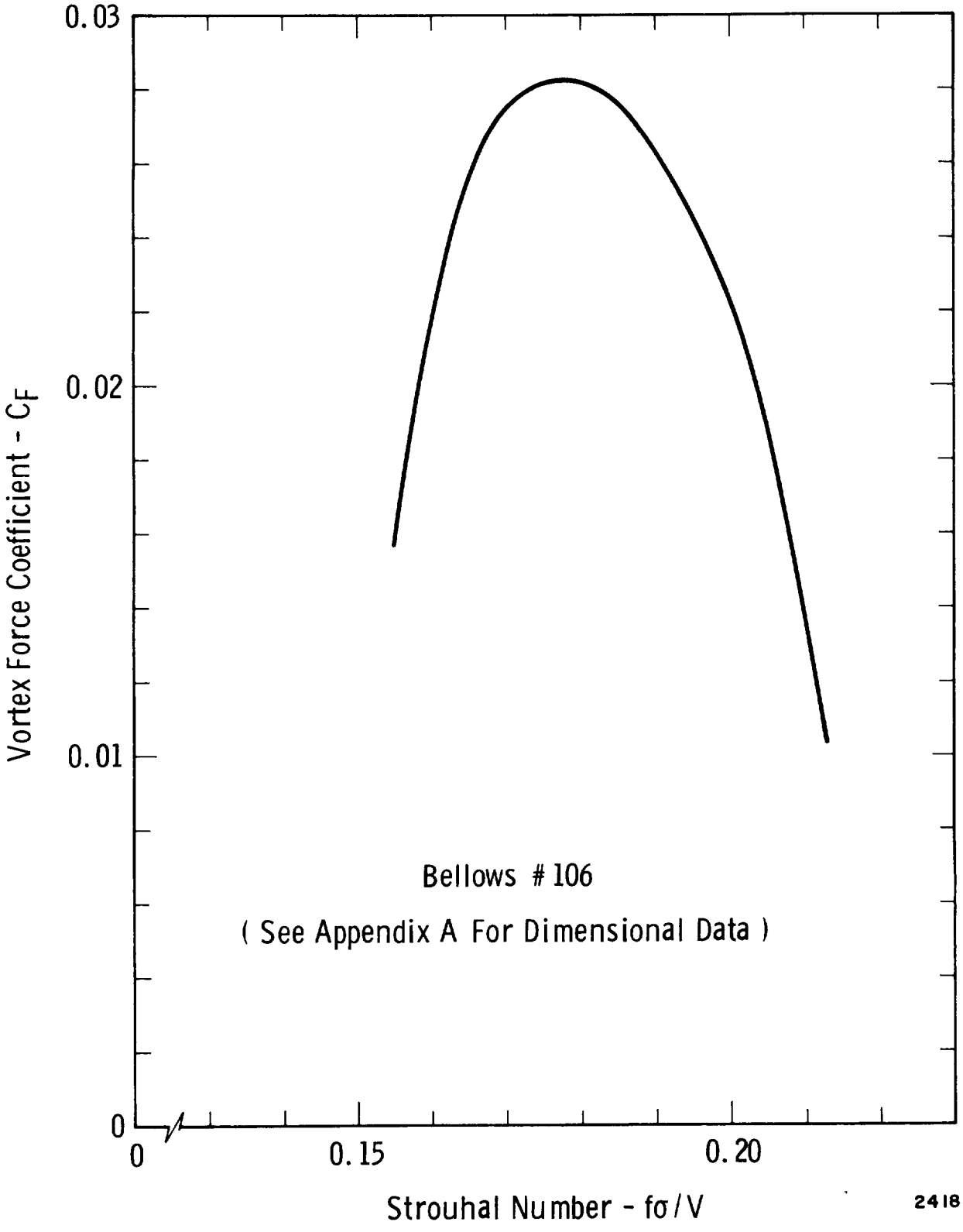

Figure 35. Vortex Force Coefficient Data For Bellows Number 106

pitch to convolution tip width (λ/σ), the smaller the peak C_F value. This trend was also seen in the results of the single convolution test model discussed earlier; see Figure 25. Unfortunately, the bellows tests discussed above did not provide the range of convolution geometry required to adequately determine C_F as a function of geometry. Therefore, a special test procedure was developed to allow a better study of geometry effect.

Initial Study of Bellows Geometry Effects

Several tests were initially performed in which the effect of bellows convolution geometry on the vortex force was determined. This was accomplished in a rather unique manner by step-wise stretching and compressing the test bellows so as to alter the convolution pitch. The advantages of this method are at least twofold; first, it allows geometry to be varied rather independent of other property variations, and second, it results in a hardware savings since more data can be obtained from a single test item.

Figure 36 shows a series of photographs of a sectioned bellows mounted in a stretching fixture and positioned in three different pitch configurations. Figure 37 gives flow-induced strain data taken from a bellows identical to the one shown in Figure 36. The data represents the observed peak flow-induced strain for each pitch setting. Figure 37 also shows this same data reduced to the vortex force coefficient form. Notice that the force coefficient generally decreases as the pitch increased; this trend is in agreement with the single convolution test model results and other bellows tests. Also, however, Figure 37 shows an obvious trend of "optimum" pitch values which produce minimum local C_F values. This trend has been observed in several bellows tests and can probably be explained by vortex reinforcement. These "optimum" pitch values can be correlated with the parameter λ/σ and are most pronounced for the first few modes of a free bellows. The higher modes of a free bellows and flex hose modes don't seem to have these "optimum" pitch values; they apparently operate in a "vortex reinforcement condition" for all λ/σ values by a natural and slight, "tuning" of the shedding frequency.

Summary of Initial Studies of Force Coefficient

In the foregoing sections, vortex shedding force coefficient data has been presented as derived from essentially three different kinds of tests. First, the results of the idealized single convolution model tests were given. These tests yielded force coefficient data for two different convolution configurations; the two configurations had the same convolute height h and the same tip width, but different pitches. Second, complete force coefficient data was obtained from tests of a number of "calibrated" bellows having various convolution geometries. Finally, a limited amount of test data was

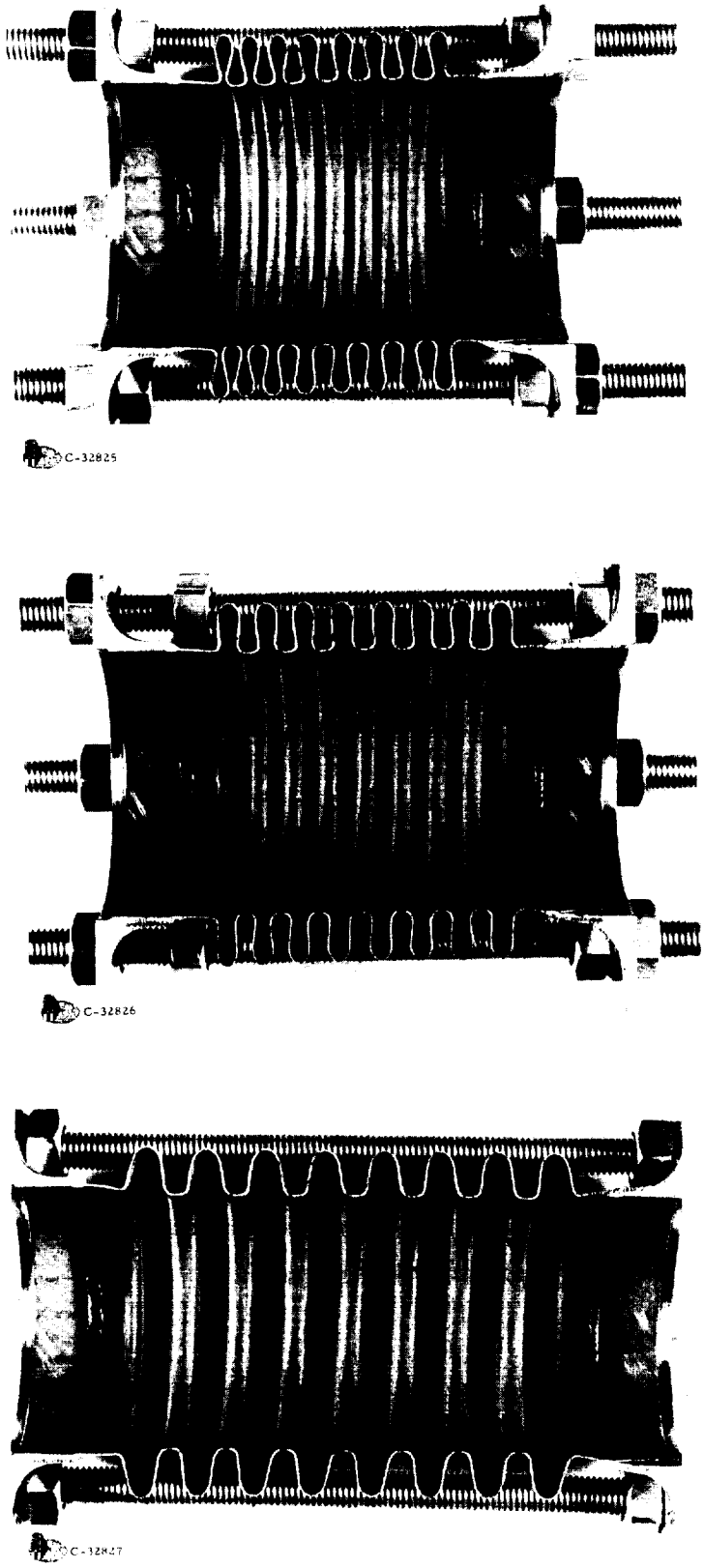

FIGURE 36. PHOTOGRAPHS OF STRETCHED AND COMPRESSED BELLOWS

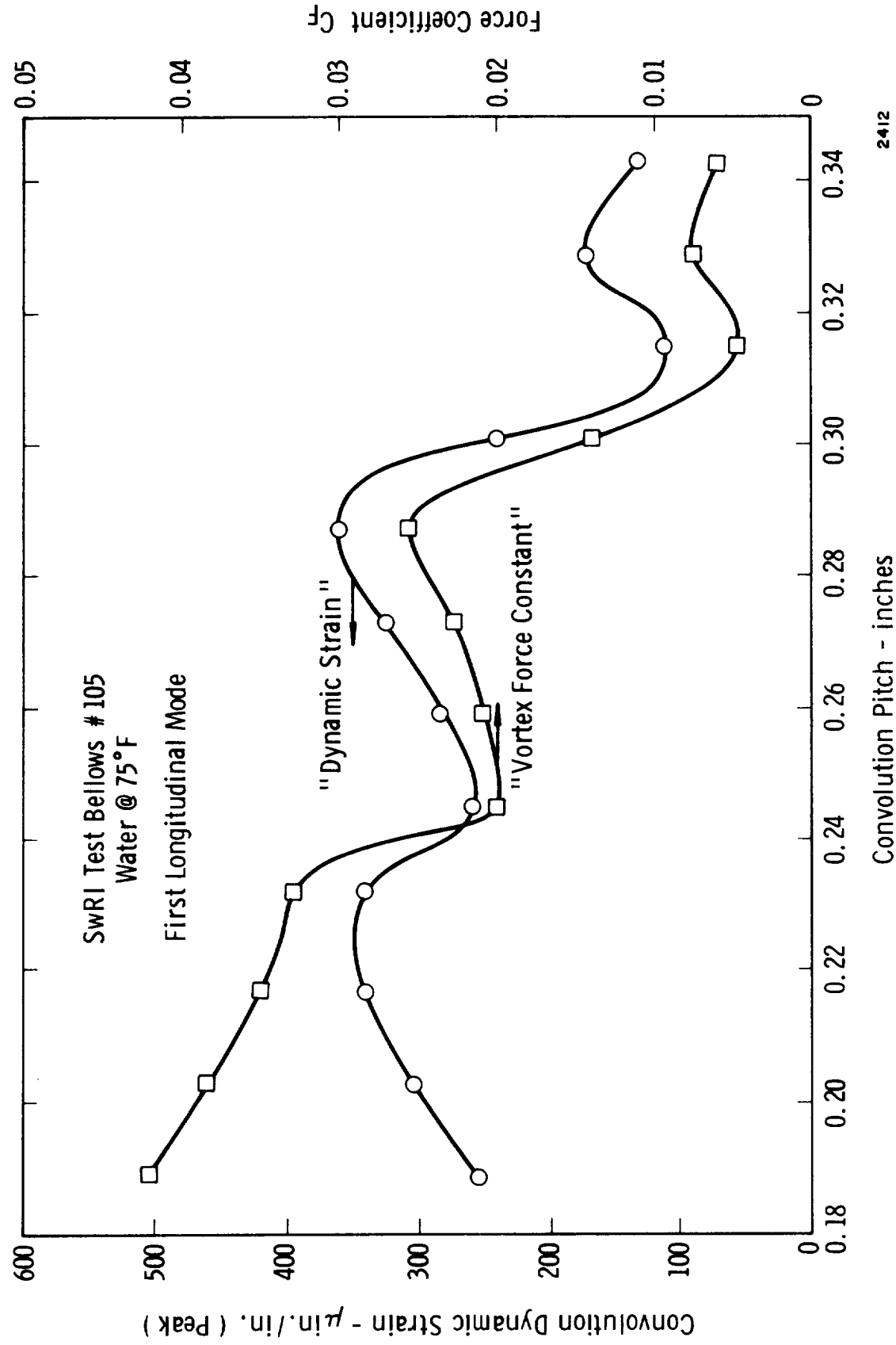

Figure 37. Response Of Test Bellows As A Function Of Pitch - Bellows Stretched To Change Pitch

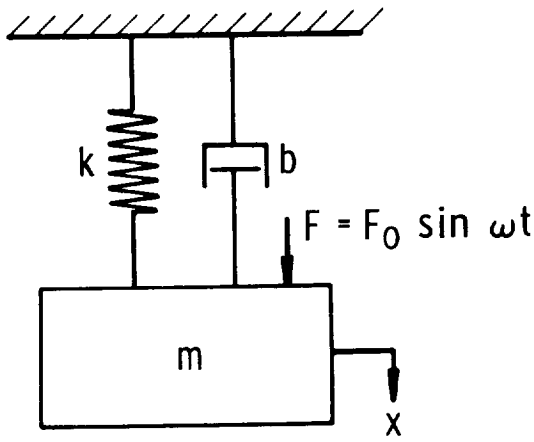

$$m\ddot{x} + b\dot{x} + kx = F_0 \sin \omega t$$

Figure 38. Linear Second-Order System

obtained by a bellows stretch-compression pitch changing scheme. Comparison of all of this force coefficient data shows consistent results which gives credence to the bellows flow-induced vibration model developed in the previous sections.

Figure 15 shows two different curves representative of all initial available force coefficient data which was obtained from the various sources. This data was originally presented in Reference 1, and does not reflect the results of bellows size scale effect, which was part of a subsequent investigation to be discussed in Section II. 5. One curve is for use with the first few modes of a free bellows, and reflects the apparent vortex reinforcement trend discussed above. The other curve is for the higher longitudinal free bellows modes, flex hose modes and the convolute local bending mode.

The data presented in Figure 15, when used with the damping model discussed in the following section, has been found valid for use with bellows of all sizes. This model has been computerized, as discussed in Appendix A, and may be conveniently employed to calculate the bellows stress indicator.

III. 4 Bellows Damping

An extremely important factor, which provides a limiting condition on the amplitude of the vibrations resulting from bellows flow excitation, is the damping of the coupled bellows-fluid system. The vortex force and mechanical model concept discussed earlier includes no damping so that, ideally, the vibration amplitudes would be infinite. Some damping is present, however, in all real structures and it serves to limit the vibration amplitudes to finite values.

By way of review, consider the elementary linear second-order system shown in Figure 38. The forced response amplitude of this system, subject to a harmonic excitation $F_o \sin \omega t$, is of the form

$$x(\omega) = \frac{F_o/k}{\left\{\left[1-\left(\frac{\omega}{\omega_o}\right)^2\right]^2 + 4\zeta^2\left(\frac{\omega}{\omega_o}\right)^2\right\}^{1/2}}$$

where

$$\omega_o = (k/m)^{1/2}, \qquad \zeta = b/2\,(km)^{-1/2}$$

At resonance (the frequency ω_r for which $x(\omega)$ is a maximum, the amplitude may be written as

$$x(\omega_r) = \frac{F_o Q}{k}$$

where

$$Q = \left\{ \left[1 - \left(\frac{\omega_r}{\omega_o} \right)^2 \right]^2 + 4\zeta^2 \left(\frac{\omega_r}{\omega_o} \right)^2 \right\}^{-1/2}$$

In terms of the values of the mechanical elements of the system in Figure 38, Q may also be written as

$$Q = \frac{1}{2\zeta} = \frac{(km)^{1/2}}{b}$$

Figure 39 illustrates a typical response curve for the system shown in Figure 38 where the amplitude of the force F_o has been held constant, and the frequency of excitation varied. As shown, the value of Q physically represents the ratio of the vibration amplitude at resonance to the vibration amplitude in the limit of zero frequency. Also, the value of Q may be expressed in the form

$$Q = \frac{f_r}{\Delta f}$$

where f_r is the system resonant frequency and Δf is the bandwidth at the halfpower point (0.707 times the resonant amplitude); see Figure 39.

Because the value of Q is so important in the prediction of bellows flow-induced vibration amplitudes, and even for proper data reduction as discussed earlier, a large number of bellows mechanical vibration tests were conducted from which Q values could be obtained. Figure 40 shows the test set-up used for the mechanical vibration tests. Each bellows was mounted in a special fixture which rigidly connected the end flanges. The reason for this was to ensure that the vibration modes excited would be the same as those observed in the flow-excitation tests.

Figures 41 and 42 show Q values obtained from the forced vibration tests. In general, the following trends are noted (see also Figure 43):

(a) The bellows damping is generally most sensitive to peak strain amplitudes, with the damping increasing as strain increases.

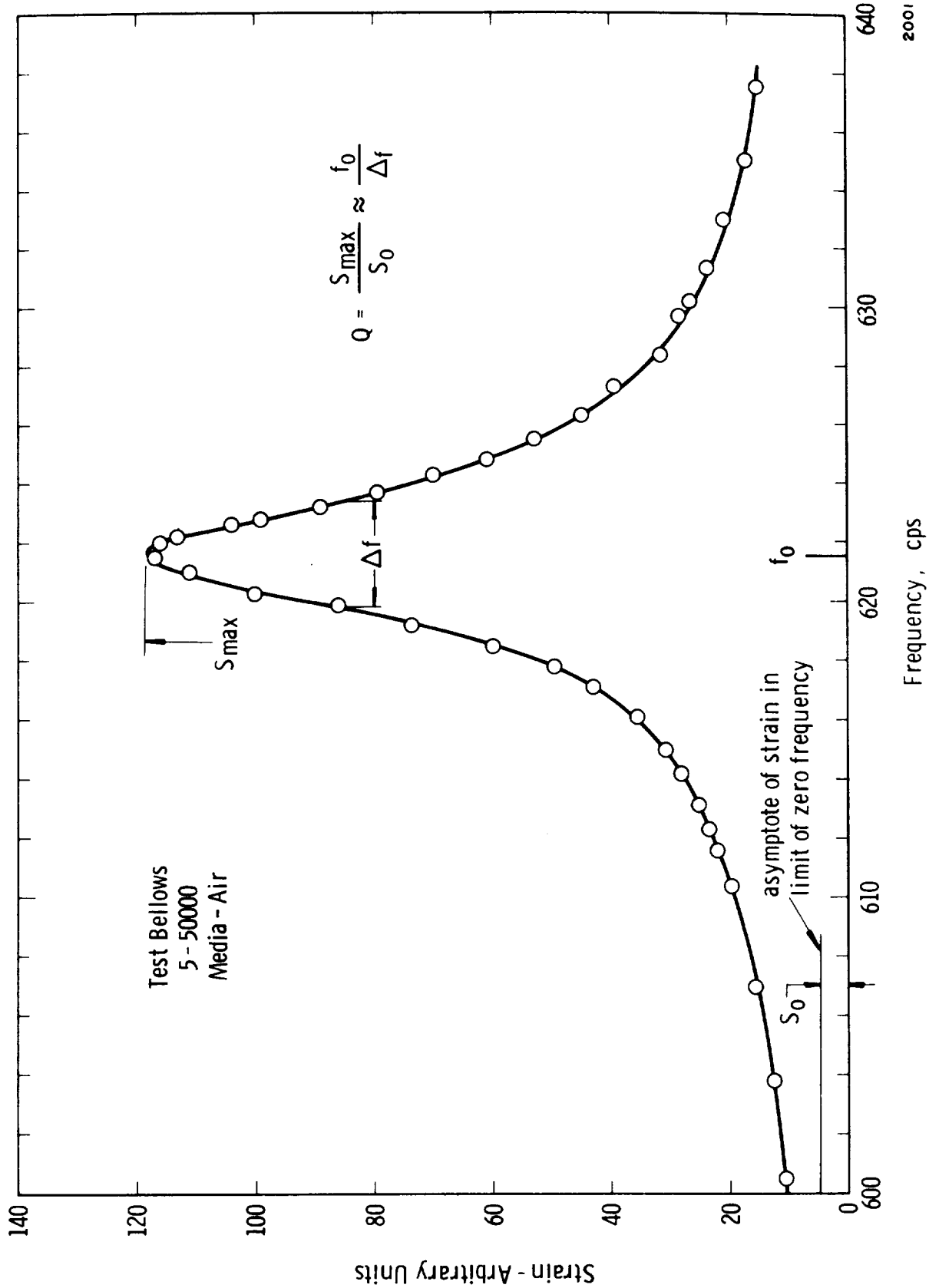

Figure 39. Example Bellows Forced Response Data For Constant Level Acceleration Input

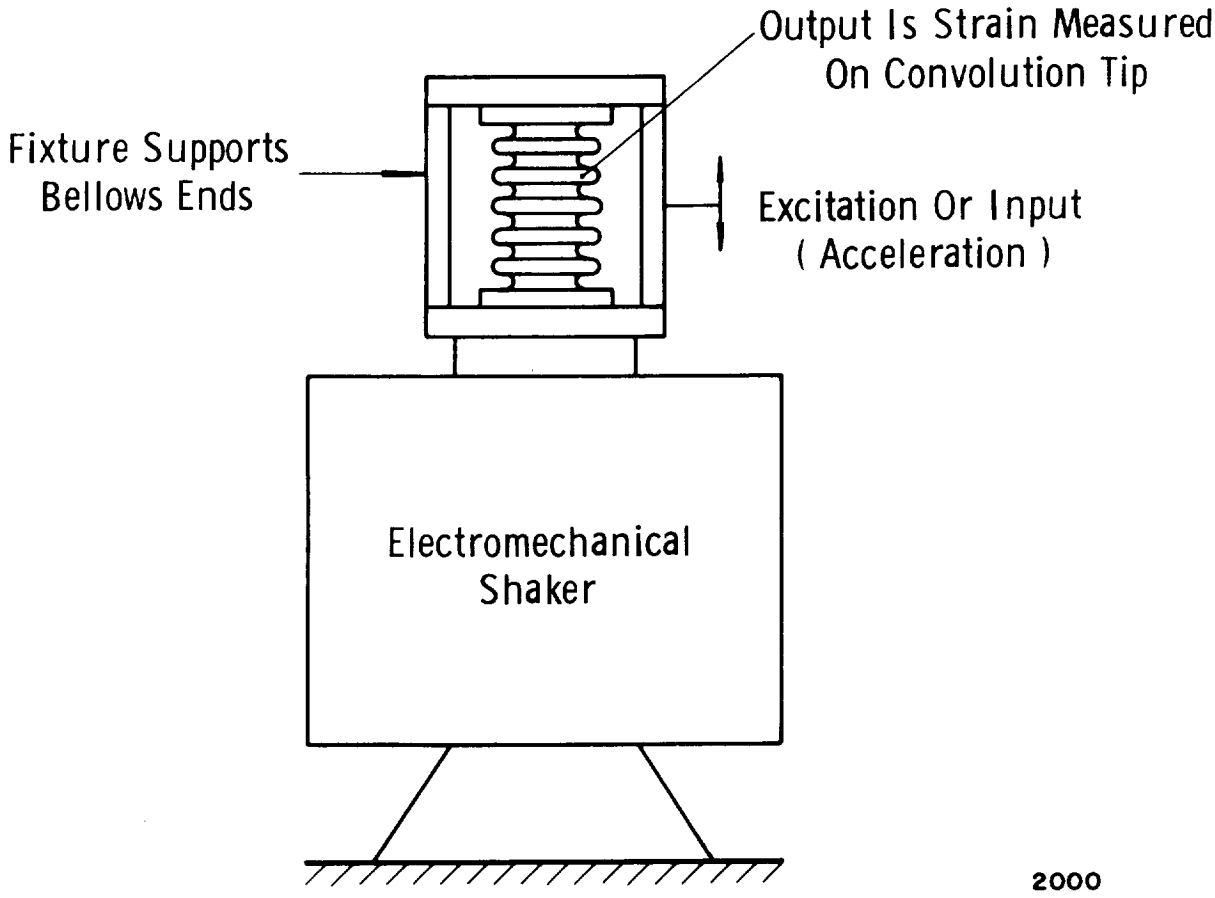

Figure 40. Schematic Of Bellows Damping Measurement Test Setup

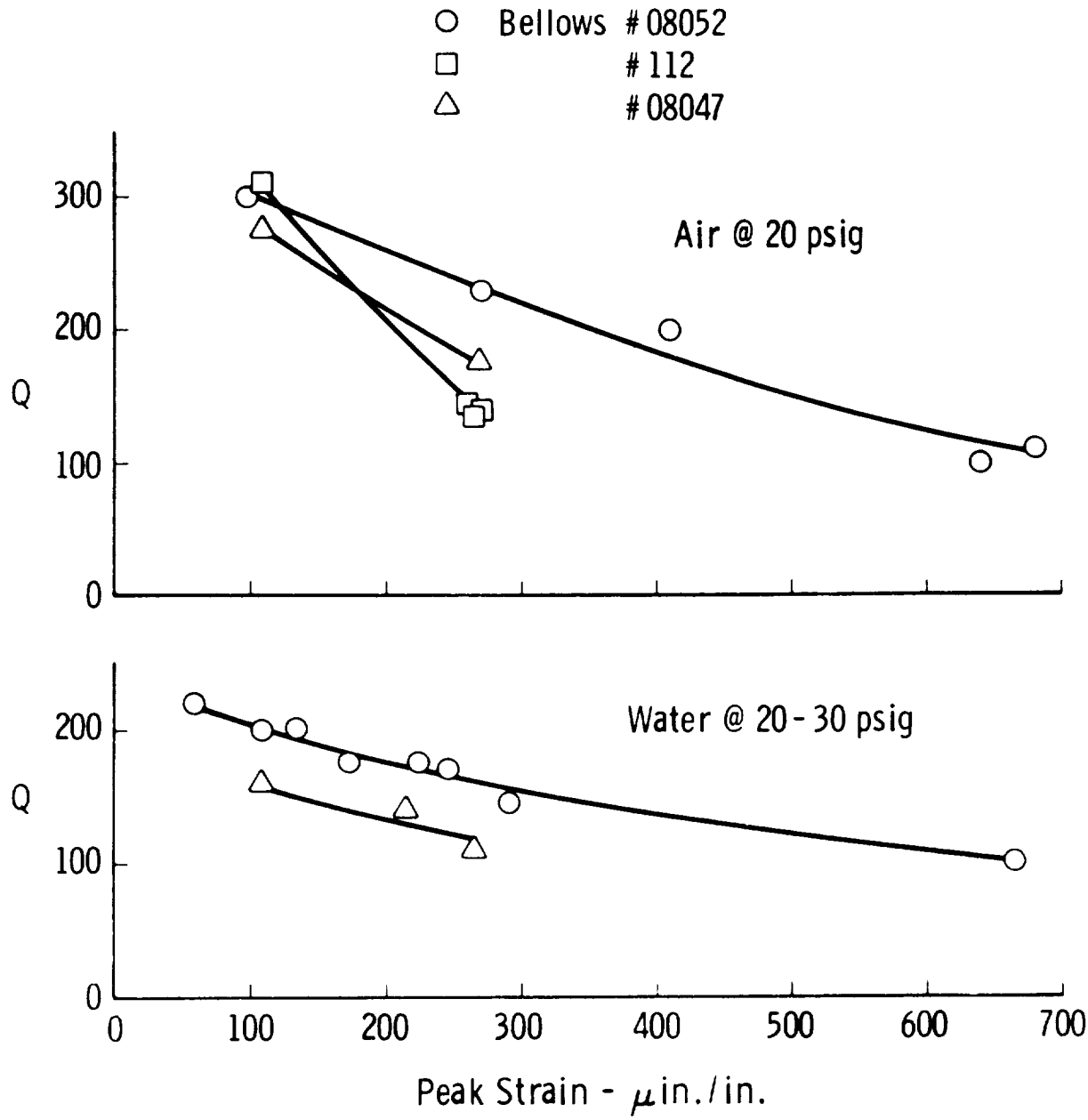

Figure 41. Q Values For Single Ply Bellows

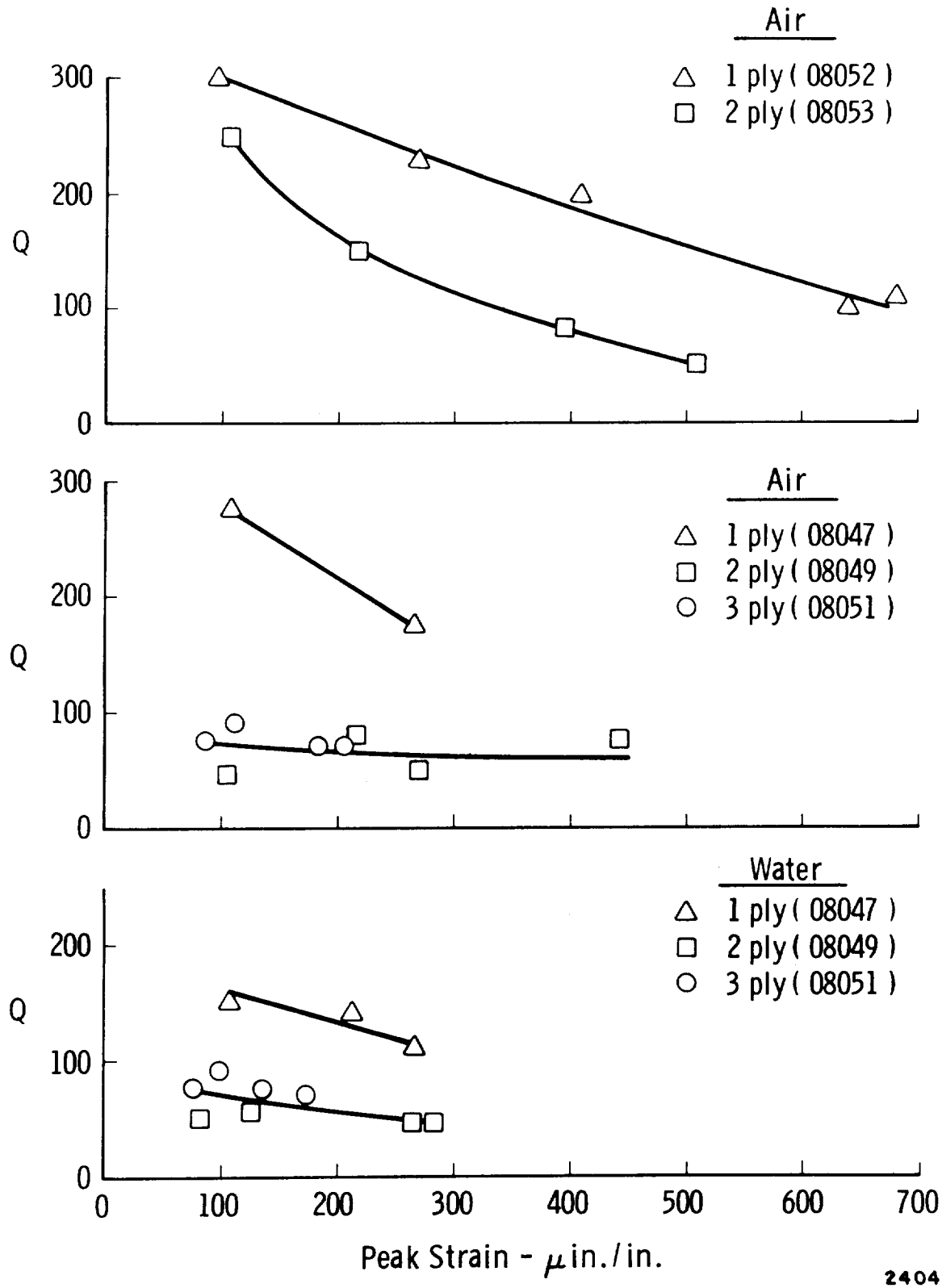

Figure 42. Q Values For Multiple-Ply Bellows

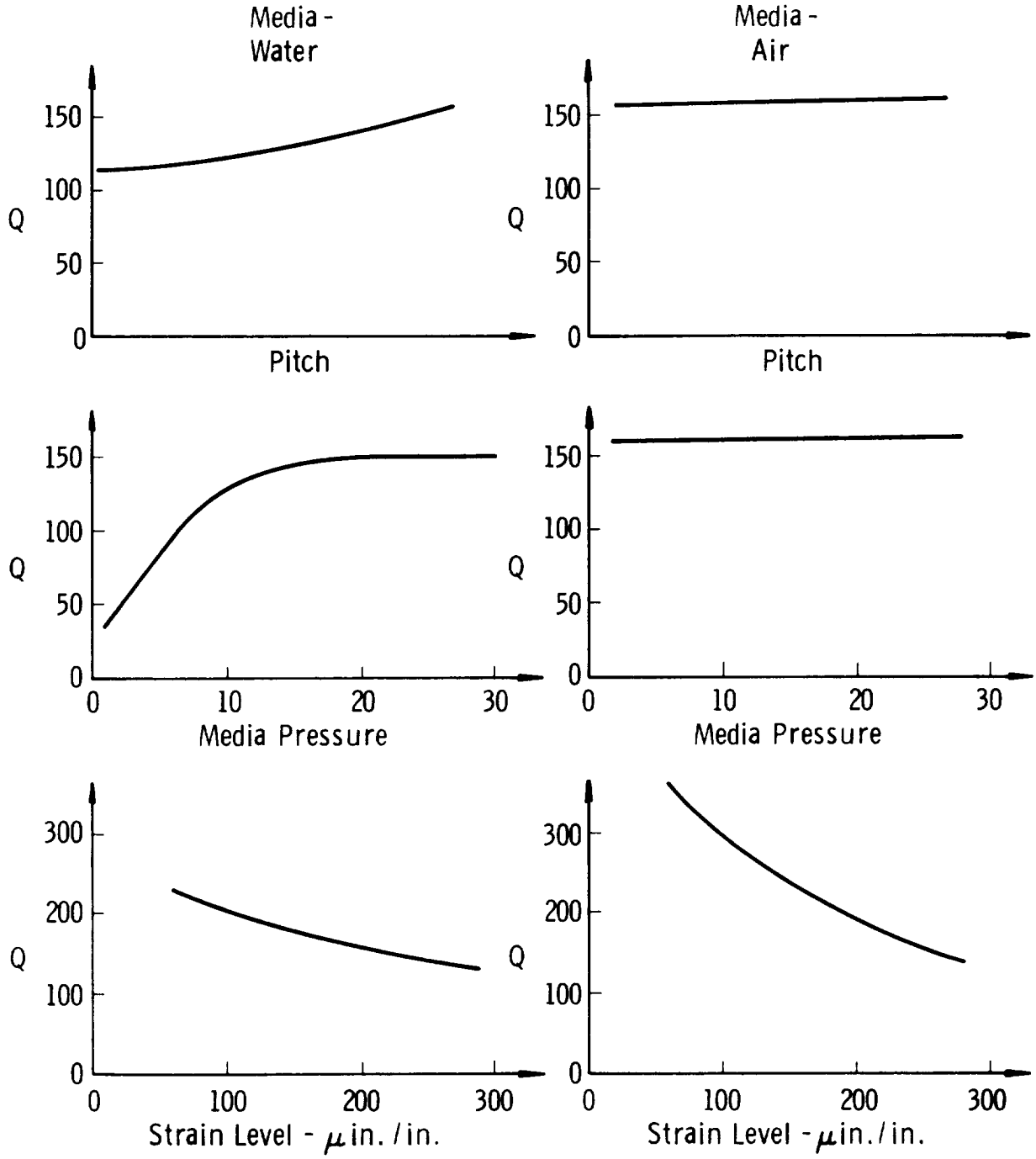

Figure 43. Trend Of Q With Various Parameters

(b) Single-ply bellows of different configurations, tested under similar conditions (same strain level, same internal media, etc.) do not necessarily have the same Q values.

(c) For one configuration of bellows, increasing the number of plies from one to two significantly increases the damping (reduces Q); however, going to three plies adds little more damping, if any, over the two-ply configuration.

(d) For bellows with a liquid as the contained media, damping may greatly increase at low absolute pressures.

The fact that damping increases as the strain level increases means that the damping is a nonlinear function of amplitude and, therefore, the linear model in Figure 37 is not necessarily valid. Valid Q values can, however, still be assigned if it is realized that they depend on strain level. The fact that the bellows damping is nonlinear is really no surprise, since structural damping is often of this nature (see Lazan's discussion of hysteretic damping in Reference 12).

The second trend noted above is that bellows with different configurations do not necessarily have the same Q values for similar test conditions. This is caused by a lack of a proper correlation model for the bellows damping. In other words, from development of an analytical model which allows prediction of damping in terms of convolution configuration, strain level, etc., then the damping data should "correlate". A better approach to the damping model, as a function of convolute geometry and operating conditions has been successfully undertaken, and is discussed in Section III. 5. The model presented here is still of validity for a "quick look" at a bellows design.

Table II and Figure 14 summarize the results of the initial damping study and give estimates of conservative Q values for various situations. The user of this data is advised to always tend toward the higher Q values where a choice must be made.

III. 5 Size Scale Effects and Refined Model

In order to determine the effect of bellows size scale and of convolute geometry on the vortex force coefficient and the damping, bellows of varying sizes were purchased and tested. Appendix B describes these test bellows which were of three different internal diameters; 3 inch, 6 inch and 14 inch. The three inch bellows consisted of fourteen different geometric types, as shown in Table VII. These bellows have been classified into four different "families" as illustrated in Table VIII. The first family, consisting of

TABLE VII. THREE INCH BELLOWS GEOMETRIC SPECIFICATIONS

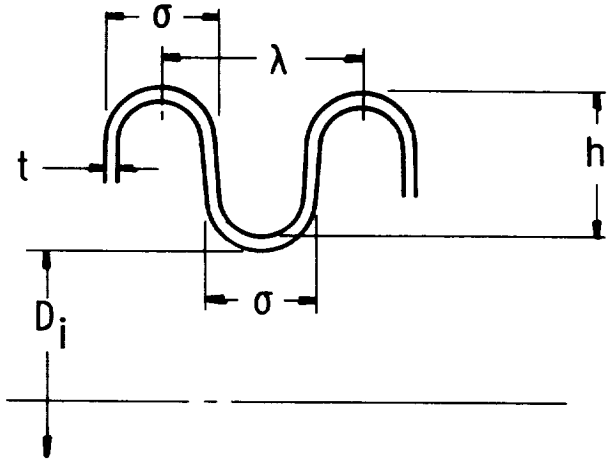

N_c = No. of Convolutions, N_p = No. of Plys, L = Live Length

Bellows: $D_i = 3.0$, $\lambda = 2\sigma - 2t$ (U-shaped). $\lambda = 2(\sigma - t)$

Specimen No.	h	t	σ	N_c	N_p
1	.2	.004	.12	13	1
2	.2	.008	.12	13	1
3	.3	.004	.12	13	1
4	.3	.006	.12	13	1
5	.3	.008	.12	13	1
6	.3	.008	.08	19	1
7	.3	.008	.20	7	1
8	.3	.010	.12	13	1
9	.3	.012	.12	13	1
10	.4	.008	.12	13	1
11	.5	.008	.12	13	1
12	.5	.010	.12	13	1
14	.3	.004	.12	13	2
15	.3	.006	.12	13	2

TABLE VIII. ILLUSTRATION OF RELATIONSHIP OF CONVOLUTE GEOMETRY FOR THE SINGLE-PLY, THREE-INCH TEST BELLOWS

t ↓ \ h →	0.2	0.3	0.4	0.5	0.6
0.004	$\sigma = 0.12$ (1)	$\sigma = 0.12$ (3)			
0.006		$\sigma = 0.12$ (4)			
0.008	$\sigma = 0.12$ (2)	(7) $\sigma = 0.20$ (5) $\sigma = 0.12$ (6) $\sigma = 0.08$	$\sigma = 0.12$ (10)	$\sigma = 0.12$ (11)	
0.010		$\sigma = 0.12$ (8)		$\sigma = 0.12$ (12)	
0.012		$\sigma = 0.12$ (9)			

bellows ①, ④, ⑩ and ⑫ have constant values of the parameter (h/t), hence, they have similar spring rate values, but differing convolute heights, h. These bellows would be expected to reveal the influence of convolute height on the force coefficient and the damping. A second family of bellows have the same h value (0.3 inches) and the same convolute tip width (J = 0.12), but varying ply thickness. These bellows were selected to show the influence of spring rate on C_F and Q. A third bellows family had constant t and σ values, but varying h values. The fourth family had the same values of h and t but differing σ values.

Each of these bellows was prepared for testing by instrumenting with convolute tip strain gages to allow monitoring of flow-induced strain. Each was next subjected to a force-strain and force-deflection test to establish actual overall spring rate, and the displacement-strain calibration. Table IX gives the overall spring rate and displacement-strain calibration for the three inch test bellows.

Following the above initial preparation, each bellows was flow tested in water at three different pitch conditions which were created by the stretch-compression technique. Each test consisted of a slow flow sweep, with the strain level monitored on an X-Y plotter displaying strain versus flow velocity. From each test strain-velocity plot, the peak flow-induced strain for each vibration mode was noted and recorded. These results are summarized in Table X.

Complimenting the above work, similar flow tests were performed on the 6 inch and 14 inch bellows. Each of these items was instrumented with a strain gage and calibrated as discussed above. The flow test results are given in Table XI.

A preliminary data reduction was performed for each set of test data presented in Tables X and XI. This data reduction scheme involved first calculating the experimental value of the product $C_F Q$ using the equation

$$C_F Q = 2 S_p \frac{dx}{dS} \frac{k_A}{A_p P_d}$$

where

S_p = observed flow-induced strain (zero-peak value)

$\frac{dx}{dS}$ = overall bellows spring rate

A_p = projected convolute height

P_d = dynamic fluid pressure $(1/2\,\rho V^2)$

TABLE IX.

THREE INCH BELLOWS MECHANICAL PROPERTY DATA

BELLOWS NUMBER	SPRING RATE Ka - lbs / in	STRAIN DEFLECTION ds/dx - min/in^2
1	67.5	7,230
2	380	11,000
3	898	2,220
4	105	9,200
5	108	6,090
6	83.1	4,620
7	262	6,730
8	252	7,500
9	343	7,600
10	47.6	3,830
11	30.8	3,250
11B	21.4	2,740
12	49.0	3,510
12B	48.4	3,100
14	32.7	3,120
15	91.5	4,330

Bellows Number	(ins)	Excitation Velocity (fps)	Excitation Frequency (HZ)	Peak Strain (μ in/in)	Static Pressure (psig)
1	.224	10.4		400	20
1	.224	20.6		820	20
1	.224	31.1		910	20
1	.232	11.6		560	20
1	.232	22.6		850	20
1	.232	34.0		1020	20
1	.232	44.0		1110	20
1	.242	12.2		520	20
1	.242	24.0		800	20
1	.242	35.0		1160	20
2	.231	23.2		1000	20
2	.231	43.0		1660	20
2	.236	22.3	430	1250	20
2	.236	40.8	830	2375	20
2	.236	56.0	1220	2500	20
2	.241	24.6		1060	20
2	.241	42.4		1600	20
3	.202	6.6		120	7.5
3	.202	8.2		300	7.5
3	.202	13.0		300	7.5
3	.237	7.0	140	75	10.0
3	.237	9.0	185	190	10.0
3	.237	12.5	235	230	10.0
3	.237	20.5		930	10.0
3	.237	24.5	800	1320	10.0
3	.237	31.0		1130	10.0
3	.237	46.0		3250	10.0
3	.241	6.8		110	11.0
3	.241	10.2		200	11.0
3	.241	13.2		300	11.0
3	.241	17.4		340	11.0
3	.241	23.0		700	11.0
4	.207	6.2		280	20
4	.207	11.2		460	20
4	.207	17.0		610	20
4	.207	27.4		550	20
4	.207	33.0		1680	20
4	.224	6.0		310	20
4	.224	12.4		560	20
4	.224	18.4		660	20
4	.224	29.2		600	20
4	.240	6.8		380	20
4	.240	14.6		710	20
4	.240	21.2		700	20
4	.240	33.2		680	20
5	.225	9.0		410	20
5	.225	18.5		780	20
5	.225	26.5		850	20
5	.236	9.4	175	580	20
5	.236	17.7	340	990	20
5	.236	26.6	500	1280	20
5	.236	34.6	640	1000	20
5	.236	50.8	875	1100	20
5	.236	56.0	990	1550	20
6	.135	9.2		180	20
6	.135	13.4		200	20
6	.135	22.0		180	20
6	.145	9.6		220	20
6	.145	14.4		280	20
6	.145	23.2		740	20
6	.154	10.0		260	20
6	.154	14.4		300	20
6	.154	20.8		300	20
6	.154	37.0		1350	20
7	.352	22.4		700	20
7	.372	25.4		880	20
7	.372	32.9		400	20
7	.392	29.0		920	20
8	.211	12.0		60	20
8	.211	17.2		340	20
8	.211	25.2		840	20
8	.211	37.4		920	20
8	.22	12.8		160	20
8	.22	18.0		380	20
8	.22	27.2		940	20
8	.22	38.2		1040	20
8	.23	13.4	250	710	20
8	.23	26.1	500	1250	20
8	.23	38.8	725	1030	20
8	.23	48.9	925	580	20

Bellows Number	(ins)	Excitation Velocity (fps)	Excitation Frequency (HZ)	Peak Strain (μ in/in)	Static Pressure (psig)
9	.208	14.0		200	20
9	.208	27.2		728	20
9	.208	39.2		840	20
9	.217	14.4		290	20
9	.217	19.4		160	20
9	.217	28.0		820	20
9	.217	40.6		1010	20
9	.228	14.8		300	20
9	.228	20.0		270	20
9	.228	28.4		790	20
9	.228	40.8		940	20
10	.212	6.5		50	20
10	.212	9.7		300	20
10	.212	14.0		320	20
10	.212	18.0		200	20
10	.212	39.0		4000	20
10	.212	44.0		7000	20
10	.221	6.8		70	20
10	.221	9.8		340	20
10	.221	14.8		380	20
10	.237	5.0	100	240	20
10	.237	9.5	190	190	20
10	.237	15.0	265	430	20
10	.237	33.0		2500	20
10	.237	37.5		3500	20
10	.237	50.0		5000	20
10	.246	6.0		180	20
10	.246	10.6		410	20
10	.246	15.8		405	20
11	.205	6.2		180	20
11	.205	8.4		240	20
11	.224	3.8		20	20
11	.224	6.4		210	20
11	.224	8.7		265	20
11	.224	14.4		360	20
11	.224	30.0		8000	20
11	.244	3.9		90	20
11	.244	6.4		250	20
11	.244	9.0		330	20
12	.200	6.4		130	20
12	.200	9.0		160	20
12	.200	11.8		170	20
12	.220	7.0		180	20
12	.220	9.8		200	20
12	.239	2.5		65	20
12	.239	7.4		235	20
12	.239	10.8		280	20
12	.239	13.6		275	20
12	.239	38.0		7200	20
14	.208	3.5		35	20
14	.208	9.2		200	20
14	.208	13.5		250	20
14	.221	5.0	80	70	20
14	.221	10.0	175	350	20
14	.221	14.6	260	450	20
14	.221	20.0	330	565	20
14	.221	24.0	400	465	20
14	.221	28.0	455	325	20
14	.225	5.0	100	50	20
14	.225	10.0	180	220	20
14	.225	15.8	270	300	20
14	.225	20.5	345	425	20
14	.225	26.0	415	425	20
14	.225	32.0	485	300	20
15	.203	907.0	140	25	20
15	.203	13.2	270	220	20
15	.203	20.0	390	350	20
15	.203	26.0	500	200	20
15	.203	40.0	690	1150	20
15	.221	7.5	160	75	20
15	.221	14.5	290	400	20
15	.221	22.0	400	500	20
15	.221	29.0	525	375	20
15	.221	44.0	740	1100	20
15	.238	8.5	175	140	20
15	.238	16.6	300	525	20
15	.238	25.0	435	650	20
15	.238	33.0	545	475	20
15	.238	47.0	790	1175	20

TABLE X. Experimental Data--3" Diameter Test Bellows With Internal H_2O Flow

Bellows #	Velocity (fps)	$\frac{dx}{ds}\left(\frac{\text{in}}{\mu\text{-in/in}}\right)$	S_{peak} (μ in/in)	k_A (# l in)	$\frac{1}{2}\rho V^2$ (psi)	$C_f Q$
1D	35	.000168	1100	165	8.25	1.25
2D	29	---	775	159	5.65	---
3D	35	.000195	1050	156	8.25	1.31
1E	33	.0002	1050	154	7.32	1.50
1F	33	.000189	800	175	7.32	1.23
1G	52.5	---	1100	595	18.5	---
2G	52.5	---	1050	538	18.5	---
3G	43	---	825	555	12.4	---
4G	50	.000173	1000	555	16.8	1.25
5G	43.5	---	850	555	12.7	---
1H	45	---	1000	485	13.6	---
2H	45.5	---	850	572	13.9	---
3H	45	.00039	1000	523	13.6	1.09
5H	45	---	1000	500	13.6	---

TABLE XI. FLOW TEST DATA FOR 6-INCH AND 14-INCH BELLOWS

The resultant experimental values of $C_F Q$ are given in Tables X and XI.

Part of the original data reduction process consisted of utilizing the original Q model given in Figure 14 to then reduce the data to a final experimental C_F for each test bellows. The results of this initial data reduction scheme were disappointing since the C_F values thus obtained showed poor agreement with the initial model presented in Reference 1, and in Figure 15. The problem with this initial data reduction reduced to one of an improper damping model as reflected in Figure 14.

A closer examination of the above difficulty led to the following conclusions:

(1) The vortex force coefficient model presented in Figure 15 is generally valid but some bellows do not display as great an increase in C_F for $\lambda/\sigma = 2.2$ as indicated in that figure.

(2) The bellows damping increases as the space between convolutes is decreased, hence the Q value is reduced as λ/σ is reduced.

(3) The bellows damping is more strongly a function of bellows spring rate than is reflected in the original damping model given in Figure 14 and Table II.

(4) The bellows damping is a function of mode number, reflecting the effect of frequency.

Based on the above, a new model of the damping, or Q value, was clearly necessary. Various correlations of the data were investigated, based on simple models of the bellows damping, until a valid model was found. In the final form it has been found convenient to not separate the quantity $C_F Q$ into the two individual components, but rather to have a single model for the product quantity.

The final model is based on a nondimensional equation relating convolute displacement to geometric, flow and dynamic parameters, or

$$\frac{x}{\sigma} = \frac{C_F Q A_p (1/2 \rho V^2)}{D_m N_p \sigma N (SSR)} \left(\frac{h}{\delta}\right)$$

The model equation above has been used as a basis for correlating the product

$C_F Q$ with known geometric or flow parameters. In this correlation, $C_F Q$ has been plotted versus the quantity

$$\frac{(\frac{1}{2} \rho V^2) \ A_p}{N K_A N_c \sigma} \ (\frac{h}{\delta})$$

The final correlation was shown in Figure 18, and is seen to depend on the mode number relation to the number of convolutes.

This model, giving the product of $C_F Q$, is more accurate than the previous model which gives C_F and Q separately. The new model is somewhat more difficult to use, however. The old model gives the most conservative values of Stress Indicator (highest values) for a given bellows. Therefore, it may indicate a borderline failure situation which the improved $C_F Q$ model will show to be safe. The user is warned to perform flow verification of those bellows which are predicted to be borderline cases.

III. 6 Fatigue Studies

The Stress Indicator versus cycles-to-failure correlation discussed in Section II. 5 was initially developed in the early part of 1969. The original correlation was based on limited test results, but showed promise of being a simple and direct approach to bellows design for prevention of flow excitation failures. To validate this approach for a typical range of bellows flow conditions and geometries, a large number of specimens were studied and flow tested to failure. Table XII gives the dimensional data on the bellows which were "fatigue" tested.

Bellows of the three different inside diameters and convolute geometries indicated in Table XII were instrumented, bench tested, and flow tested. Flow tests included determination of response as well as fatigue life.

Instrumentation and Bench Tests

Strain gages were mounted on each bellows to measure strain on the outside surface of a convolute crown in the axial direction. The gages were standard, constantan, foil type construction. Grid sizes were 1/32" or 1/16" depending on the bellows size. No attempt was made to temperature compensate the gages since the strain to be measured was dynamic or short term static in nature. The gages were bonded with Eastman 910 or epoxy and coated with a commercial strain gage sealer after the lead wires had been soldered in place. The photographs in Figure 44 show a typical gage installation.

Bellows Number	Di (inches)	h (inches)	t (inches)	σ (inches)	λ/σ	Nc	NP
SwRI-A	3.0	0.2	0.008	0.12	1.57	13	1
SwRI-B	3.0	0.3	0.008	0.12	1.89	13	1
SwRI-C	3.0	0.3	0.010	0.12	1.92	13	1
SwRI-D	6.0	0.3	0.008	0.12	1.87	13	1
SwRI-E	6.0	0.3	0.008	0.12	1.87	14	1
SwRI-F	6.0	0.3	0.008	0.12	1.87	12	1
SwRI-G	6.0	0.45	0.016	0.16	1.81	13	1
SwRI-H	14.0	0.6	0.016	0.24	1.87	13	1
SwRI-I	14.0	0.6	0.020	0.30	1.87	19	1

TABLE XII. DIMENSIONAL DATA FOR FATIGUE BELLOWS

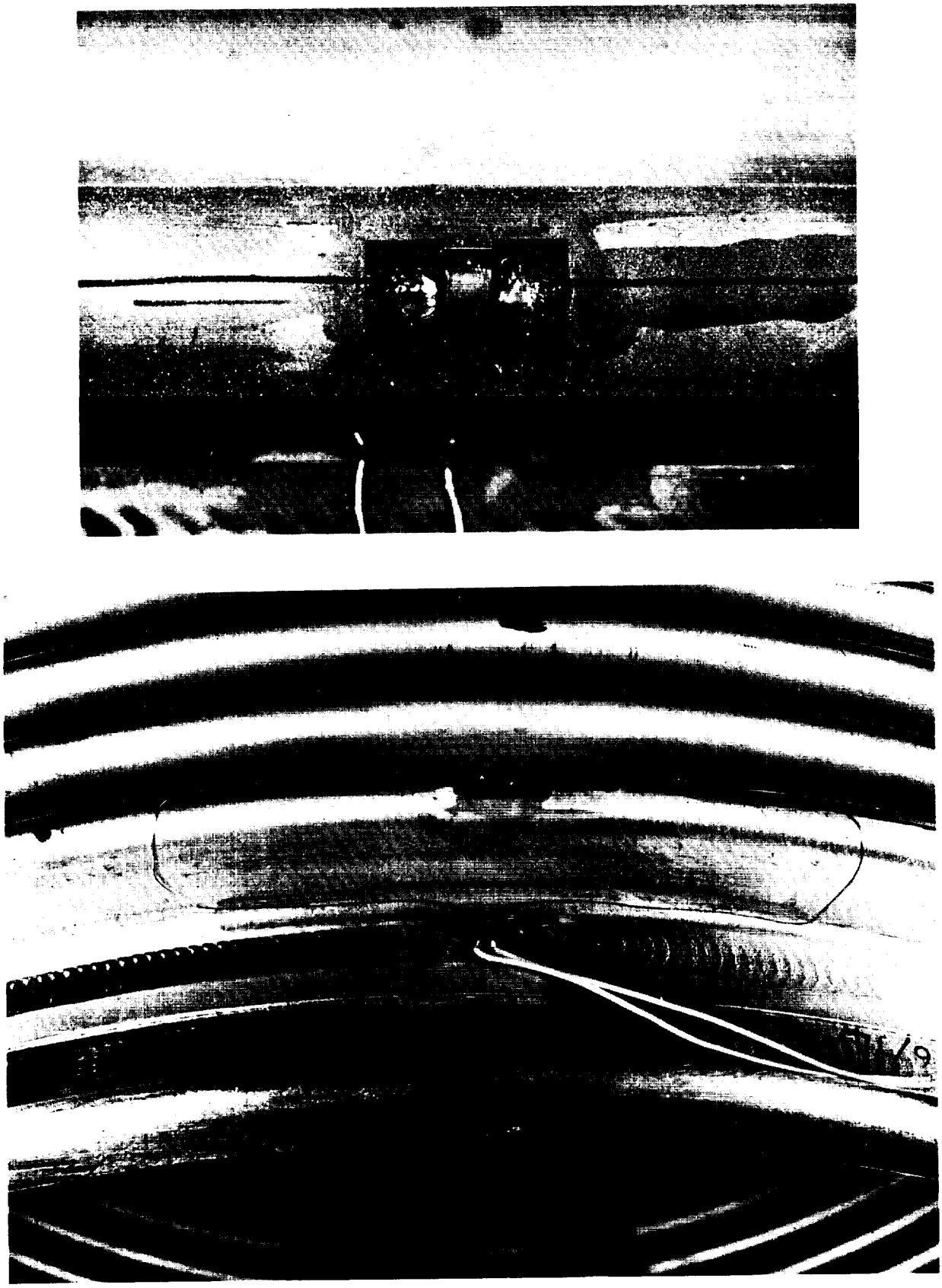

FIGURE 44. STRAIN GAGE INSTALLATION ON 14-INCH BELLOWS

Bench tests were performed to determine load versus deflection and deflection versus strain. The results of these tests are shown in Figures 45 through 51. This was done by loading the bellows in compression with calibration weights while measuring the deflection with a dial indicator and the strain with a Budd static strain indicator.

Flow Response and Fatigue

For the flow tests, the bellows were held in the flow loop with a fixture which was very rigid in comparison with the stiffness of the bellows itself. Figure 52 shows a typical installation. The flow media in all cases was water. At least one example of each bellows configuration was tested to determine mode shapes, mode frequencies, and dynamic strain levels throughout the range of fluid velocities. The mean fluid velocity was recorded at the peak of each mode. Figures 53 through 57 show results of these tests.

After the tests described above had been performed for one representative bellows, all the bellows of the same geometric configuration were fatigue tested. The fatigue tests were carried out in increments of 10^7 strain cycles or more at a given strain level. Usually the first step was carried out at a strain level below the endurance limit, and subsequent steps were carried out at higher levels until failure occurred. In some cases the first step was begun above the endurance limit, and the bellows were broken in less than 10^7 total accumulated strain cycles. Dynamic strain level, strain frequency, flow rate, and test time were recorded for each step.

In order to minimize the effect of static strain upon the fatigue life, the bellows were mounted in the test section at their natural manufactured lengths; and the flow system static pressure was held to the minimum required to prevent cavitation inside the bellows. However, the strain due to the system static pressure was checked and found to be negligible when analyzed according to the modified Goodman law.

Following all flow tests, the results were reduced to the form of calculated Stress Indicator versus cycles-to-failure data points for each distinct bellows. These data points were then plotted in a log-log form, as was the preliminary data shown in Figure 17. Figure 58 shows the final results in comparison with the Safe Operating and High Failure Probability limits which were shown in Figure 17. It may readily be noted from the results shown in Figure 58 that the most recent failure data, which covers a wide range of bellows sizes and geometries, verifies the original Safe Operating limit.

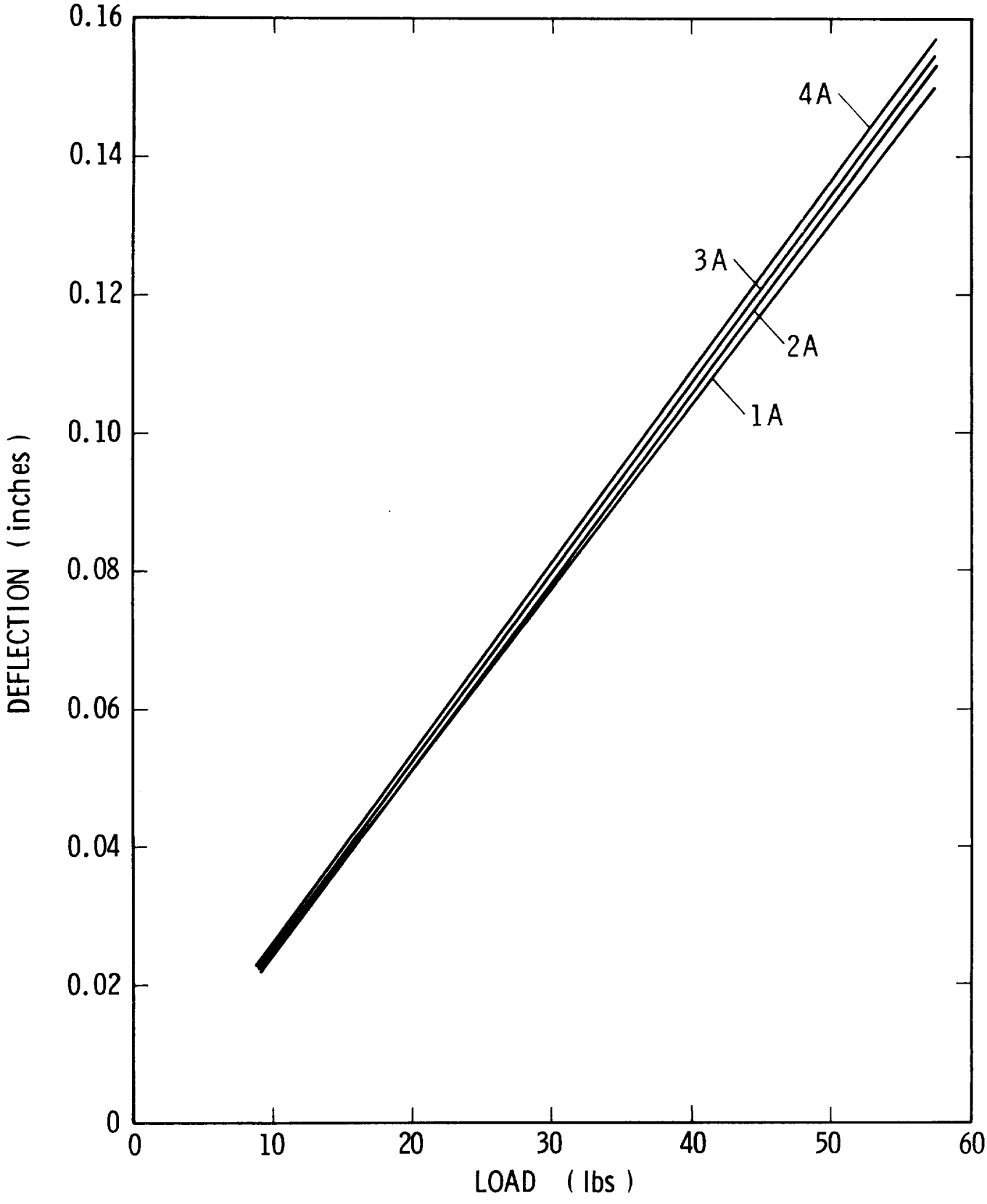

Figure 45. Load versus Deflection for SwRI - A Series Bellows

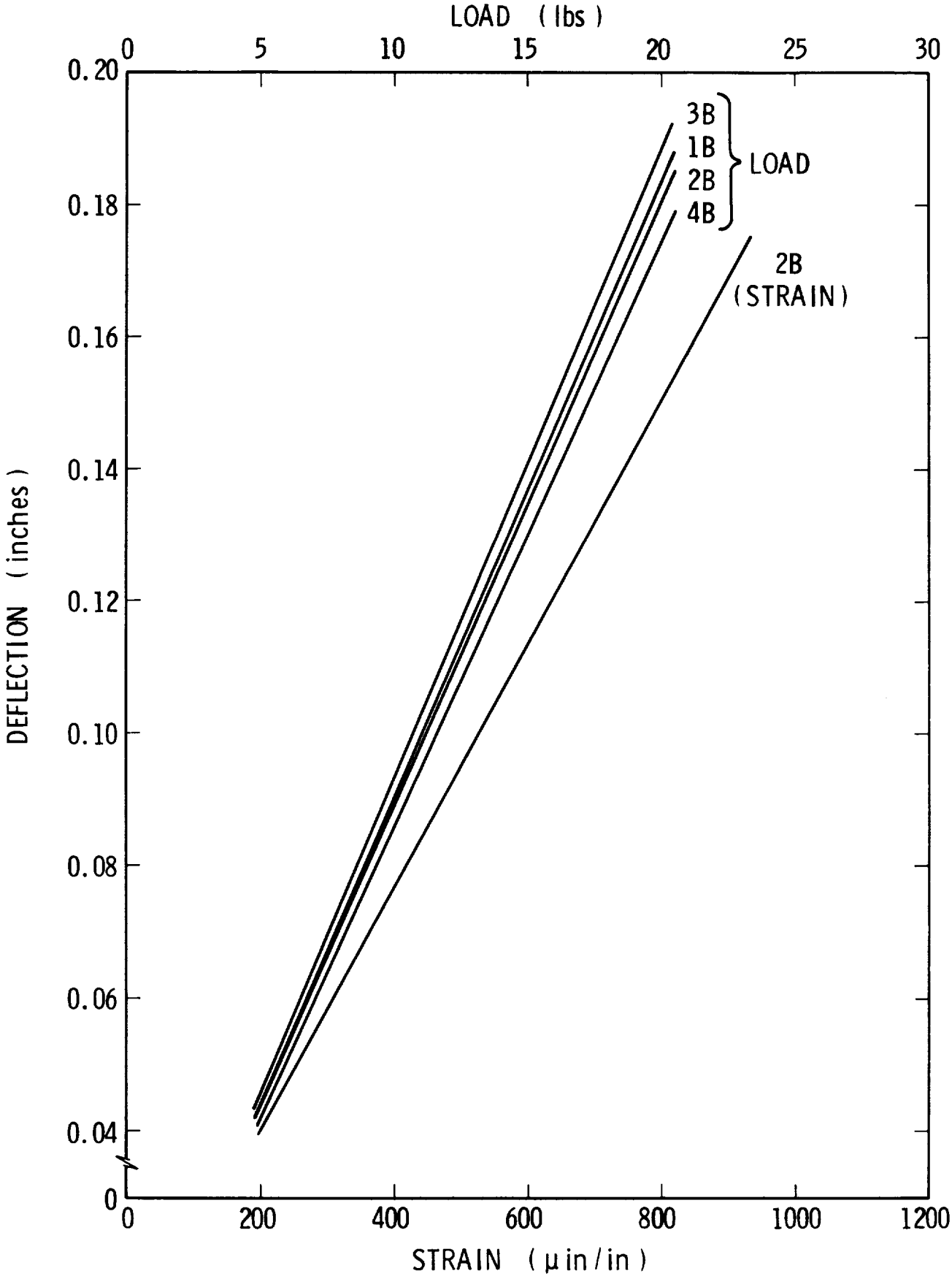

Figure 46. Load-Deflection and Strain-Deflection Characteristics for SwRI-B Series Bellows

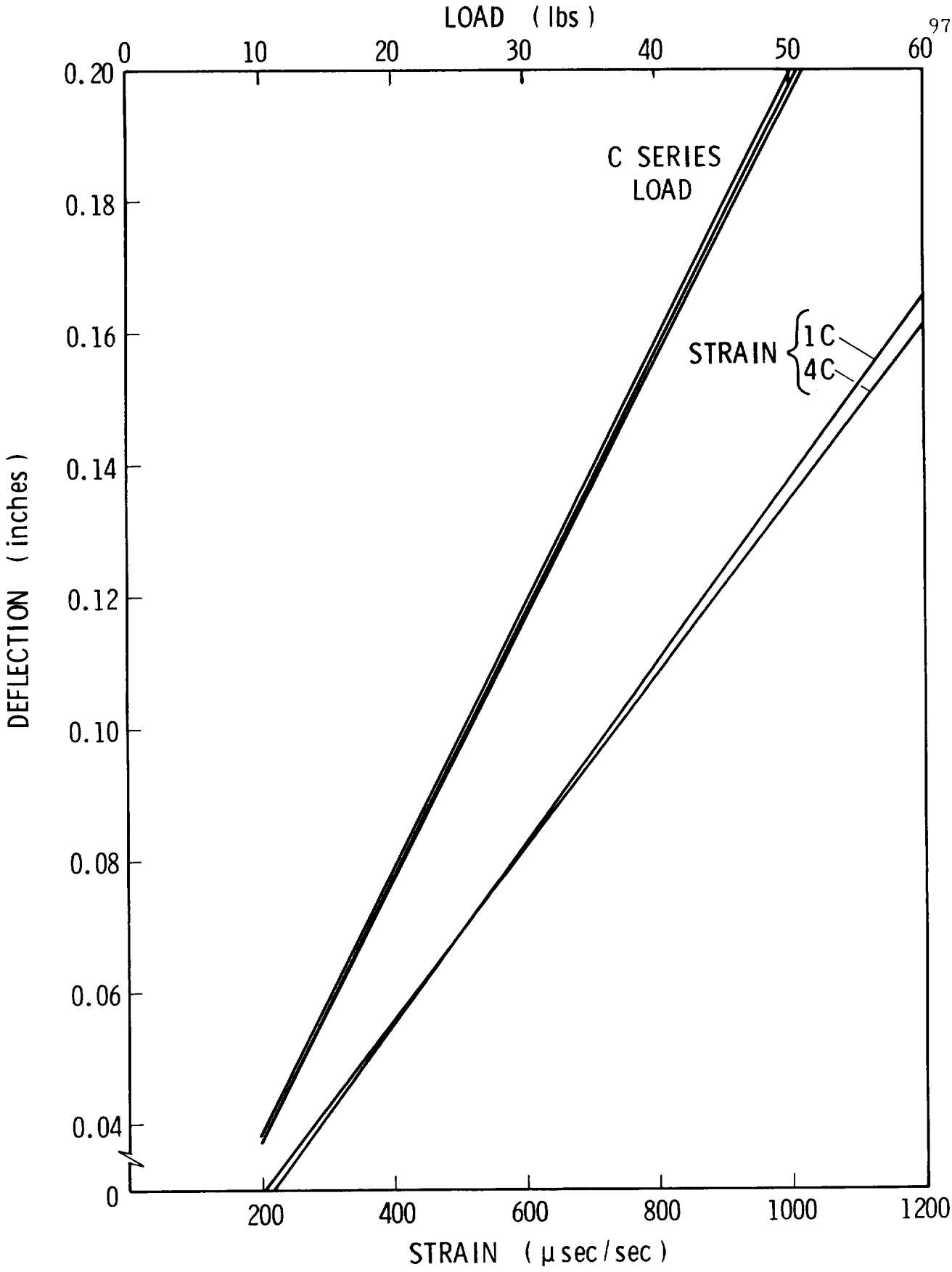

Figure 47. Load-Deflection and Strain-Deflection Characteristics for SwRI-C Series Bellows

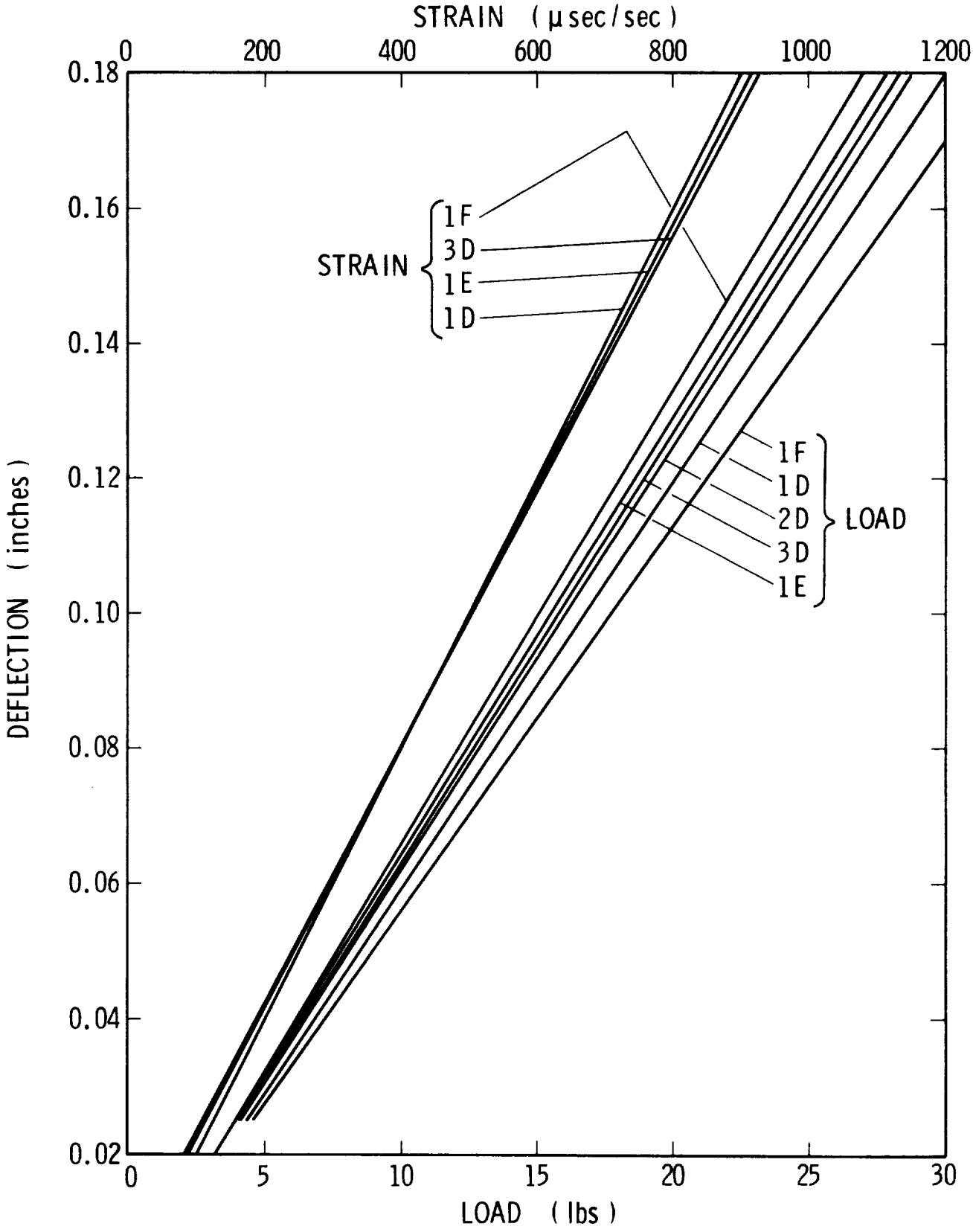

Figure 48. Load-Deflection and Strain-Deflection Characteristics for SwRI-D, E & F Series Bellows

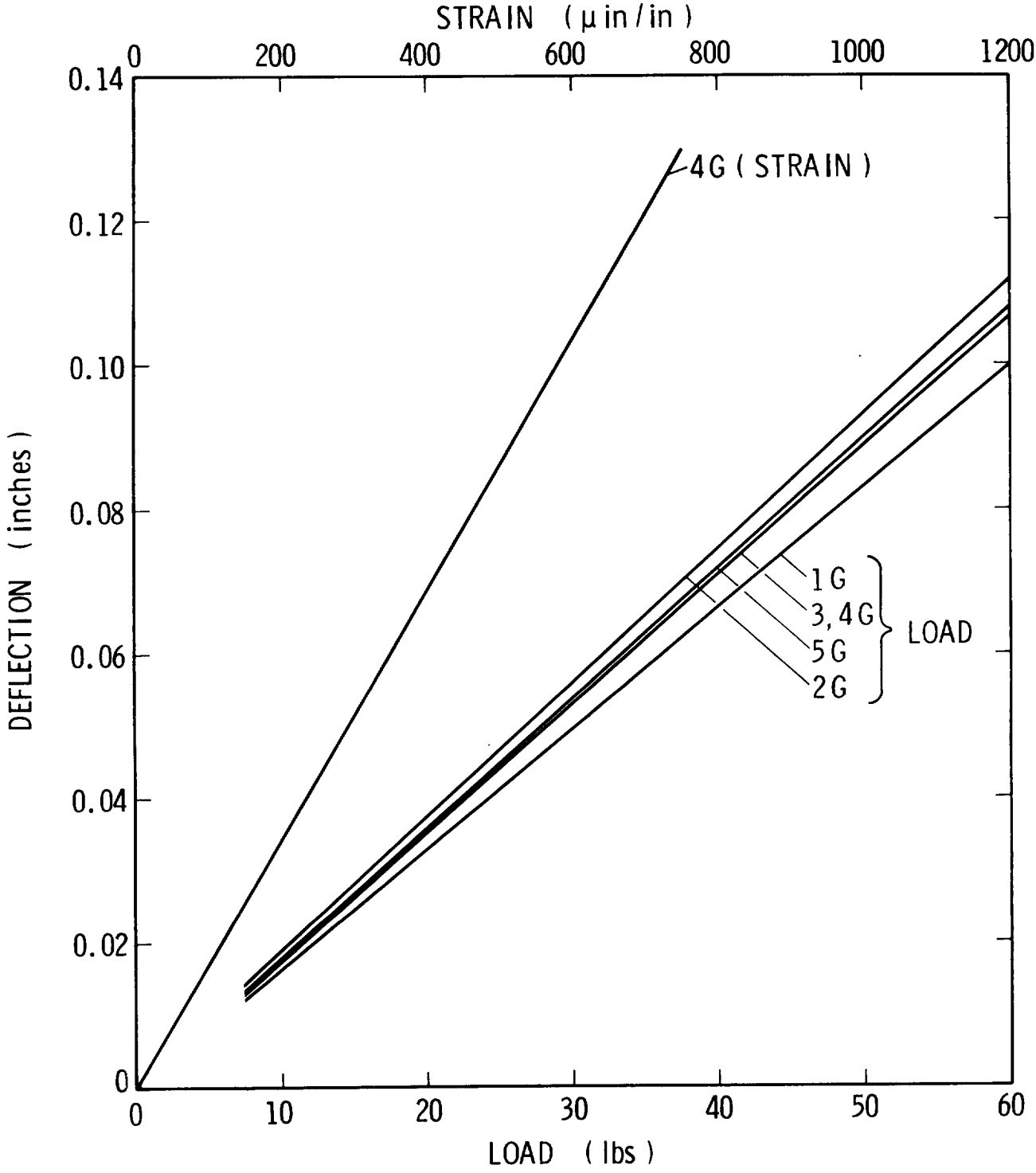

Figure 49. Load-Deflection and Strain-Deflection Characteristics of SwRI-G Series Bellows

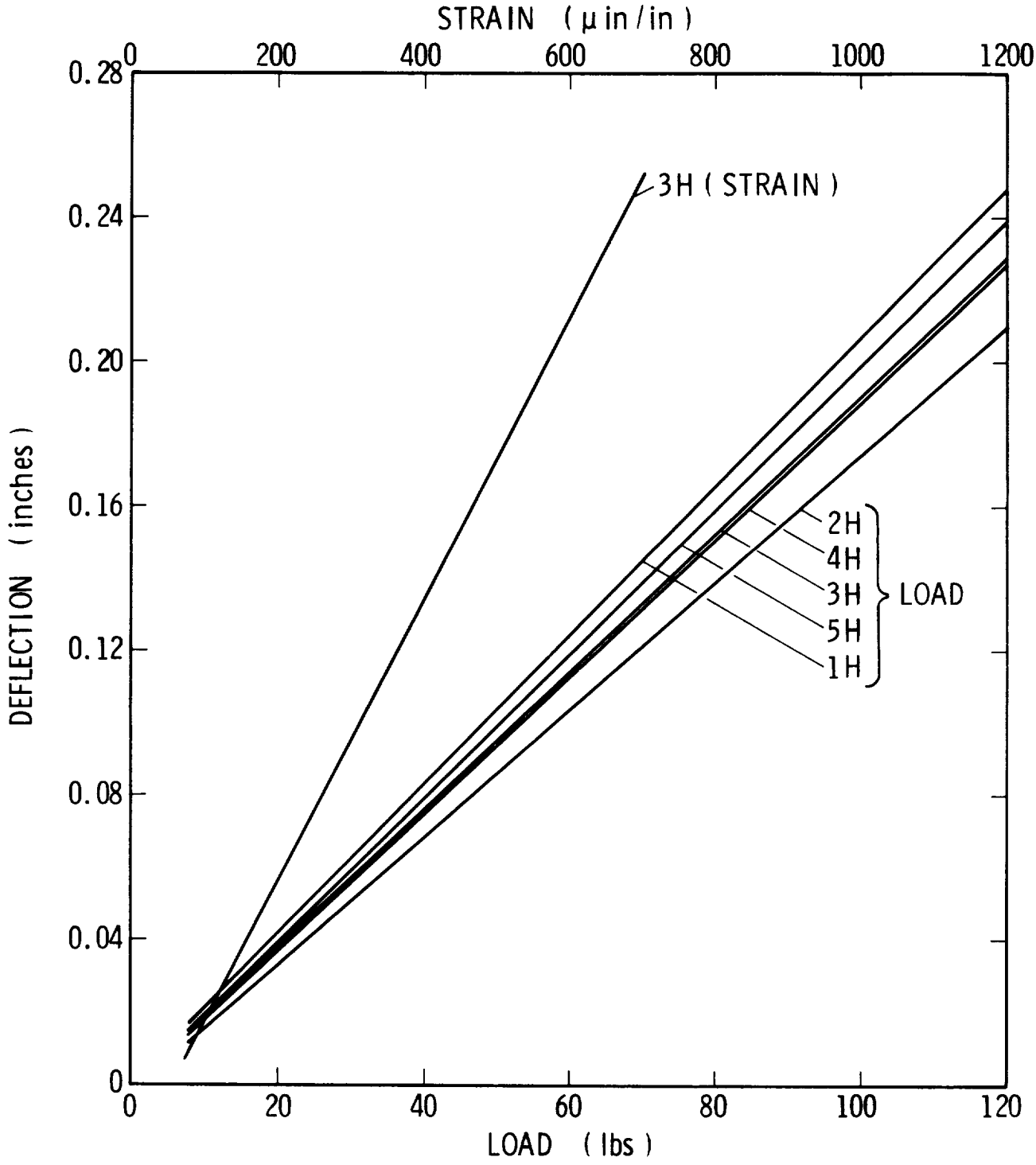

Figure 50. Load-Deflection and Strain-Deflection Characteristics of SwRI-H Series Bellows

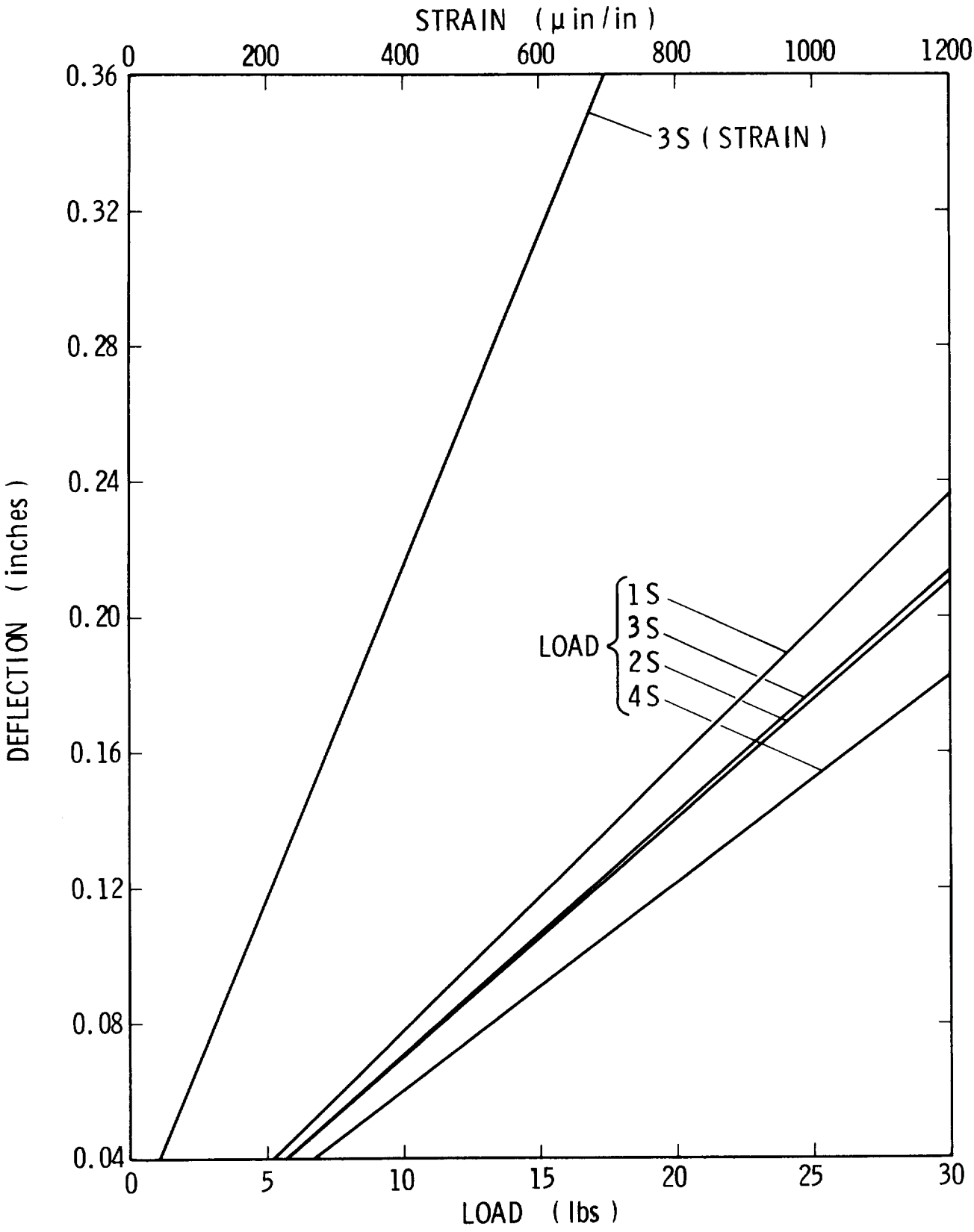

Figure 51. Load-Deflection and Strain-Deflection Characteristics for SwRI-S Bellows

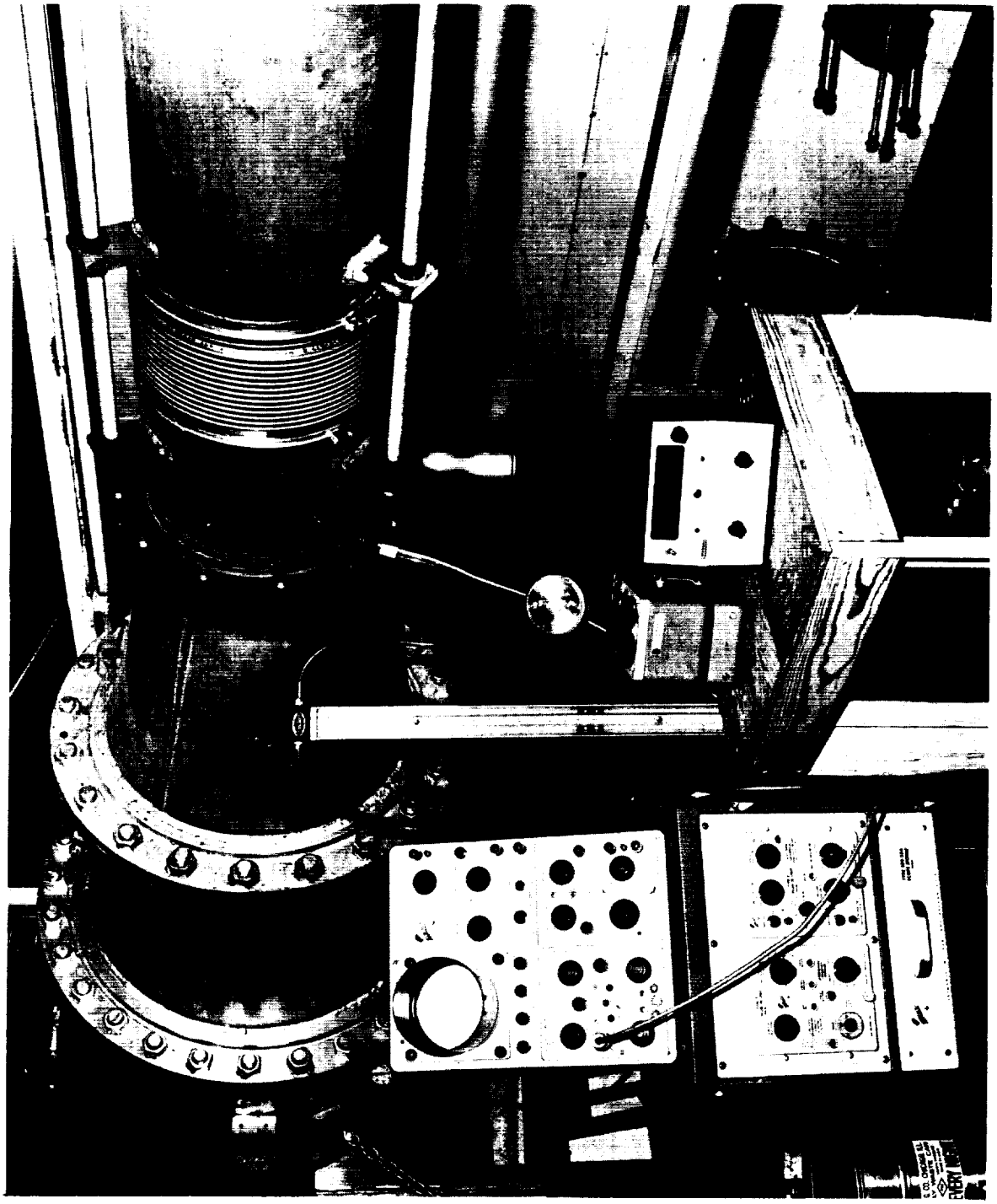

FIGURE 52. INSTALLATION OF BELLOWS IN FLOW LOOP

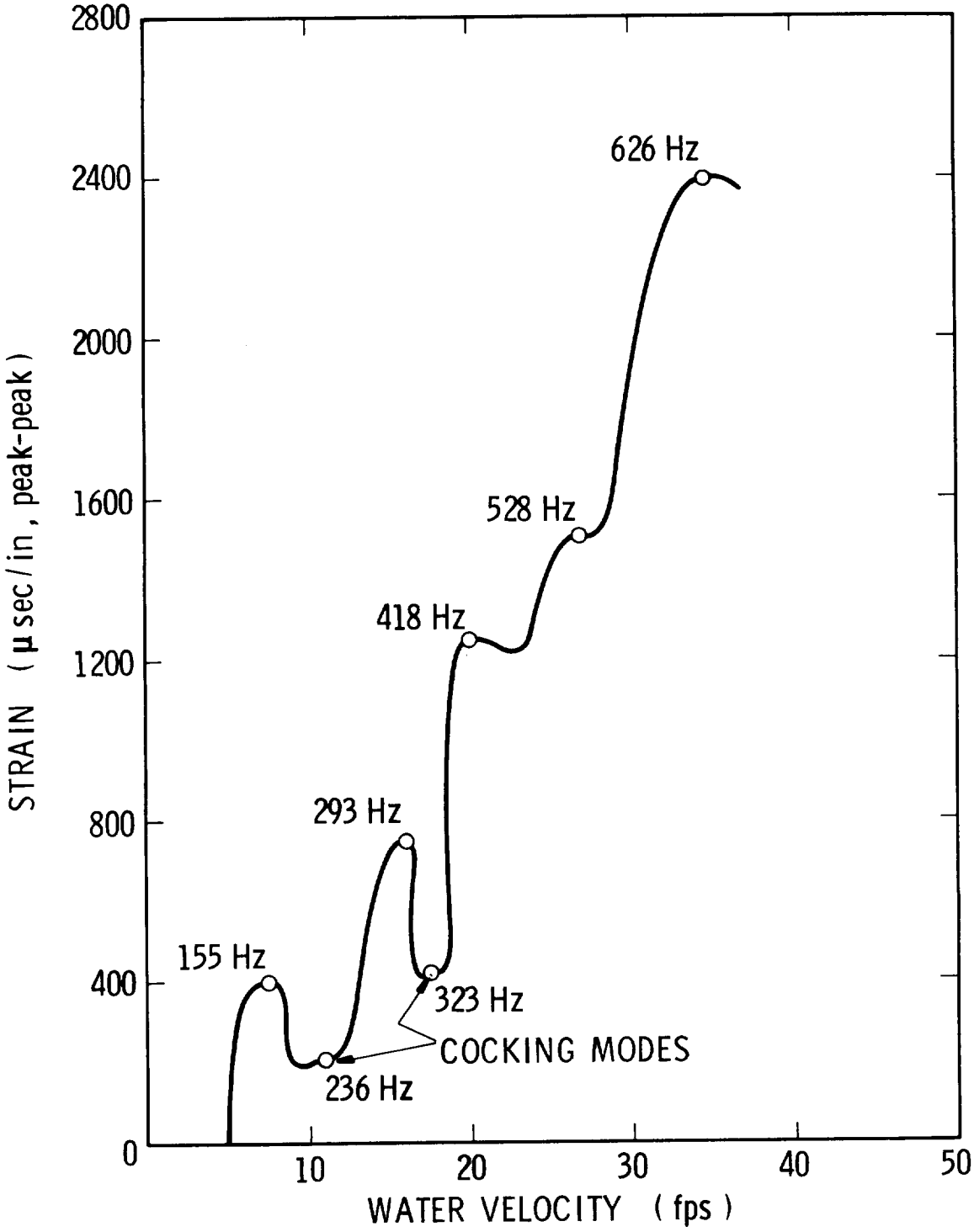

Figure 53. Mean Flow Velocity versus Dynamic Strain
SwRI-D Series (Typical)

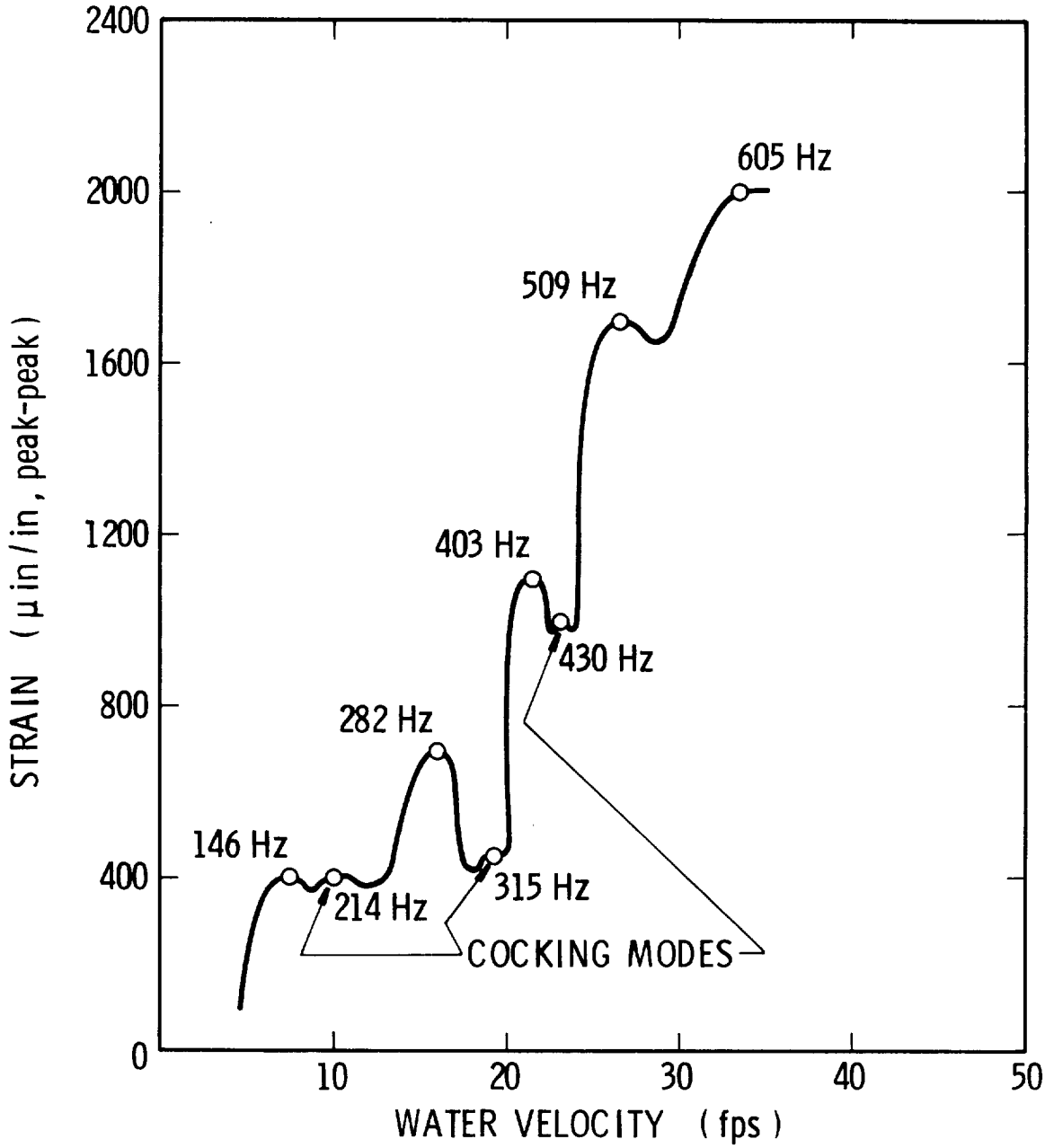

Figure 54. Mean Flow Velocity versus Dynamic Strain for SwRI-E Series (Typical)

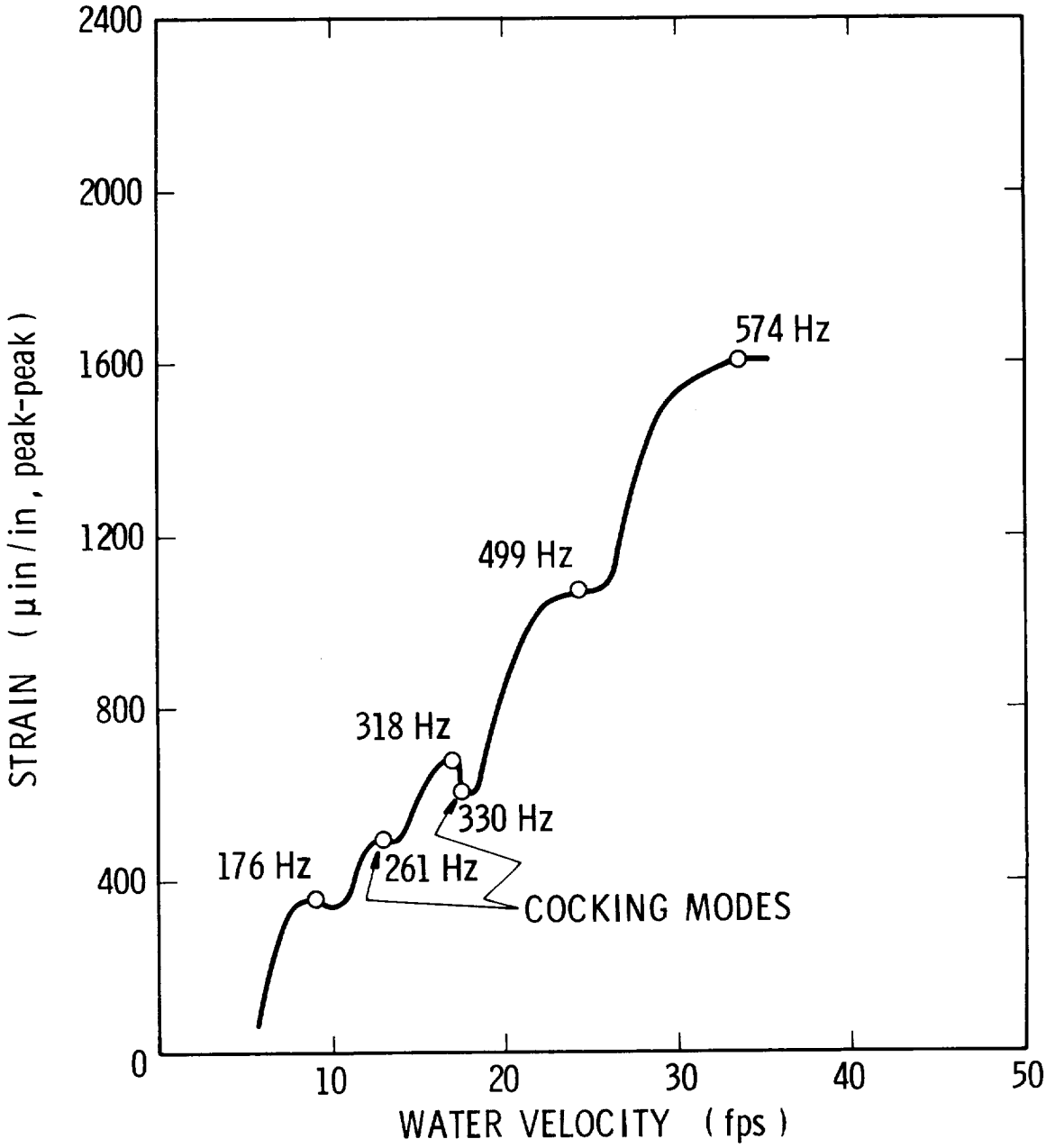

Figure 55. Mean Flow Velocity versus Dynamic Strain for SwRI-F Series (Typical)

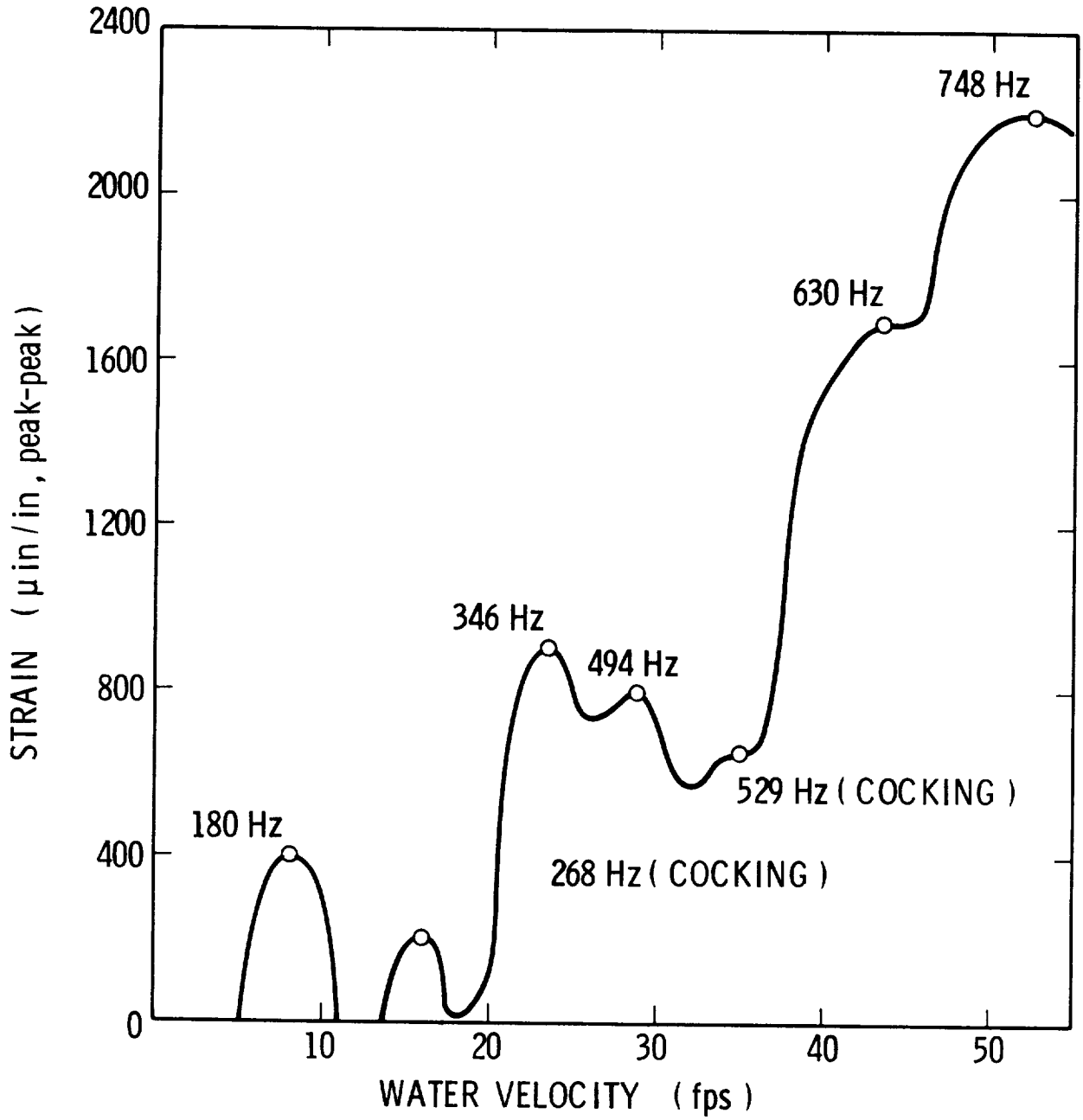

Figure 56. Mean Flow Velocity versus Dynamic Strain for SwRI-G Series (Typical)

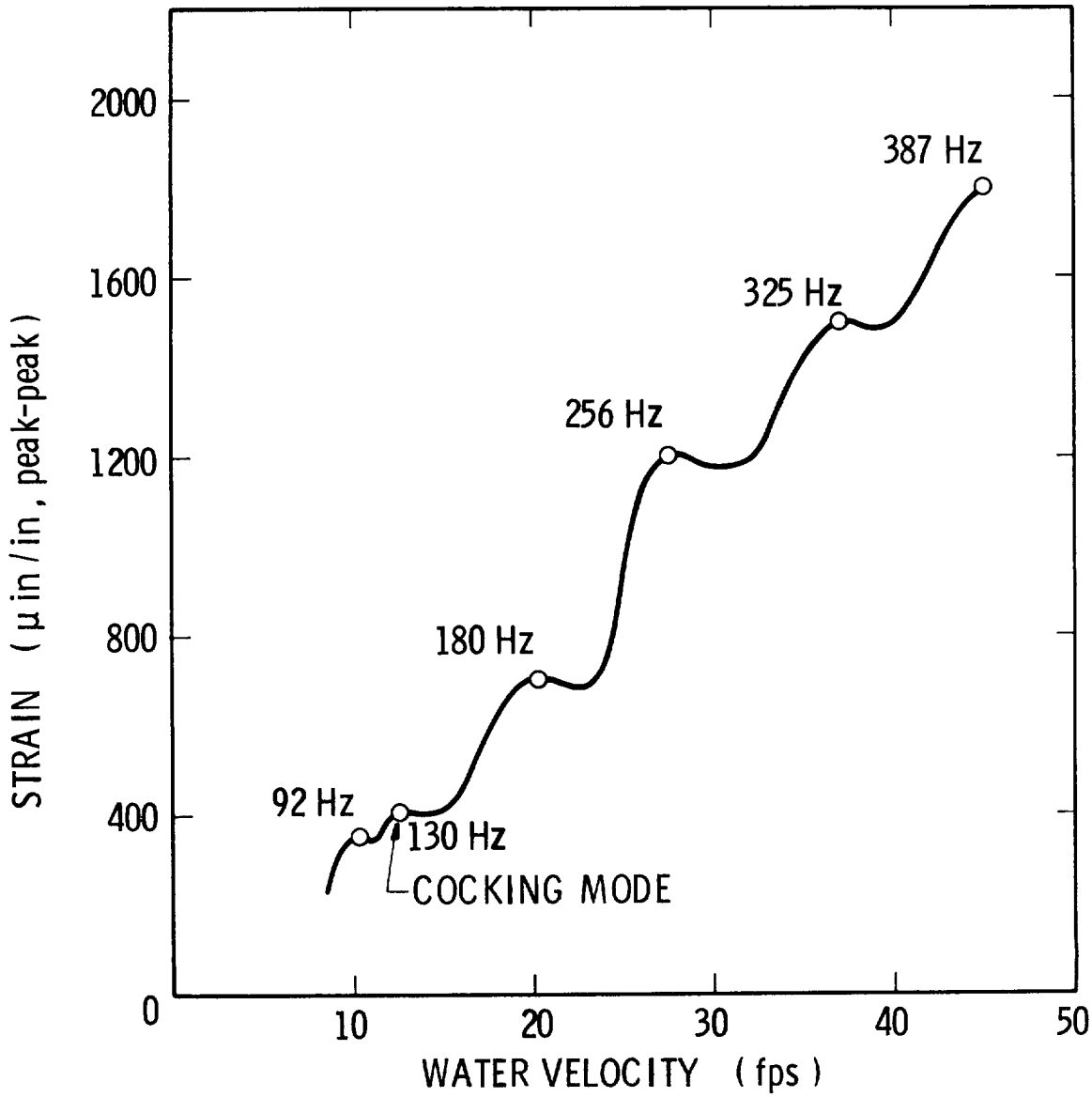

Figure 57. Mean Flow Velocity versus Dynamic Strain for SwRI-H Series (Typical)

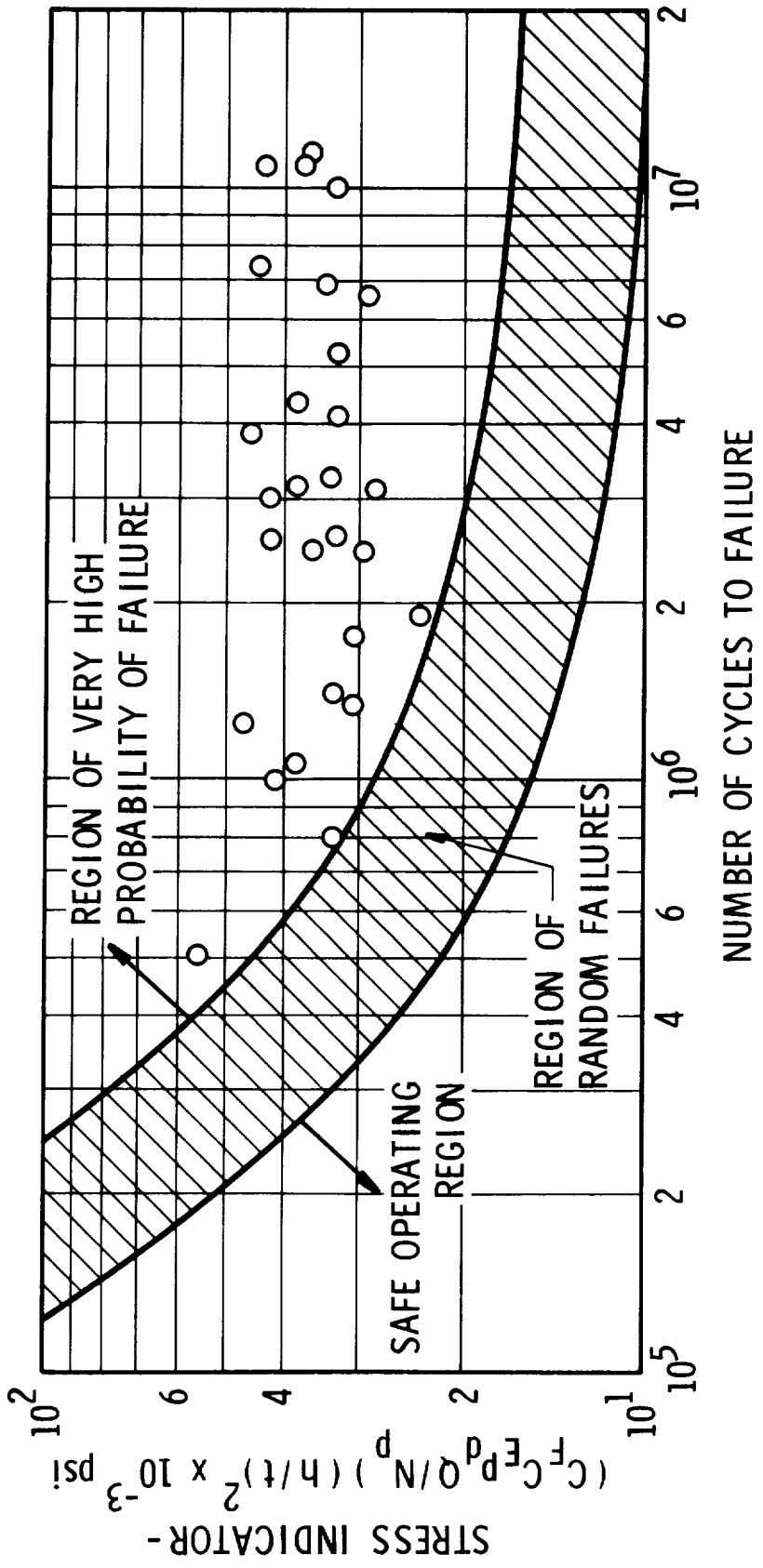

Figure 58. Final Bellows Fatigue Life Data

Section II discusses the use of the failure data for design and analysis purposes.

III. 7 Other Influences

In practice, it has been found that several factors, in addition to those already discussed, can have an influence on the magnitude and character of bellows flow-induced vibrations; these factors are, (a) presence of an upstream elbow, (b) angulation of the bellows, (c) non-rigidly attached piping, and (d) acoustic resonances of the duct system. The first three influences are discussed briefly in this section and the subject of "acoustic resonance effect" is treated in a subsequent section.

Upstream Elbow Effect

Because it had been observed that some bellows installed immediately downstream of a duct bend were seemingly more susceptible to flow-induced failure problems than those in straight sections, a small investigation was undertaken to study this. One of the calibrated test bellows was placed in the flow system, and located immediately downstream of a short-radius 90-degree elbow. Flow-induced strain amplitudes were than monitored as a function of the mean internal fluid velocity. The test was repeated with the same bellows in a straight run with all other conditions kept the same.

Figure 59 shows the results of these tests. Notice that two things have changed about the response of the bellows with the elbow present, compared with the response with no elbow. First, the mean fluid velocity range over which flow excitation occurs has been shifted down by about 45 percent. Second, note that the strain level for a given mode of vibration has significantly increased, or that the strain amplitude at a given fluid velocity has increased.

The explanation for the difference in bellows vibration with, versus without, an upstream elbow is that the velocity profile is skewed or distorted because of the presence of the elbow (see Figure 59). This causes an excessive dynamic fluid loading on the convolutions downstream of the outer bend region and possibly a reduced loading downstream of the inner region; the net effect is an increased effective value of the fluid velocity along the surface of the bellows, causing the vortex shedding to lock-in on the bellows vibration at a lower-than-normal mean fluid velocity.

While further tests must be performed to better quantify the influence of an upstream elbow on bellows vibration levels, we can say for the present that an increase in stress level by a factor of about 2 is possible for a given mean velocity. Elbows with more generous radii of curvature, or located further upstream, would most likely not cause this great an increase in flow-induced stress levels.

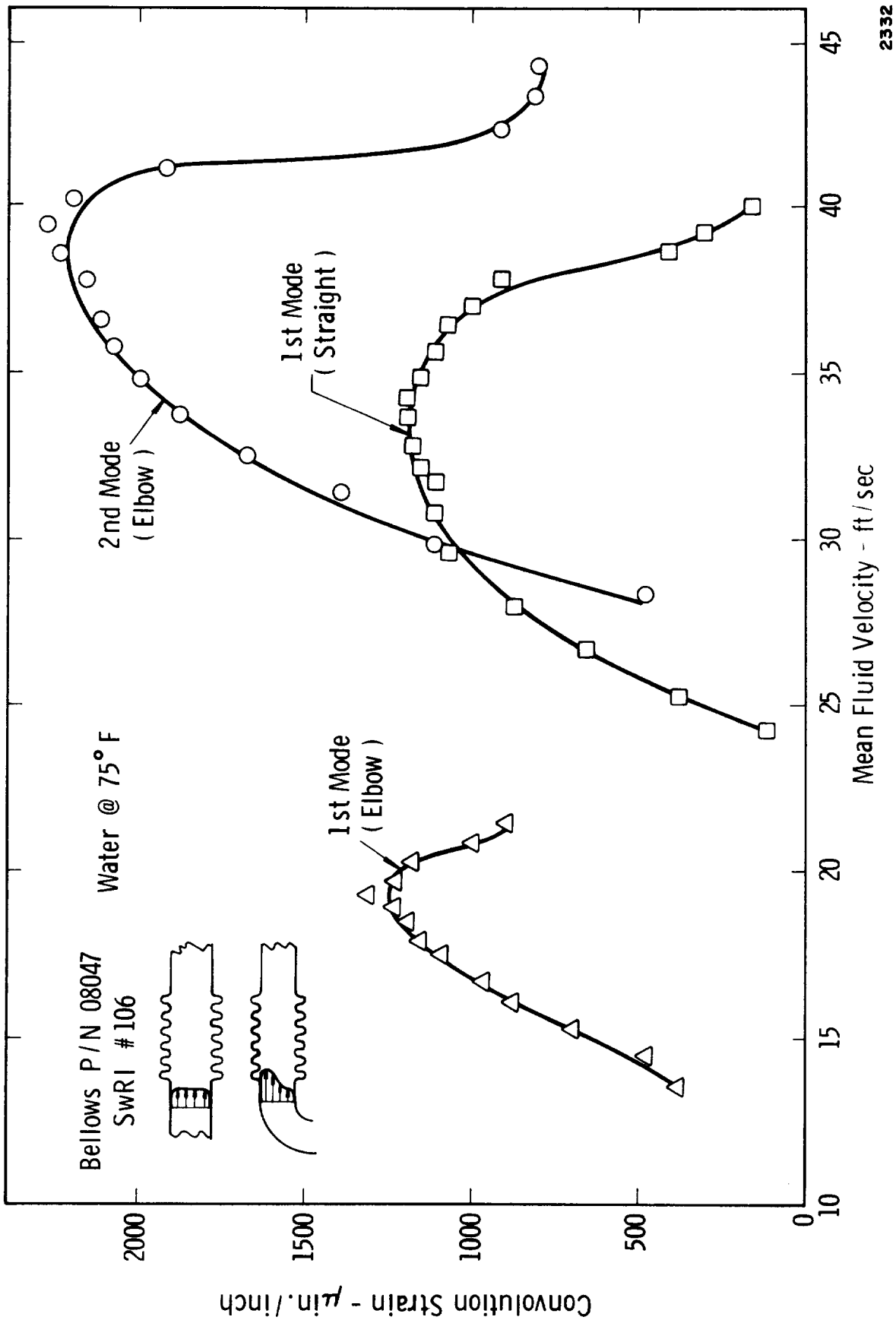

Figure 59. Bellows Flow-Induced Strain With And Without Upstream Elbow

Non-Rigid Ducting

As might be expected, if the ducting attached to the ends of a bellows is not rigid then the character of the flow-induced vibration can be changed compared with the ideal case of perfectly rigid attachments. There are apparently two ways that the bellows vibrations can be affected; first, the modal frequencies can be changed (generally lowered), and second, additional damping can be "added" or energy dissipated through the attachments.

For most cases, the modal frequencies of a bellows will not be significantly changed because of flexible attachments. The reason for this is that the bellows is generally so much more flexible than the attached ducting, particularly in the longitudinal or axial direction. Apparently, however, significant damping can be introduced by allowing duct flexibility as evidenced by some of our experimental observations. While we can't at this time report any quantitative results, the reader should take note of these observations. Whenever a bellows is undergoing a qualification test, our observations indicate that particular care should be exercised so that the bellows attachments are at least as rigid as in the actual installation. This should help ensure that the flow-induced vibration levels attained in the qualification test are at least as great as the actual installation.

Angulation of Bellows

At the present time, we have no quantitative information to report concerning the effect of angulation on bellows flow-induced vibrations. It would seem, based on the results of the upstream elbow tests discussed above, that angulation might lead to an increase in vibration levels because of the excess fluid loading on the outer bend region. Also, however, angulating a bellows might cause a change in the mode frequencies and damping. At this time, effect of angulation must be considered unknown and we caution the reader to be conservative in dealing with this situation.

IV. BELLOWS FLOW-INDUCED VIBRATIONS WITH CRYOGENIC FLUIDS

IV. 1 Introduction

Heat transfer effects as well as vortex, acoustic, geometric and cavitation influences must sometimes be considered in obtaining an understanding of the flow-induced vibrations in flexible metal bellows. The consequences of heat transfer in the case of cryogenic flow in bellows are of particular interest since large temperature differences exist between the flowing liquid and the bellows environment which could lead to a phase change near the inside bellows wall. Vapor formation will result in a "killing off" of the vortex shedding, and a change in the bellows flow response. Even low rates of heat transfer, which do not produce large scale boiling, may raise the vapor pressure near the wall so cavitation can occur and suppress the flow induced vibration. In addition to vapor effects on the flow induced vibration, frost buildup and liquid condensation on the outside bellows surface will affect the heating rate and add damping to the bellows structure, thus influencing its operating characteristics. Another question regarding bellows operation is the change in the bellows characteristics at extremely low temperatures in contrast to conditions tested in air and water at near ambient conditions. Once the bellows response to heat transfer is established, a more realistic evaluation of bellows performation in the field will be available in order to establish failure criteria under operating conditions.

The objective of the work reported in this section was to perform a theoretical and experimental study of heat transfer with respect to its effect on the flow-induced response of bellows when gas is formed in the convolutes and/or frost or liquid accumulates on the bellows exterior. The following questions are typical of those discussed in this section:

(a) How does bellows response in liquid nitrogen (LN_2) compare to test results for water and air?

(b) In practical situations, can heat transfer change the physical properties of the fluid in the bellows convolutions sufficiently to influence the vortex excitation phenomena?

(c) If heat transfer does have an effect under certain conditions, can these conditions be predicted and how do they relate to the physical properties of the cryogenic liquid?

(d) What effect does the external buildup of ice, slush and liquid have on the problem?

(e) What influence do changes in convolution geometry have on a possible heat transfer effect?

(f) What is the most realistic, and/or severe, method of testing a bellows to account for possible heat transfer and external damping effects; that is, what test procedure will most likely show failure-prone bellows?

The results presented in this section were initially reported in Reference 2 as Interim Report No. 2 for the contract.

IV. 2 Experimental Facility

Cryogenic Flow Loop

A special cryogenic flow loop was designed and fabricated for the purposes of this study. The loop is shown in Figures 60and 61before and after the insulation was installed. The pump is a standard centrifugal cryogenic unit, designed for liquid oxygen service, which was converted from electric motor drive to a hydraulic motor drive to provide a variable speed capability. The pump rating is 600 GPM at 110 ft total head when pumping liquid oxygen. The flow rate is measured with a turbine type flow meter which was calibrated in place with a pitot tube using water as the flow medium.

The flow loop has a total capacity of approximately 90 gallons. The system is filled from a 1500-gallon dewar which is installed adjacent to the laboratory. Any liquid remaining in the loop after completion of a test can be pumped back into the dewar.

Insulation of the loop consists of 2-inch thick styrofoam panels built into a box-like enclosure. A small amount of boiloff gas from the loop is vented into the enclosure to prevent any possible dangerous buildup of oxygen. The insulation is quite adequate for the short term tests such as those performed in this program. Liquid loss resulting from heat transfer was small compared to pumping loss. The styrofoam panels are easily removed when necessary for repair or modification of the loop.

The test section of the loop can be isolated by closing the upstream and downstream valves. The test piece can then be replaced without draining the system. The downstream valve can also be used to increase the back pressure in the test section during flow tests. System pressure can be controlled by manually venting gas or by setting an automatic relief valve.

Instrumentation

All bellows installed in the cryogenic flow loop described above were instrumented as illustrated in the schematic drawing shown in Figure 62. Four copper-constantane thermocouples were provided in order to monitor (1) the upstream fluid temperature, (2) downstream fluid temperature, (3) the bellows metal or skin temperature, and (4) the surrounding temperature of the environment in which the bellows were placed. All of these thermocouples were referenced to -320^{o}F (boiling point of liquid nitrogen

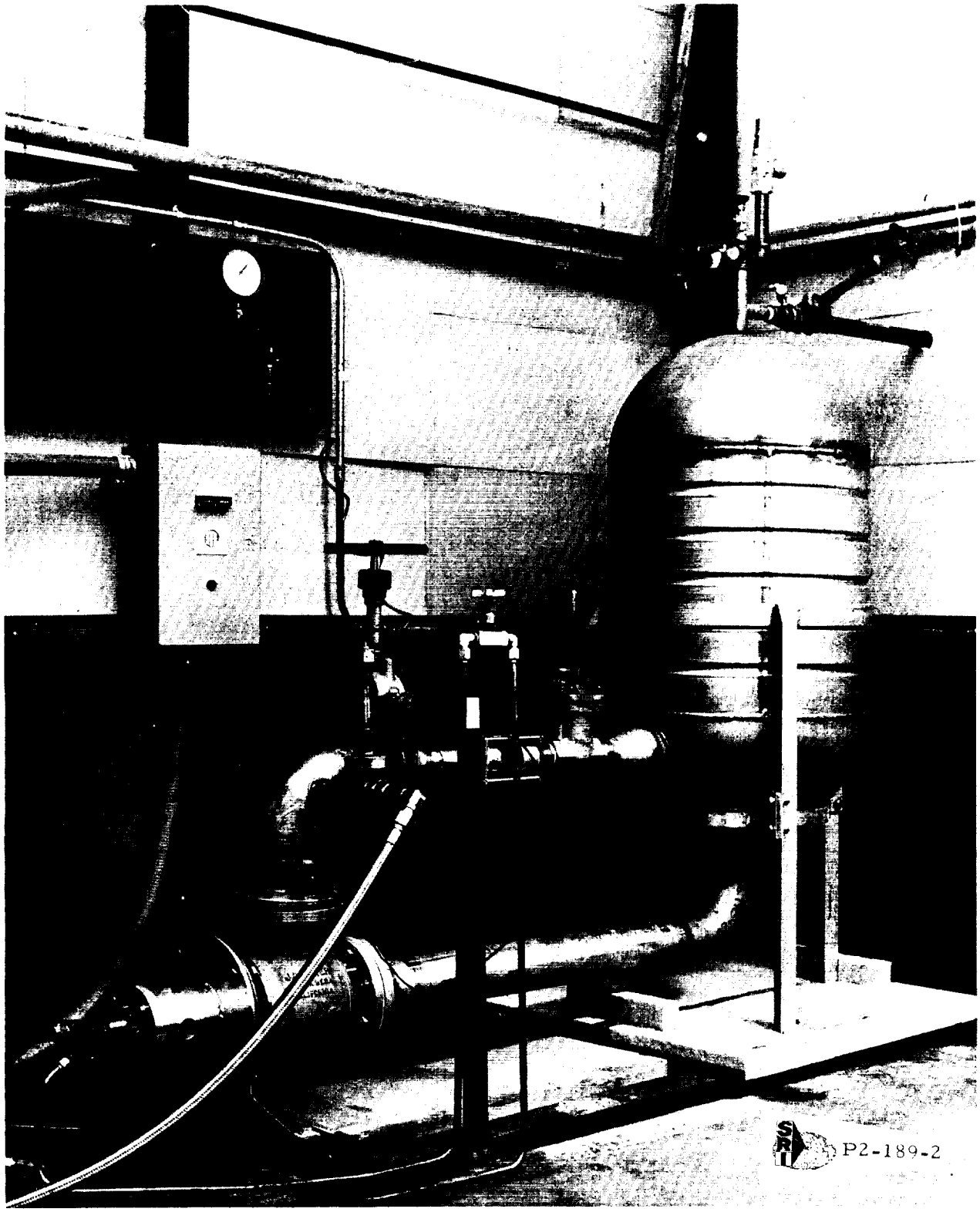

FIGURE 60. CRYOGENIC FLOW LOOP WITHOUT INSULATION

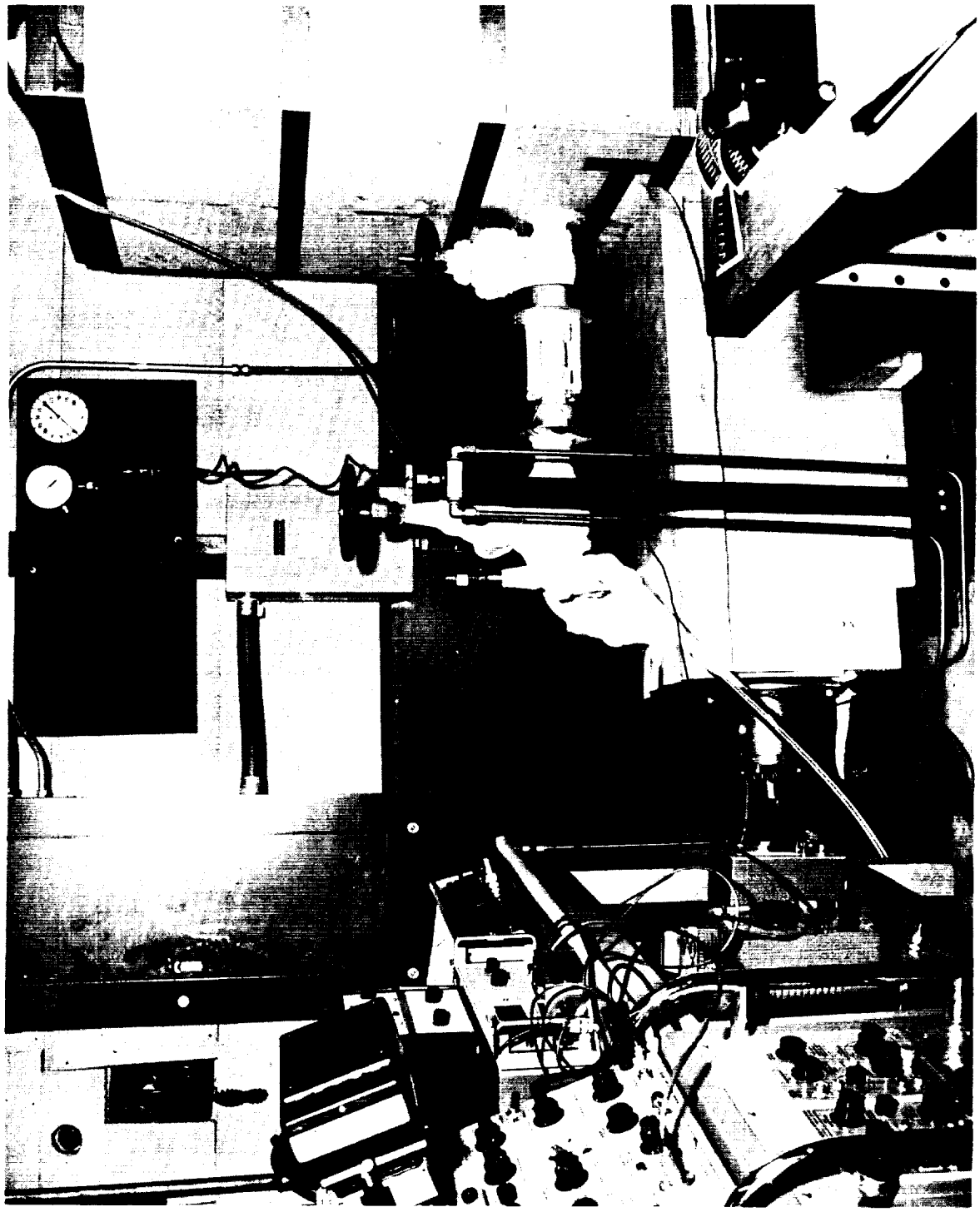

FIGURE 61. CRYOGENIC FLOW LOOP WITH INSULATION

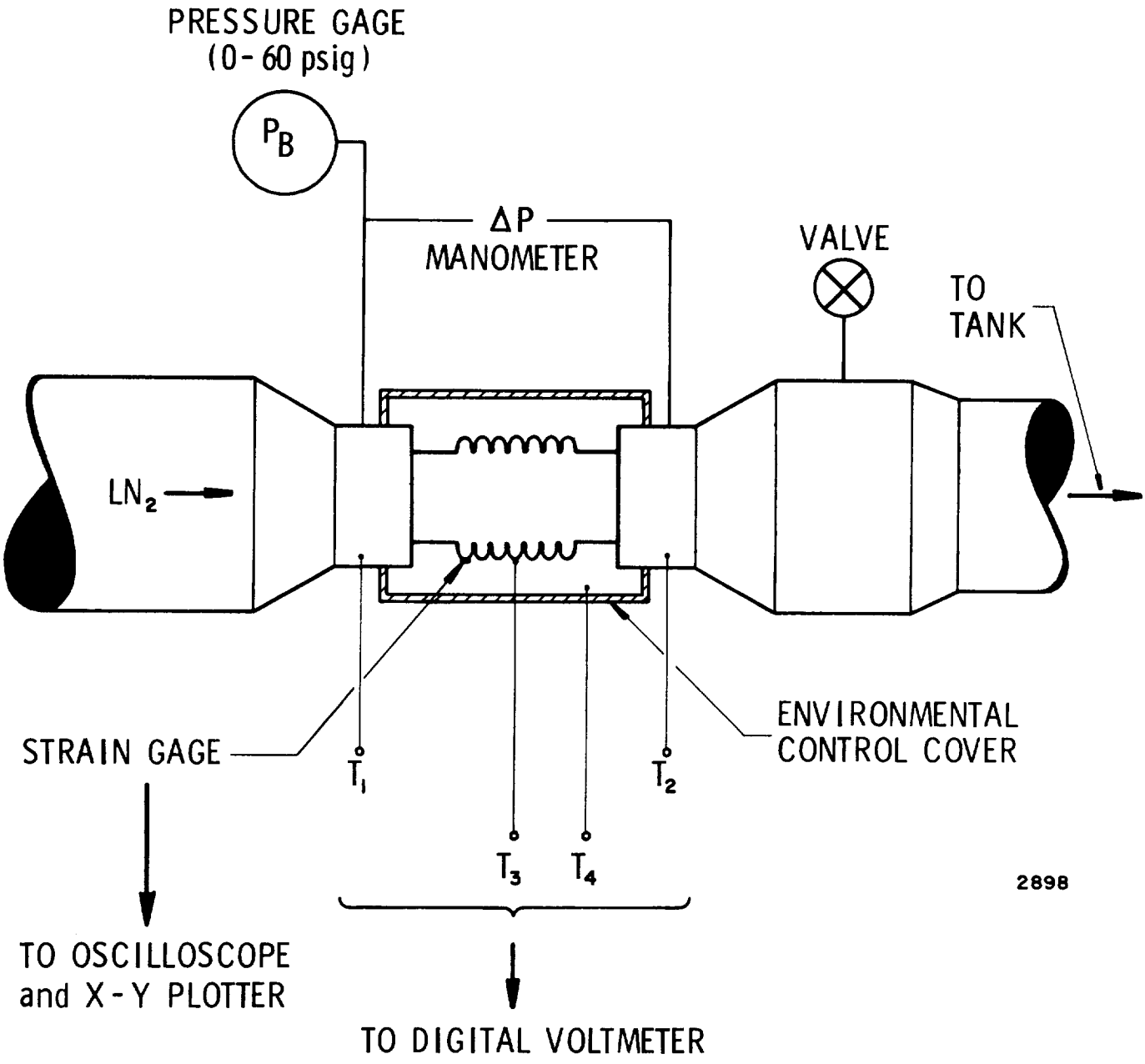

Figure 62. Instrumentation Schematic

at standard conditions) in order to provide accurate results. A digital voltmeter was employed in conjunction with the thermocouples, and the accuracy was established to be $\pm$ 0.5 degrees F.

Bellows pressure was measured with a bourdon pressure gage, while the pressure drop across the bellows was measured with a mercury manometer. The static pressure of the system was measured with the same bourdon gage when the flow velocity was zero, and is referred to in the report as P_T (tank pressure or static system pressure). The downstream valve shown in Figure 62 was used to create the back pressure (P_B-P_T) required to excite the bellows vibration.

Dynamic strain was monitored through the use of 1/32-inch gages mounted on the first convolution tip of each bellows. Since the strain frequencies were expected to be relatively high, ordinary constantane foil type gages were used without temperature compensation. These gages are less expensive than those produced specifically for use at cryogenic temperatures, and they can readily be obtained in configurations which are convenient for bellows applications.

The fact that the apparent strain curve for constantane has a very large slope at cryogenic temperatures is of little consequence since the strain readout equipment was AC coupled, and the temperature changes were slow compared to the strain frequency.

The strain gages were installed with a 100% solids epoxy adhesive. Bellows surface preparation consisted of light sandblasting and application of a degreaser. The gages were positioned by the holding-tape technique, and the adhesive was cured under a light clamping force. Following strain gage installation, each bellows was tested to obtain static force-deflection and strain-deflection curves. This provided experimental spring rate values which allowed more accurate mode frequency calculations. The force-deflection and strain-deflection data for the six bellows tested in the cryogenic flow facility are shown in Figures 63 and 64.

At the cryogenic temperatures, considerable "zero drift" occurred with the strain gages, and the question was raised as to the reliability of the strain gage readings at these extreme temperatures under a dynamic situation. According to the manufacturers' specifications, the gage factor would change only 4% at these temperatures. As a check, one of the bellows was mounted on a mechanical shaker with one end fixed rigidly and the other free to move with the shaker (Figure 65). A dial deflection gage was used

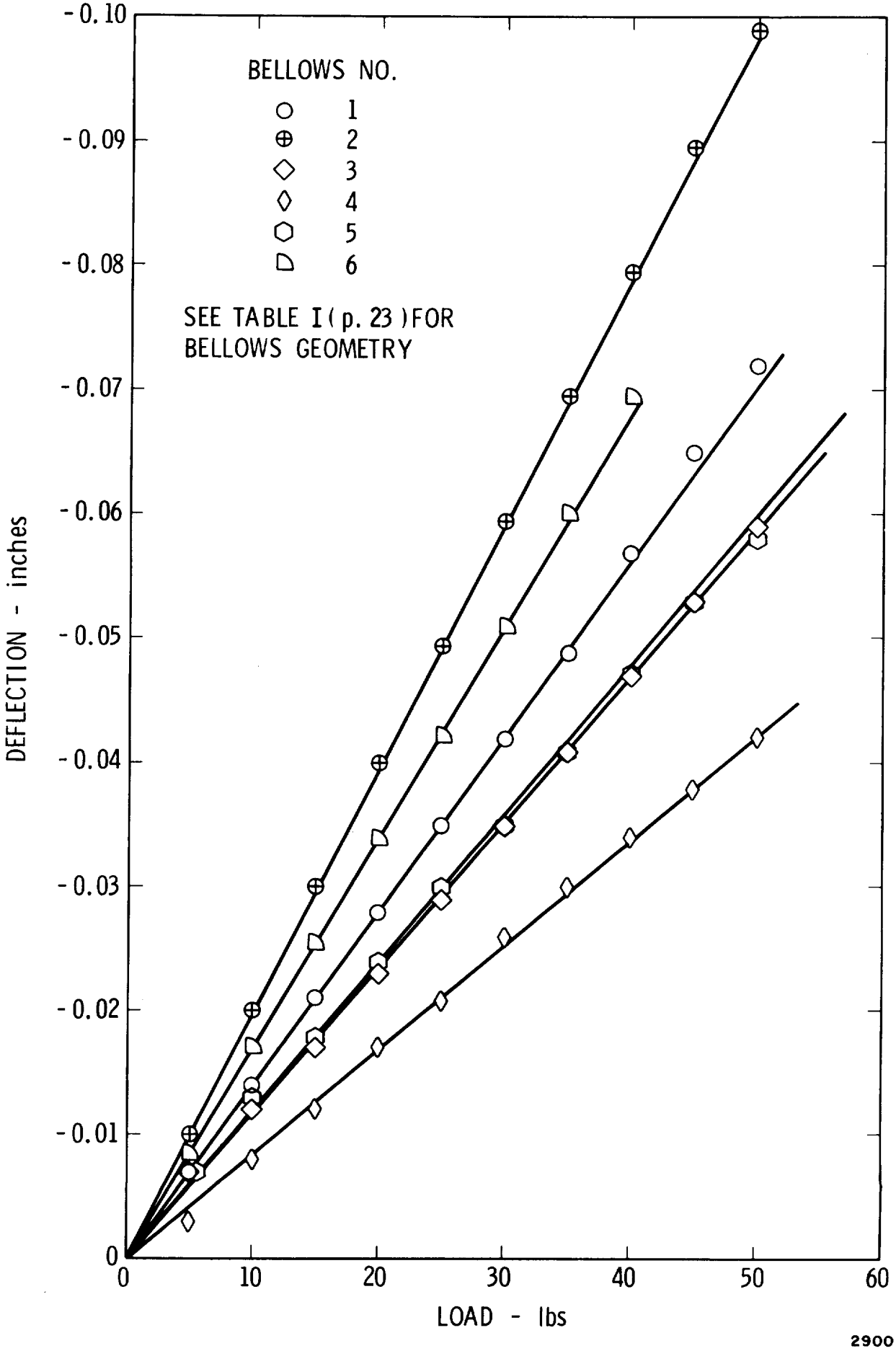

Figure 63. Load - Deflection Data For Test Bellows

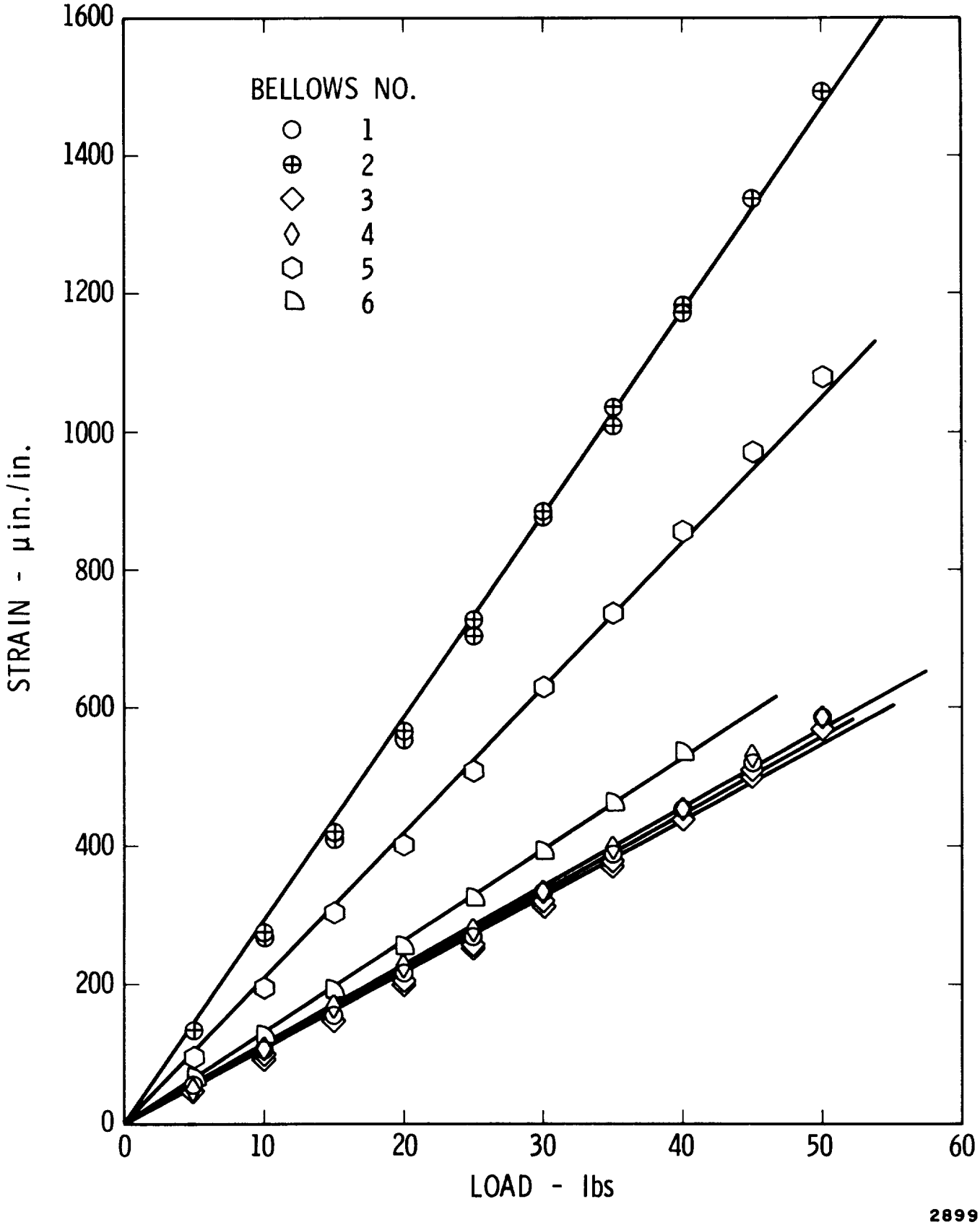

Figure 64. Strain - Load Calibration For Test Bellows

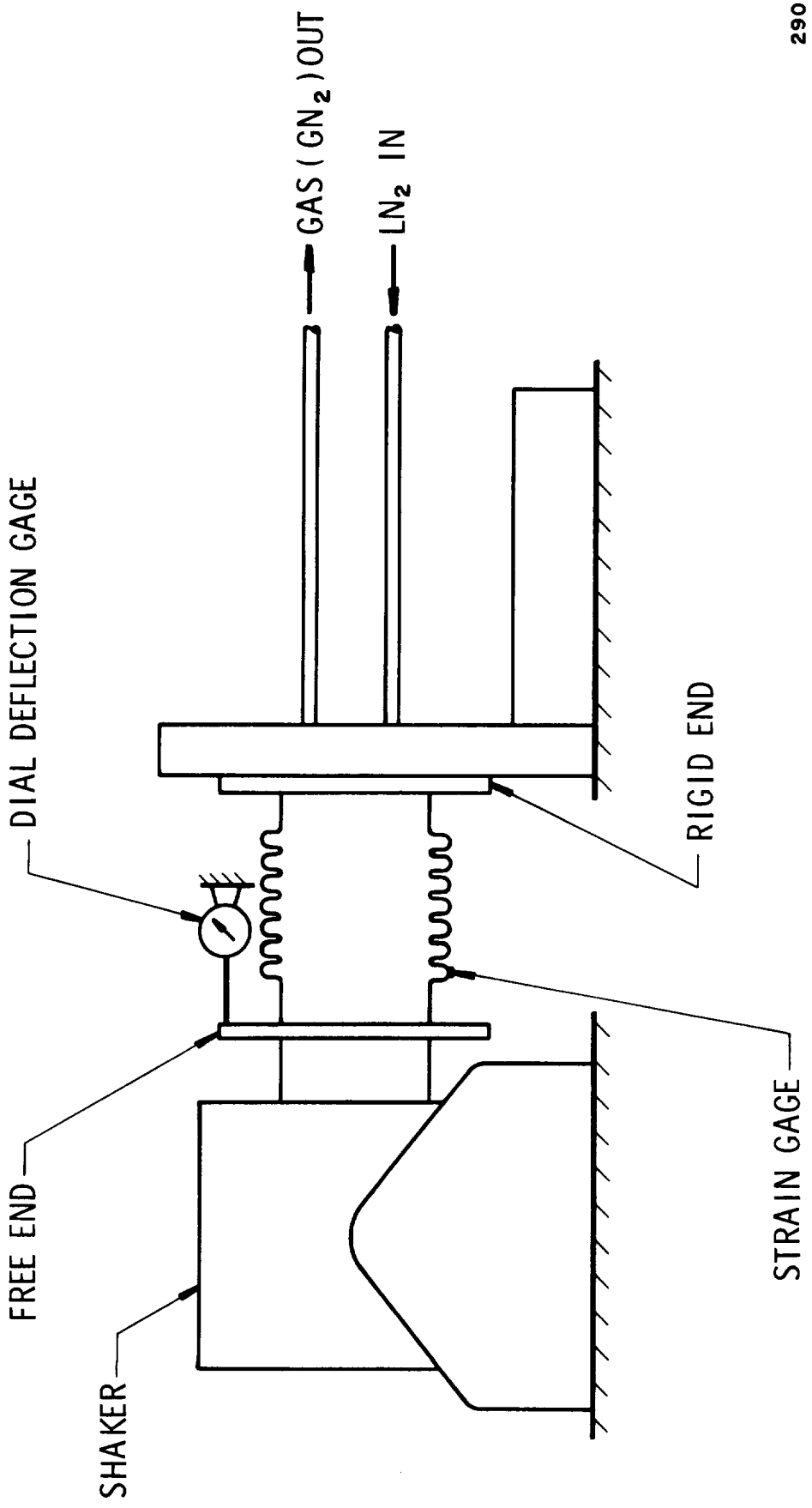

Figure 65. Strain Gage Temperature Calibration Set Up

to measure the movement of the free end while the shaker vibrated at a low frequency to simulate a dynamic loading on the bellows. This test was conducted with the bellows at room temperature, and again at -320°F by filling the bellows with boiling liquid nitrogen. The strain-deflection data for both temperatures is shown in Figure 66. The change in slope represents a change in gage factor of 4.5% at the cryogenic temperature which is very near the manufacturers specifications, therefore the dynamic strain data was verified for the low temperature conditions encountered in the tests.

The strain gage readout circuit consisted of a standard DC powered bridge which was AC coupled to an audio-frequency amplifier. The strain signal was displayed on an oscilloscope, and also plotted as a function of fluid velocity on an X-Y recorder. The DC equivalent of peak-to-peak strain was recorded as the ordinate, and the fluid velocity was recorded as the abscissa. A DC signal directly proportional to fluid velocity was obtained by connecting the turbine meter output to a frequency-DC converter.

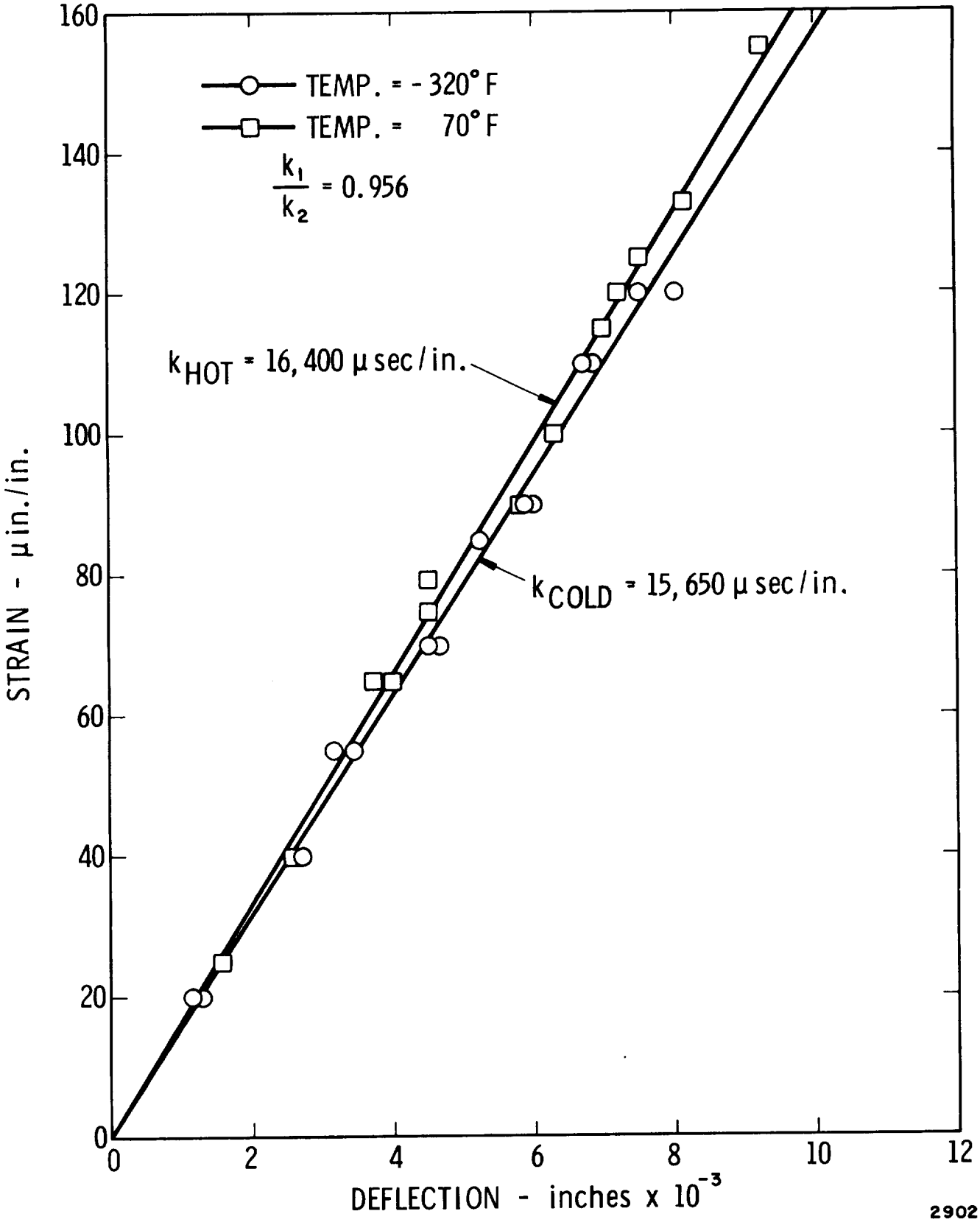

Figure 66. Strain Gage Calibration versus Temperature

IV. 3 Experimental Results

Introduction

The cryogenic flow loop described in the previous section was utilized to study bellows flow excitation for a number of fluid and surrounding conditions. Initially, a number of exploratory tests were conducted simply to get a feel for the overall problem. Following this, detailed tests of various kinds were conducted. To obtain a comparison of bellows response with LN_2 versus water, a series of tests were conducted with identical bellows using both mediums, but with heat transfer effects maintained at a minimum. Heat transfer effects with LN_2 were then studied by controlling the bellows environmental conditions (temperature, frost buildup and convection rate) and recording the strain levels at different flow rates and pressures. Finally, pressure drop data was obtained under varying heating rates and operating conditions to yield additional information on bellows operating characteristics. The results of these tests are discussed in the following sections.

Description of Test Bellows

Throughout this study, six different test bellows were employed. Dimensional data for these bellows is given in Table XIII.

Bellows #1, #2, and #6 have basically the same convolute geometry, except the pitch has been varied from the original configuration (#6) by stretching in one case (#1) and compressing in the other case (#2). Similarly, bellows #3, #4, and #5 have essentially the same geometry except for the pitch and were derived by the stretch and compression technique.

Initial Test Results and Effect of Back Pressure

When the testing of bellows with liquid nitrogen was first begun, it was observed that no matter what tank or system pressure the flow loop was operated at, the bellows would not vibrate except at the higher velocities, where low-level vibration of the higher frequency modes occurred. It was assumed that since the liquid nitrogen was so near the liquid-vapor line, a very small reduction in pressure, or increase in temperature, would cause cavitation, and hence, reduce or kill the vortex shedding excitation mechanism. (This assumption was later proved to be correct and is discussed in greater

Table XIII

Dimensional Data

Bellows #1 (Long 2.22)	Bellows #2 (Short 2.22)
I.D. = 1.49 h = .312	I.D. = 1.49 h = .36
O.D. = 2.22 λ = .345	O.D. = 2.22 λ = .187
Dm = 1.85 σ = .125	Dm = 1.85 σ = .125
N_c = 7 t = .013	N_c = 7 t = .013
N_p = 1 LL= 2.75	N_p = 1 LL = 1.5
Bellows #3 (2.02 Nom)	Bellows #4 (Long 2.02)
I.D. = 1.46 h = .27	I.D. = 1.46 h = .25
O.D. = 2.02 λ = .22	O.D. = 2.02 λ = .282
Dm = 1.74 σ = .144	Dm = 1.74 σ = .144
N_c = 8 t = .013	N_c = 8 t = .013
N_p = 1 LL = 1.52	N_p = 1 LL = 1.95
Bellows #5 (2.02 short)	Bellows #6 (2.22 N)
I.D. = 1.46 h = .28	I.D. = 1.49 h = .345
O.D. = 2.02 λ = .156	O.D. = 2.22 λ = .250
Dm = 1.74 σ = .125	Dm = 1.85 σ = .125
N_c = 8 t = .013	N_c = 7 t = .013
N_p = 1 LL = 1.25	N_p = 1 LL = 2.0

ID	=	internal diameter
OD	=	outside diameter
D_m	=	mean diameter
N_c	=	number of convolutes
N_p	=	number of plys
h	=	convolute height
λ	=	convolute pitch
σ	=	convolute tip width (internal)
t	=	ply thickness
LL	=	live length

detail in a later section of this report.) The first attempt to correct this condition and produce stronger flow excitation was to close a valve on the tank and let the pressure of the system build up. However, it soon became obvious that this was simply moving the fluid state to a point further along the liquid-vapor line, since the temperature was also increasing with the pressure (along the equilibrium or liquid vapor line). In order to increase the pressure at the bellows, and hopefully induce vibrations of the lower modes, a valve was installed into the loop (Figure 62) downstream of the bellows. This valve was used to restrict the flow and cause an increase in pressure in the bellows greater than the system pressure. This allowed an increase in pressure and only slight, if any, temperature increase in the bellows or test section. Therefore, the state of the fluid in the bellows could be arbitrarily adjusted away from the liquid-vapor line.

By closing the downstream valve in increments, successive increases in the bellows pressure was produced. The effect of increasing this back pressure can be seen in Figures 67 through 72 which present the maximum strain level recorded versus the bellows pressure at various values of the tank system pressure (P_T) for the six test items. In all cases it can be seen that the strain increases with increasing back pressure (P_B-P_T) up to a maximum where it levels off and becomes invariant with further increases in bellows pressure. More information of this phenomena is provided in a later section where the effects of heat transfer into the bellows is discussed.

Comparison of Liquid Nitrogen to Water

To provide a direct comparison of flow induced vibration phenomena with LN_2 and water, a series of tests were conducted in which heat transfer effects were minimized as much as was practical. The resultant data should, therefore, reflect basically any possible difference in the vibrations because of differences in the two flow media or because of bellows material property changes with temperature. To reveal possible geometry effects, all six test bellows were used for this series of tests.

Flow-induced vibration test results for the six bellows, with both water and LN_2 flows, are given in Figures 73 through 78. In all cases the data shown is for the first or lowest frequency longitudinal mode. In obtaining the LN_2 data, each bellows was run with a back pressure sufficient to minimize possible cavitation suppression of the vortex shedding. Also the bellows exterior was subjected to a cold GN_2 purge to prevent frost or liquid condensation which might cause unwanted external damping.

The test data presented in Figures 73, 74 and 75 show excellent agreement of the peak flow-induced strain levels for the two test liquids. In each case, the maximum strain is greater for water flow than for the

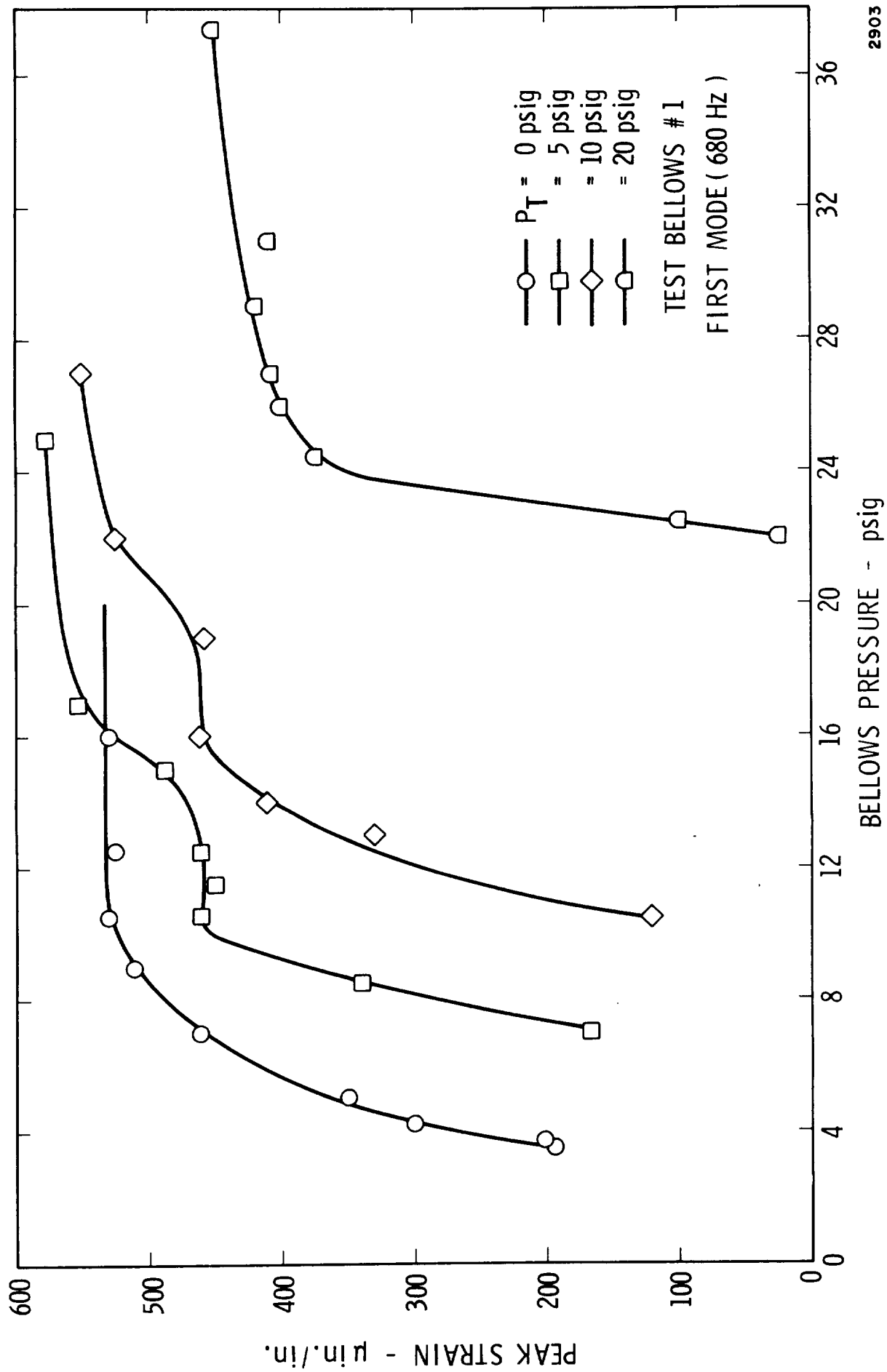

Figure 67. Pressure Sensitivity Of Flow Excited Bellows (# 1) With LN_2 Flow

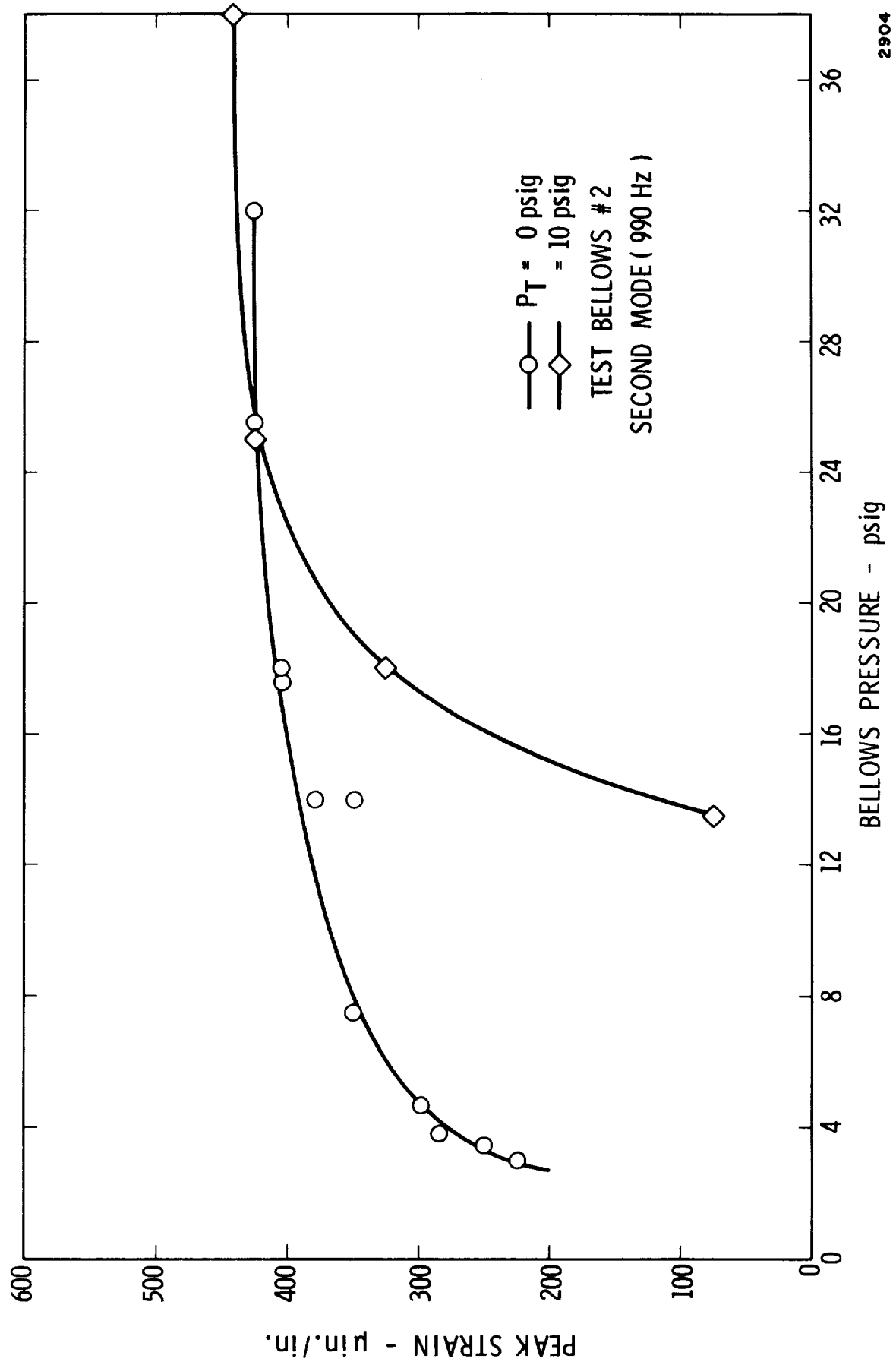

Figure 68. Pressure Sensitivity Of Flow Excited Bellows (# 2) With LN_2 Flow

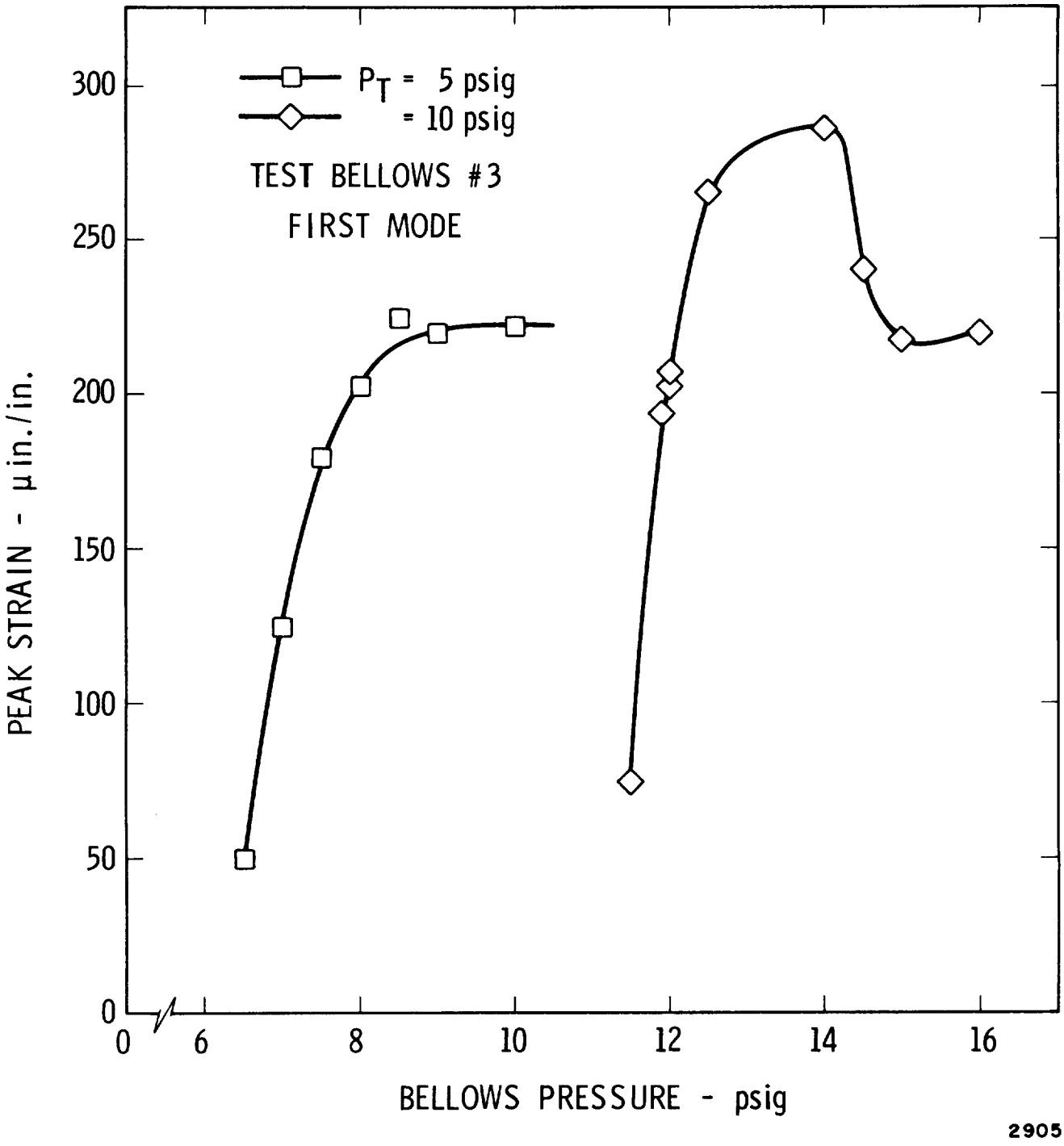

Figure 69. Pressure Sensitivity Of Flow Excited Bellows (# 3) With LN_2 Flow

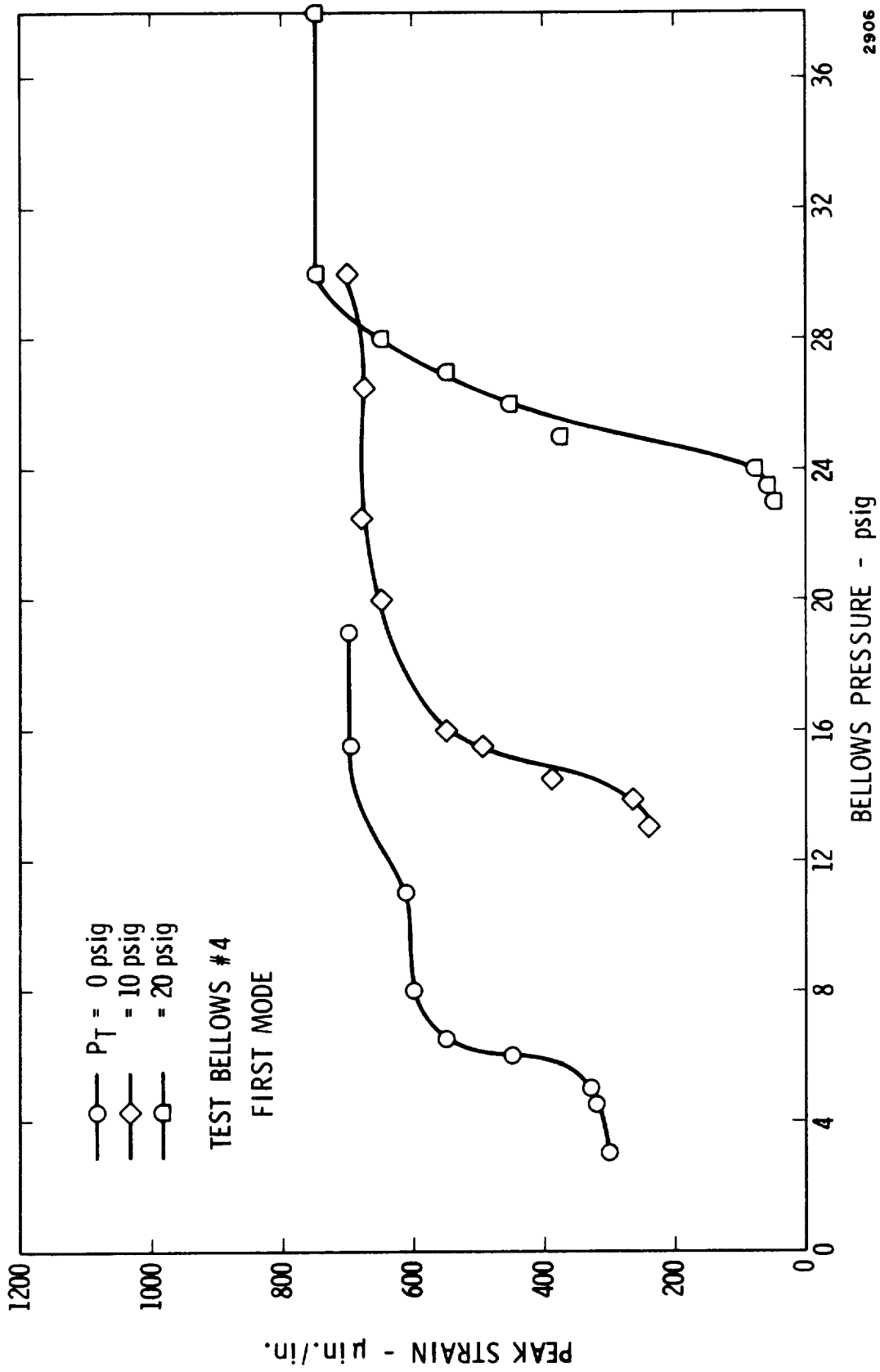

Figure 70. Pressure Sensitivity Of Flow Excited Bellows (# 4) With LN_2 Flow

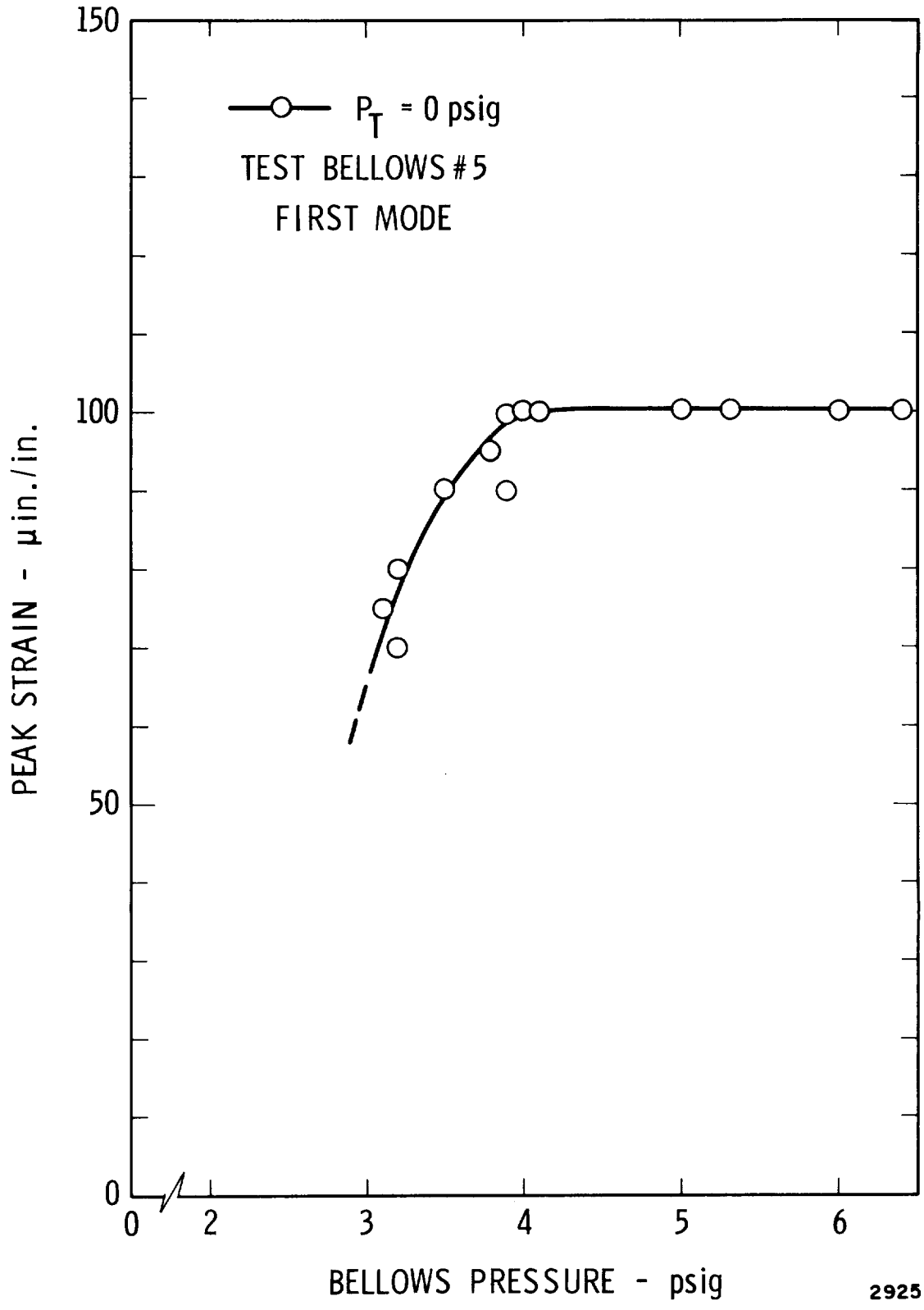

Figure 71. Pressure Sensitivity Of Flow Excited Bellows (#5) With LN_2 Flow

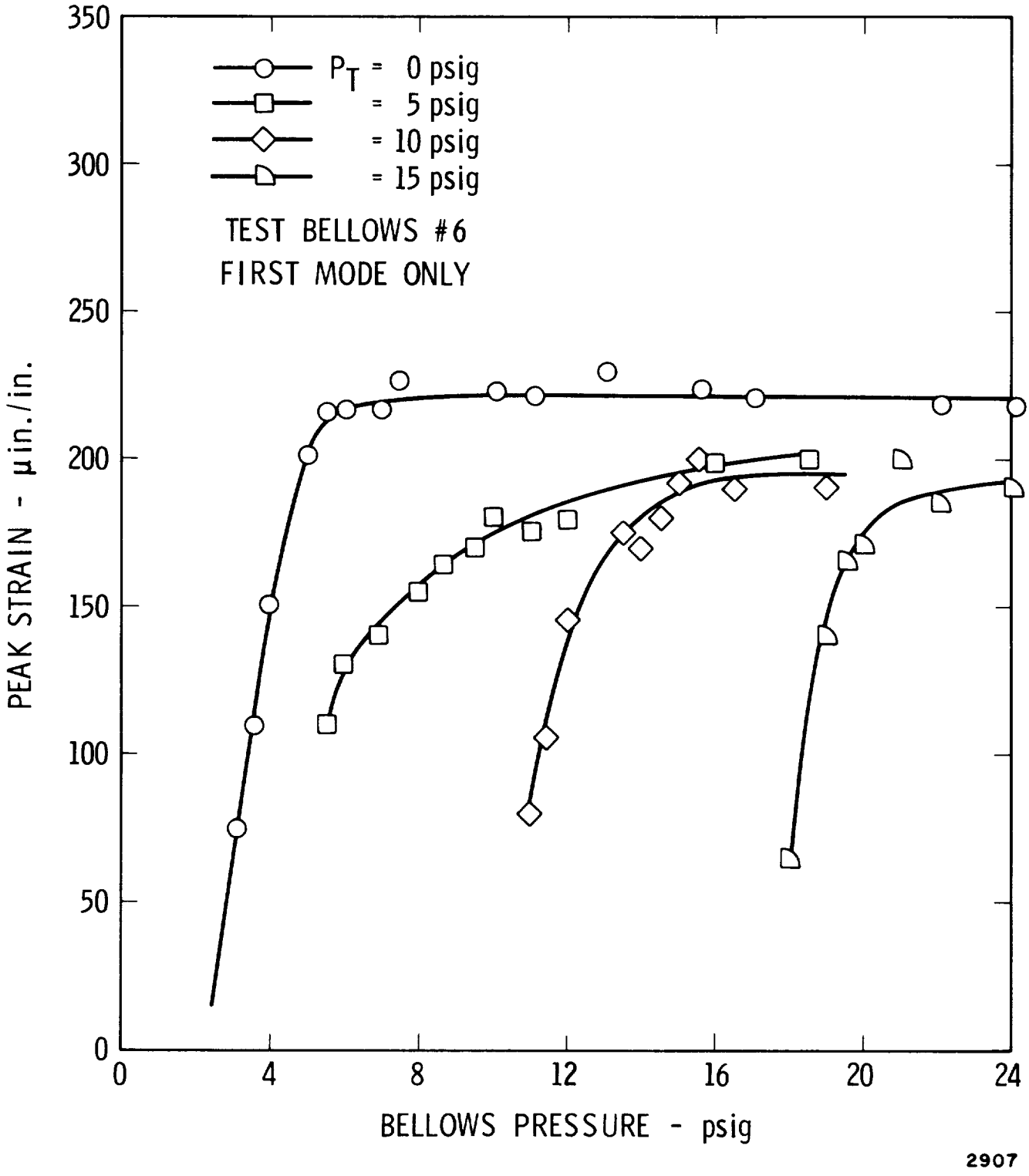

Figure 72. Pressure Sensitivity Of Flow Excited Bellows (# 6) With LN_2 Flow

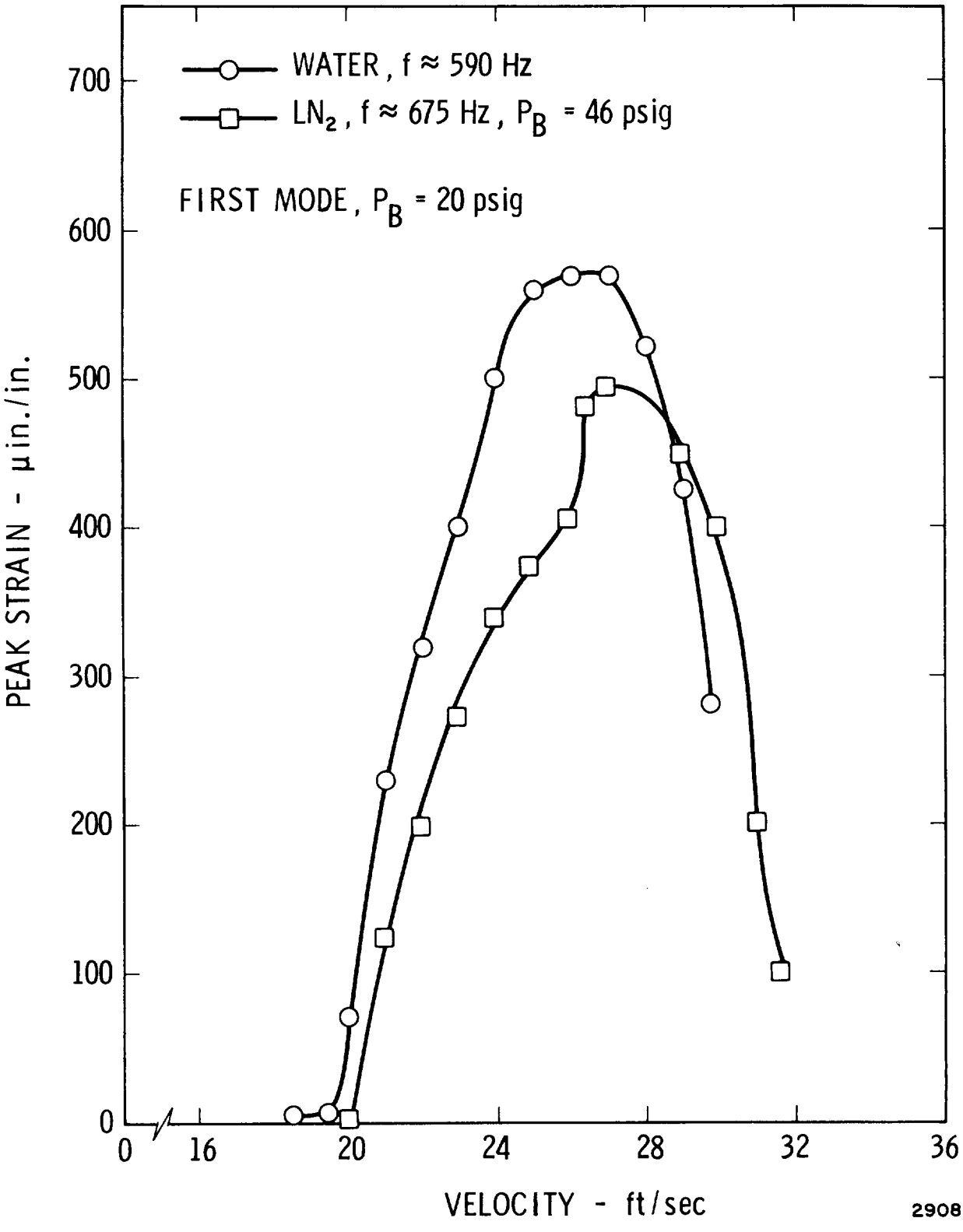

Figure 73. Comparison Of Flow-Induced Vibration With Water And LN_2, Bellows #1

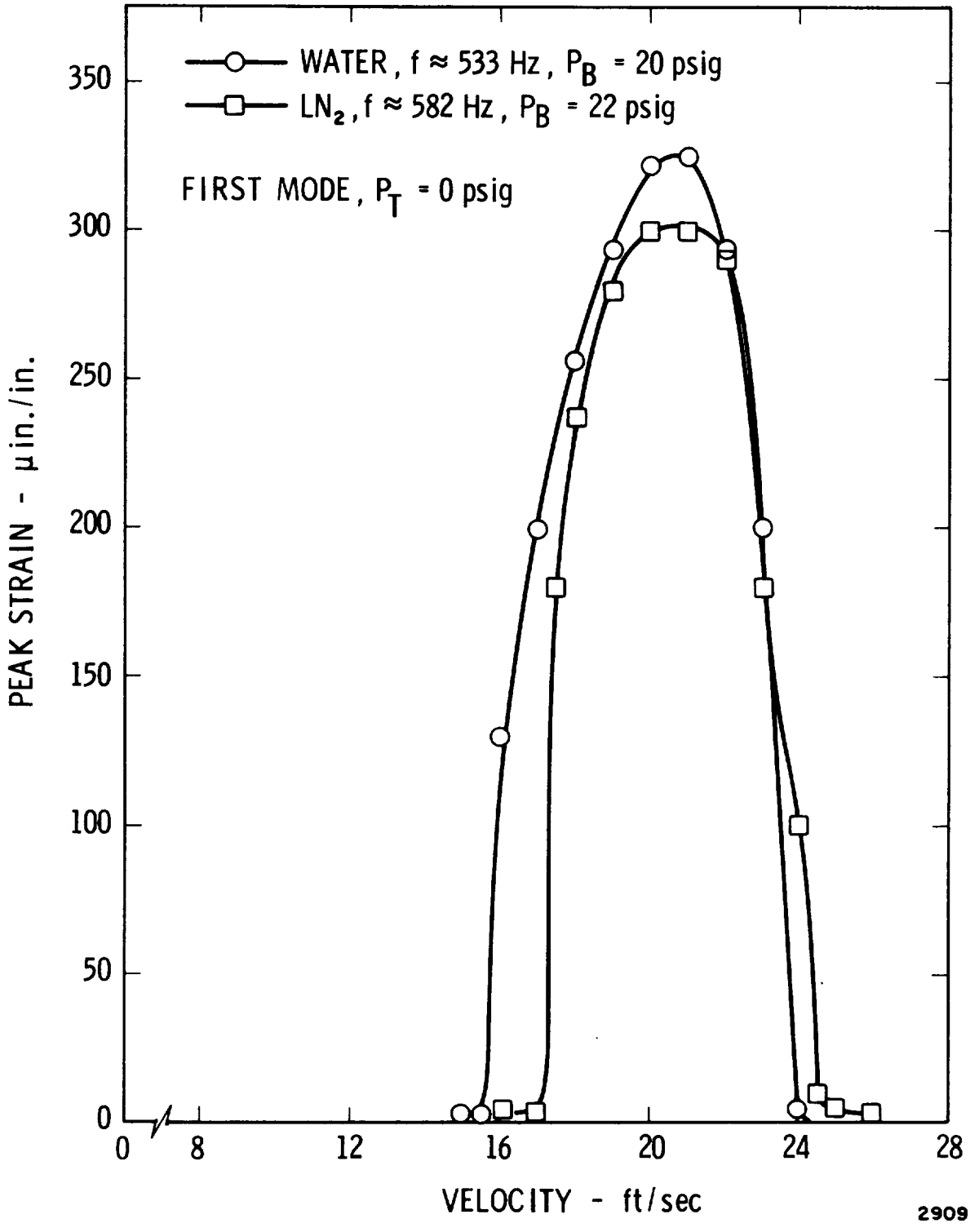

Figure 74. Comparison Of Flow-Induced Vibration With Water And LN_2, Bellows #6

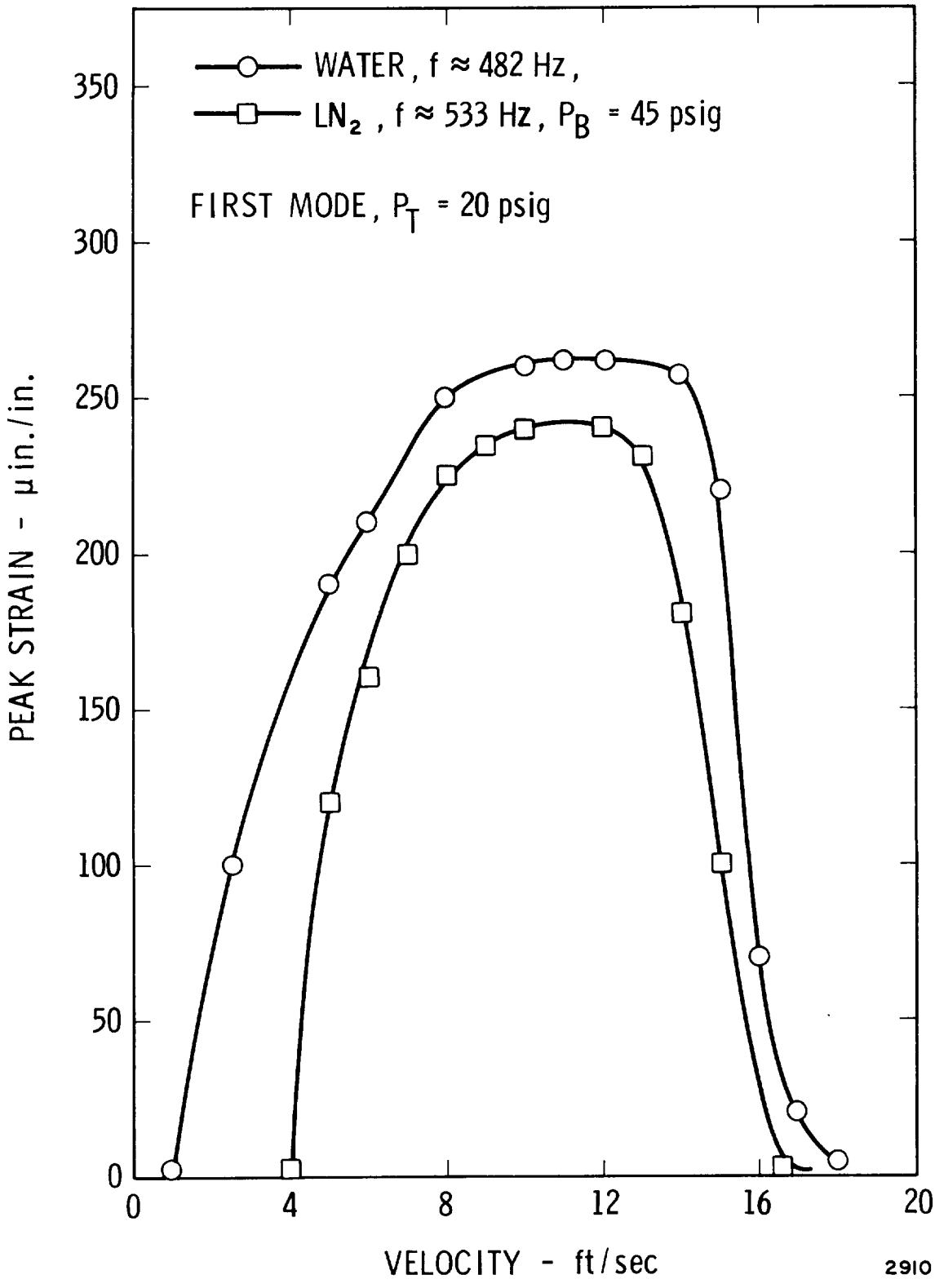

Figure 75. Comparison Of Flow-Induced Vibration With Water And LN_2, Bellows #2

LN_2 flow. This is to be expected since the LN_2 was less dense than the water, hence the vortex shedding excitation force, which is proportional to $1/2\,\rho\,V^2$, was less. The results given in Figures 73, 74 and 75 were for one series of bellows having essentially the same convolute geometry, except for the pitch.

Figures 76, 77 and 78 show a comparison of flow-induced vibration data for the second series of bellows with similar convolute geometry, except for pitch. This data does not show as good a correlation of the LN_2 and water results as did the results for the first bellows series (Figures 73, 74 and 75). The primary disagreement is in the velocity at which the peak strain occurs, since the LN_2 results peak at a velocity which is about 10 percent higher than the peak for the water data. Still, the agreement is good enough that we can conclude there are no major discrepancies between flow-induced vibration results for water and LN_2, if no cavitation suppression occurs and no external damping media is allowed to form.

Based on these results, we conclude that the theory presented in Sections II and III is valid for cryogenic fluids, as well as water, except for the limitations noted above which reduce the dynamic strain levels, hence are suppression effects. The remainder of this section is devoted to further discussion of results of studies of the suppression effects.

Bellows Response With Heat Transfer

Initial studies with a two-dimensional clear plastic flow channel and bellows segment revealed that the vortex shedding phenomena responsible for bellows flow induced vibrations could be completely suppressed by vapor addition in the convolute sections. This suppression was accomplished by passing water through the channel at the proper velocity for vibration and then blowing small air bubbles into the convolutes. The vortex shedding and bellows vibration was easily observed by injecting ink upstream of the convoluted segment, and viewing the shedding with a strobe light set near the shedding frequency. Once this condition was established, air bubbles injected into the convolutes completely killed off the shedding process and the convolute vibrations ceased. This observation led to the conclusion that if vapor, created by either cavitation, heat transfer, or a combined cavitation/heat transfer effect, was formed in a bellows flowing a liquid, then the flow induced response could be altered.

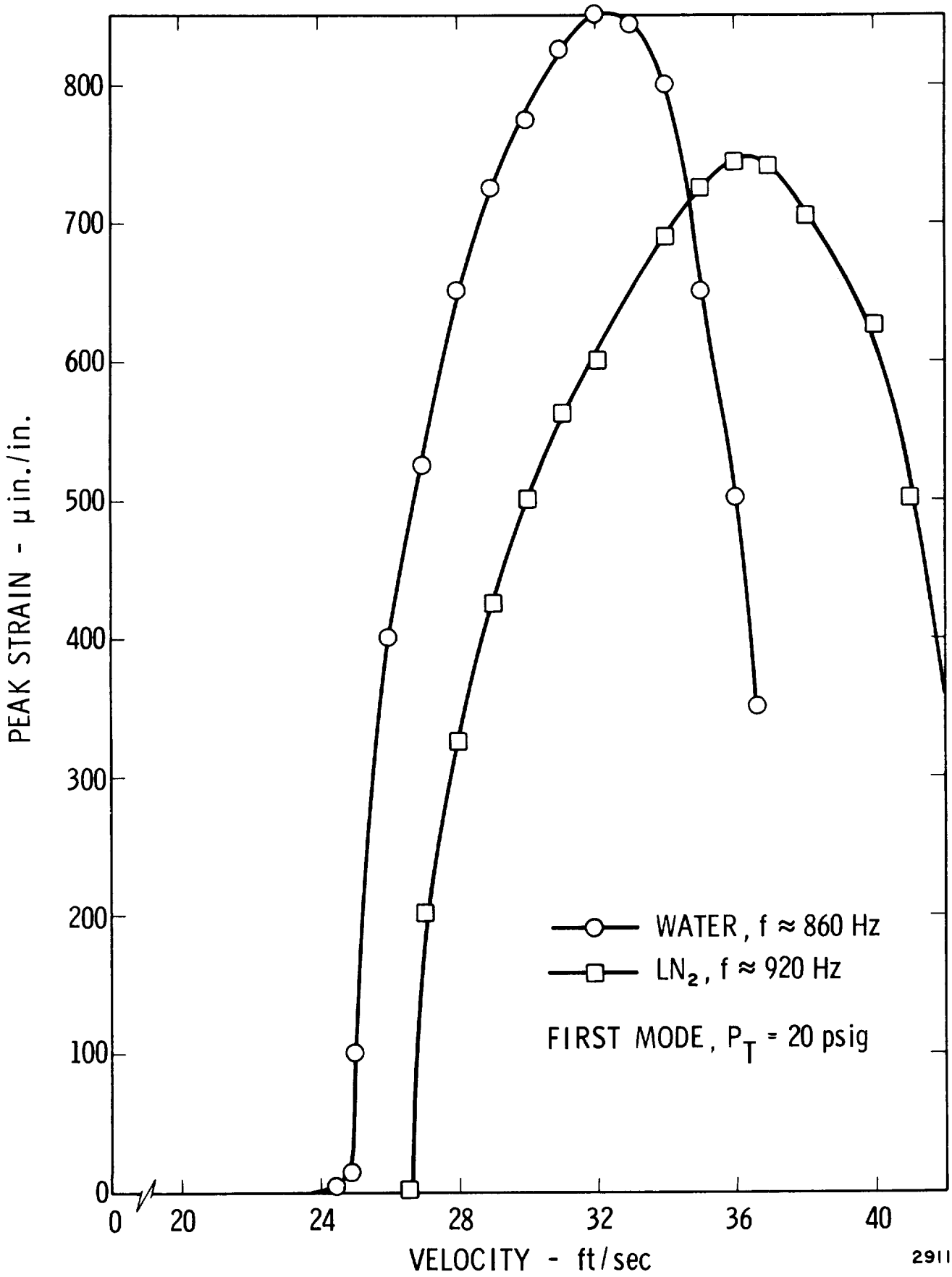

Figure 76. Comparison Of Flow-Induced Vibration With Water And LN_2, Bellows #4

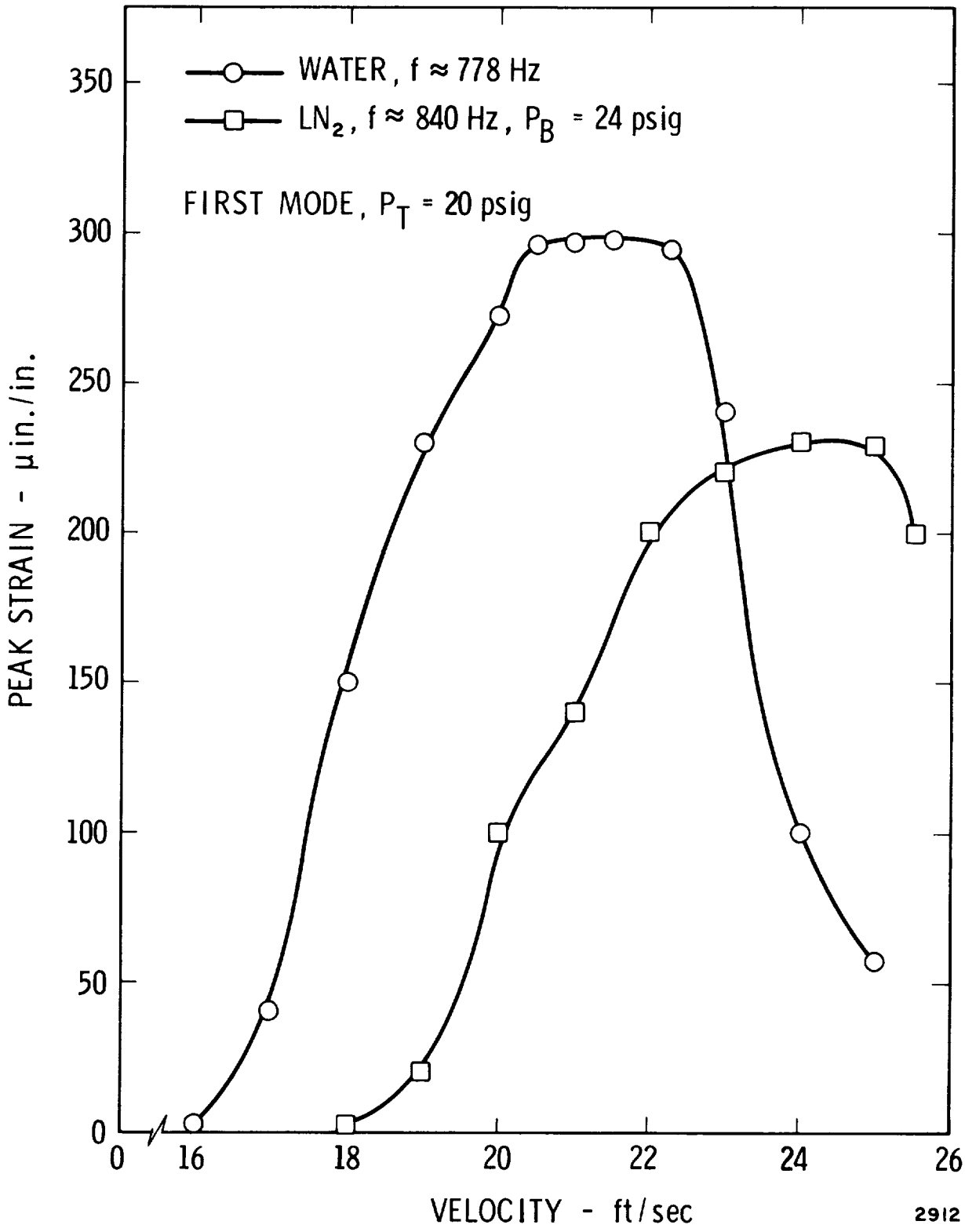

Figure 77. Comparison Of Flow-Induced Vibration With Water And LN_2, Bellows #3

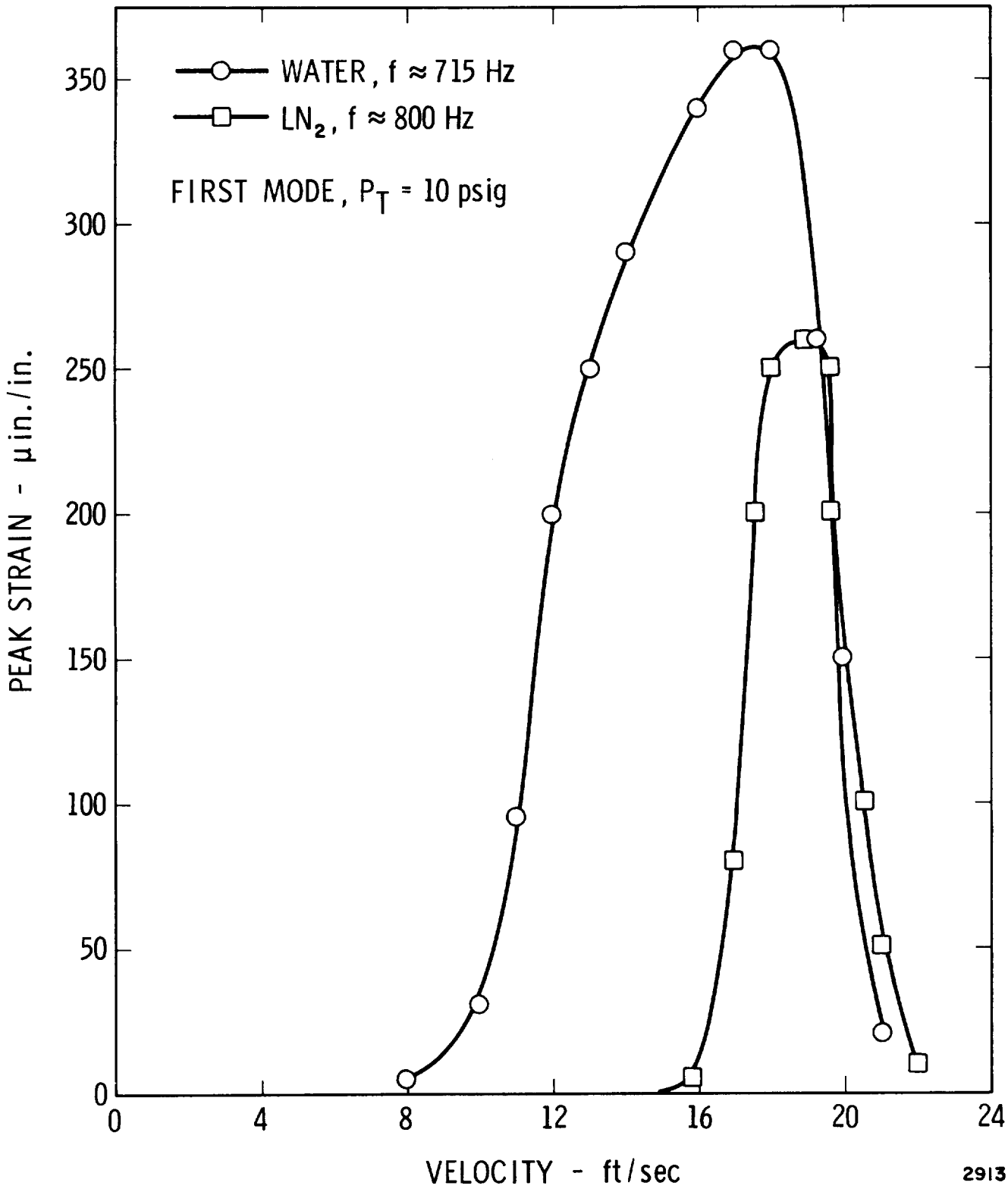

Figure 78. Comparison Of Flow-Induced Vibration With Water And LN_2, Bellows #5

To provide initial quantitative information of the effects of heat addition during operation of flow excited bellows, a duct was designed to surround the bellows completely so that hot air could be passed over the convolutes. A thermocouple was located at both the entrance and exit of this duct so that the change in air temperature could be recorded as it passed over the cold bellows containing flowing LN_2. From thermodynamics, the heat added or removed per-unit mass of a gas at constant pressure is given by

$$d\dot{Q}^* = c_p dT \tag{22}$$

where c_p is the specific heat at constant pressure of gas (air). For a flowing gas losing heat between arbitrary points 1 and 2, Equation (22) becomes

$$\dot{Q}^* = \dot{w}\, c_p\, (T_2 - T_1) \tag{23}$$

where $\dot{w}$ is the weight flow per unit time. This expression represents the heat input per unit time into the bellows section. In the experiment, the heating air weight flow, $\dot{w}$, was produced by a blower with a 20 amp heating element located at the entrance of the duct, and was calibrated by measuring the velocity and, hence, mass flow at the duct entrance. Since some of the heat was lost into the duct itself and not all absorbed by the bellows, a calibration of heat ($\dot{Q}^*_d$) lost to the duct alone was also made. This value was always subtracted from the total heat lost per unit time, $\dot{Q}^*$, to obtain the actual heat per unit time added to the bellows section alone, $\dot{Q}^*_B$, or

$$\dot{Q}^*_B = \dot{Q}^*_T - \dot{Q}^*_{duct} \tag{24}$$

With the flow loop operating at a velocity which produced maximum excitation of the first mode of the bellows, the heating rate was increased with time, and the resulting strain or stress amplitude was recorded. Typical results are shown in Figure 79, and these results indicate that increasing the heating rate produced a corresponding decrease in strain until a point was reached where the vibration was completely suppressed. Therefore, it was concluded that heat transfer did affect bellows response in a manner similar to vapor addition in the two dimensional visualization flow channel.

Bellows usually operate under conditions of approximately steady state heat transfer, therefore the results in Figure 79 for transient heating are not typical of bellows environmental conditions but do indicate the possible effects from heat transfer. Since vapor formation in the bellows

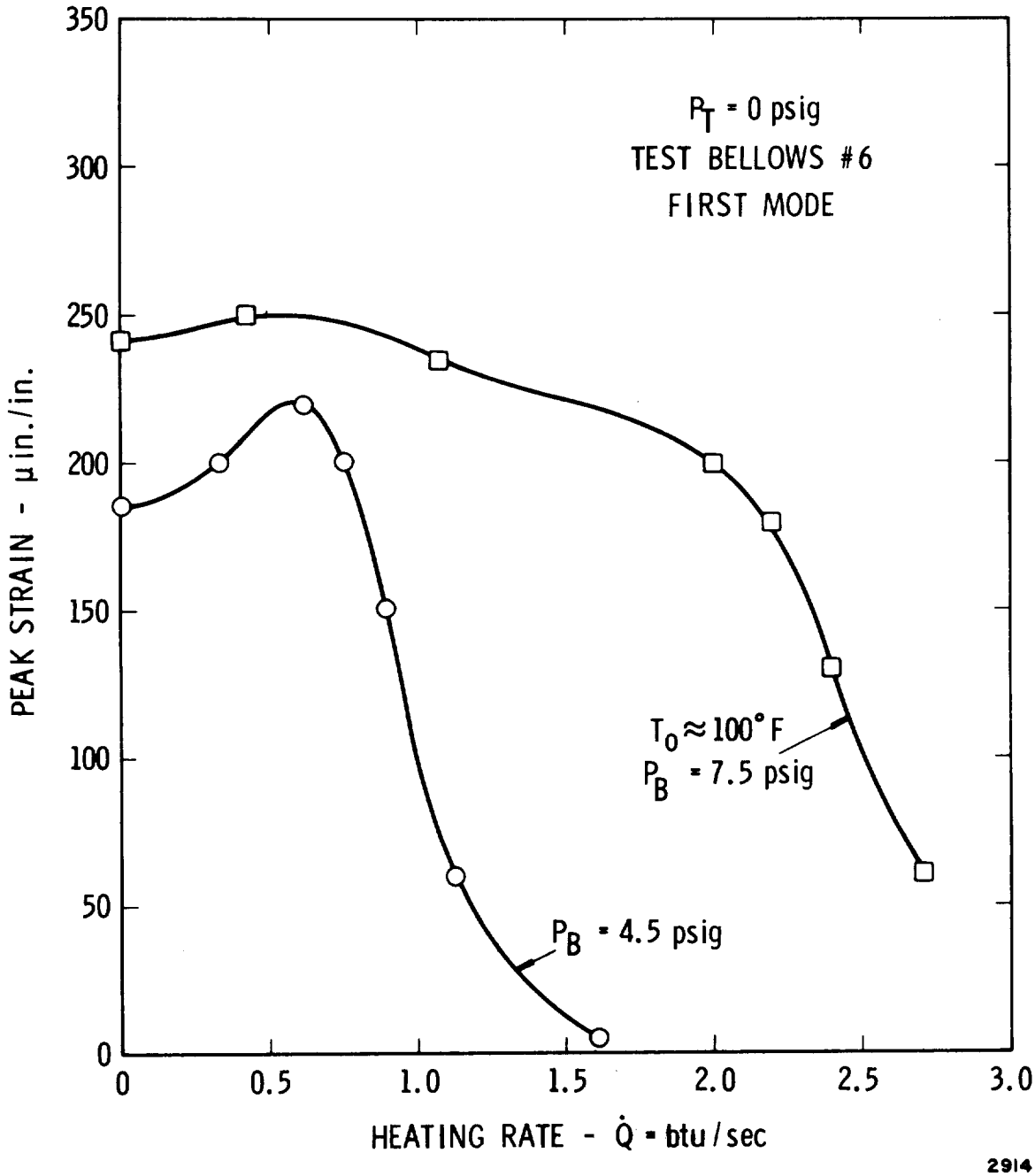

Figure 79. Effect Of Heating Rate On Maximum Strain Level

convolutes will be affected by operating pressure, (compare the results for P_B = 7.5 versus 4.5 in Figure 79) a test was conducted to determine the effect of bellows pressure on strain response with constant heat input. To produce these conditions, a bellows with flow excitation of its first mode was surrounded with cold GN_2 to maintain constant heat transfer, and the operating pressure was varied from 0 to 25 psig. Figure 80 shows the test results. This data is similar to that shown in Figures 67 to 72 for various bellows geometries. The strain response versus operating pressure shown in Figure 80 indicates that there is some minimum pressure at which the bellows will vibrate and produce maximum flow-induced strain. This pressure is indicated as P_{Bmax} in Figure 80 and is, then, the lowest operating pressure at which maximum strain will occur. As the pressure is decreased below P_{Bmax} the strain amplitude decreases rapidly until zero strain is recorded at P_{Bmin}, the highest operating pressure for no flow-induced vibration. Below P_{Bmin} no condition of flow excitation is observed. Therefore, under conditions of constant heat transfer there is a minimum operating pressure which will allow flow excitation to occur and produce vibrational strains in the bellows structure.

To better define the effects of heat transfer on P_{Bmax} and P_{Bmin}, additional experimental results were obtained at different levels of heating. Four conditions of heating were obtained by producing four levels of environmental temperatures, in the following ways:

(a) Surrounding the bellows with cold N_2 gas, $T_0 = -200^{\circ}F$

(b) Surrounding the bellows with cold N_2 gas-air, $T_0 = -145^{\circ}F$

(c) Surrounding the bellows with air, $T_0 = 45^{\circ}F$

(d) Surrounding the bellows with heated air, $T_0 = 285^{\circ}F$

For each of the four conditions of T_0, the bellows was operated at flow velocities corresponding to peak excitation of the first vibrational mode, and strain data was obtained over a range of operating pressures. The free stream temperature was $-320^{\circ}F$ (saturation temperature at 1 ATM in LN_2) for each heating level, and no frost was allowed to build up on the bellows external surface. At each test condition thermocouples recorded environment, skin and stream temperature. The results in Figure 81 show that as additional heat is added to the bellows, i.e., increasing T_0, the values of P_{Bmax} and P_{Bmin} are also increased. The same trend with increasing T_s is also shown in Figure 82 for a condition where the environmental temperature was held constant, and four levels of stream temperature

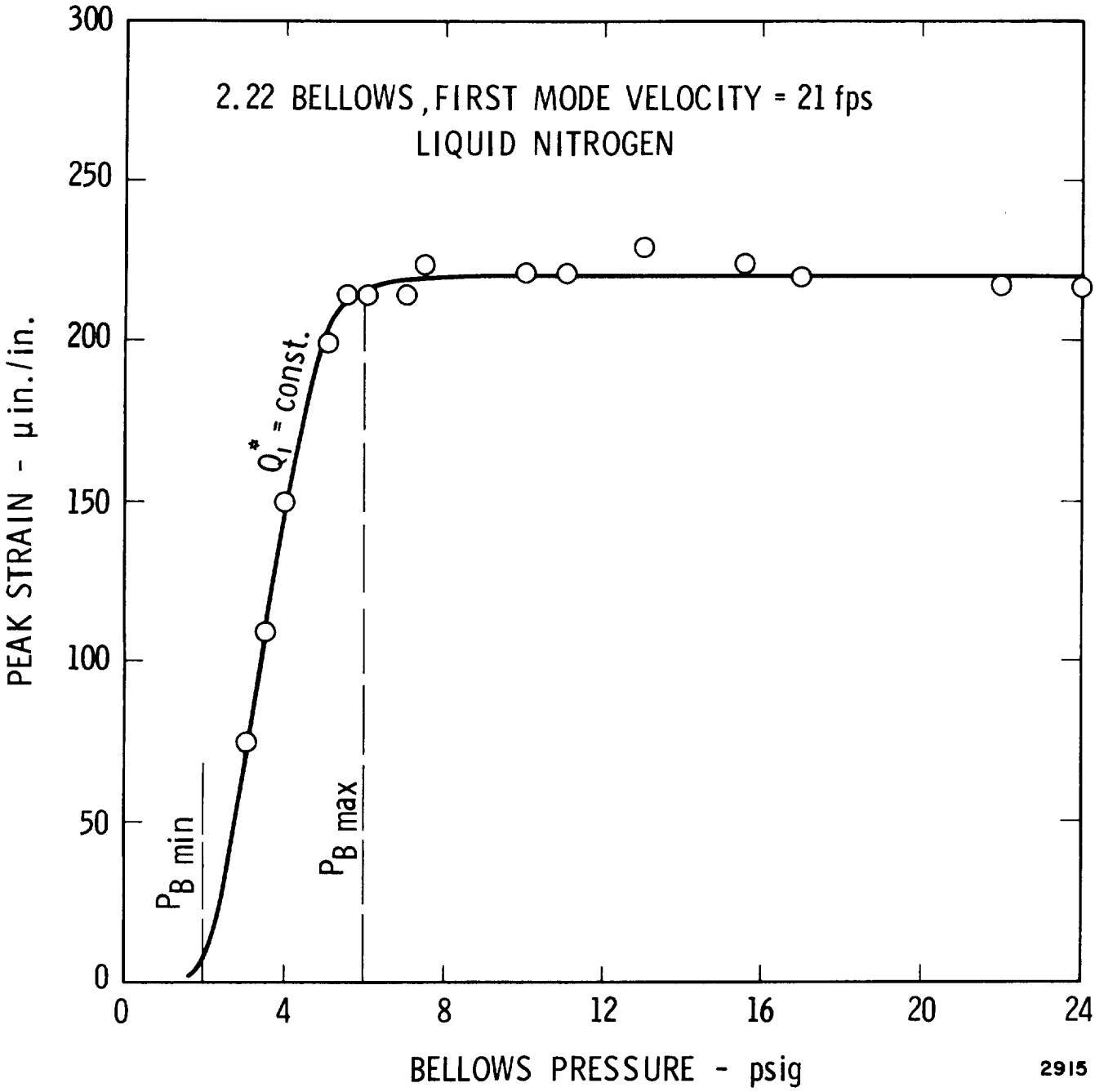

Figure 80. Effect Of Increasing Bellows Pressure On Maximum Strain Level

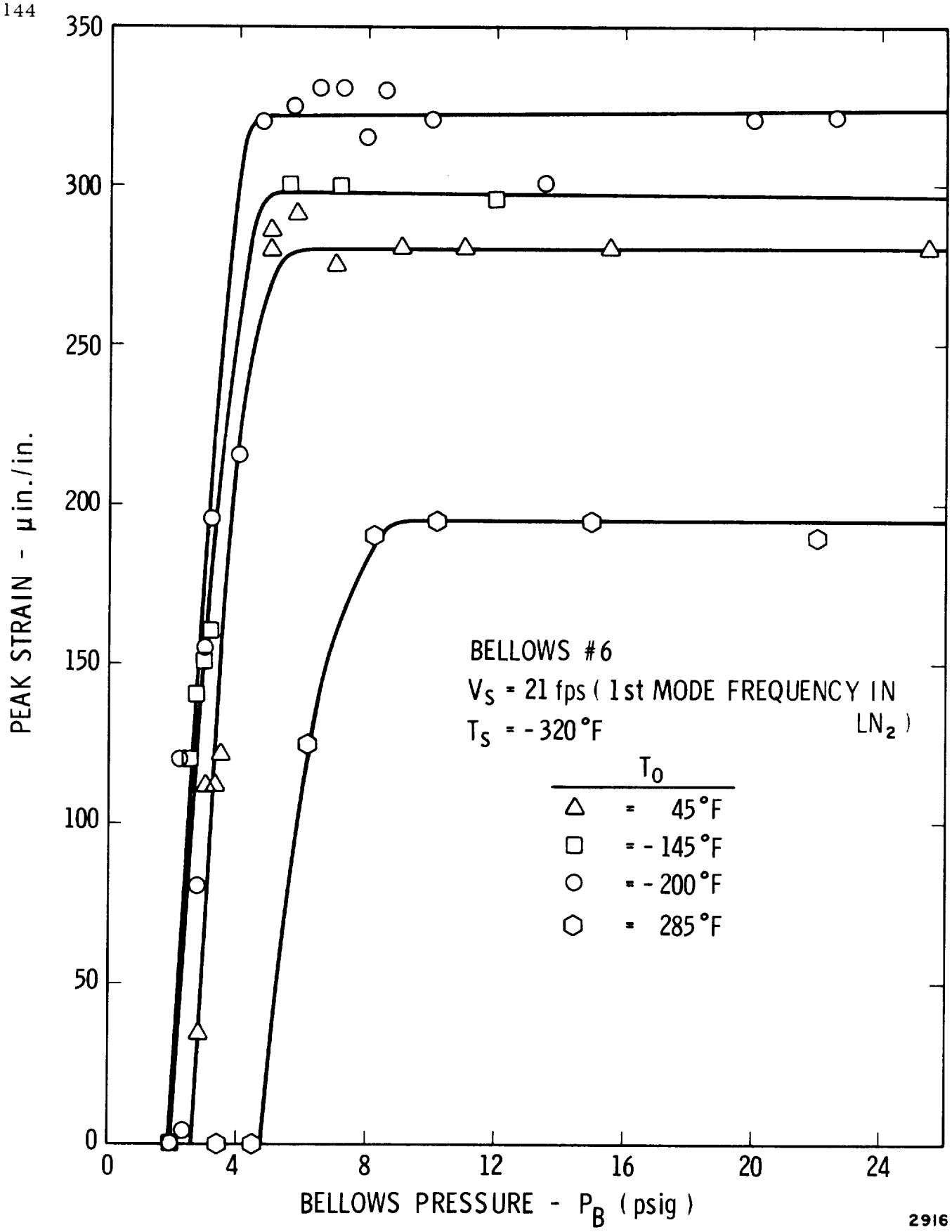

Figure 81. Effects Of Heat Transfer On Bellows Pressure At Zero And Maximum Strain With Different Environmental Temperatures

were used. The stream temperatures were increased by allowing the static LN_2 tank pressure to increase, which raised the system LN_2 temperature before it flowed through the bellows. The higher stream temperatures resulted in higher operating pressures required to insure peak strain.

The results in Figure 82 indicate that increased levels of heat transfer result in vapor formation at the low-operating pressures, hence producing a damping or complete suppression of the flow excitation. Increasing the operating pressure to P_{Bmax} will cause a recovery of the flow induced dynamic strain. The effect of an increased heat transfer rate is a corresponding shift of P_{Bmax} or P_{Bmin} with increasing stream temperature. Thus operating pressure must be increased to suppress vapor formation and maintain peak strain if

(a) The liquid is flowing at a given stream temperature and additional heat is transferred through the bellows wall raising the inside wall temperature and causing vapor formation in the convolutes, or

(b) The liquid stream temperature is increased by some change in operating conditions upstream of the bellows.

The bellows flow velocity required to produce peak flow-induced strain remained unchanged with changing heat transfer rates. The results in Figure 83 reveal this fact for the first mode frequency, which shows the peak excitation resulted at approximately 21 fps for all four environmental temperatures. An investigation of the theoretical bellows frequency change with large temperature changes supports the experimental results, showing no frequency shift should occur with different levels of bellows temperature. That is, the bellows frequency is given by

$$fo = \frac{1}{2\pi} \left(\frac{k}{m}\right)^{1/2} \tag{25}$$

where k is the bellows spring rate and m an elemental model mass composed of fluid and metal contributing terms. Large changes in temperatures will affect the spring rate k because of changes in Young's modulus, and will affect the model mass by changing the fluid mass from a liquid to a gas. However, these effects on the natural frequency are negligible, as the frequency decreases only 3 percent for changes in Young's modulus for stainless steel over a temperature range from -300°F to 100°F, while mass changes produced by the liquid vaporizing creates a frequency increase of 5 percent. The combined effect of both a change in Young's modulus and the model mass is a 2 percent increase in the bellows frequency for the 400°F temperature change. This change is considered insignificant since peak strain occurs over a band of frequencies larger than $\pm$ 2 percent of the mean.

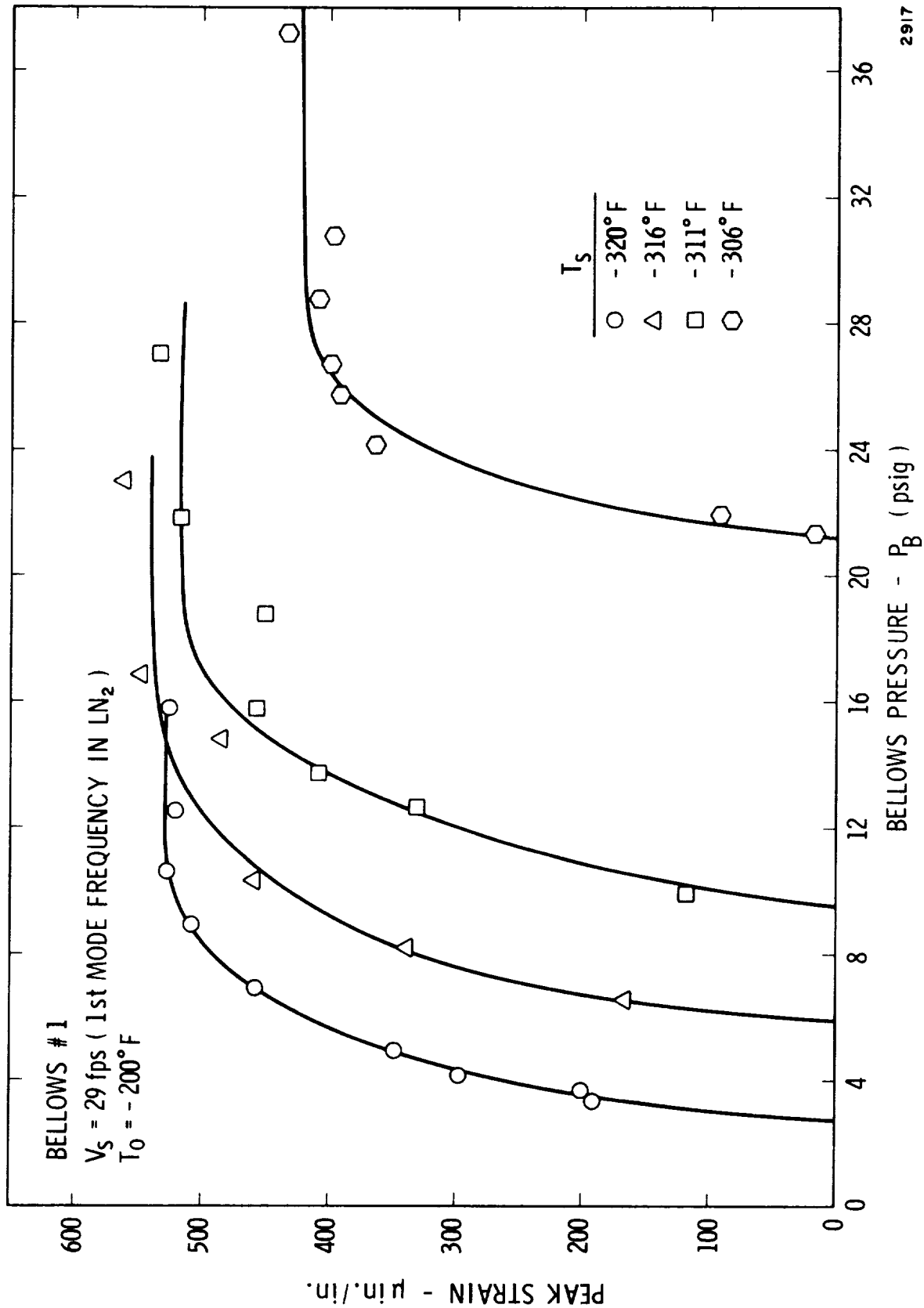

Figure 82. Effects Of Heat Transfer On Bellows Pressure At Zero And Maximum Strain With Different Stream Temperature

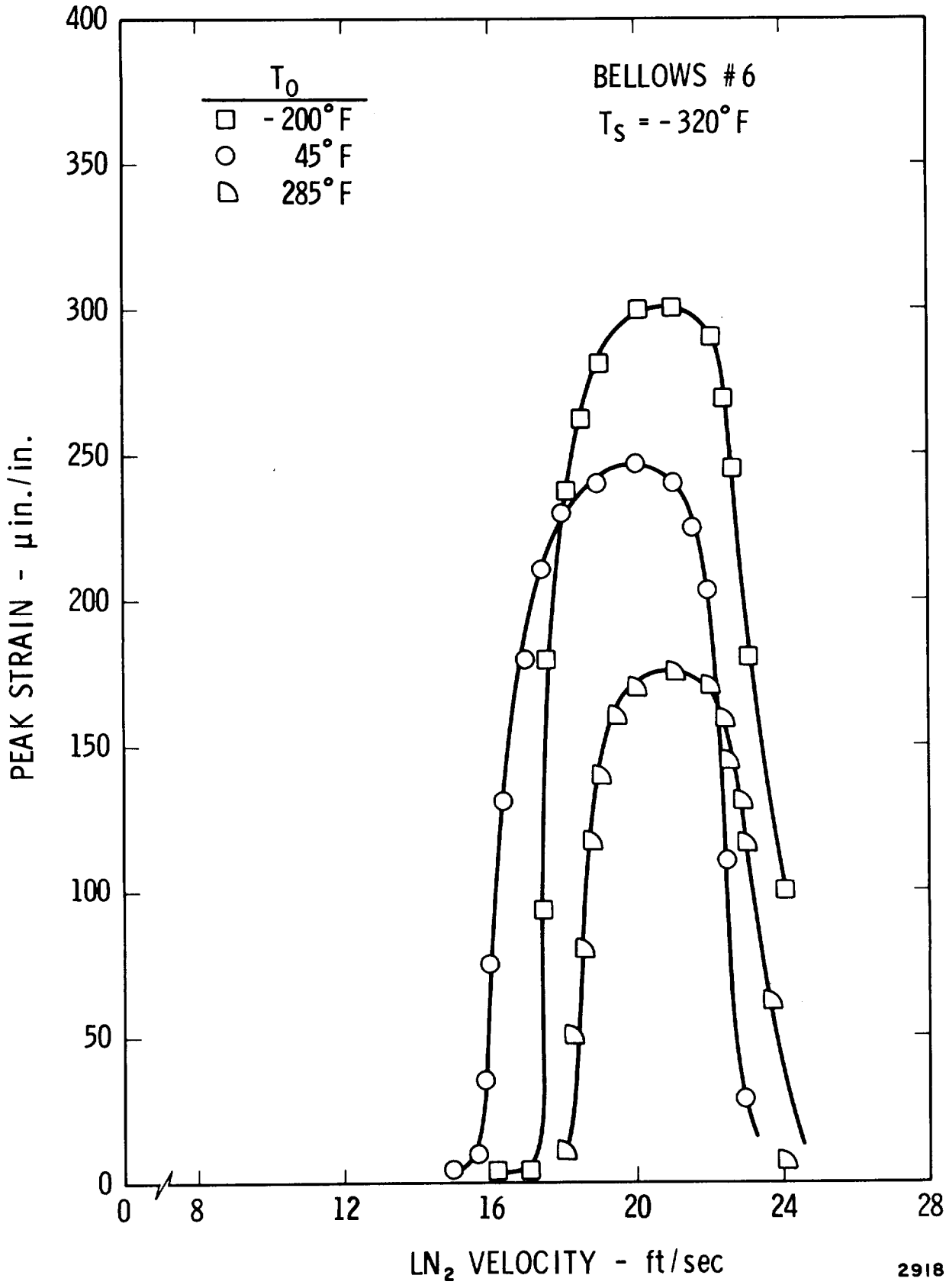

Figure 83. Effect Of Environmental Temperature On First Mode Frequency

Pressure Drop Data

The pressure drop across the bellows was recorded during tests to establish heat transfer effects with LN_2. The results of the pressure drop versus operating pressure are presented in Figure 84 for the case of $T_0 = -200^{\circ}F$. Results at the other test environmental conditions indicate the same trend in pressure drop across the bellows. The results in Figure 84 show that below P_{Bmin} an increase in pressure causes a decrease in pressure drop resulting from a reduction in the vapor formation in the flowing LN_2. Near P_{Bmin} additional increases in pressure cause enough suppression of the vapor phase so that vortex shedding begins to occur, and this causes disturbances in the flow and an increase in the pressure drop. Increasing pressure from P_{Bmin} to P_{Bmax} creates an increase in the pressure drop as the vibrational amplitudes build to a maximum. Increasing the pressure above P_{Bmax} results in decreasing the pressure drop since vibrational effects remain constant but the flow media progressing further into the liquid phase. Although results were not obtained at pressures higher than 20 psig, it is expected that the pressure drop would level off at the higher pressures and remain at a constant value.

The pressure drop data presented here indicates that bellows heating will not only create a change in the vibrational characteristics of bellows but will also alter their pressure drop characteristics.

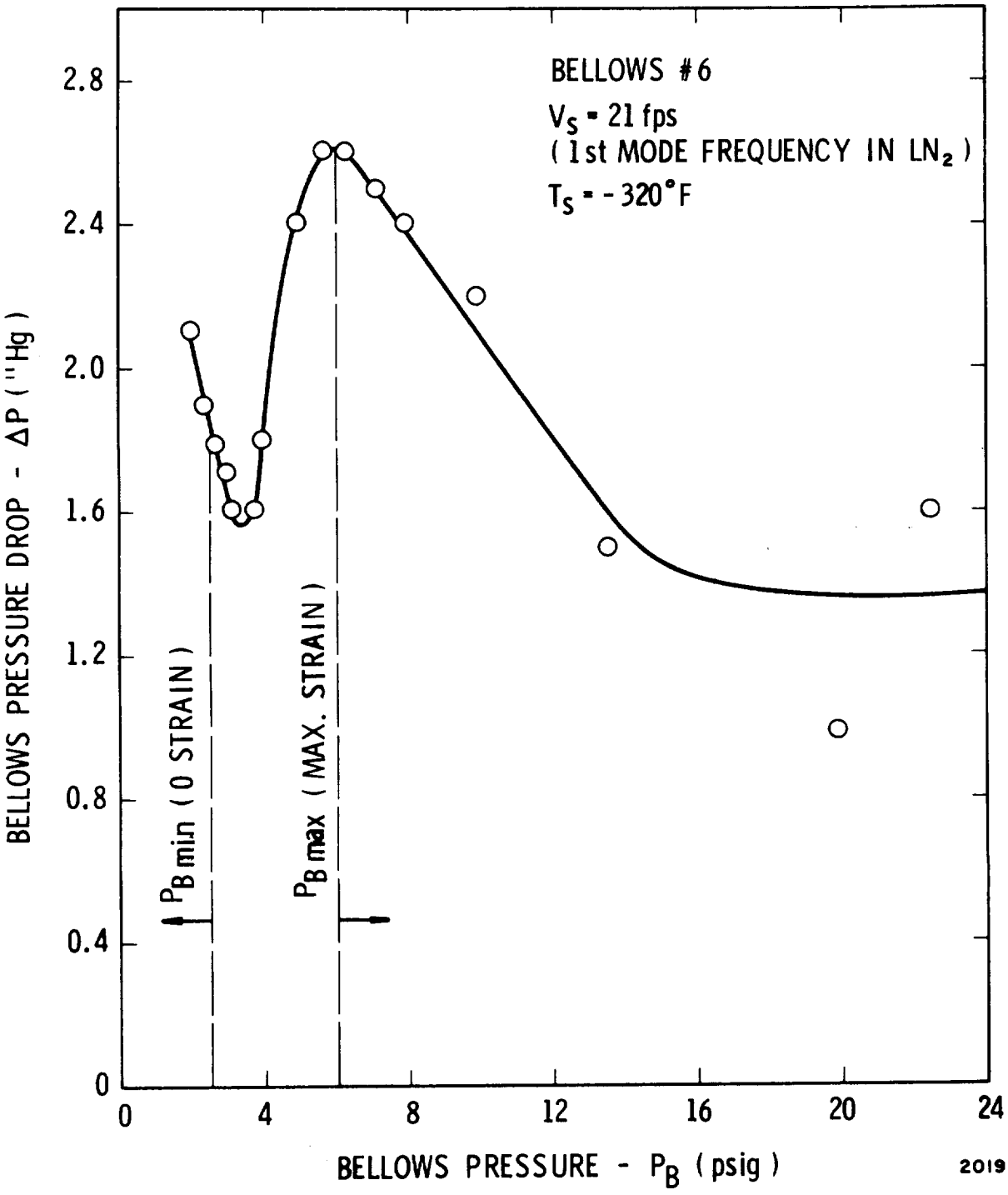

Figure 84. Bellows Pressure Drop versus Operating Pressure

IV.4 Heat Transfer Analysis

Introduction

The experimental results presented in the preceding section indicate that heat transfer to a flowing cryogen through a bellows wall can change the flow-induced response of the bellows by altering the vortex shedding phenomena. A concept of how this likely occurs is illustrated in Figure 85. For a condition of no heat transfer, the vortex shedding phenomena will behave as illustrated in Figure 85 . If, however, the fluid is heated somewhat, and the internal pressure is low enough, then cavitation in the vortex formation and shedding region can occur, and this will tend to reduce the vortex force; see Figure 85 . For even greater heating inputs, local boiling can occur in the convolutes as well, as shown in Figure 85 , this likely corresponds to a condition of complete suppression of the vortex shedding phenomena.

In order to gain a better understanding of the heat transfer effects, and to obtain a method for predicting the operating conditions at which the bellows response characteristics are altered, a heat transfer model has been developed. The model may be used to predict temperature distributions across the bellows between the environment and the flowing medium. A knowledge of this distribution, combined with a defining cavitation number, allows the operating pressures at the initial points of maximum and minimum dynamic strain to be correlated and predicted. The effect of frost formation on these pressures is also obtained, and a limiting frost thickness is determined for different environmental conditions.

Heat Transfer Model Development

Geometry

The bellows geometry, Figure 86, for purposes of setting up a heat transfer model, was assumed to be a thin walled cylinder of radius, r_m, equal to the mean radius of the bellows and of length ℓ corresponding to the actual expanded length along the convoluted surface. This length is given in terms of the bellows geometric parameters as

$$\ell = 2N_c \left(\frac{Do-Di}{2}\right) + \left(2N_c - 1\right) \sigma , \qquad (26)$$

and the corresponding wall area is

$$A_w = 2\pi r_m \ell$$

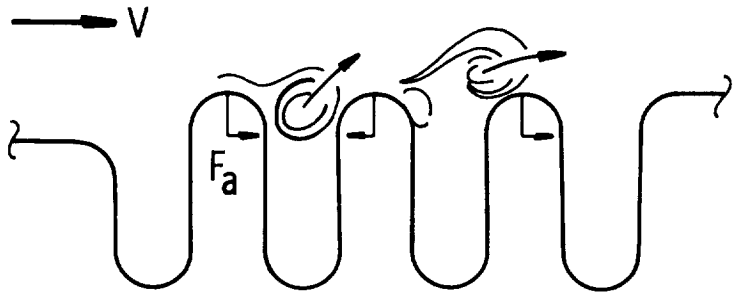

(a) NO HEAT INPUT - CONVENTIONAL VORTEX PHENOMENA

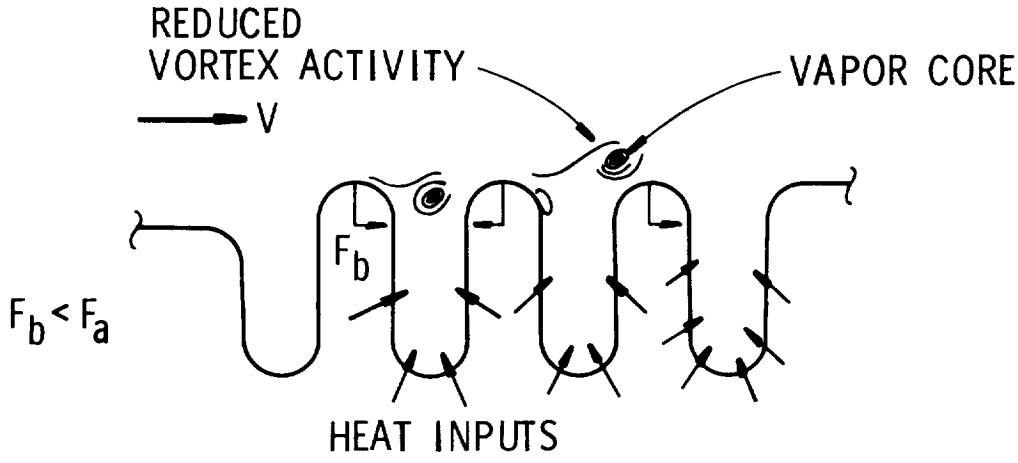

(b) EXTERNAL HEATING - VAPOR CORE IN VORTEXES

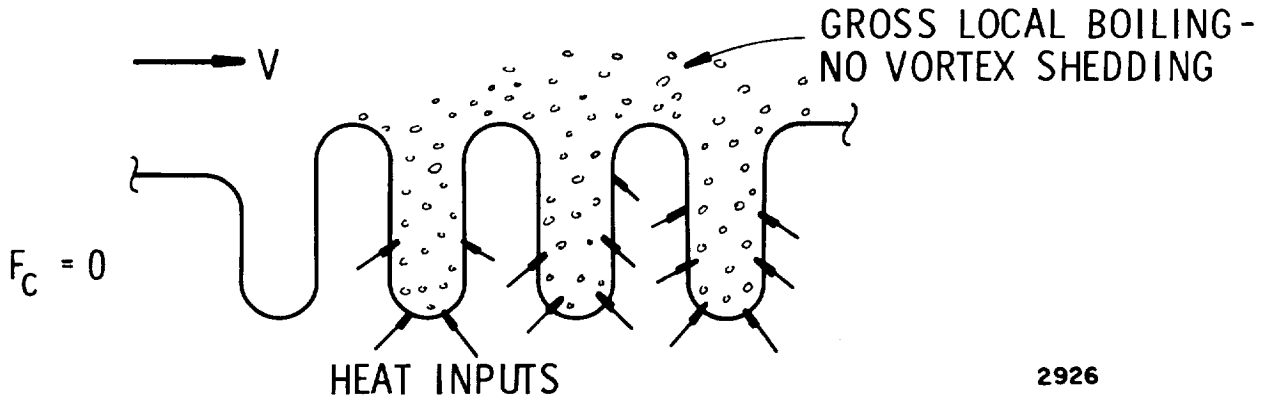

(c) EXTERNAL HEATING - GROSS BOILING

Figure 85. Illustration Of Heating Effect On Bellows Vortex Shedding Flow Excitation

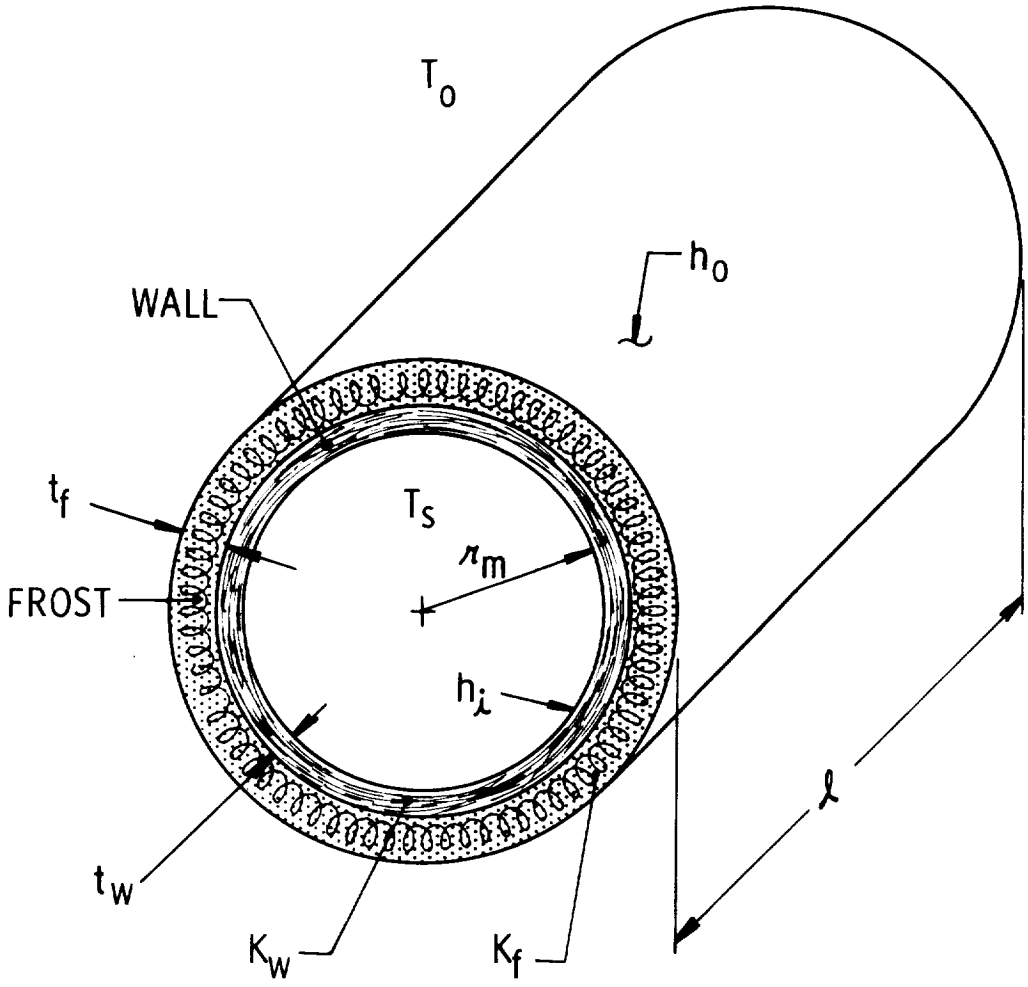

$$r_m = \frac{r_i + r_o}{2}$$

$$\ell = N_c \left(\frac{r_o - r_i}{2}\right) + (2N_c - 1)\ \sigma$$

$$A_{wi} = 2\pi r_m \ell$$

$$A_{wo} = 2\pi\ (r_m + t_w + t_f)\ell$$

Figure 86. Bellows Geometry for Heat Transfer Model

Heat Transfer

The heat transfer was assumed to be one-dimensional steady-state conduction and convection in the radial direction of the thin-walled cylinder, with no conduction along its length.

The heat transferred between the bellows environment, at temperature T_0, and the flowing liquid at T_s is given by

$$\dot{Q}^* = \frac{T_0 - T_s}{\Sigma R} \tag{27}$$

where

$$\Sigma R = R_1 + R_2 + R_3 + R_4$$

which is the total resistance to heat transfer caused by the thermal potential, T_0-T_s. The resistances are defined as follows:

$$R_1 = \frac{1}{A_{wo}\, h_o} \tag{28}$$

which is the convection resistance between the environment and the outside surface (frost or wall).

$$R_2 = \left[\ln\left(\frac{r_m + t_w + t_f}{r_m + t_w}\right)\right]\left(\frac{1}{2\pi \ell\, K_f}\right) \tag{29}$$

is the conduction resistance of the frost at thickness t_f and having a thermal conductivity K_f;

$$R_3 = \left[\ln\left(\frac{r_m + t_w}{r_m}\right)\right]\left(\frac{1}{2\pi \ell\, K_w}\right) \tag{30}$$

is the conduction resistance of the wall at thickness t_w and with thermal conductivity K_w;

and

$$R_4 = \frac{1}{h_i A_{wi}} \tag{31}$$

is the convection resistance between the inside wall and the free stream.

In order to utilize these equations to obtain heating rates and temperatures, a knowledge of the inside and outside convection coefficients, h_i and h_o, must be known as well as the bellows geometry, and thermal conductivity, K_w, and the frost conditions, t_f and K_f. The most difficult parameter to estimate is the inside heat transfer coefficient, h_i, which depends on the state of the LN_2 in the convolutes. That is, can the heat transfer between the inside wall and the stream be described as

(a) Forced convection with minimum boiling ($T_{wi} - T_s < 5^o$)

(b) Forced nucleate boiling ($5^o < T_{wi} - T_s < 20^o$)

(c) Forced unstable film boiling ($20 < T_{wi} - T_s < 60^o$), or

(d) Forced film boiling ($T_{wi} - T_s > 60^o$) ?

The temperature ranges given above are for pool (static fluid) boiling, but a review of experimental data of forced flow boiling heat transfer to cryogenic fluids indicates that these ranges are approximately correct for forced flow boiling also. While a tremendous amount of work has been done on pool boiling of liquids, few correlations exist for forced flow boiling heat transfer. Some experimental work and a few analytical studies are available as a guide.

If Case (a) represents the heat transfer in the convolutes then the work of Nunner (14) can be used to estimate h_i, thus

$$\frac{Nu_d}{Re_d Pr^1} = \frac{0.0384\,(Re_d)^{-1/4}}{1 + A\,(Re_d)^{-1/8}\,(P_r{}^1 - 1)} \tag{32}$$

where

$$P_r{}^1 = P_r\,(f/f_o) \tag{33}$$

$$A = 1.5\,(P_r{}^1)^{-1/6}$$

and the bellows friction factor, f^*, and that for a smooth pipe, f_o^*, are determined for the bellows Reynolds number, Re_d.

If Case (b) is valid where nucleate boiling dominates, then from Reference 15, h_i is given by

$$\frac{C_p(T_{wi} - T_s)}{h_{fg}} = a \left\{ \frac{h_i(T_{wi} - T_s)}{\mu_\ell\, h_{fg}} \right\}^{1/3} \cdot \left\{ \frac{\tau}{g(\rho_\ell - \rho_v)} \right\}^{1/6} P_r{}^{1.7} \tag{34}$$

where $0.0022 < a < 0.015$.

For Case (c) Bromley (16) estimated h_i by

$$h_i = C \left\{ \frac{V_\infty K_v \rho_v \lambda^1}{D_w (T_{wi} - T_s)} \right\}^{1/2} \tag{35}$$

where

$$\lambda^1 = h_{fg} \left\{ 1 + \frac{0.4 (T_w - T_s) C_{pv}}{h_{fg}} \right\}$$

and C = 2.7 for forced flow over horizontal tubes.

Once the state of the fluid in the convolutes has been determined then either Equation (32), (34) or (35) may be used in the analysis. If unstable film boiling exists ($20 < Tw-Ts < 60^\circ F$) no analytical method is available, and an extrapolation between nucleate and film boiling must be used.

The outside convection coefficient, h_o, can be determined from correlations for the forced flow of air over cylinders, by

$$\frac{h_o D_o}{K_{air}} = C \left(\frac{V_{air} D_o}{\nu_{air}} \right)^m \tag{36}$$

where C and m are functions of Reynolds number, or from the literature when natural convection is considered. Typical values of h_o for natural convection of air to cylinders range from 1 to 5 Btu/hr ft^2 $^\circ F$.

Pressure at Peak and Zero Strain

With the heat transfer model in hand, the bellows inside wall temperature can be determined by

$$T_{wi} = T_s + \overset{*}{Q} R_4 \tag{37}$$

Knowing T_{wi}, an estimate of the bellows operating pressure at peak and zero strain can be obtained from a set of cavitation numbers defined as

$$\sigma_m = \frac{P_{Bmax} - P_v @ T_{wi}}{q_\infty} \qquad \text{(Cavitation number at peak strain)} \tag{38}$$

$$\sigma_o = \frac{P_{Bmin} - P_v @ T_{wi}}{q_\infty} \qquad \text{(Cavitation number at zero strain)} \qquad (39)$$

where P_v at T_{wi} is the vapor pressure corresponding to the inside wall temperature and q_∞ is the dynamic stream pressure. The vapor pressure, P_v, is given by the relation (Reference 17)

$$\text{Log}_{10}\ P_v\,(\text{ATM}) = A_1 + A_2/T_{wi} + A_3\,T_{wi} + A_4\,T_{wi}^2 + A_6\,T_{wi}^3 + A_6\,T_{wi}^4 + A_7\,T_{wi}^5 \qquad (40)$$

where

$A_1 = 5.27805(10^{-1})$

$A_2 = 3.0507339(10^{-2})$

$A_3 = 1.6441101(10^{-1})$

$A_4 = 3.1389205(10^{-3})$

$A_5 = 2.9857103(10^{-5})$

$A_6 = 1.4238458(10^{-7})$

$A_7 = 2.7375282(10^{-10})$

and T_{wi} in ^oK.

The cavitation numbers at peak and zero strain, together with the inside wall temperature, LN_2 flow velocity and density, allow P_{Bmax} and P_{Bmin} to be calculated.

To determine P_{Bmin} and P_{Bmax} for a given bellows operating and environmental condition:

(a) Calculate T_{wi} from heat transfer analysis.

(b) Determine P_v at T_{wi}

(c) Calculate P_{Bmin} from σ_o (determined experimentally)

(d) Calculate P_{Bmax} from σ_m (determined experimentally)

The experimentally determined cavitation numbers are presented in the next section.

Results

Cavitation Numbers at Peak and Zero Strain

The model presented in the preceding section requires a knowledge of the cavitation number in order that an estimate of the operating pressures at peak and zero strain may be made. The experimental P_{Bmax} and P_{Bmin} data presented in Figures 81 and 82, together with the heat transfer model (which yields P_v at T_{wi}) allowed σ_o and σ_m to be determined. To utilize the heat transfer equations, the inside convection coefficient h_i was determined from Equation (32), and the outside coefficient h_o was assumed to be 4 Btu/hr ft^2 ^oF. Use of Equation (32) to determine h_i was based on the fact that experimental values of outside bellows skin temperature obtained in the testing revealed that the wall temperature remained near the stream temperature. This indicates that the inside heat transfer is the result of forced convection. A value of 4 Btu/hr ft^2 ^oF was chosen for h_o since the bellows environment was calm, but bellows vibrations caused some agitation of the air near the convolutes. Work on natural convection from vibrating wires (7) indicates that the assumption of h_o = 4 Btu/hr ft^2 ^oF is valid. Fluid and thermal properties in Equation (32) were evaluated at the stream temperature. Usually, an evaluation of properties is made at some stream temperature between stream and wall values. This requires an accurate guess of T_{mean}, or use of an iteration procedure until the guessed and calculated values correspond. Since wall and stream temperature values were within a few degrees, using the stream temperature to determine h_i should result in negligible error.

Vapor pressures corresponding to T_{wi} calculated from the model, and combined with experimental values of P_{Bmax} and P_{Bmin} were used to determine σ_o and σ_m from Equations (38) and (39). The results are presented in Figure 87. The average cavitation number at initial maximum strain (σ_m at P_{Bmax}) for the eight experimental conditions is 2.25. The cavitation number at initial zero strain (σ_o at P_{Bmin}) is 0.4 for the eight experimental conditions. These cavitation numbers are reasonable considering initial cavitation usually occurs when the cavitation number is reduced to near one, and gross cavitation occurs between zero and one. These results indicate that when operating conditions are such that the cavitation number nears σ_m initial cavitation begins and vortex shedding is damped; see Figure 85b. When σ_o is approached, vortex shedding is completely suppressed; see Figure 85c.

Operating Pressures for Different Environmental Conditions

The cavitation numbers given in the previous section, together with the heat transfer analysis have been used to predict P_{Bmax} and P_{Bmin} under more general conditions than those tested. The computations were made by

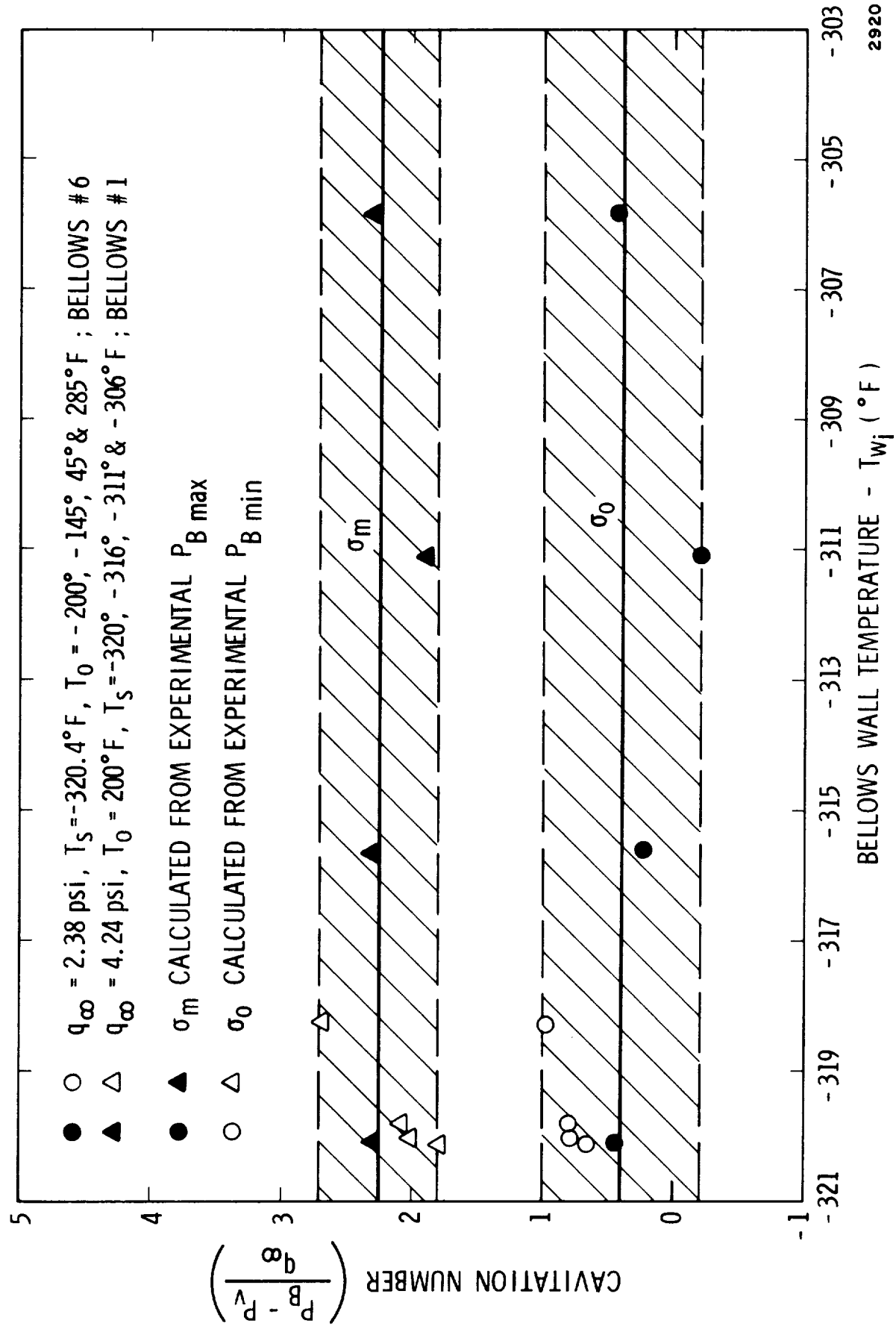

Figure 87. Experimental Cavitation Numbers At Maximum Strain (σ_m) And At Zero Strain (σ_O)

a digital computer, since the equations are cumbersome and not conducive to hand calculations. A listing of the program is provided in the Appendix. The computation proceeds as follows:

(a) Bellows geometry and LN_2 flow velocity and temperature are introduced into the program.

(b) Equation (32) is used to determine h_i with LN_2 properties evaluated at T_s.

(c) Environmental temperature T_0, outside convective coefficient h_o and frost thickness t_f were allowed to vary.

(d) Frost thermal conductivity (8) is assumed to be 0.030 Btu/hr ft ^oF, and bellows wall conductivity 10.0 Btu/hr ft ^oF for stainless steel.

(e) Equations (38) and (42) are used to determine the heat transfer resistances.

(f) Equation (27) is used to calculate the heat transfer.

(g) Equation (37) is used to obtain T_{wi} and Equation (40) to determine P_v.

(h) P_{Bmin} is then determined from Equation (39) for σ_o range of 0 to 1.0 and P_{Bmax} for σ_m from 1.75 to 2.75.

(i) P_{Bmax} and P_{Bmin} are determined for a range of T_0 from -200 to 280^oF and for h_o varying between 2 and 20 Btu/hr ft^2 ^oF (from natural to forced convection on the outside bellows surface). Frost thickness is varied from 0 to 1 inch at each condition of T_0 and h_o.

The results of the previous calculation procedure indicate that the largest resistance to heat transfer from the environment to the fluid flowing in a bellows occurs from the outside convection characteristics and from the insulating effect from the frost. The thin bellows wall offers little resistance to heat flow, and the inside convection resistance is small because of the forced flow over the rough convoluted surface. Since the inside convection resistance is small, the inside wall temperature remains only a few degrees above the stream value, and use of Equation (32) remains

valid. Equation (32) is also considered ideal for estimating h_i since it was shown to fit experimental data taken on pipes artificially roughened by attaching various size rings to the inside surface. The rings would be directly analogous to the convoluted section of a bellows. The friction factor, f^* used in Equation (32) was determined from previous friction factor data (1) obtained for 2-inch diameter bellows over a range of Reynolds numbers.

No Frost Formation

The results of this analysis are presented in Figures 88 and 89 for a 2-inch diameter bellows flowing LN_2 at a velocity of 21 fps, corresponding to the first mode frequency, and with no frost formation on the bellows exterior surface. The values of P_{Bmax} and P_{Bmin} were determined from σ_o and σ_m equal to 0.4 and 2.25, respectively. The results indicate that

(a) Increasing the outside convection coefficient from 2 to 12 Btu/hr ft ^oF, with a constant environmental and stream temperature, causes a corresponding increase in the value of P_{Bmax} and P_{Bmin}. The range on h_o represents natural convection (h_o = 4 Btu/hr ft^2 ^oF) to forced convection at h_o = 12 Btu/hr ft^2 ^oF, representing a wind velocity of 40 mph from Equation (36).

(b) Increasing T_0 at a constant h_o and T_s also results in a corresponding increase in P_{Bmax} and P_{Bmin}.

Frost Formation

The effects of frost formation are presented in Figures 90 and 91 for the same bellows and flow conditions as for the no-frost case. In this case environmental temperature is held constant at 80^{o}F and the effects of frost thickness with varying outside convection conditions are presented. The limiting frost thickness is determined by examining the frost temperature at the outside surface as given by

$$T_{fo} = T_{wi} + \dot{Q}^* R_2$$

Once the frost thickness has increased to a point where the temperature drop across the frost is such that T_{fo} = 32^{o}F, then no additional frost buildup will occur. The limiting thickness will depend on the total heat

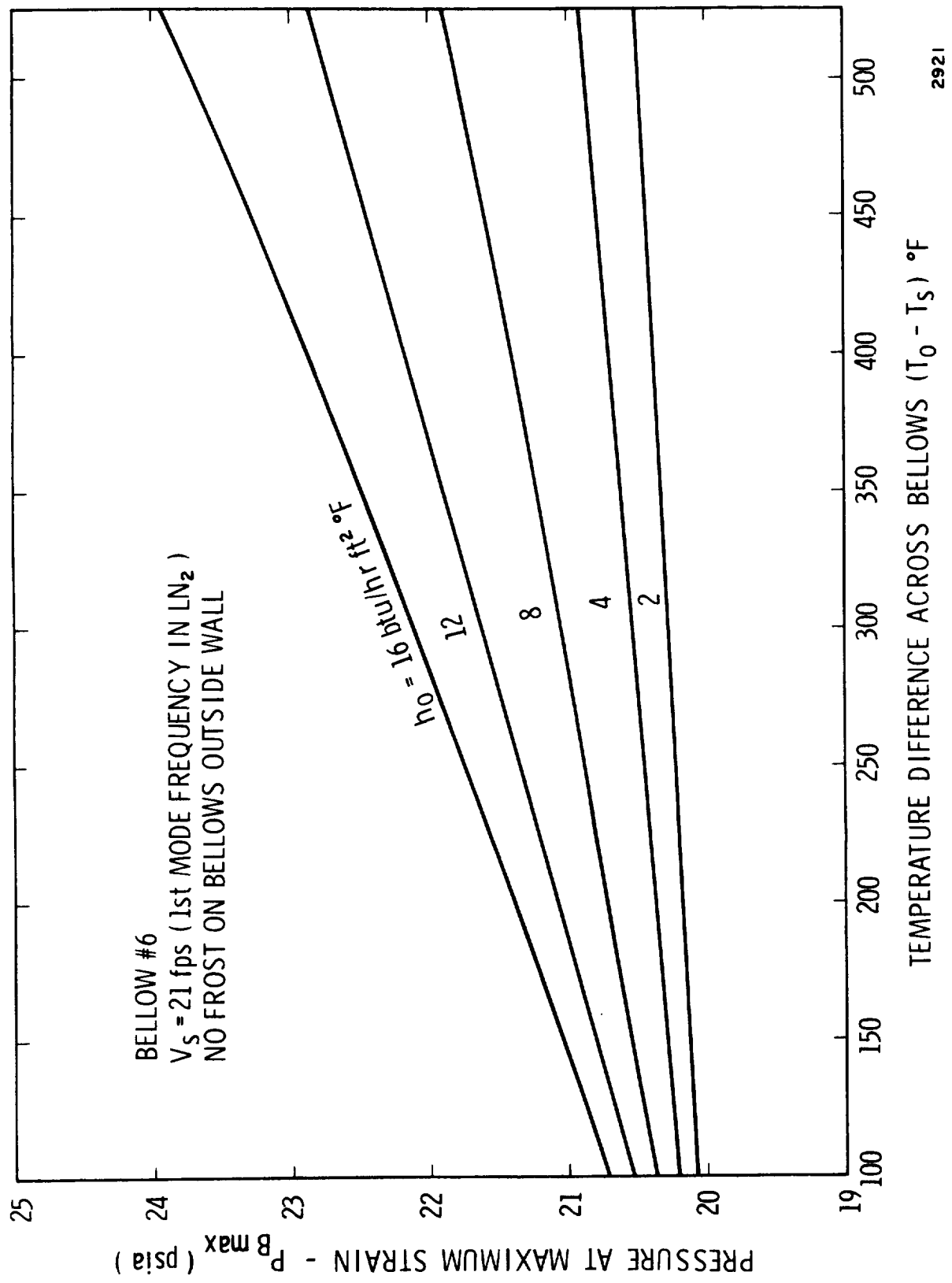

Figure 88. Bellows Pressure At Maximum Strain With No Frost On Wall

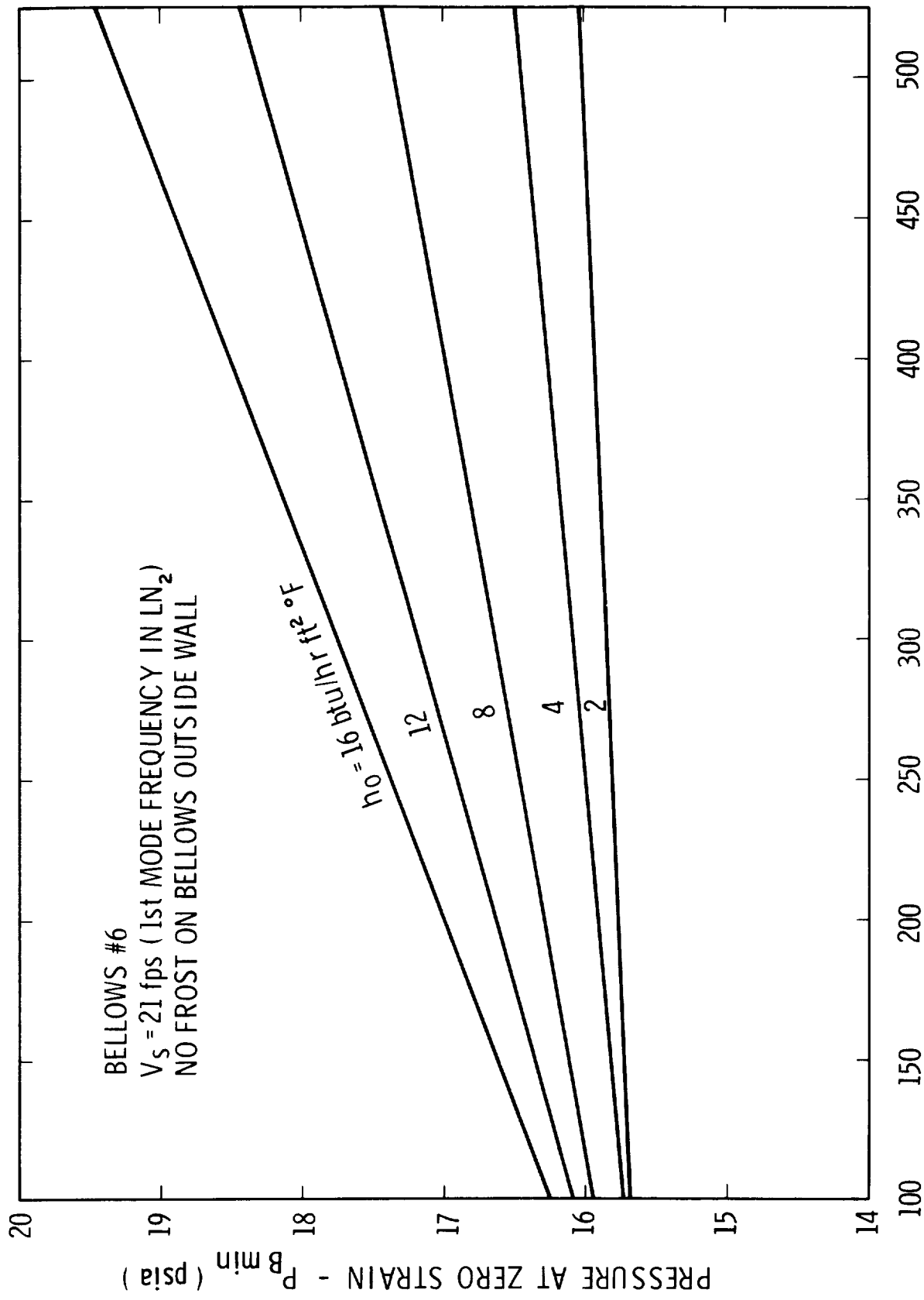

Figure 89. Bellows Pressure At Zero Strain With No Frost On Wall

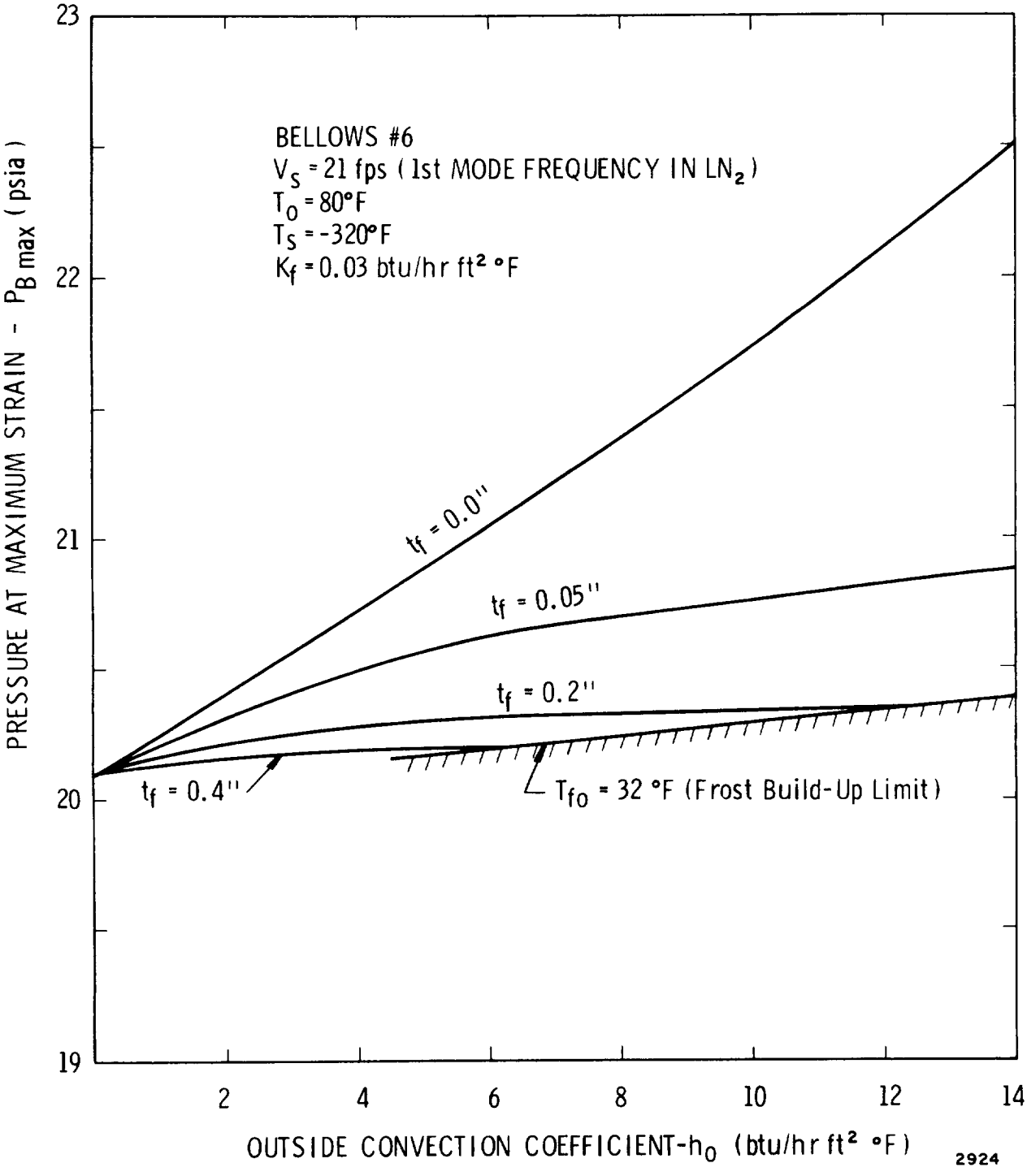

Figure 90. Bellows Pressure At Maximum Strain With Frost Build-Up

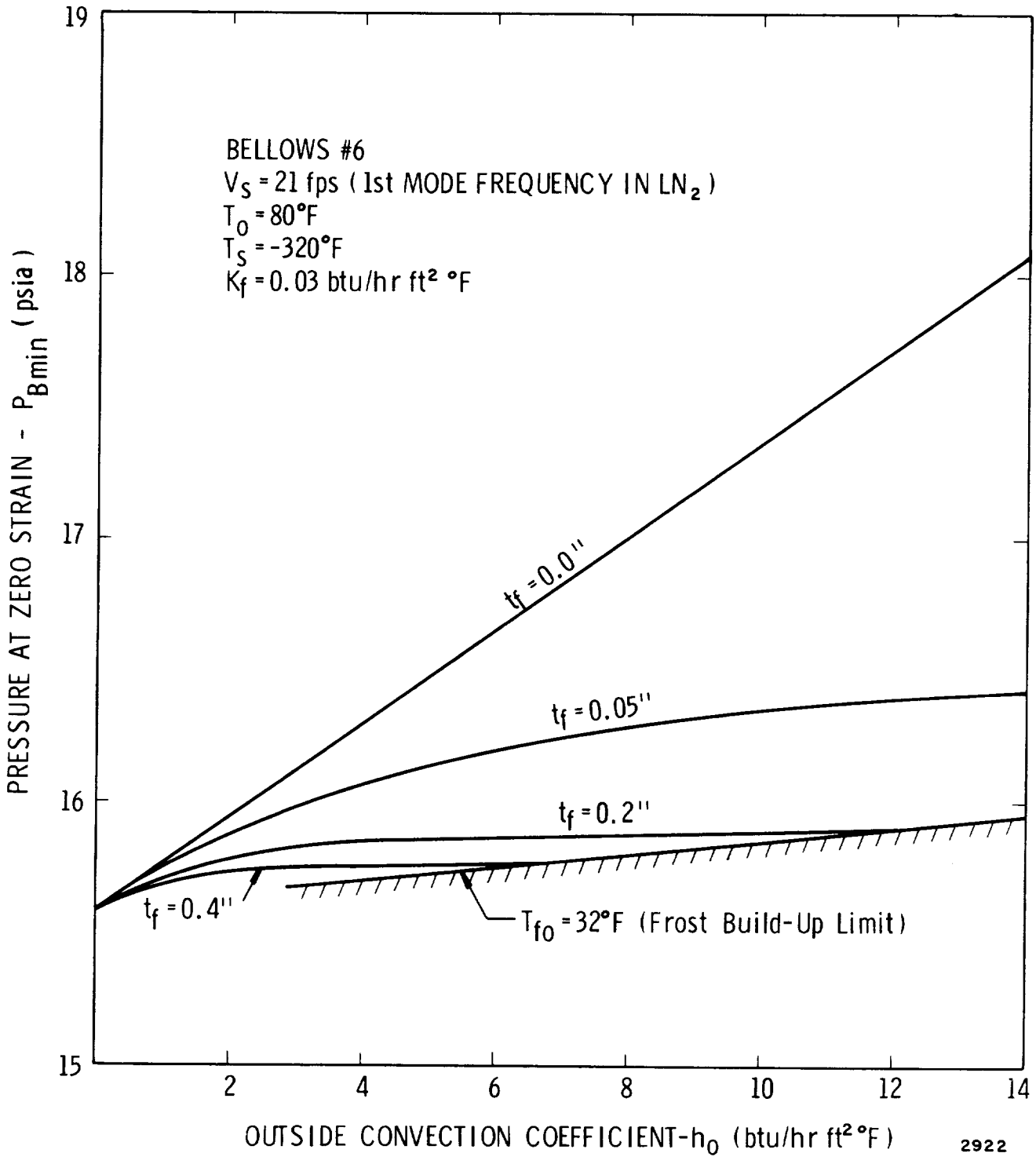

Figure 91. Bellows Pressure At Zero Strain With Frost Build-Up

transfer, Q, as determined from the environmental and stream conditions. This maximum thickness is shown in Figures 90 and 91. These results indicate that:

(a) For a given convection coefficient h_o, frost buildup insulates the bellows, reducing P_{Bmin} and P_{Bmax}.

(b) Increasing h_o at a given frost thickness results in an increase in P_{Bmax} and P_{Bmin}.

The results of the effects of frost buildup on the operating characteristics of bellows are considered adequate to indicate the expected bellows response when frosting occurs. However, it should be pointed out that assuming a constant thermal conductivity of 0.03 Btu/hr ft ^{o}F under varying conditions of frost formation is a simplification of the problem. The nature of frost formation on cryogenic feed lines is extremely complicated and depends on the relative humidity, the temperature and other factors. Experimental values of frost thermal conductivity vary, and the choice of the frost conductivity was made after a review of the literature, and is considered to be adequate for this analysis.

Geometric Effects

An examination of the heat transfer model presented in this report will show the effects of bellows geometry on the combined heat transfer/cavitation phenomena that alters bellows flow induced response. Consider Equations (28) and (32) for determining the heat transfer and bellows inside wall temperature, respectively. If the heat transferred per unit wall area is based on the inside wall area, A_{wi}, then Equation (28) becomes

$$\frac{\overset{*}{Q}}{A_{wi}} = \frac{T_o - T_s}{A_{wi}\,\Sigma R} \tag{41}$$

and Equation (32) can be written as

$$T_{wi} = T_s + \frac{\overset{*}{Q}}{A_{wi}}\, R_4\, A_{wi} \tag{42}$$

If $\overset{*}{Q}/A_{wi}$ and $R_4 A_{wi}$ are dependent on bellows geometry then T_{wi} and P_v will also depend on geometry.

First, examining the term $R_4 A_{wi}$, we find

$$R_4 A_{wi} = \frac{1}{h_i} \tag{43}$$

Therefore, $R_4 A_{wi}$ is independent of geometry except as h_i is altered by changes in convolute shape.

Next, examine $\dot{Q}^*/A_{wi}$

$$\frac{\dot{Q}^*}{A_{wi}} = \left(\frac{T_o - T_s}{A_{wi}}\right)\left\{\frac{1}{A_{wo}h_o} + \frac{1}{2\pi\ell}\left[\frac{1}{K_f}\ln\left(\frac{r_m + t_f + t_w}{r_m + t_w}\right) + \frac{1}{K_w}\ln\left(\frac{r_m + t_w}{r_m}\right)\right] + \frac{1}{A_{wi}h_i}\right\}^{-1} \tag{44}$$

for the case of a thin walled cylinder where the thickness is such that

$$\frac{r_2 - r_1}{r_1} < 0.1 \tag{45}$$

then $\ln(r_2/r_1)$ can be estimated within 5 percent by $(r_2 - r_1)/r_1$.

Therefore, the wall and frost resistances can be estimated by

$$R_2 = \frac{t_w}{K_w A_{wi}} \tag{46}$$

$$R_3 = \frac{t_f}{K_f A_{wo}} \tag{47}$$

if condition (45) is valid. Condition (45) is valid for 2-inch diameter bellows with frost thickness of 0.1 inch or less, and the assumption becomes more accurate for larger diameter bellows at greater frost thicknesses.

Utilizing R_2 and R_3 as given by Equations (46) and (47) yields

$$\frac{\dot{Q}^*}{A_{wi}} = \left(\frac{T_o - T_s}{A_{wi}}\right)\left\{\frac{1}{A_{wo}h_o} + \frac{t_w}{A_{wi}K_w} + \frac{t_f}{A_{wo}K_f} + \frac{1}{A_{wi}h_i}\right\}^{-1} \tag{48}$$

and since

$$A_{wo} \cong A_{wi} \qquad \text{for condition (45)}$$

then

$$\frac{\overset{*}{Q}}{A_{wi}} = (T_o - T_s)\left\{\frac{1}{h_o} + \frac{t_w}{K_w} + \frac{t_f}{K_f} + \frac{1}{h_i}\right\}^{-1} \tag{49}$$

the expression for heat transfer through a slab of area A_{wi}.

Since the wall resistance (t_w/K_w) is negligible compared to the other resistances and t_w is small for most bellows, the resulting expression for $\overset{*}{Q}/A_{wi}$ is independent of bellows geometry and is only a function of the environmental conditions. Therefore, the inside wall temperature used to determine the vapor pressure will be strongly dependent on the bellows inside and outside conditions (i.e., T_0, T_s, t_f, K_f, h_i and h_o) and only a weak function of bellows geometry. This will be true only if the simplifying assumption of heat transfer to a thin walled cylinder is an accurate model and if the bellows is small enough to prevent sufficient heat transfer from producing an appreciable temperature drop between bellows inlet and exit. The restriction on constant stream temperature between the bellows entrance and exit should be valid for short bellows under the low rates of heat transfer represented by the environmental conditions considered.

Next, the effect of geometry on P_{Bmax} and P_{Bmin} must be considered. Solving (38) and (39) for P_{Bmax} and P_{Bmin} yields

$$P_{Bmax} = P_{v@T_{wi}} + \sigma_m \, q_\infty \tag{50}$$

and

$$P_{Bmin} = P_{v@T_{wi}} + \sigma_o \, q_\infty \tag{51}$$

The effect of bellows geometry on P_v was shown to be minor, leaving only σq_∞ to be analyzed. No experimental data is available on cavitation numbers at maximum and minimum strain except for the 2-inch bellows. It is assumed that σ_o and σ_m will not change drastically with bellows geometry changes. However, the bellows velocity at which vortex shedding occurs is dependent on bellows geometry and the different modes of vibration will occur at different velocities. This change in velocity with geometry and vibrational mode will change the σq_∞ terms in Equations (50) and (51) resulting in changing the values of P_{Bmax} and P_{Bmin}. The results of geometry effects can be summarized as follows:

(a) Bellows geometry differences for short bellows will produce negligible changes in the calculated vapor pressure for a given set of environmental and flow conditions. Therefore, results presented in Figures 88 to 91 for a 2-inch bellows should be valid for other diameters flowing LN_2 at 21 fps and -320°F.

(b) Bellows geometry differences will change the estimate of P_{Bmax} and P_{Bmin} since geometry affects the velocity for a given vibrational mode.

General Remarks

All results are presented for velocities corresponding to the first vibrational mode. No data has been taken at higher mode frequencies to confirm the accuracy of this analysis. Also, Equation (32) used to determine h_i will be affected by changes in Reynolds number through changing V_∞ and D_m. When forced convection on the outside wall of the bellows becomes severe enough, the inside wall temperature will exceed the point where boiling heat transfer can be ignored. Under these unusual conditions, Equations (33) and (34) should be used only as an order of magnitude estimate of h_i as they do not directly apply to cryogenic flow in a pipe. Also, the validity of Equation (23) is questionable at Reynolds numbers much above 10^6 as the data this equation was based on covers an Re range up to 10^5.

In general, the analysis should be adequate to yield an accurate estimate of operating pressures to insure that cavitation does not occur under a given environmental situation.

IV.5 External Damping

Introduction

The prior discussions in this section have been devoted primarily to one type of mechanism which can suppress bellows flow excitation where cryogenic liquids are the flow media. This suppression was caused by vapor formation in the flowing liquid which directly affected the vortex shedding phenomena, and reduced the magnitude of the periodic force. Another possible suppression mechanism where cryogens are the flow media is the extra damping introduced by the external buildup of some combination of ice, frost, or condensed air. Experiments have been conducted to determine the damping introduced by these three types of external media, and the results are described in the following discussions.

Frost and Ice Damping

Frost buildup alone on a bellows with an internal cryogen flow has a minor to negligible effect on the amplitude of flow-induced vibrations. Several experiments were conducted to determine if the vibration was suppressed by frost formation, and in all cases where frost alone was present, no truly significant reduction was noted. This was true even for heavy frost buildups. Figure 92 illustrates frost conditions typical of those for which tests were conducted.

The fact that frost alone yielded negligible external damping is understandable since this media has a very low mass, based on total volume occupied, and may be easily "crushed". Therefore, when bellows vibrations occur, the built-up frost offers negligible resistance to convolute motion.

External ice buildup with internal cryogen flow may or may not cause suppression of the flow-induced vibrations. As might be expected, if the ice buildup is of sufficient magnitude so that the spaces between the convolutes are largely filled with ice, then no vibrations will occur.

When thinner ice coatings are present, low energy vibrations are completely suppressed, but high energy level vibrations cause the ice coating to crack and fall off so that the original or undamped (external damping) vibration amplitude is restored. Figure 93 illustrates this phenomena. The top strain-velocity curve illustrates flow-induced vibrations of a bellows with no external damping media. Figure 93 illustrates the behavior of a bellows with a light ice buildup. Note that the first mode (lower energy level mode)

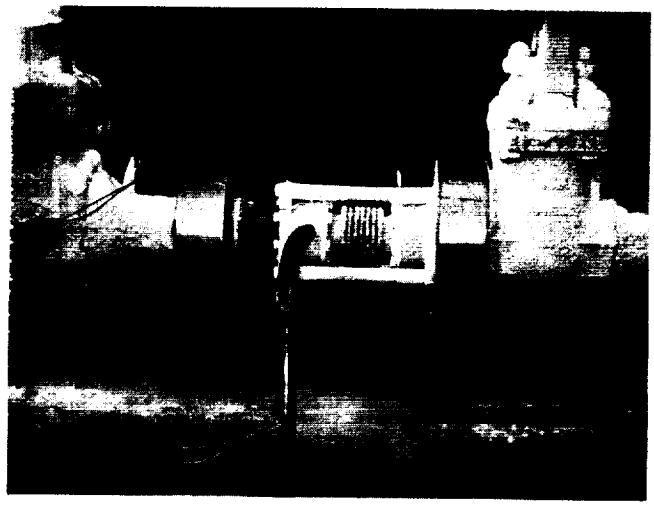

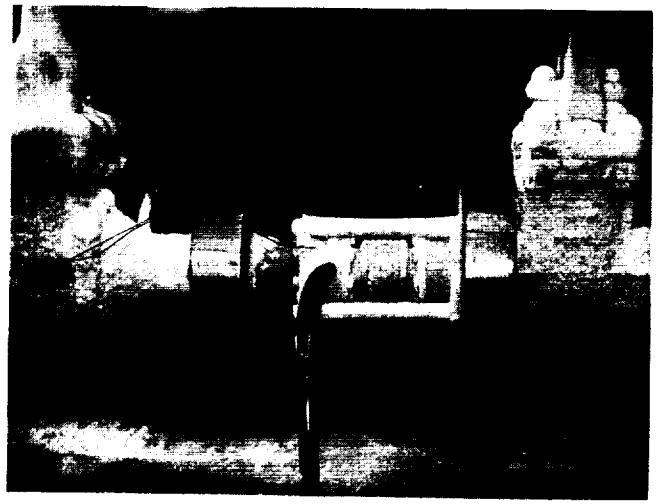

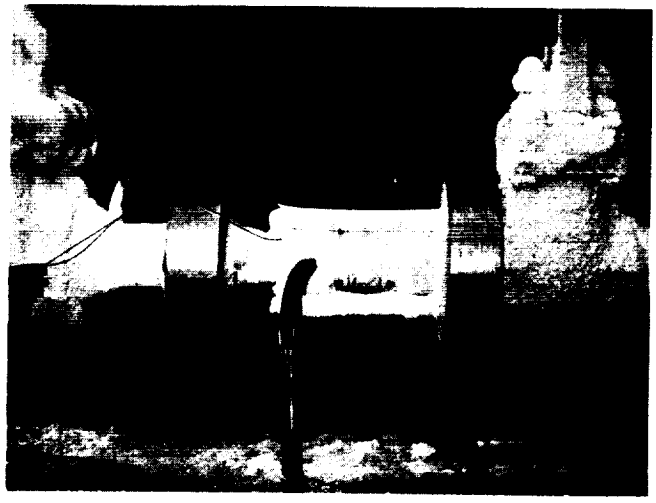

FIGURE 92. PHOTOGRAPHS OF FROST BUILDUP ON TEST BELLOWS WITH INTERNAL LN_2 FLOW

is completely suppressed. The second mode, however, is only suppressed up to a certain maximum velocity where breakup of the ice occurs and the original vibration amplitudes are thereby restored.

External Liquid Damping

Experiments conducted in the laboratory revealed that bellows damping, because of the presence of an external liquid, can be quite significant. Since such a condition generally occurs only where liquid hydrogen or helium is the flow media, our experiments were conducted under simulated conditions employing external water damping on bellows flowing water and air. In conjunction with these experiments, an analysis was performed to develop a mathematical model for this type of damping.

Figure 94 illustrates the mechanism believed to be responsible for damping of a bellows covered on the outside by a liquid. As shown, vibratory motion of the convolutes causes the external liquid to be periodically forced in and out of the space between convolutes. Estimates of the Reynolds number typical for this periodic motion show that a transient turbulent situation likely exists. Therefore, it is reasonable to expect that this external periodic fluid motion will produce a damping force on the vibrating convolutes. This force, because of the turbulent dissipation mechanism, will be proportional to the convolute relative velocity to the second power.

Based on the above hypothesis for external liquid damping, a mathematical model has been developed for the convolute vibrations for a case where external damping alone is present (no conventional damping). The results have been formulated in terms of a Stress Indicator equation, to be compatible with earlier results, and this equation is

$$SI_e = \frac{\epsilon \delta t E N_p}{f h^3} \sqrt{\frac{C_F p_d}{\rho_e}} \quad , \epsilon \approx 0.25 \qquad (52)$$

where

SI_e = Stress Indicator for external damping alone
ϵ = Empirical constant, $\epsilon \approx 0.25$
E = Young's modulus for bellows material
t = Bellows wall thickness per ply
δ = Space between convolute tips
N_p = Number of plys
f = Bellows vibration frequency
h = Convolute height
C_F = Vortex force coefficient
p_d = Internal dynamic fluid pressure
ρ_e = External media mass density

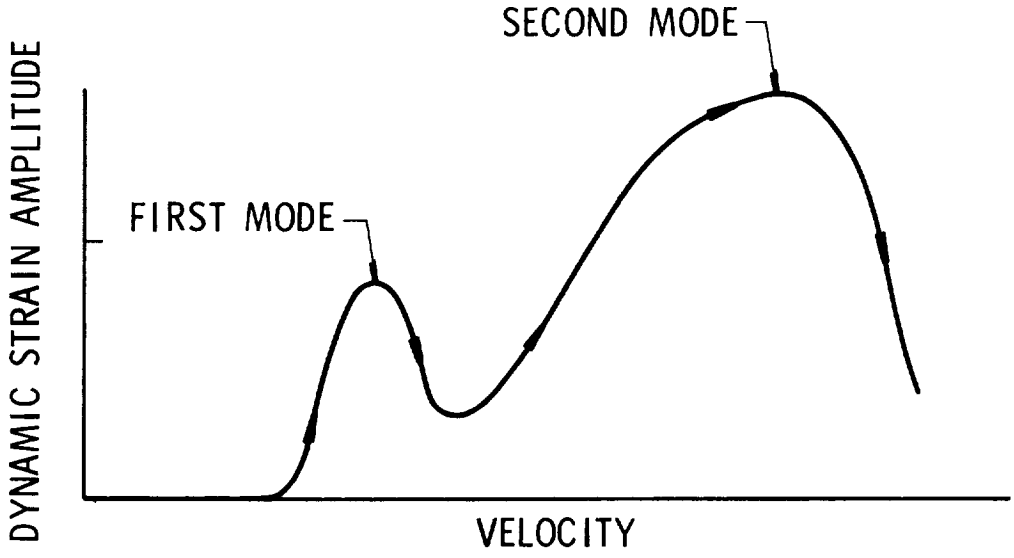

(a) STRAIN-VELOCITY PLOT WHERE NO EXTERNAL ICE IS PRESENT

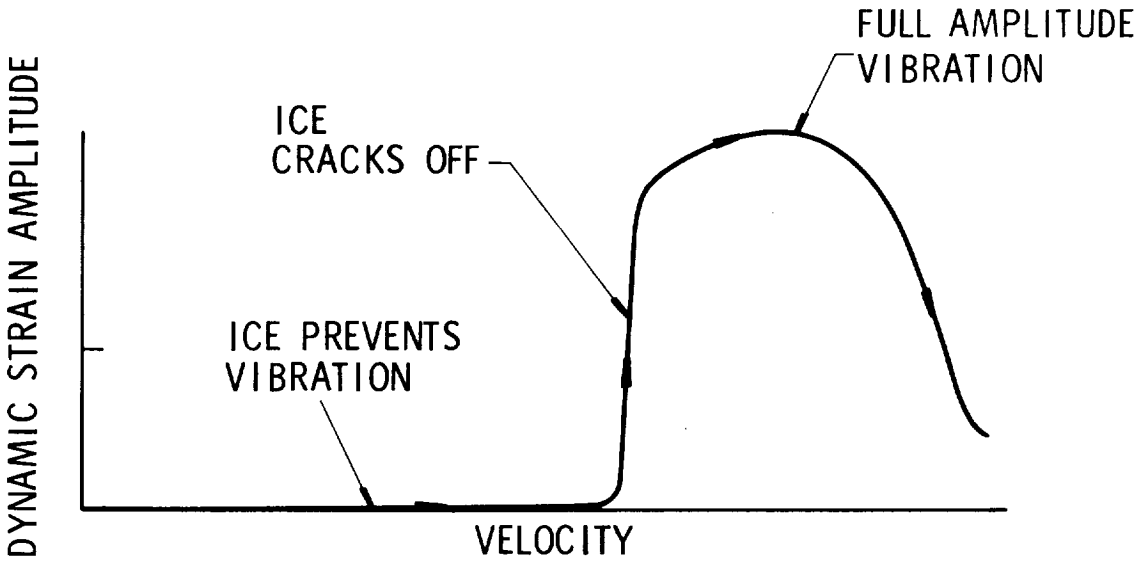

(b) STRAIN-VELOCITY PLOT WHERE THIN ICE COAT IS PRESENT

2927

Figure 93. Illustration Of Bellows Flow-Induced Vibration With And Without External Ice Builtup For Velocity Upsweep

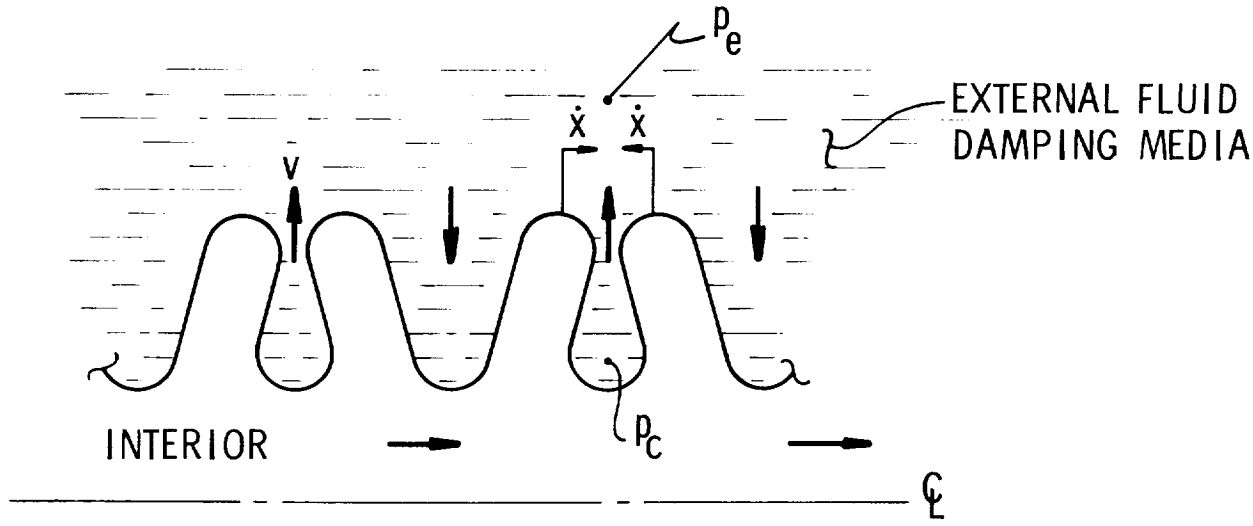

- CONVOLUTE RELATIVE VELOCITY $2\dot{x}$ GIVES DISCHARGE VELOCITY OF

$$v \approx \frac{\dot{x}h}{\delta}$$

- THIS FLUID MOTION, IF TURBULENT, GIVES A PRESSURE DIFFERENTIAL OF

$$|p_c - p_e| \approx \epsilon_1 \rho v^2$$

WHERE ϵ_1 IS AN EMPIRICAL CONSTANT

- THIS PRESSURE DIFFERENTIAL MAY BE INTERPRETED AS A FLUID DAMPING FORCE

$$F_d = (\pi D_m h)(\epsilon_1 \rho v^2) = b\dot{x}^2$$

2930

Figure 94 . Illustration Of External Fluid Damping Mechanism

Since some conventional damping is always present, Equation (52) does not indicate the true bellows flow-induced stress level, but only the external damping limited part. To get the true or correct Stress Indicator, it is necessary to combine the conventional value and the external damping value. This may be done by the expression below, or

$$SI_c = \left\{ \frac{1}{\frac{1}{SI} + \frac{1}{SI_e}} \right\} \tag{53}$$

where

SI = Stress Indicator for Conventional Damping (see Reference 5)

SI_e = Stress Indicator for External Damping Alone (see Equation (52)).

IV.6 Application of Results

Summary of Use of Results

This section has described results of an investigation of bellows flow-induced vibrations where a cryogen is the flow media. It has been demonstrated that the phenomena is predictable by the method presented in Section II , except for two important limiting cases. First, if boiling and/or cavitation occurs in the bellows, then the vortex shedding, hence vibrations, will be suppressed. Second, the presence of an external buildup of frost, ice or condensing liquid can also suppress the vibrations. The data in Section II provides an upper-limit prediction of vibration amplitudes, and the phenomena described herein are vibration suppression mechanisms.

From the standpoint of a designer or test engineer, it is important that these possible suppression mechanisms be recognized so that the worst-case condition is examined in any design or test activity. The case history reported in Section II is dramatic evidence of the importance of recognizing these suppression mechanisms.

As an aid to the reader, the following sections have been prepared summarizing a procedure which might be followed in predicting these flow-excitation suppression effects.

Suppression by Internal Vapor Formation

Utilizing the heat transfer analysis presented in this report to determine when flow excitation of a bellows will be suppressed proceeds as follows:

(a) Using the results of Section II , determine the flow velocity where flow excitation is expected.

(b) Calculate the internal heat transfer coefficient h_i from Equation (32) by determining the Reynolds number Re_d and Prandtl number P_r at the stream conditions, and friction factor ratio f*/fo* from Section II. Base the Nusselt number Nu on D_o, and base Re_d on D_i for a conservative h_i estimate.

(c) Determine the external heat transfer coefficient h_o from a knowledge of bellows environmental conditions. Use Equation (36) for forced flow over the bellows or any other suitable expression for the expected bellows environmental condition, (i.e., natural or forced convection or condensation). If frost is present, estimate its thickness and conductivity.

(d) Calculate the overall heat transfer from Equation (49).

(e) Calculate the bellows inner wall temperature T_{wi} from Equation (42).

(f) Determine the cryogen vapor pressure P_v at temperature T_{wi} from Equation (40) for LN_2 or an appropriate expression for other cryogenics.

(g) Using the cavitation number limits σo and σm of 0.4 and 2.25, respectively, calculate the operating pressures P_{Bmin} and P_{Bmax} from Equations (50) and (51). These defining cavitation numbers resulted from LN_2 experimental data but should be adequate for predicting strain suppression with other liquids as the flowing medium.

(h) If the bellows operating pressure is above P_{Bmax}, flow-induced response is possible and predictable by the method of Reference 1. If the operating pressure is between P_{Bmax} and P_{Bmin} some damping of the response is expected. If the operating pressure is below P_{Bmin}, no flow-induced response will occur.

External Damping Vibration Suppression

The damping effect of frost alone can be neglected. Thus, for liquid oxygen and liquid nitrogen flows where a buildup of frost alone is usually the case, the results of Section II apply but the possibility of internal vapor formation exists, and must be examined by the above procedure.

Ice formation may or may not produce a damping effect, depending on the level of buildup. In the laboratory, ice occurred only by deliberately pouring water on the bellows, or by periodic melting of the frost layer with external heating. Ice buildup should be treated as a very special case, the effect of which can only be accurately determined from laboratory testing.

External liquid (air) condensation will generally occur only for liquid hydrogen or cold helium flows. An estimate of the vibration severity with this damping mechanism present may be made by the procedure given in Section IV.5.

Realistic Testing

It should be evident from the results in this report that in performing flow-induced vibration tests on a bellows with internal cryogenic liquid flows, one must properly allow for possible vapor formation or external damping. If the bellows is to be operated under conditions where no external heating or damping media buildup is possible, such as in a vacuum, then the bellows should be tested under the same conditions. The only possible shortcut found in the laboratory was to use an external purge of the cold boil-off gas from the test to minimize heating and external damping effects. This means use cold GN_2, GOX or GH_2 where LN_2, LOX or LH_2 are the flow media, respectively. Practical difficulties may make it easier to go ahead and provide an external vacuum environment rather than use this procedure, however.

For monitoring flow-induced vibrations of bellows, experience has shown that only convolute strain measurements are absolutely reliable. Other monitoring methods such as duct vibration, internal pressure measurements, and external acoustic emission have been evaluated. In general, these other methods are undesirable, except for providing qualitative information, because they give output signals with an unrealistic frequency content. Examination of the spectral content of a duct acceleration signal, for example, often shows vibrational energy at the actual bellows frequency plus several harmonics of this frequency. A convolute strain signal from the same bellows will only reveal significant energy at the actual bellows frequency.

Because of the high frequencies involved, and the severity of the vibrations, proper mounting of strain gages can be a problem. Thorough cleaning of the convolute surface and use of an epoxy for mounting the gages has resulted in reliable installations in our laboratory. Only very fine lead wires (≈ 0.005 inch) should be soldered directly to the convolute strain gages. These fine wires should be attached to the main signal leads at terminal strips cemented on the duct adjoining the bellows. A fine coat of rubber cement should be put on the small lead wires to provide some damping and help prevent wire fatigue failures. Care must be taken to ensure that the output instrumentation has adequate frequency response for the signals anticipated.

Example Situation

Reference 9 discussed bellows flow induced response changes with changing environmental conditions, and resulted from an investigation into the failure of a braided bellows (J-2 engine, ASI line) carrying LH_2 with an external vacuum environment. The failure was attributed to the bellows

being qualification tested in a normal atmospheric environment which created suppression of the flow-induced vibrations, hence, did not allow maximum vibratory strain to occur. The authors of Reference 9 indicated that air condensing between the convolutes and the braid caused suppression of the bellows vibrations. However, the authors seem to relate this to a heat transfer effect, which is highly unlikely. By their own calculations the bellows wall temperature with film condensation was -396°F with the hydrogen flowing at -400°F and 1000 psia (our own analysis confirms this). A 4° change in temperature between the wall and bulk flow at 1000 psi was too small to cause a density gradient sufficient to influence the vortex shedding.

The mechanism responsible for the reduced response under these conditions was most likely the added damping action of the external liquid air. Application of the external liquid damping model (see Section IV.5) to this ASI line case, indicates that this particular suppression mechanism could have reduced the flow-induced vibrations to about 20 percent of the vibration level observed with an external vacuum.

In Reference 9, the conclusion that heat transfer caused the vibration suppression of the ASI line was based, in part, on a test where hot helium gas at a mean temperature of 285°F was blown over the bellows surface. It appears from the figures in Reference 9 that this forced heating created a fluid temperature in the convolutes of -330°F compared with -400°F in the bulk flow. This type of temperature change could have produced a sufficient density gradient in the convolutes to suppress the vortex shedding and reduce the vibrational response. However, the amount of heat transferred with the hot helium was about 17 greater than for the case with condensing air, assuming the inside wall heat transfer coefficient didn't change. Therefore, the two cases were not analogous, and the reduced bellows response, in our judgment, was created by a different phenomena for each case. That is, with condensation, liquid air damped the response, while for the hot helium test a density gradient in the convolutes probably suppressed the vortex shedding.

It should be noted that, since the tests in Reference 9 were performed at pressures above the critical pressure (1000 versus 188 psia), the state of the hydrogen in the bellows was not well defined in terms of being a liquid or vapor. At super-critical pressures a liquid and vapor phase cannot exist simultaneously, and any large temperature difference that exists between the bellows wall and bulk flow as the result of heat transfer will only cause a density reduction of the fluid in the convolutes which could lead to a change in the vortex shedding.

IV.7 Conclusions from Heat Transfer Study

A number of conclusions have been derived from the study reported in this section; these are:

(a) Vibrations excited in bellows by the internal flow of a cryogenic liquid are caused by the same fluid-elastic instability reported in Section II for internal water and air flows.

(b) Where no internal boiling or phase change occurs, and where no frost, ice or condensed liquid appears on the bellows exterior, the flow-induced vibration with an internal cryogen is predictable by the method reported in Section II.

(c) If a phase change of the flowing media occurs and/or external frost, ice or condensed liquid is allowed to form, then the bellows vibration amplitudes, hence, the dynamic strain levels, will be reduced from the condition of (b).

(d) The conditions under which an internal phase change will produce suppression of the bellows flow-excitation are predictable. An analysis for making this prediction is presented in this report.

(e) The presence of frost on a bellows can produce a negligible reduction of the vibration amplitudes by virtue of some added damping.

(f) If built up prior to the initiation of flow, a heavy ice layer can completely suppress flow-induced vibrations of bellows. If, however, the ice is formed after flow-excitation is initiated, the convolute vibrations will prevent large buildups by causing the ice to crack and fall off. Ice buildup on a bellows is generally a rare occurrence unless water is purposely poured over the cold convolutes.

(g) Condensation of significant quantities of gas constituents from the ambient surroundings can produce a significant damping of the bellows flow-induced vibrations. This condensation would be most pronounced for internal liquid hydrogen or cold helium flows. A model for predicting vibration amplitudes when an external liquid is present is given in this section.

V. BELLOWS VIBRATIONS WITH GASES

V. 1 Introduction

Bellows vibration response when the internal flow medium is a gas, can be significantly altered especially at high flow velocities. This results from acoustic loading which can increase the number of degrees of freedom of a bellows system by producing additional bellows acoustic modes. Preliminary observations of acoustical resonance in bellows with gas flows were reported in Reference 1. It was noted that the bellows showed virtually no response up to rather high flow velocities where quite suddenly the vibration response became very pronounced. This sudden onset of vibration response was accompanied by significant acoustic radiation from the entire test loop, indicating that acoustical resonance existed. When this condition was established, it was observed that the vibration was much more severe than it should have been which was attributed to an enhancement of vortex shedding by the acoustic resonance. Preliminary data obtained with both air and freon as the internal flow media exhibited the same characteristics with the exception that the critical flow velocity with freon was about half that experienced with air. This was expected, however, since the speed of sound in freon is approximately half that of air, and reducing the speed of sound will cause a reduction in the acoustic resonance frequency, hence the flow velocity required to give a resonant condition. Additional testing (Reference 1) was also conducted to map the acoustic pressure field inside a bellows by use of a small microphone, and the results are shown in Figure 95. It was determined that a coupled radial-axial acoustic mode existed with a maximum sound pressure level occurring in the radial direction near the internal bellows diameter. It was also determined that the acoustic field was being excited by the vortex shedding from the bellows convolutions and, in turn, the acoustic resonance enhanced the vortex shedding, causing greater than expected resonance levels. It was reasoned that the sudden occurrence of this phenomenon at some critical flow velocity was that: At low fluid velocities (i.e., low vortex frequencies) the acoustic wavelengths were too long to fit in the bellows in the radial direction. Therefore, the radial acoustic waves which were generated experienced pure attenuation. When a high enough shedding frequency was achieved (hence, a high fluid velocity), the wavelengths were short enough to fit radially and therefore, radial resonance condition would couple with the axial acoustic mode. As a result of this preliminary work, it was concluded that the effect of radial acoustic resonance in bellows leads to generally increased flow-induced stress levels and sharp increases in the sound level in duct systems.

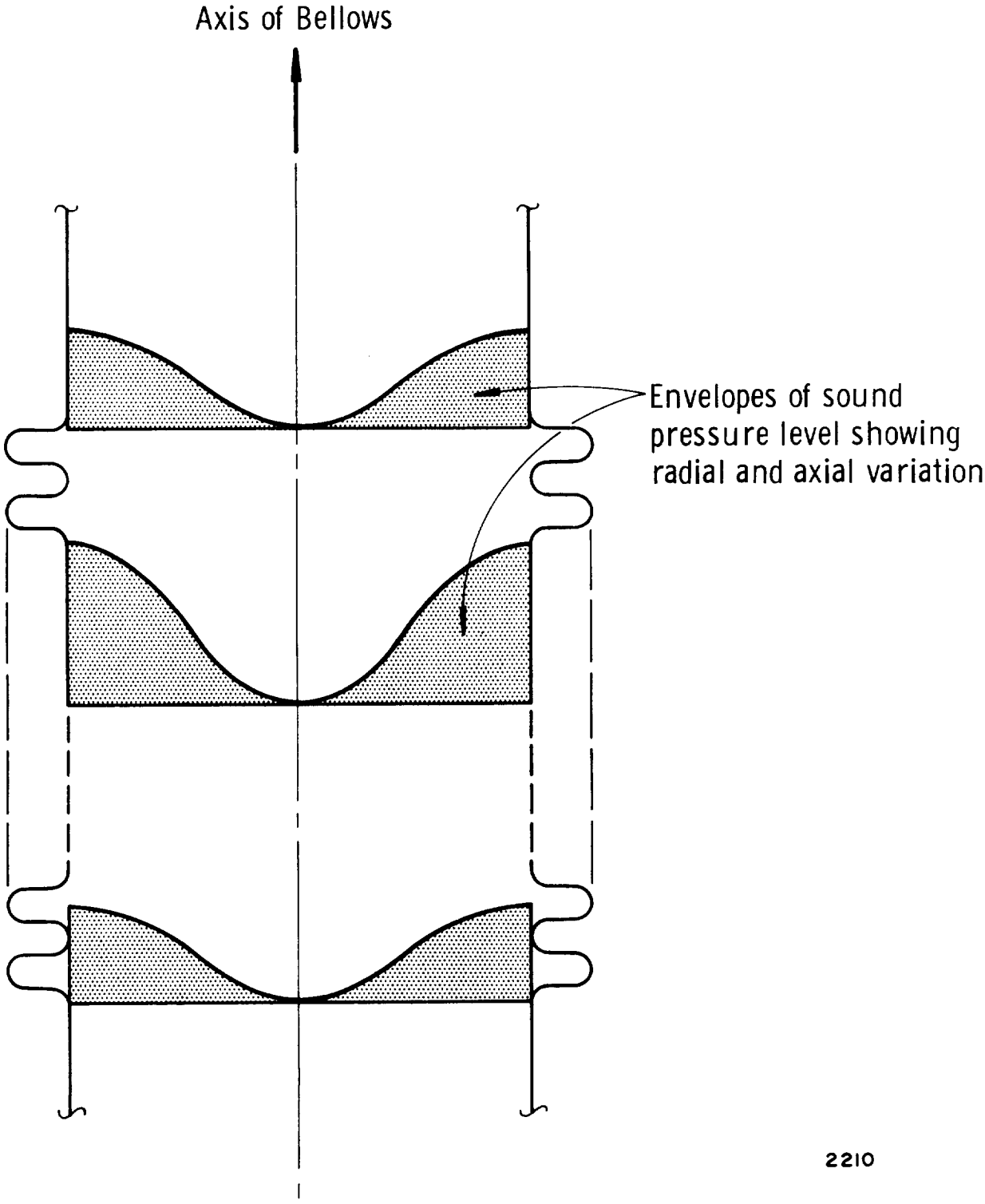

Figure 95. Illustration Of Acoustic Pressure Level Variation With Radial And Axial Position In Bellows

V.2 Experimental Results

Subsequent to the preliminary results reported in Reference 1, additional experimental tests were conducted to provide data for determining the effects of acoustic induced bellows vibrations with internal gas flows. A 1.5-in. I.D. specimen was extensively investigated in the SwRI gas flow loop. The tests were conducted with one end of the bellows open and with the gas exhausted into the atmosphere. Strain data were recorded over an air velocity range from 0 to 350 feet per second. Also, acoustic sound pressure level data were obtained by use of a microphone. As expected, the peak sound levels occurred at the same flow velocities (and frequencies) that the peak convolute strain was observed, as shown in Figure 96. This particular test bellows showed strong response at 5200, 6100 and 7700 cps, which are all above the highest longitudinal mode frequency of 5100 cps. In order to verify that the excitation was purely acoustically oriented, the bellows was covered on the outside with epoxy to completely prevent any convolute motion. Subsequent sound pressure level measurements again showed peak responses at the three frequencies, 5200, 6100 and 7700 cps.

Additional tests were performed to determine the effect of changing duct acoustic impedance on the bellows vibration. Tests were performed with another 1.5-in. I.D. bellows exhausting to the atmosphere but with different lengths of exhaust ducting adding to the open end. Figure 97 shows the results of this testing. A significant difference in convolute dynamic strain characteristics for each downstream duct length is noted. Also noted is the significance of the maximum peak strain occurring at an exit exhaust duct length of 2.25 in., which is almost precisely a 2.5 inch wavelength (at the particular frequency for which the strain peaked in Figure 97) from the open end of the duct to the mid-axial point of the bellows. Previous measurements of sound pressure levels indicate the pressure to be a maximum at the mid-axial point. Since the pressure level must be near zero at the duct open end, it is expected that the acoustic resonance phenomena could be enhanced at total duct lengths of 1/2, 1-1/2, 2-1/2, etc., wavelengths. This geometric configuration should, therefore, result in an optimum reinforcement.

Additional experimental gas flow tests were performed with the 3-in. diameter test specimens indicated in the previous table. Both freon and air were used as the internal flow media for all testing with these bellows. For the wide range of bellows tested, the acoustical resonance started when the vortex frequency became high enough to produce a sound wavelength about equal to the bellows diameter where wavelength and vortex frequency are related by

$$\lambda_s = C_o/f$$

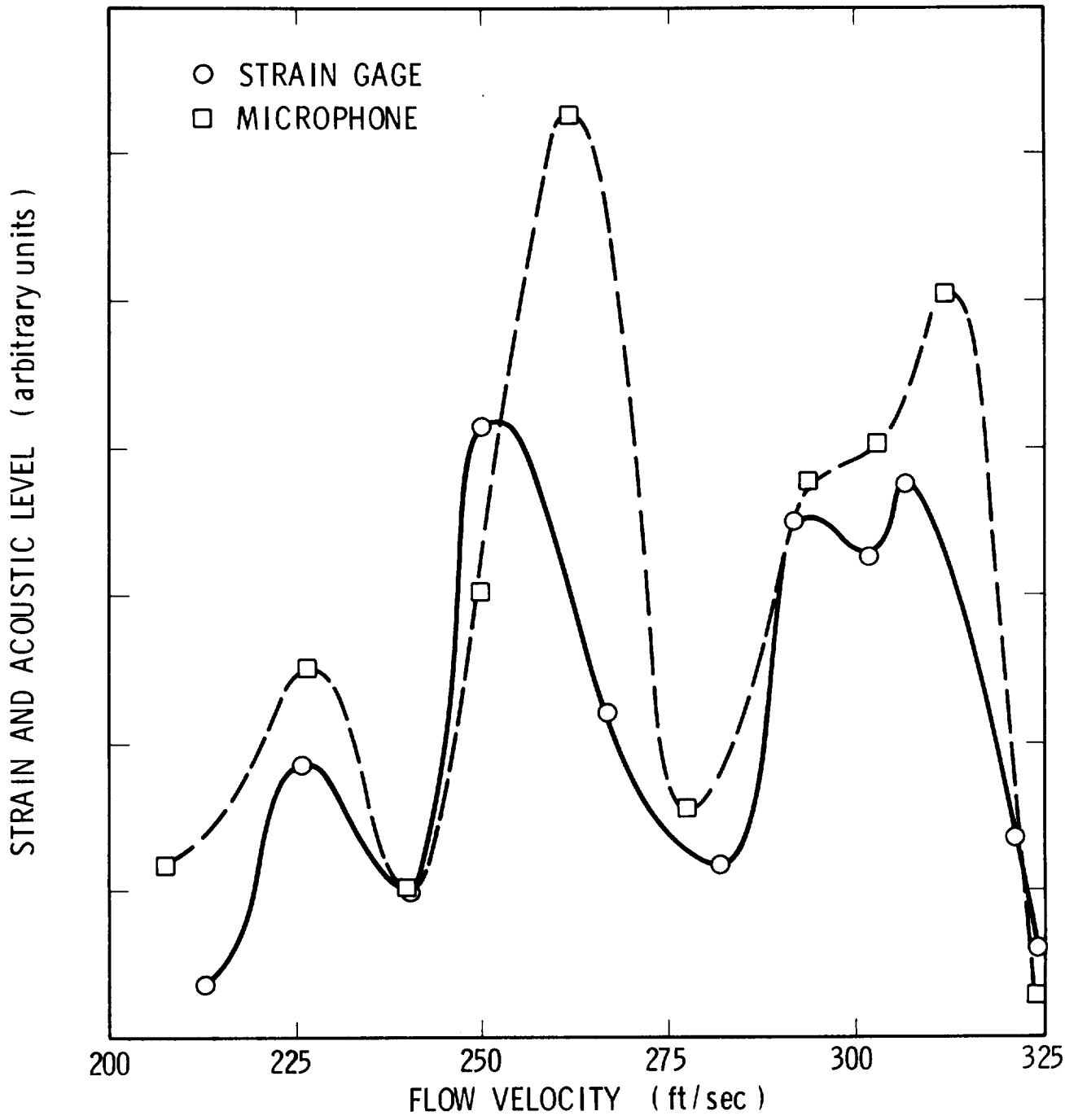

Figure 96. Comparison of Convolute Dynamic Strain and External Acoustic Sound Pressure Level (Air Flow)

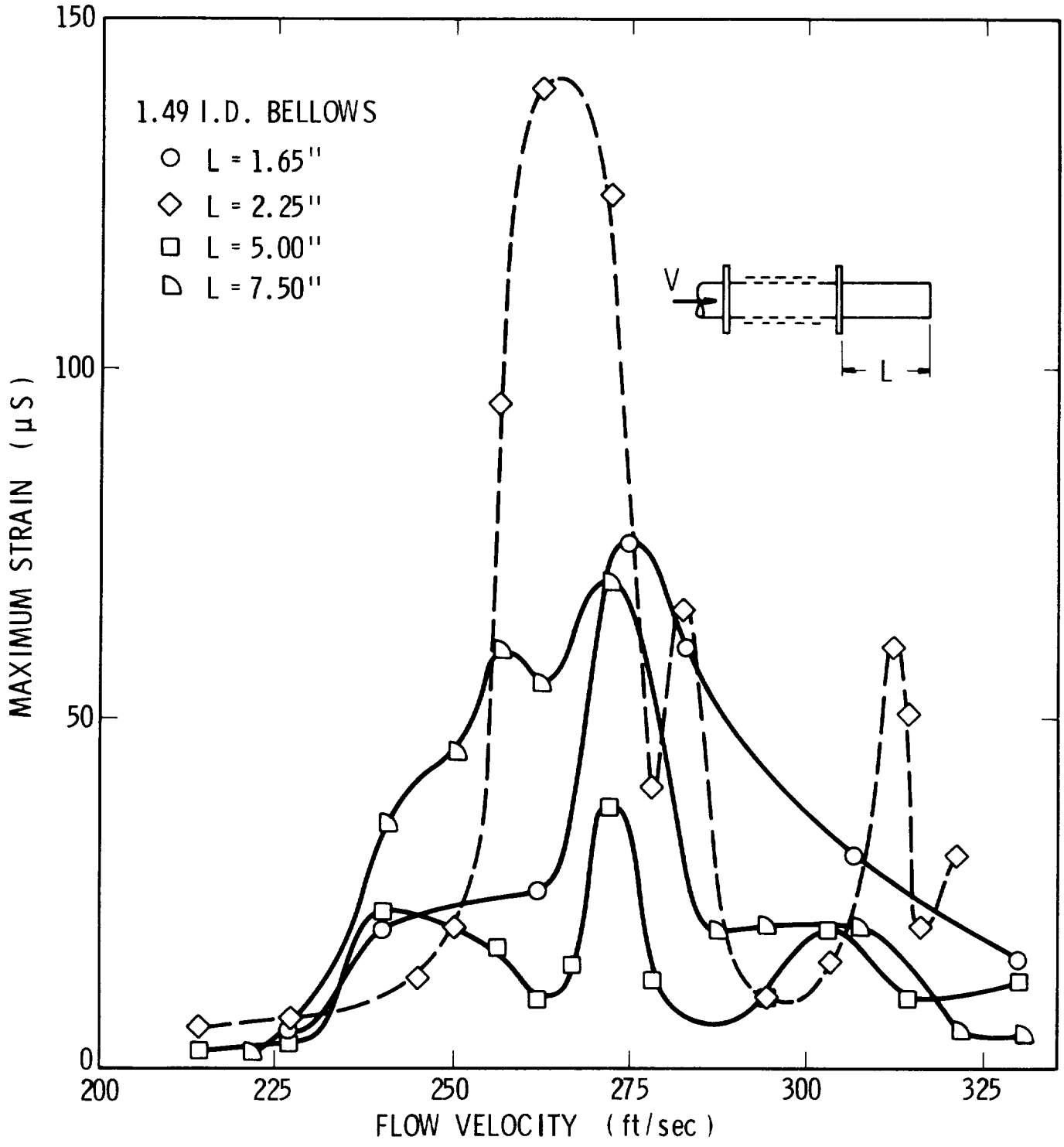

Figure 97. Effect of Exit Duct Length on Bellows Vibration Amplitude With Acoustic Resonance (Air Flow)

where λ_s = sound wavelength, c_0 = speed of sound in gas, f = vortex shedding frequency. Vibration response data for the 3-in. I. D. test bellows are shown in Figures 98, 99 and 100. These results are typical of those obtained with the other 3-in. test bellows.

Bellows No. 12 has 13 convolutes and, therefore, the longitudinal vibrational model predicts a 25-degree-of-freedom system with the highest vibrational mode being the 25th. Figure 98 shows a low level strain response occurring at the 25th mode and below this velocity no appreciable strain level is recorded. However, at approximately 190 feet per second, a high level strain resonance was recorded accompanied by an intense noise level. Estimating the acoustic resonance condition by comparing the calculated acoustic wavelength λ_s with the bellows diameter (where $f = V_g S/\sigma$) indicates an acoustic wavelength of 3. 15 in., which compares closely with the 3-in. I. D. of the test specimen.

Figure 99 shows bellows flow response with internal freon (F-12) flow for three cases of expansion and compression of the bellows length. The results for all three cases indicate the same trends as the previously exhibited air data. For bellows No. 3, the highest predicted longitudinal vibrational mode (the 25th) occurs at approximately 55 feet per second. However, no appreciable strain is recorded (Figure 99) until the flow velocity reaches approximately 80 to 100 fps. Similar response is shown in Figure 100 for test bellows No. 4. Also shown in Figures 99 and 100 are the effects of bellows length and pressure on the acoustic flow-induced response. The results indicate that some change in flow response is observed when the above parameters are varied. However the results show that comparing the acoustic wavelength at the recorded flow velocities to the internal bellows diameters is still a good indication of expected flow regimes where acoustic resonance will occur. As a result of all our gas flow tests, we can generally say that the condition for acoustic resonance may be predicted as follows:

(1) For closed pitched convolutes, assume the bellows I. D. is equal to the starting acoustic wavelength. The corresponding resonance frequency is then calculated from $f = C_o/d$ and the frequency is related to the critical flow velocity through the Strouhal number by $V = f\sigma/s = C_o\sigma/Sd$.

(2) For straight wall convolutes, assume the starting acoustic wavelength is equal to the bellows mean diameter.

(3) For open pitch convolutes, assume λ_s is equal to the bellows O. D. less two wall thicknesses.

It should be emphasized that the above simply defines a starting condition for acoustic resonance and that as fluid velocities are further increased,

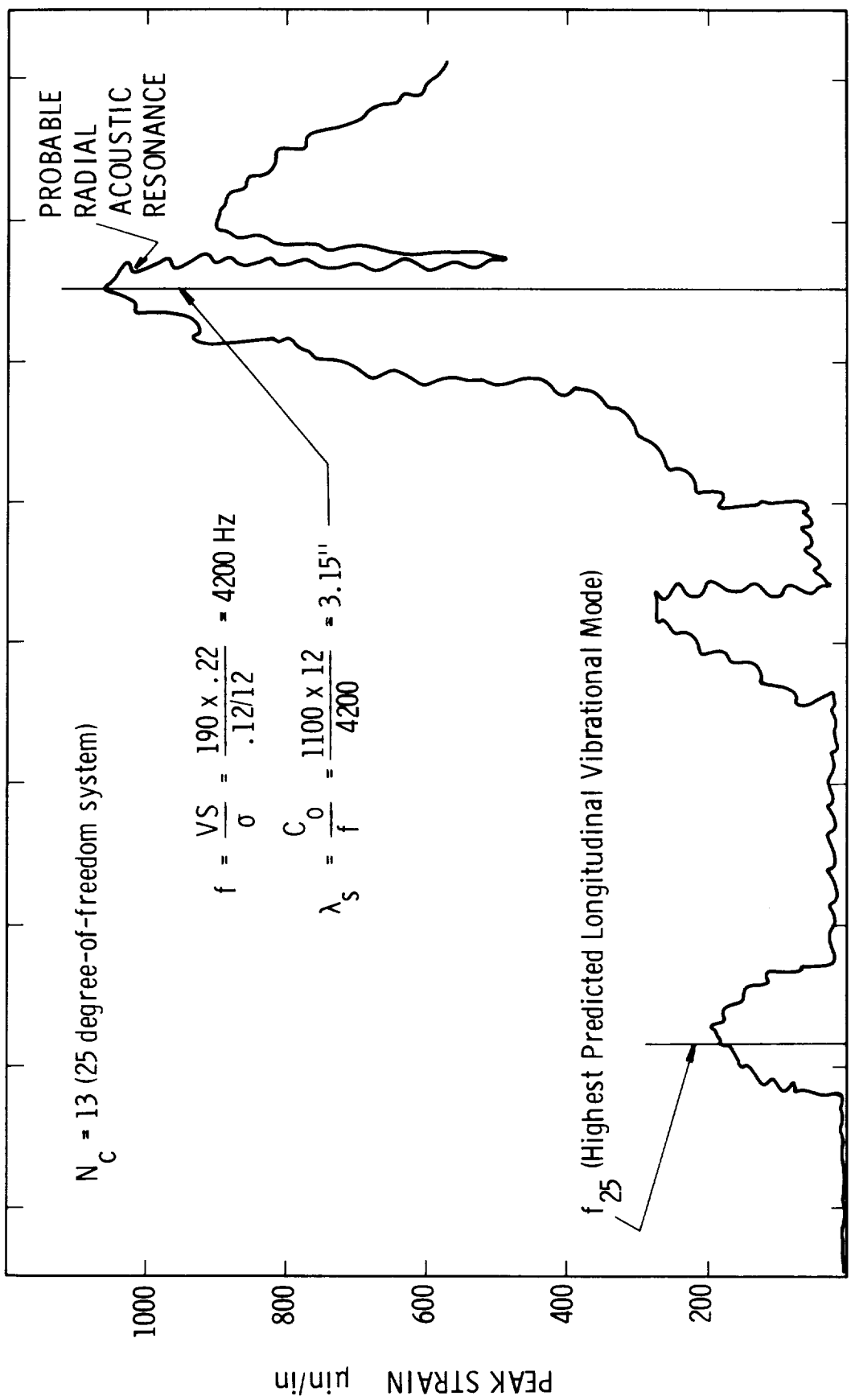

Figure 98. Flow Response for 3" ID Test Bellows #12 With Internal Air Flow

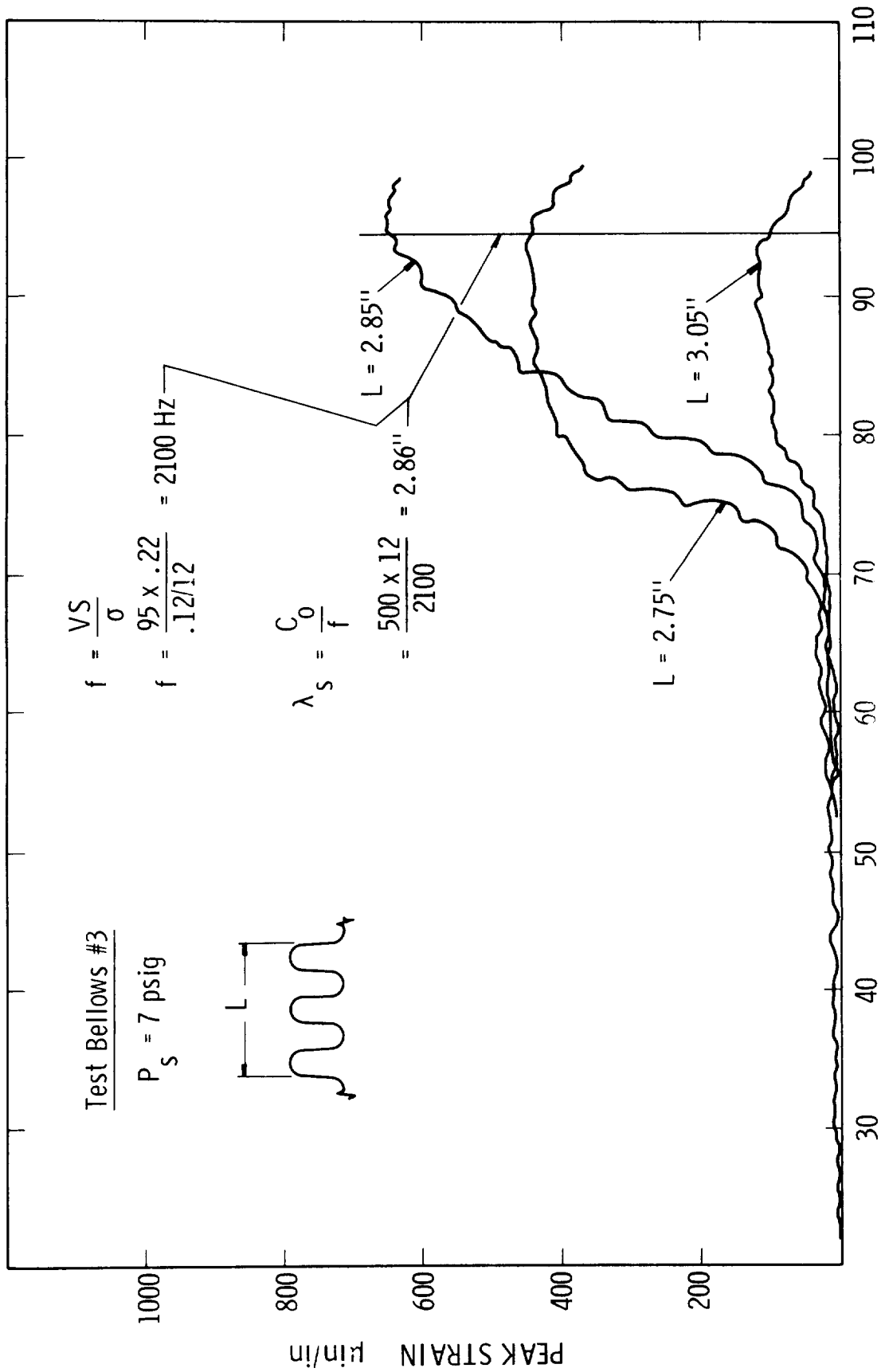

Figure 99. Effect of Bellows Length on Flow-Induced Vibrations with Internal Freon Flow

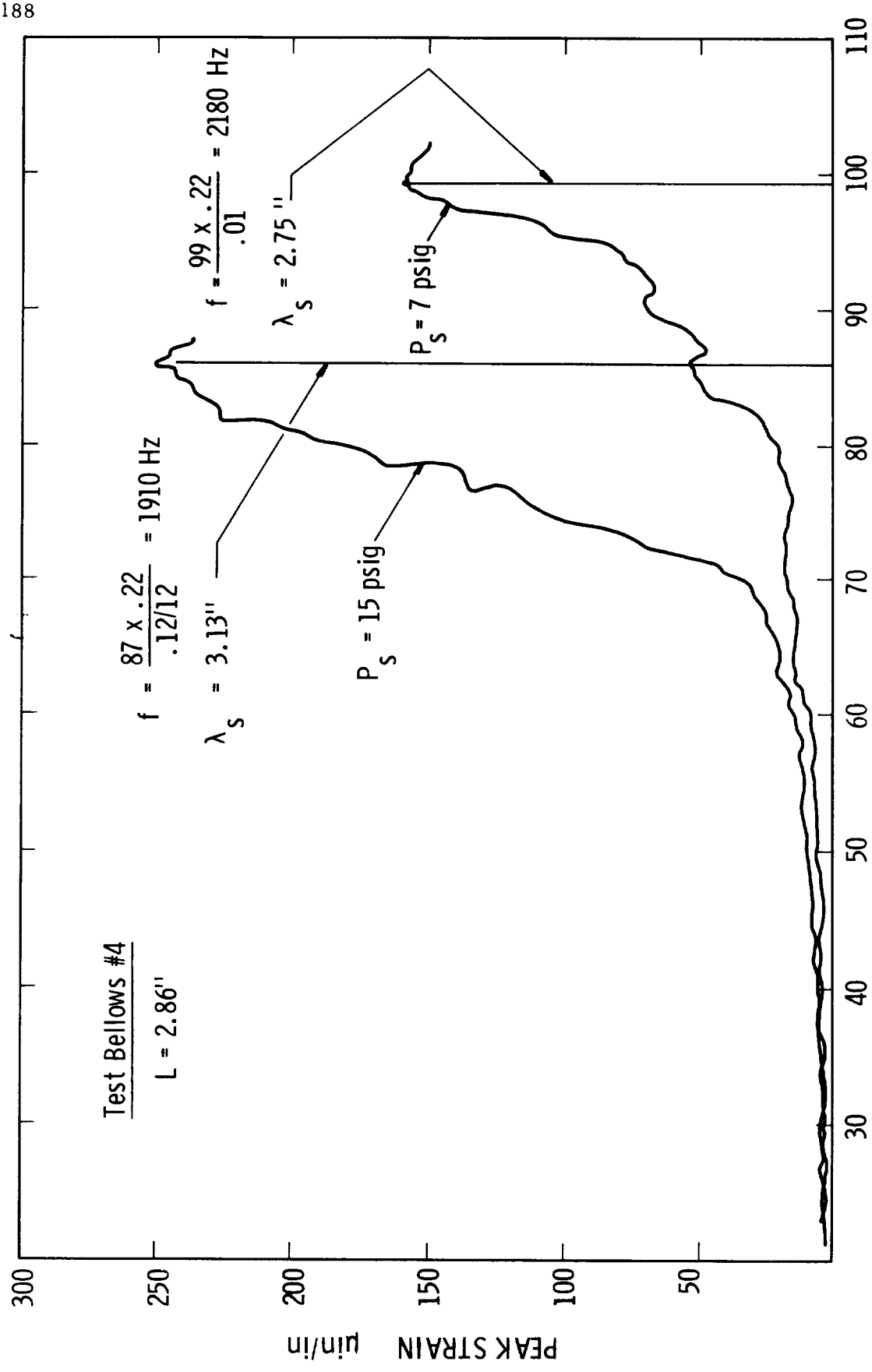

Figure 100. Effect of Bellows Static Pressure on Flow-Induced Vibrations with Internal Freon Flow

acoustic resonance is generally maintained and the vibration may become more severe depending on the presence of bellows modes which can be excited. All the above rules provide a general "rule of thumb" to determine the condition for radial acoustic resonance in bellows. A more detailed theoretical analysis was undertaken to better define the effects of acoustic resonance on bellows vibrations.

V.3 Theoretical Results

Methods for predicting higher order resonant conditions in circular fluid conduits are given in Reference 12. However, the solutions are not valid for a bellows where the convoluted wall must be treated differently from a straight wall section. For the case of a straight wall section, the fluid radial impedance is given in Reference 12 as

$$\frac{P_1}{V_r} = \left(\frac{\rho_o c_o^2}{s}\right) \left[\frac{B\,(\gamma^2 - \beta^2)\, J_o(\beta r_o)}{B\,\beta\, J_1(\beta r_o) + A\gamma\, J_1(Kr_o)}\right] \tag{54}$$

The condition of zero axial fluid velocity at the wall yields

$$B\, J_o(\beta r_o) + A\, K\, J_o(Kr_o) = 0 \tag{55}$$

and combining Equations (54) and (55) and eliminating the arbitrary constants A and B yields

$$\frac{P_1}{V_r} = \frac{(\gamma^2 - \beta^2)\,(\rho_o\, C_o^2/s)}{\left[\dfrac{\beta\, J_1(\beta r_o)}{J_o(\beta r_o)} - \dfrac{\lambda^2}{K}\,\dfrac{J_1(Kr_o)}{J_o(Kr_o)}\right]} \tag{56}$$

which is the radial impedance of the fluid at the wall. In these equations, γ is a separation constant and $J_o(\beta r_o)$ and $J_1(Kr_o)$ denote the zero and first order Bessel functions of the first kind with arguments βr_o and Kr_o, respectively. In addition, the parameters, K, γ, and β are related by

$$\beta^2 = \gamma^2 - (s/C_o)^2 = K^2 - (s/C_o)^2 + s/\upsilon \tag{57}$$

The parameter s in Equations (54), (56) and (57) is the Laplace operator, where these equations have been transformed into the Laplace domain for convenience, and υ is the kinematic viscosity of the fluid.

In order to obtain the solution for radial acoustic resonance in bellows, one must determine the fluid radial impedance at the wall in terms of the bellows wall geometry and equate the resulting expression to Equation (56). Referring to Figure 101, the difference between the pressure in the convolute and the internal flow pressure is given by

$$P_1 - P_2 = I_q \frac{dq}{dt} \tag{58}$$

Likewise the flow rate, q, from the bellows convolutes into the free stream flow is given by

$$q = C_q \frac{dP_2}{dt} \tag{59}$$

In equations (58) and (59) I_q and C_q are the bellows convolute fluid impedance and capacitance respectively and are given by

$$I_q = \rho_o h/\delta\pi D_m \tag{60}$$

$$C_q = h\sigma\pi D_m/P_o k \tag{61}$$

where D_m is the mean bellows diameter, P_o the free stream pressure and k the specific heat ratio. Transforming Equations (58) and (59) into the Laplace domain yields

$$P_1 - P_2 = I_q S Q \tag{62}$$

$$Q = S C_q P_2 \tag{63}$$

and combining Equations (62) and (63) yields

$$P_1/Q = (I_q S + 1/C_q s) \tag{64}$$

The radial velocity of the fluid into or out of the convolutes is estimated by

$$V_r = Q/A_\omega = \frac{Q}{\pi D_m} \left(\frac{1}{\delta + \sigma}\right) \tag{65}$$

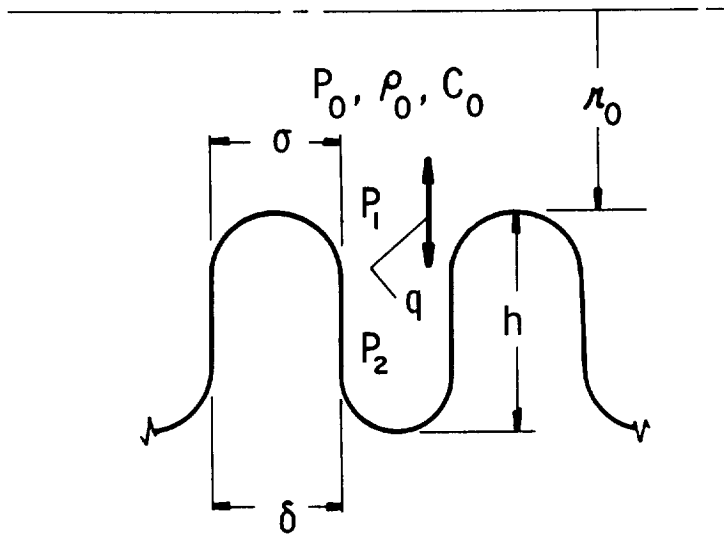

Figure 101. Important Parameters for Modeling Fluid Radial Impedance at Bellows Wall

Substitution of Equations (62), (63) and (65) into (64) yields

$$P_1/V_r = \left(\frac{2 P_o k}{h} + 2 \rho_o h s^2 \right) \quad /s \qquad (66)$$

which is the fluid radial impedance at the wall due to the bellows convolutes. Setting Equation (66) equal to Equation (56) and making the parameters nondimensional yields

$$\frac{(G_N^2 - B_N^2)}{\left[B_N \frac{J_1(B_N)}{J_o(B_N)} - \frac{G_N^2}{K_N} \frac{J_1(K_N)}{J_o(K_N)} \right]} = \frac{2 r_o}{h} + \frac{2h}{r_o} FN^2 \qquad (67)$$

Equation (67), together with Equation (57), which in dimensionless form is

$$B_N^2 = G_N^2 - FN^2 = K_N^2 + FN^2 + FN/DN \qquad (68)$$

are solved simultaneously to predict the conditions of radial acoustic resonance in bellows. In Equations (67) and (68) the dimensionless parameters are defined as follows:

$$G_N = \gamma_m r_o$$

$$B_N = \beta_m r_o$$

$$K_N = K_m r_o$$

$$FN = s r_o / C_o$$

$$DN = \upsilon / C_o r_o$$

Each set of eigenvalues K_n, γ_n and β_n (where $n = 0, 1, 2, 3\ldots$) represent a solution to Equations (67) and (68). The solution for the zeroth mode ($n = 0$) represents an axial acoustic resonance of the bellows structure. The solution for the first mode ($n = 1$) represents the first radial mode. Likewise, from $n = 2 \rightarrow \infty$ represents higher order radial modes in the bellows structure. To determine resonant conditions, Equation (67) and (68) were programmed and solved numerically on a CDC 6400 digital

computer for conditions representing the current 3-inch diameter test bellows with internal air flow. The first mode spatial attenuation versus frequency number for test bellows with convolute heights of 0.3 inch is shown in Figure 102 and the dimensionless phase velocity versus frequency number is given in Figure 103. The resonant condition (FN = 3.5) for the first radial acoustic mode in these bellows is indicated in the two figures. Thus, the first acoustic radial mode occurs at a frequency number of about 3.5 which yields a theoretical value for the first resonant frequency of 4900 Hz. The experimental first mode acoustical resonant frequencies are shown in Table XIV for 3-inch test bellows numbers 4, 5, 8 and 9 which have a 0.3-inch convolute height. Good agreement is observed between the predicted and the experimental values.

In addition, the first mode spatial attenuation versus frequency number for 3" I.D. bellows is shown in Figure 104 with internal air flow for convolute heights up to 0.5 in. The results in Figure 104 indicate that as the convolutes become deeper, the frequency number at resonance is reduced resulting in a decrease in flow velocity required to produce the first radial acoustic mode. The straight wall case presented in Figure 104 (h = 0) represents an upper limit on frequency number for the first radial mode.

The theoretical frequency number at resonance is shown in Figure 105 as a function of convolute height. Also shown on this figure is experimental data obtained for the first radial acoustic mode with the three inch bellows with internal air flow. A lock-in range is present under radial acoustic resonant conditions as is the case for longitudinal vibrational modes. The data scatter at any convolute height shown on Figure 105 is indicative of the lock-in range over which the first radial acoustic mode occurs. As noted in Figure 105, the trend in the data is in good agreement with the theoretical curve for the first radial acoustic mode.

The theoretical analysis presented in this section provides a method for determining the acoustic modes in a bellows structure which are responsible for high level vibrations with internal gas flows. Using this theory will provide a prediction of resonance conditions as a function of convolute geometry and gas properties. In general, critical flow conditions for internal gas flows can be estimated by comparing the acoustic wavelength to the internal bellows diameter. When a more detailed examination is required, the theory presented herein may be utilized.

V.4 Flex Hose Acoustic Resonance Induced Failure

During the course of the present study, an experimental investigation of the flow-induced failure of the Saturn S-II LOX pre-pressurization system

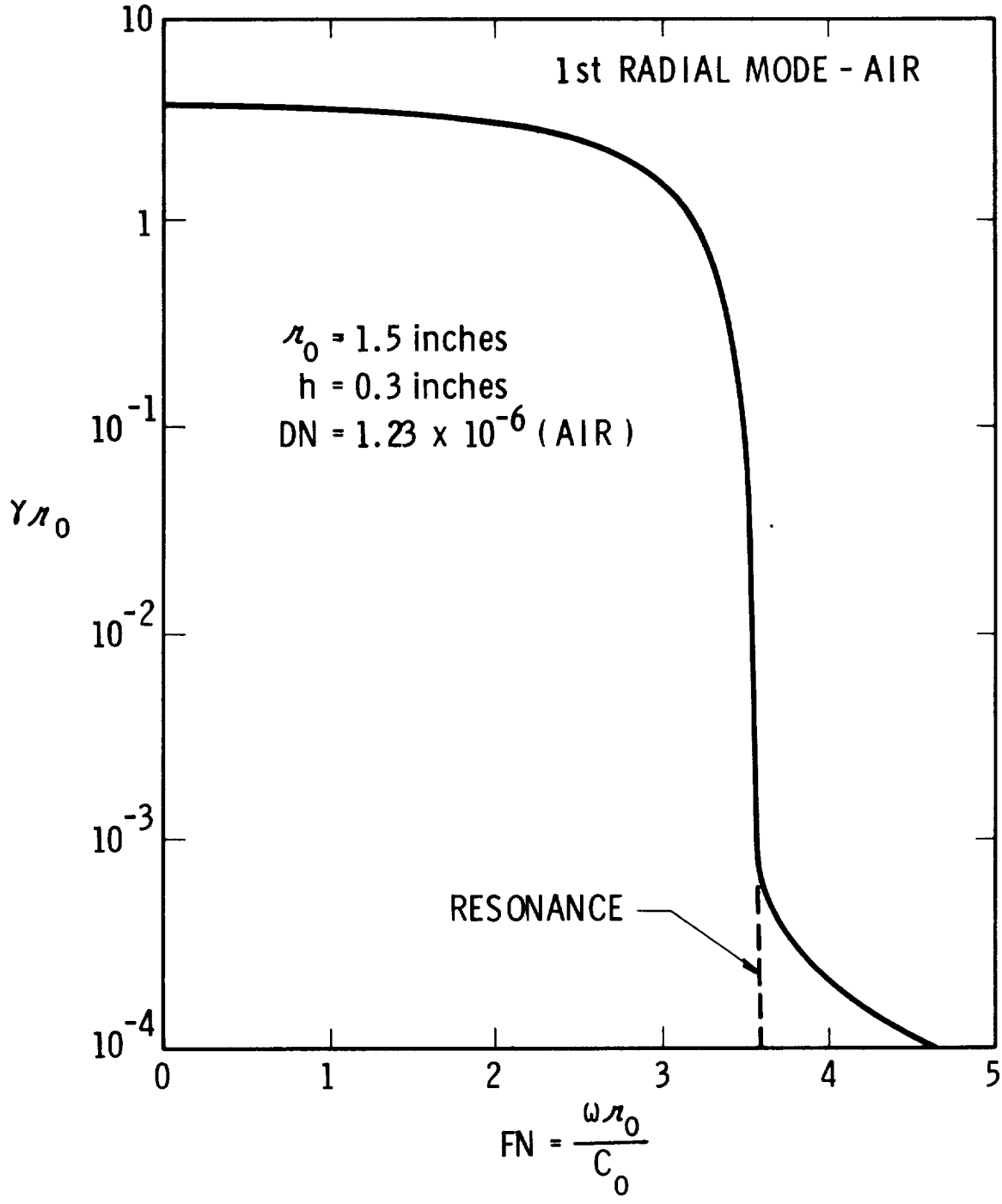

Figure 102. First Mode Spatial Attenuation versus FN for Bellows Numbers 4, 5, 9 and 10

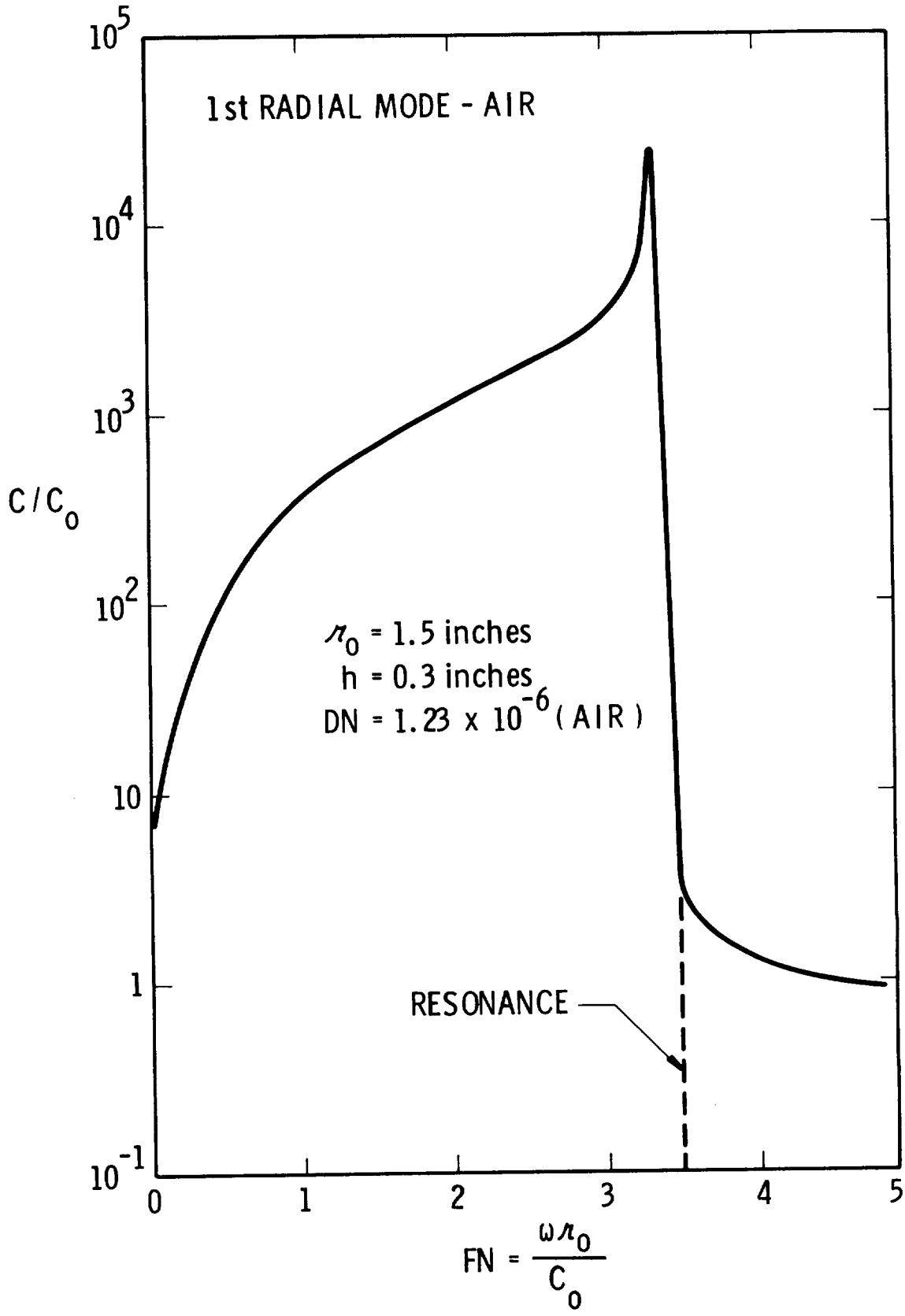

Figure 103. Dimensionless Phase Velocity, C/C_0, versus FN for Bellows Numbers 4, 5, 9 and 10

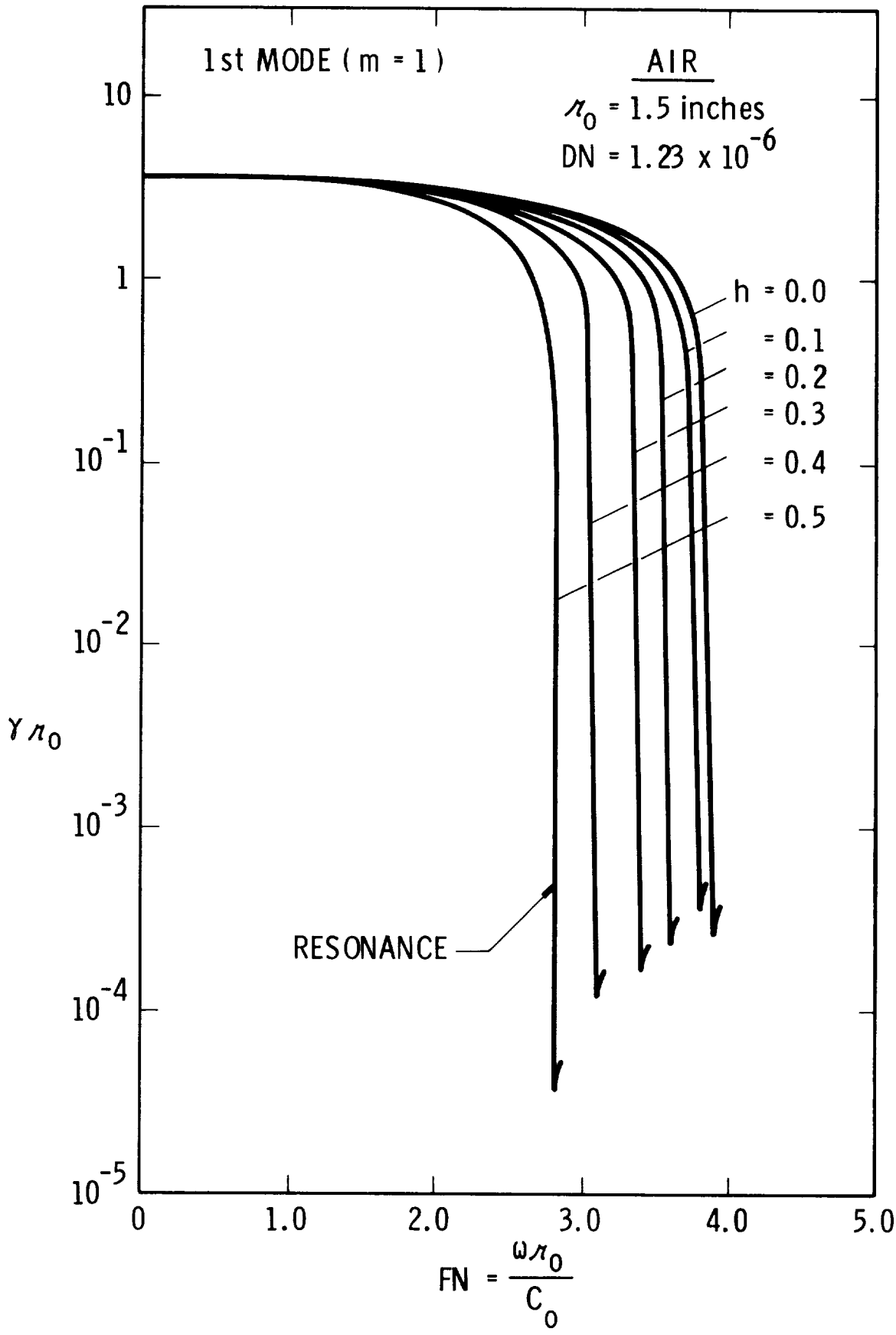

Figure 104. First Mode Spatial Attenuation versus Frequency Number

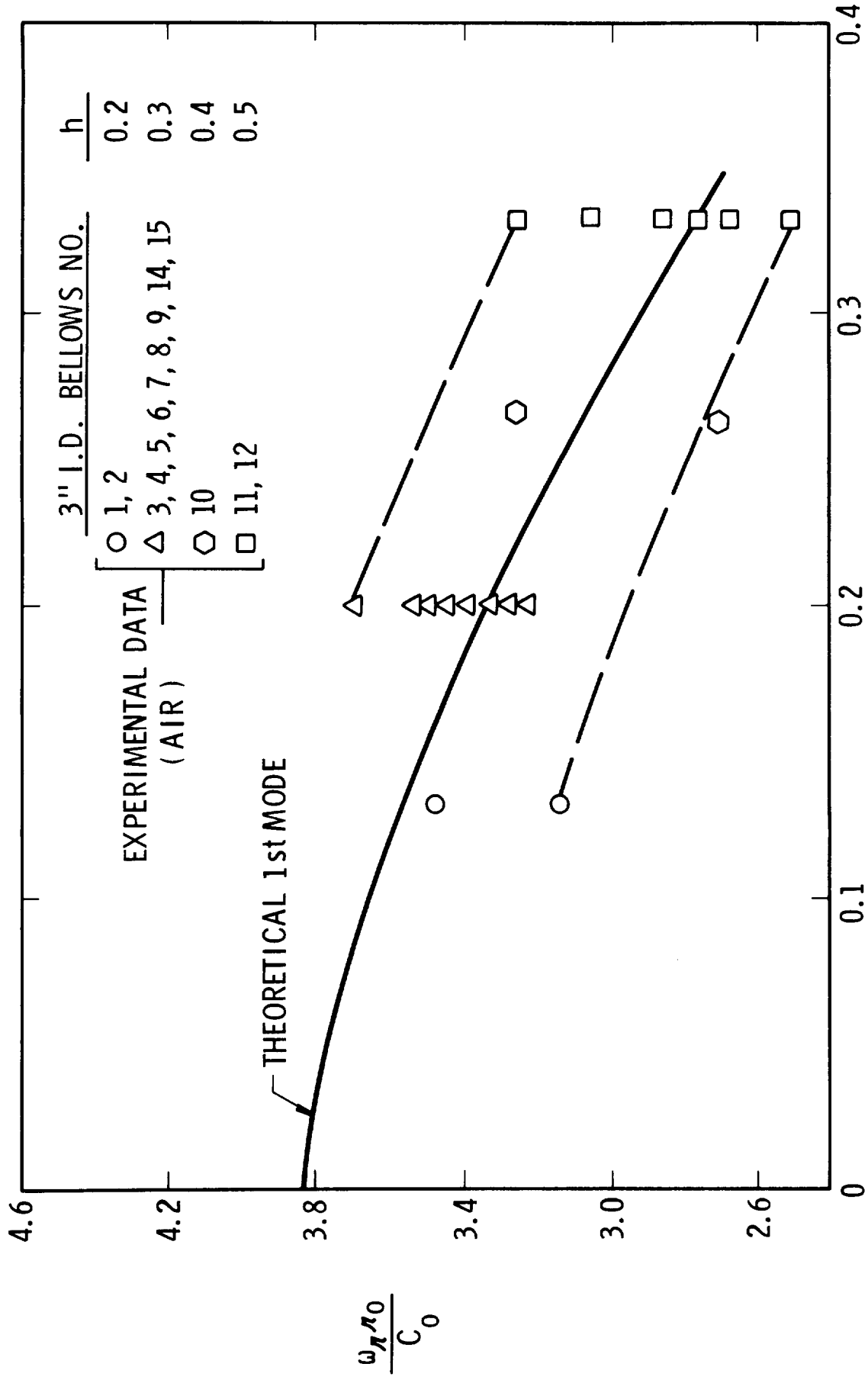

Figure 105. Comparison of Theory and Experiment for 1st Radial Acoustic Mode for 3 inch Diameter Test Bellows

TABLE XIV.

Comparison of Experimental and Theoretical 1st Mode Radial Acoustic Resonance for 3 Inch Test Bellows With Internal Air Flow

Bellows No.	r_o	h	$f_{ex(Hz)}$	$f_{th(Hz)}$
4	1.5"	.3"	5225	4900
5	1.5"	.3"	4950	4900
8	1.5"	.3"	5000	4900
9	1.5"	.3"	4650	4900

flexible hoses was conducted. This was done to assist MSFC and North American, Space Division, with an overall investigation and cure of the problem which had occurred on a vehicle. Appendix D of this report gives results of our work, while Reference 13 gives details of the overall study conducted at North American.

V.5 Stress Indicator for Gas Flows

Based on the experimental results, the Stress Indicator approach appears valid for the case of internal gas flows if the value of C_F or $C_F Q$ is increased by a factor of 5.

VI. BELLOWS LINER DESIGN AND EXTERNAL DAMPING DEVICES

VI. 1 Cone Liners for Reduction of Vibrations

A limited study of cone-shaped liners was made with the specific purpose of determining how much of the bellows must be covered by the liner to effectively stop flow-induced vibrations. The liners being considered here are simple, truncated, hollow cones formed from thin sheet metal which are mounted at the entrance of a bellows and extend into the bellows itself. The cone shape allows angular movement of the bellows but also produces a constriction, and a resulting pressure drop, which is discussed in the next section.

An initial aspect of the liner study was to determine the nature of the velocity profiles downstream of the liner; this, it was hoped, would provide some insight into how far the liner should extend into the bellows to prevent vibration. Pitot tube traverses were run downstream of convergent inserts mounted in a 2-inch ID duct to determine the shape of a fluid jet as it emerges from the end of a cone liner. The resultant velocity profiles are shown in Figure 106 where the velocity downstream has been normalized by the velocity at the center of the cone exit.

The influence of the cone angle was not very pronounced, but there was a vena-contracta present with the 30° cone which was not present with the 10° or 20° cones. This was quite noticeable from the Pitot differential pressure which represents the square of velocity. However, the actual center velocity at the vena-contracta was only about 3% greater than at the cone outlet. Comparison of the flow profiles at station #6 with and without the inserts shows that the flow is noticeably affected as far as 5 or 6 outlet diameters away from the insert. This would indicate that a considerable part of a bellows could be left uncovered when a cone-shaped liner is used.

In order to determine the extent to which this information could be applied to an actual situation, two -1/2-inch ID bellows of different convolution geometries (#110 and #112)* were flow tested with water using a movable liner that could be positioned at any axial location within the bellows. Since

---

* See Appendix B for a list of dimensional data on all test bellows.

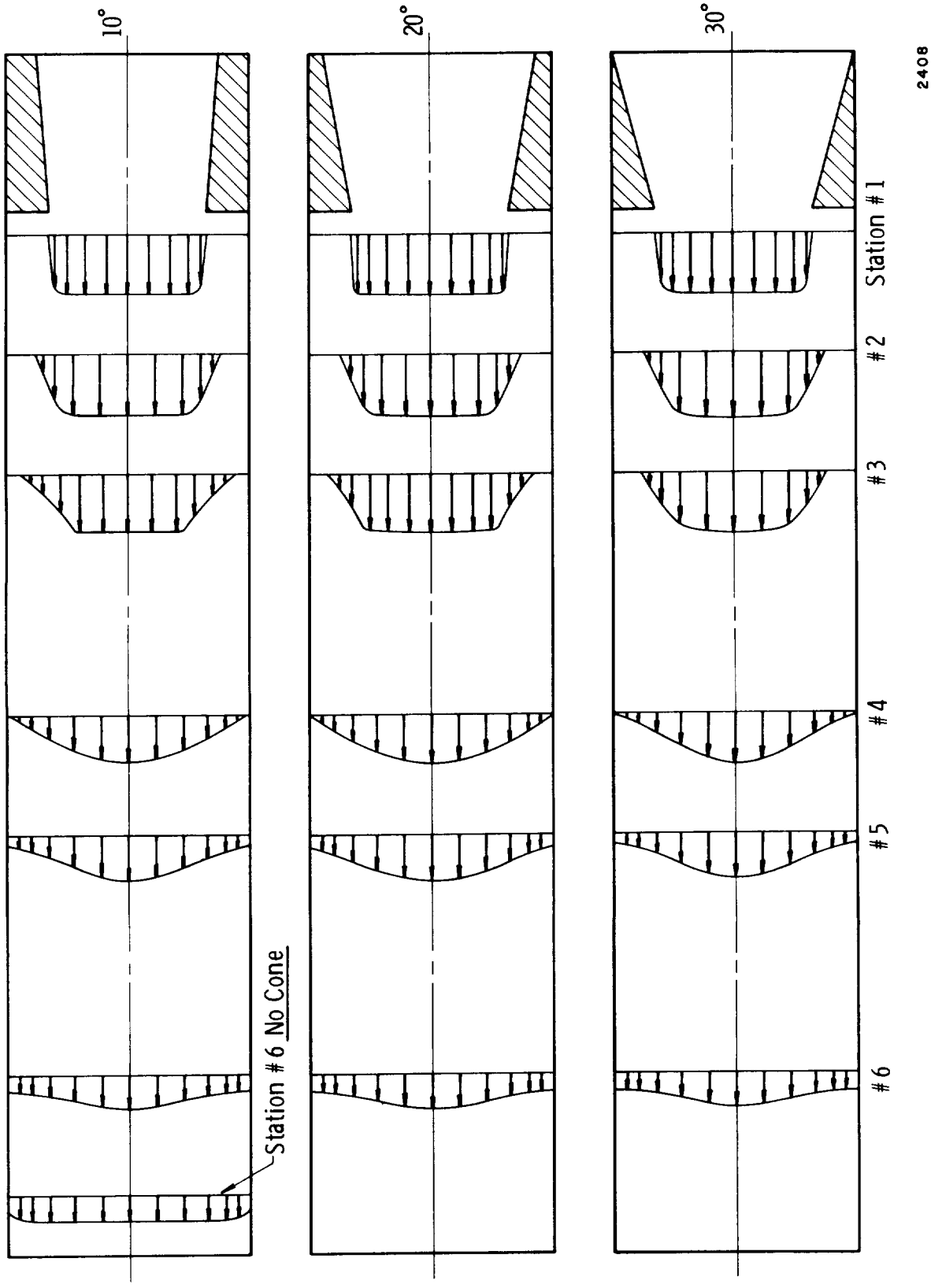

Figure 106. Flow Patterns Downstream Of Cone Shaped Liners

the effect of cone angle on the flow pattern was rather small, only one liner configuration was tested. The liner had an outlet diameter of 1-1/4", a length of 11/16", and a 10^{o} included angle. The fluid velocity was varied from 0 to 70 ft/sec based on bellows diameter and maximum dynamic strain was recorded for several liner positions. The results are shown in Figure 107.

Even with the liner completely withdrawn from the bellows, the strain level was reduced from that of an unlined bellows; this result is in agreement with the velocity profile observations. However, all modal vibrations were not stopped until the liner covered all but one or two convolution roots. The modes which were present did not occur in order. In some cases the first mode was present at two different flow rates while the second mode was completely absent over the entire flow range.

Operating the bellows at an angle did not significantly affect the dynamic strain readings for these particular bellows-liner arrangements. There probably are cases where the effects of angulation are significant.

The effectiveness of a cone liner or the effect of angulation would be difficult to predict analytically due to the highly turbulent expansion which takes place at the liner exit. The tests which have been performed can serve as a guide, but more testing of different types of bellows is required before reliable empirical design is possible. At this time, however, we offer the following design guidelines:

(1) If the bellows failure problem without a liner is severe, then the liner should cover most if not all of the active convolutions. If pressure loss is a problem, the liner might be reduced in length somewhat, possibly allowing some bellows vibration. Testing should be performed to verify the design; preferably, a "before and after" test should be conducted with one or more bellows.

(2) If the bellows vibrations are not too severe without the liner, then a very short liner extending over, say, about one-fourth of the convoluted length should offer substantial reduction in vibration levels. Again, the design should be verified with testing.

(3) On any liner design, an important consideration is weight which means the liner thickness, as well as length, should be minimized. Any proposed design should be subjected to a buckling analysis to assure that it will not collapse as a

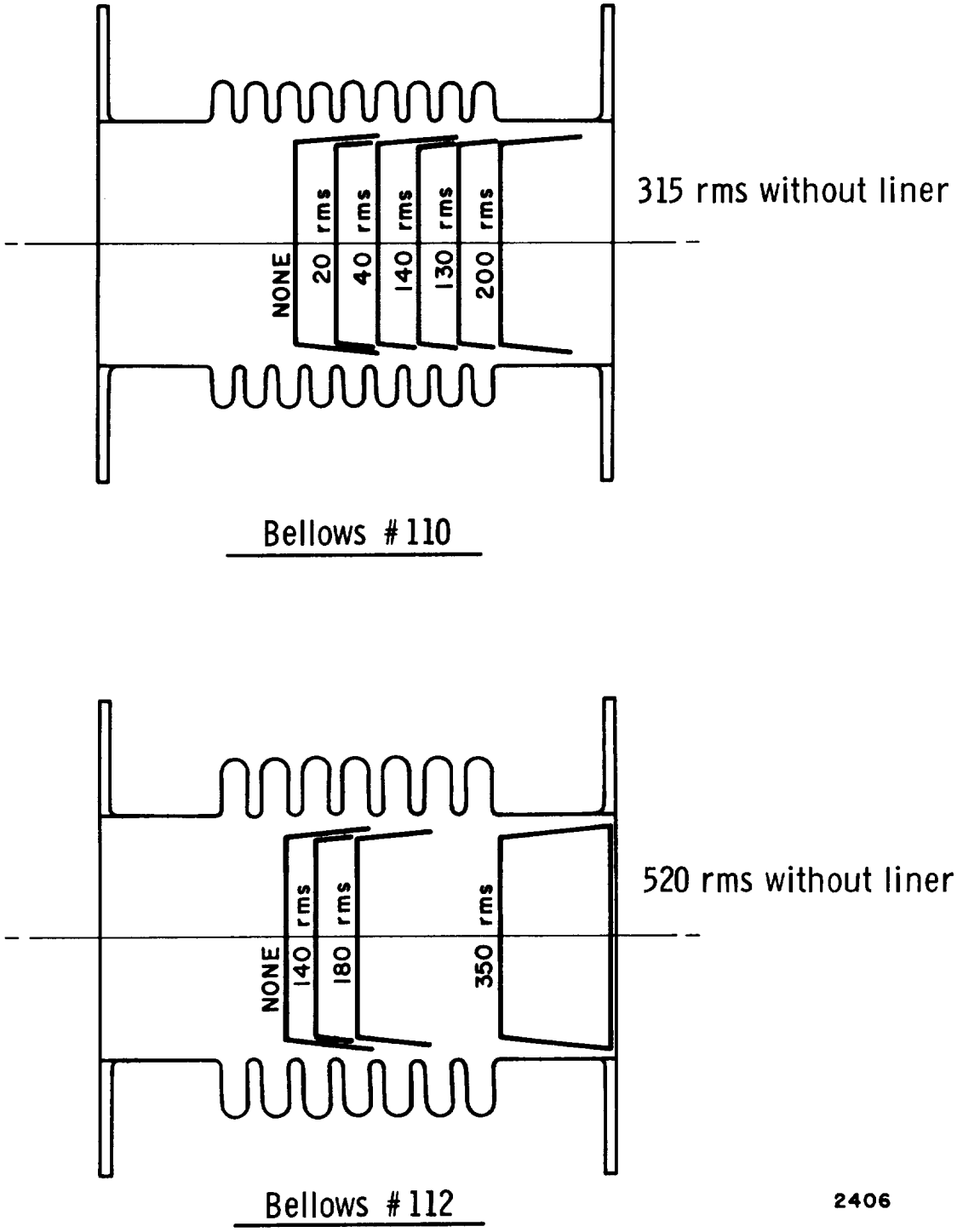

Figure 107. Maximum Dynamic Strain For Fluid Velocities From 0 - 70 ft/sec (Water - 75°F)

result of the differential pressure. Also, the designer should be aware of potential "splitting" problems caused by turbulent flow excitation of the liner. High dynamic pressure situations should be approached with care.

VI. 2 Pressure Loss of Cone Liners

An important point for consideration in regard to a proposed liner design is that the pressure loss be acceptable. It has been demonstrated that a liner can, in fact, increase the pressure drop compared with the bare bellows. The purpose of the following discussion is to demonstrate a simple procedure for estimating liner pressure drop characteristics.

Usually, a typical liner can be considered, from a fluid mechanics point of view, to consist of a contracting section followed by an expansion or, in some cases, an expansion followed by a contraction or, possibly even a series of expansions and contractions depending on the specific configuration. Assuming this to be true, then using information available in the literature for losses resulting from expansions and contractions, the liner overall pressure loss can be estimated. Figure 108 gives all of the information needed for estimating these losses. Note that for either a contraction or expansion, the pressure drop is characterized by

$$\Delta p = \frac{K\rho}{2} V_1^2 \left[1-(D_1/D_2)^2\right]^2$$

$$= \frac{K\rho}{2} V_2^2 \left[(D_2/D_1)^2-1\right]^2$$

where K is a loss factor defined in terms of the geometry of the duct as shown in Figure 108.

This prediction procedure has been checked experimentally for the liner illustrated in Figure 109 which is a conical configuration typical of a currently used design.

For a zero deflection angle, the pressure loss for this case will be the collective result of, first, the contraction in the cone section and, second, the uncontrolled expansion when the fluid exits the cone. The pressure drop will therefore be given by

$$\Delta p = \frac{\rho}{2} (K_c + K_E) \left[(D_2/D_1)^2-1\right]^2 V_2^2$$

EXPANSION

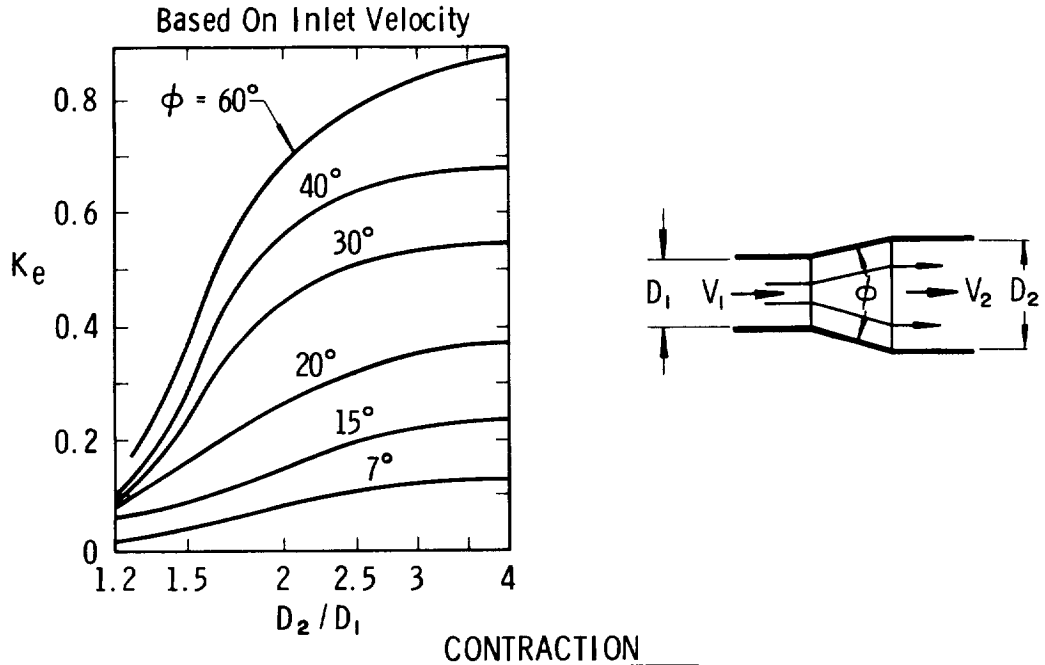

CONTRACTION

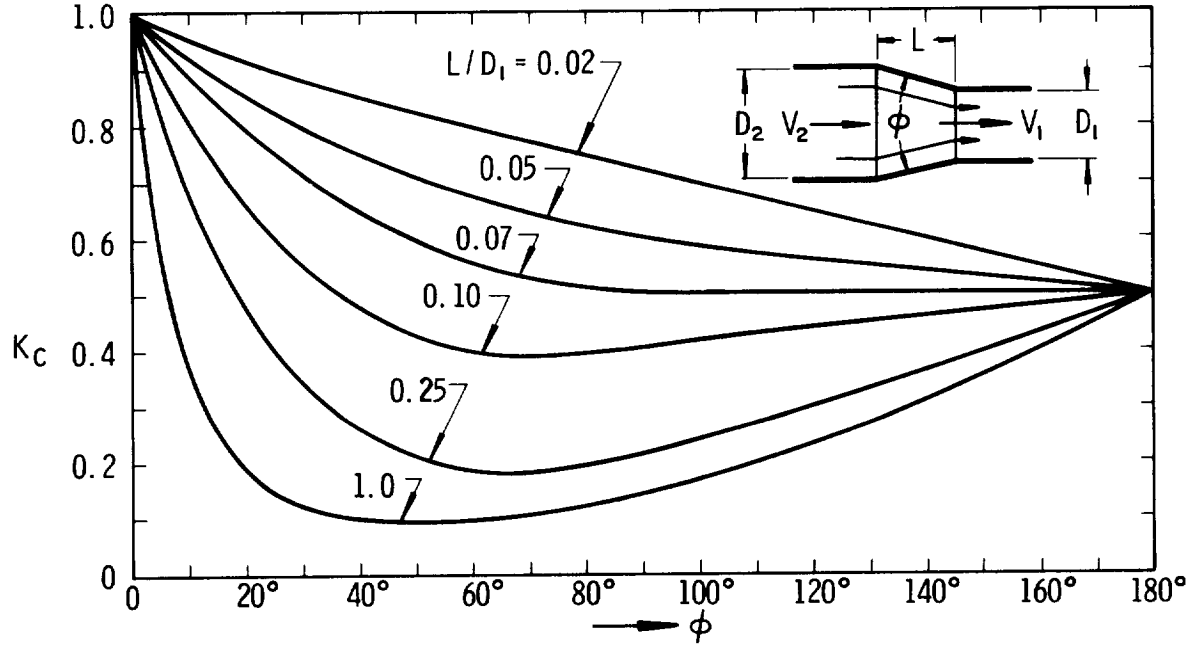

Calculations Of Pressure Drop

For Either Contractions Or Expansions, The Pressure Drop Is

$$\Delta p = \frac{K\rho}{2} V_1^2 \left[1 - (D_1/D_2)^2\right]^2 = \frac{K\rho}{2} V_2^2 \left[(D_2/D_1)^2 - 1\right]^2$$

1865

Figure 108. Flow Loss Factors For Contractions And Expansions

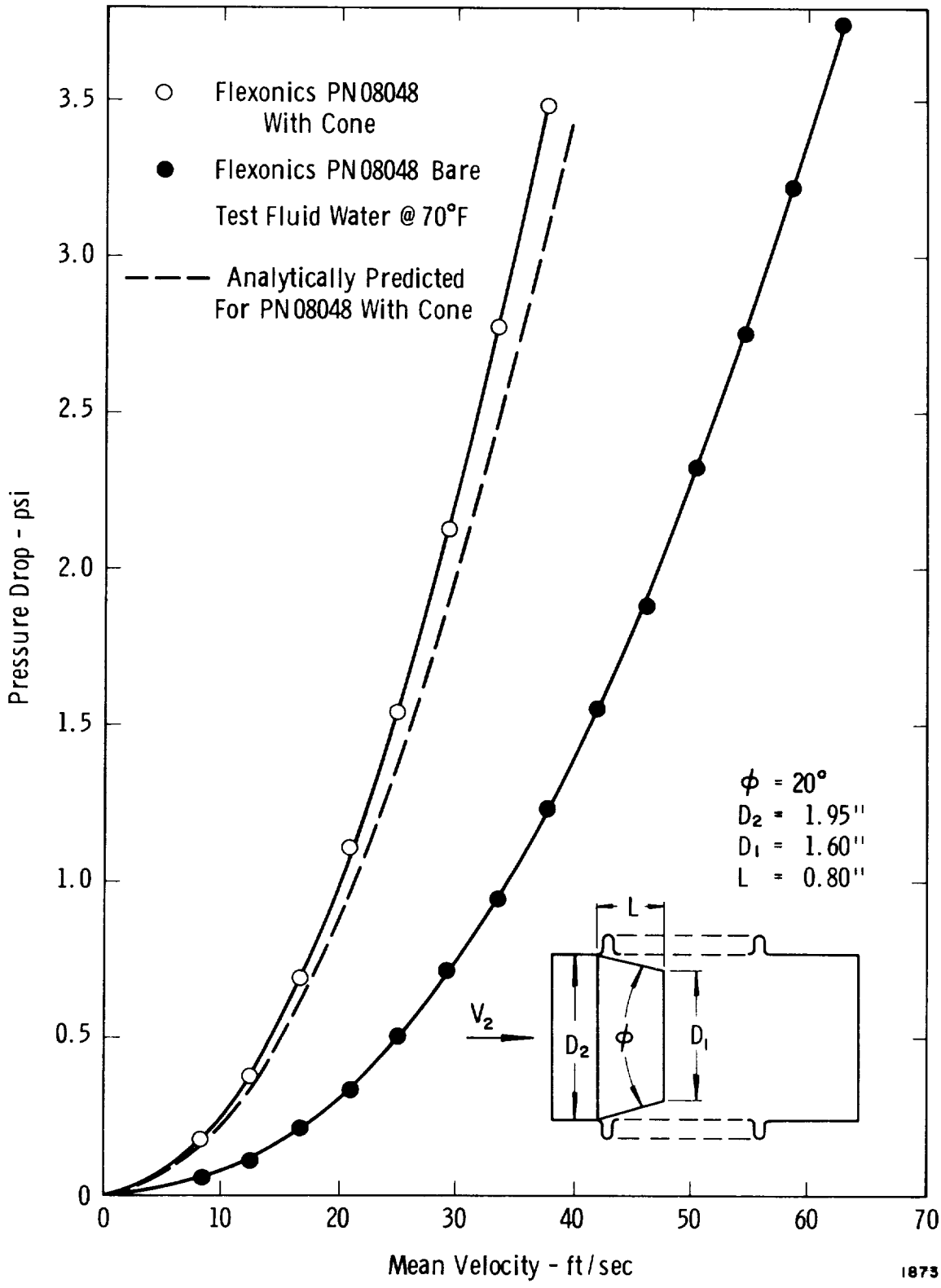

Figure 109. Comparison Of Pressure Loss For Bare Bellows And Bellows With Cone Liner

From Figure 108, the value of K_c for this cone geometry is about 0.35. The value of K_E for an uncontrolled expansion is 1.0, thus

$$\Delta p = \frac{\rho}{2} (1.35) [(1.22)^2 - 1]^2 V_2^2 = (0.324) (1/2 \rho V_2^2)$$

Figure 109 shows pressure drop as a function of mean flow velocity predicted by the above equation, and also the pressure drop obtained experimentally for this same conical liner configuration. Figure 109 also shows the experimentally obtained pressure loss for the bare bellows (no liner) used for the tests. In this case, the liner is responsible for an increase in pressure loss.

VI. 3 External Damping Devices

One possible means of reducing the stresses in a bellows resulting from internal flow is to add damping to the bellows structure. The attractive feature of this method of reducing stress is that it allows the designer to possibly "fix" a bellows which has demonstrated some fatigue tendencies, but is otherwise satisfactory. Our work to date in this area has been strictly exploratory; several external damping ideas have been tried with two basic objectives, (1) to find out in a quantitative fashion how much the damping can be increased under ideal conditions, and (2) to compare the relative increase in damping for several devices or ideas. Three types of external damping ideas have been tried thus far; these are:

(1) Filling the convolutions with some damping material, usually a viscoelastic material, such as RTV rubber, 3M strip-caulk (a putty-like material), and a polystyrene foam.

(2) Placing a metal spring or rubber "O" ring in each convolution.

(3) Wrapping the exterior of the bellows with screen wire.

Figure 110 shows a photograph of several bellows with various external damping devices added. Flow tests have been run on several of these "damped" bellows to explore very briefly their possibilities. Figures 111 and 112 show some of the test results. In Figure 111, a comparison is shown between an undamped bellows and the same bellows with two types of dampers; the external screen and the neoprene "O" rings. In general,

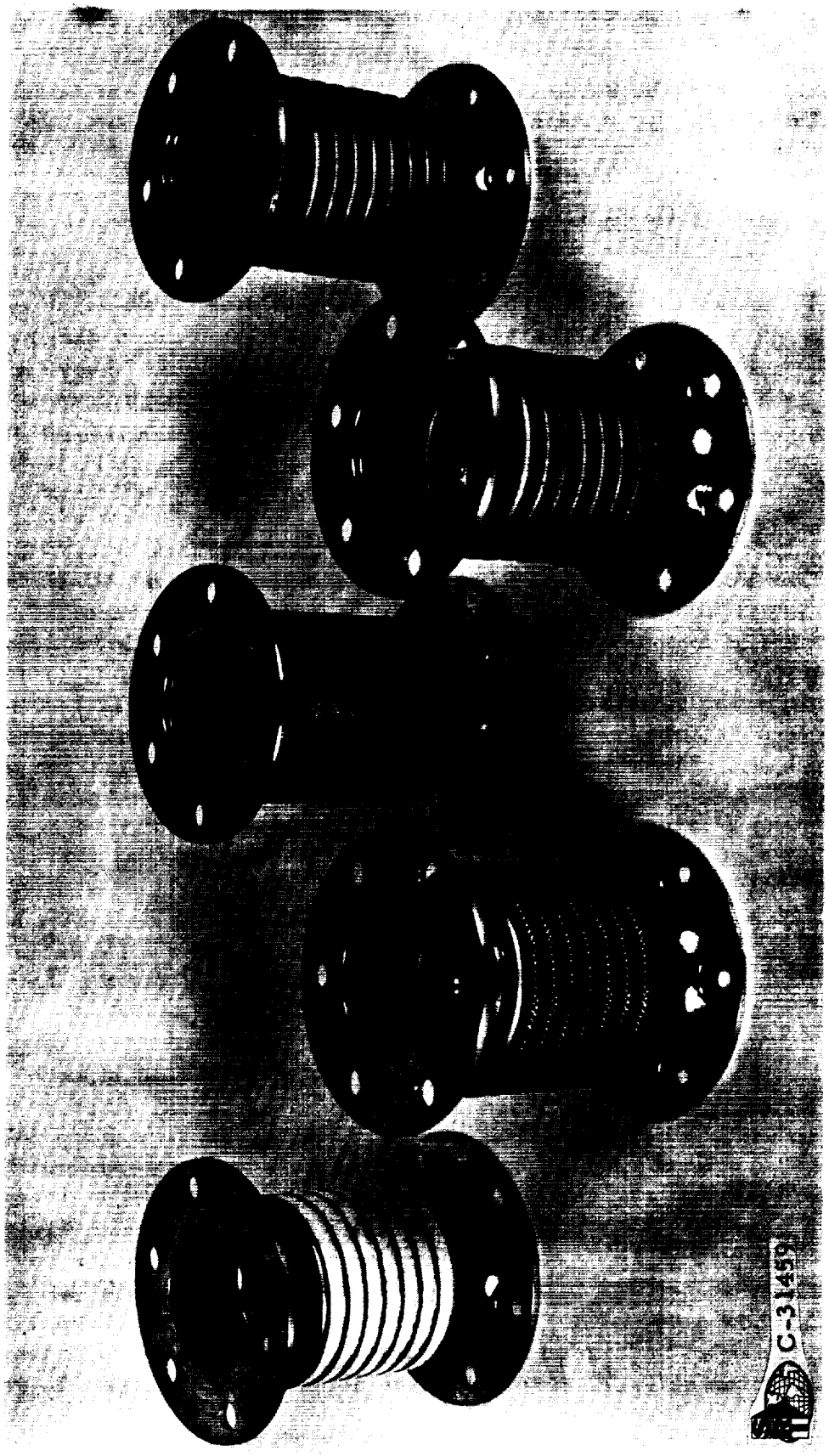

Figure 110. Photographs Of Several Bellows With Various External Damping Devices

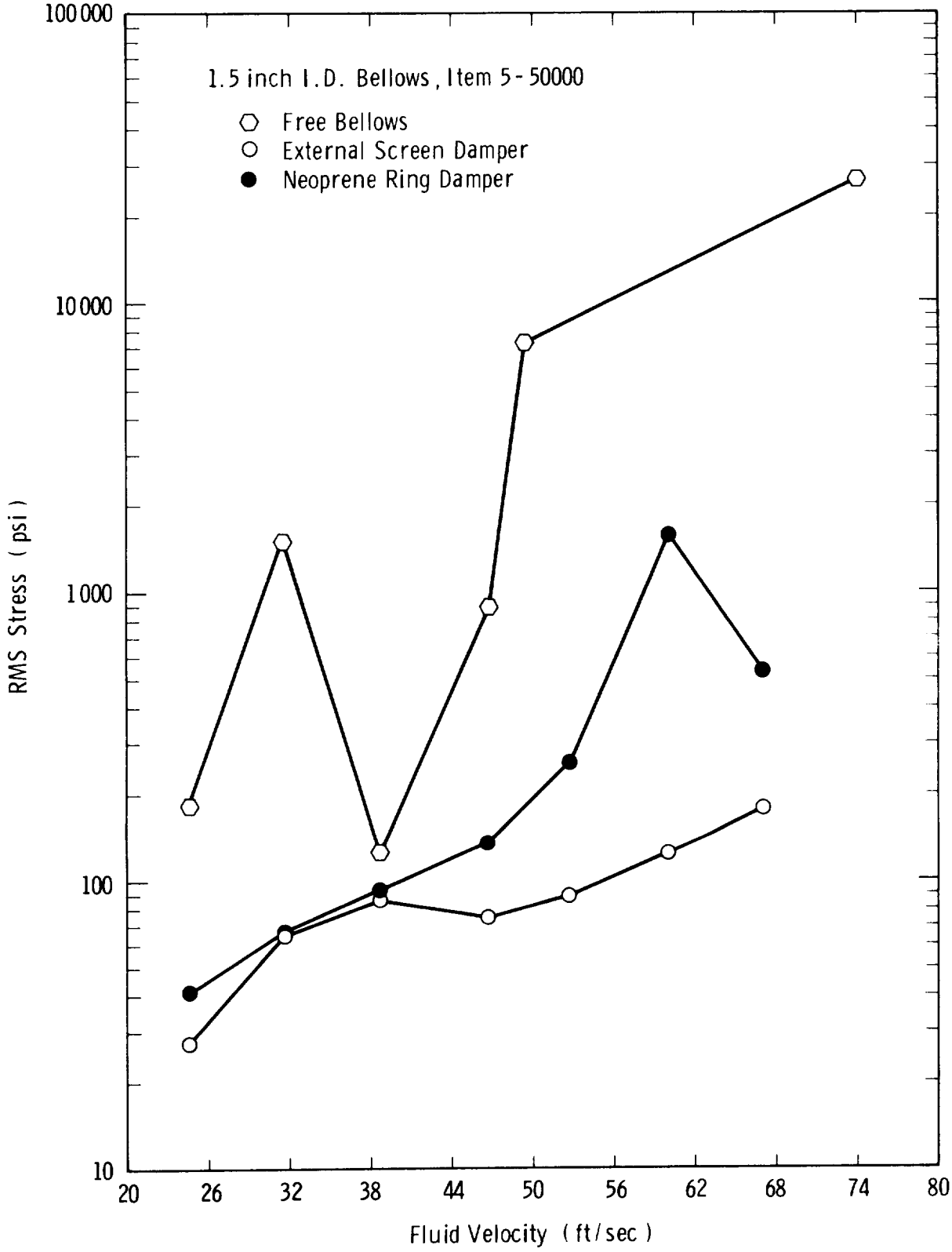

Figure 111.Comparison Of External Screen And Neoprene Ring Dampers With Free Undamped Bellows

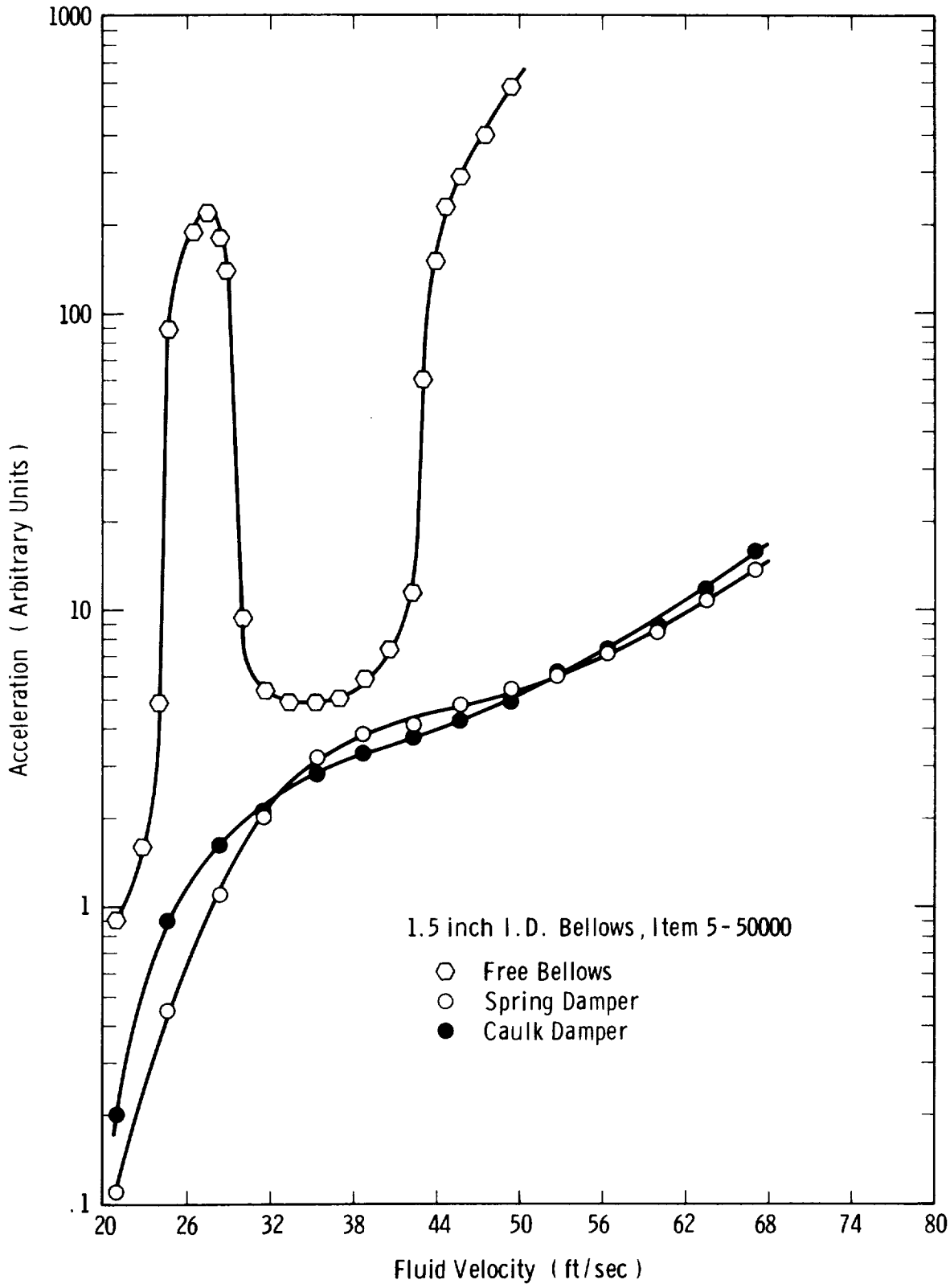

Figure 112. Comparison Of External Spring And Caulk Dampers With Free Undamped Bellows

both devices provided considerable damping; however, the "O" ring dampers allowed some resonance effect at about 60 ft/sec flow velocity, whereas the external screen did not. Figure 112 shows a comparison of an undamped bellows and two others with damping devices; one of the damped bellows had 3M strip-caulk packed in the convolutions and the other had coil springs wound around the outside of each convolution. The two damped bellows exhibited about the same vibration characteristics, as may be seen from Figure 112, and both reduced the vibration level by a considerable amount (about 2 orders of magnitude near the resonant points).

In general, we believe that these exploratory tests have demonstrated that it is, indeed, possible to add considerable damping to a bellows by use of some external device. A word of caution must be added here, however, because our tests were only conducted on free bellows and for conditions where the first few modes could be excited. For a flexible hose or the higher modes of a free bellows, it is not known what kind of device will be required. Of course, some of the devices which were tried would obviously not work for a flexible hose.

Another point which the reader will undoubtedly note is that some of the damping devices which were tried are absolutely not practical for one reason or another; for example, the external screen, as shown, would not allow a free bellows to flex; a variation of this idea will, however. Also, neoprene, the strip-caulk, and the polystyrene foam will not work at cryogenic temperatures. As mentioned previously, one objective of these tests was to find out how much damping can be introduced under ideal conditions, and this is why some impractical devices were tried. The important point of the results is that considerable damping can be added; the problem now is to discover practical devices.

VI. 4 Summary of Bellows Vibration Suppression

We have demonstrated in this chapter that both cone liners and external damping devices are effective in suppressing bellows flow-induced vibrations. Both types of devices have been used in the past by bellows manufacturers for this very purpose. Some points are important to reemphasize about the use of these devices:

(1) Cone liners can cause a significant increase in the pressure drop across the bellows.

(2) Cone liners can experience both buckling failures, because of the large differential pressure, and fatigue failures because of turbulence-induced vibrations.

(3) External damping devices can be as effective as a cone liner without causing an increase in pressure loss.

(4) Care must be exercised in the application of external damping devices to ensure that the damping is actually increased.

VII. BELLOWS AND ELBOW PRESSURE LOSS

VII. 1 Description of Pressure Loss Mechanism

As described in Section II , the general behavior of the fluid through a bellows involves a generation of vortices in the convolutions. In the absence of vibrations, the vortex motion inside each convolute is steady as was shown in Figure 4. With flow-induced vibrations, toroidal vortices are periodically shed out of the bellows convolutes as shown in Figure 7.

Regardless of whether or not there is flow-induced vibration, the generation of vortices in the convolutes causes an extraordinarily high steady flow pressure loss compared with an equivalent length of smooth tubing. Figure 114 shows a typical plot of the friction factor f as compared with friction factors for flow through tubes. Recall that the friction factor is proportional to the pressure drop in a one-diameter length of tubing (or bellows), and is related to the pressure loss and fluid conditions by the equation

$$\Delta p = (fL/D)\,(1/2\ \rho V^2)$$

Note from Figure 114 that the bellows friction factor increases drastically as the Reynolds number is increased over the range from about 10^4 to 10^6. This trend is contradictory to the observed behavior of the friction factor for turbulent flow in a pipe, which shows that f decreases as Reynolds number increases. It is our present belief that the cause for this peculiar behavior can be explained by the presence of the vortices in the convolutes, and the fact that these vortices will transition from a laminar to a turbulent condition at a higher Reynolds number than does the main stream flow. We are planning to explore this idea with a simple analysis in the near future.

VII. 2 Compiled Bellows Pressure Loss Data and Some Test Results

All pressure loss data for bellows and flex hose which was available in the open literature, or from unrestricted company reports, has been compiled. This data has been reproduced in Appendix E. This compiled data included two different correlation methods giving the friction factor f in terms of bellows geometry and Reynolds number; these two correlation methods are illustrated in Figures 114 and 115. Each of these correlations gives f, as a function of Reynolds number, in terms of a one-parameter family of curves. The parameter used in the Daniels

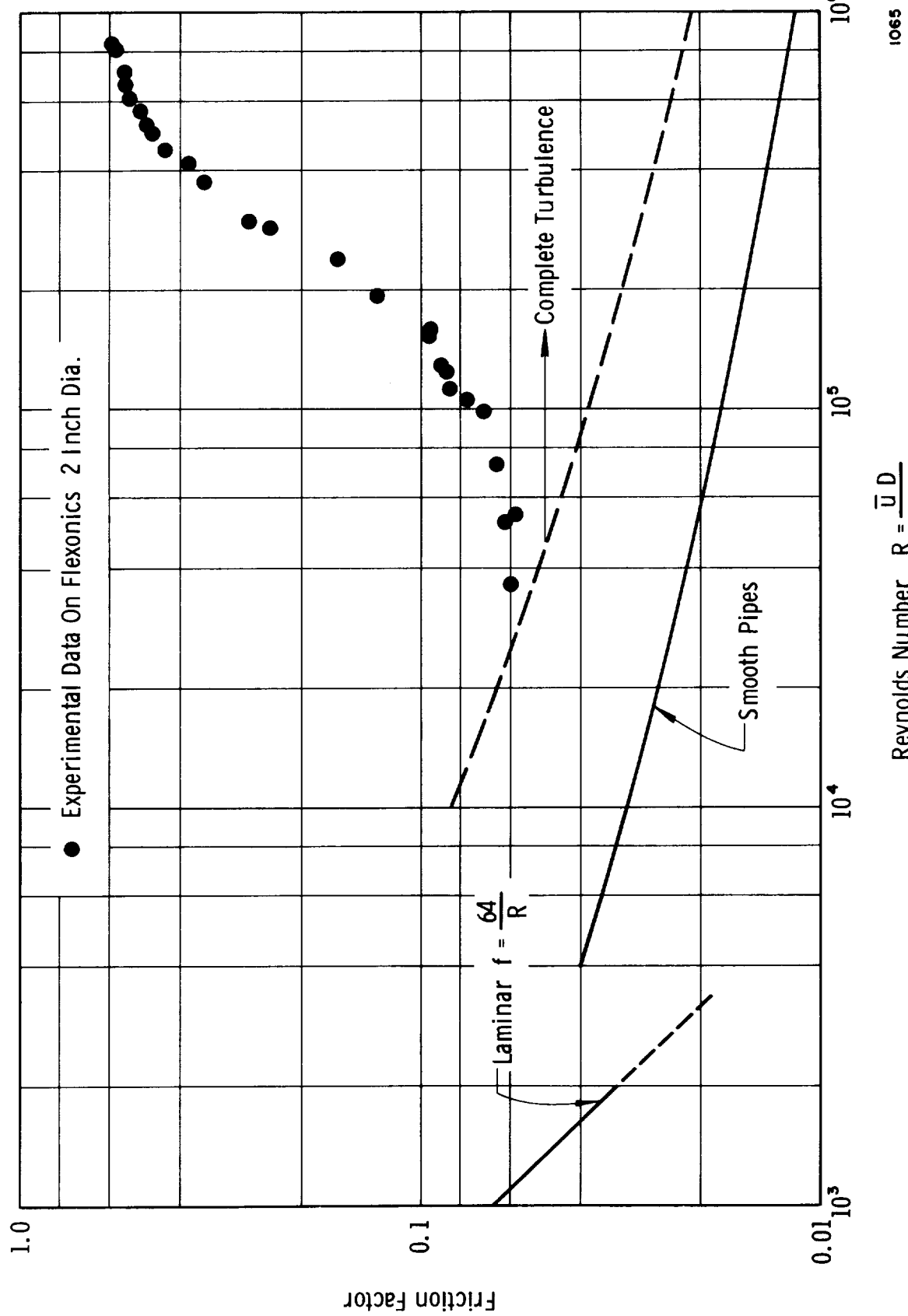

Figure 113. Comparison Of Friction Factors For Smooth Pipes And Flexible Hose

Method for Predicting Frictional Loss in Metal Bellows and Flexible Hose

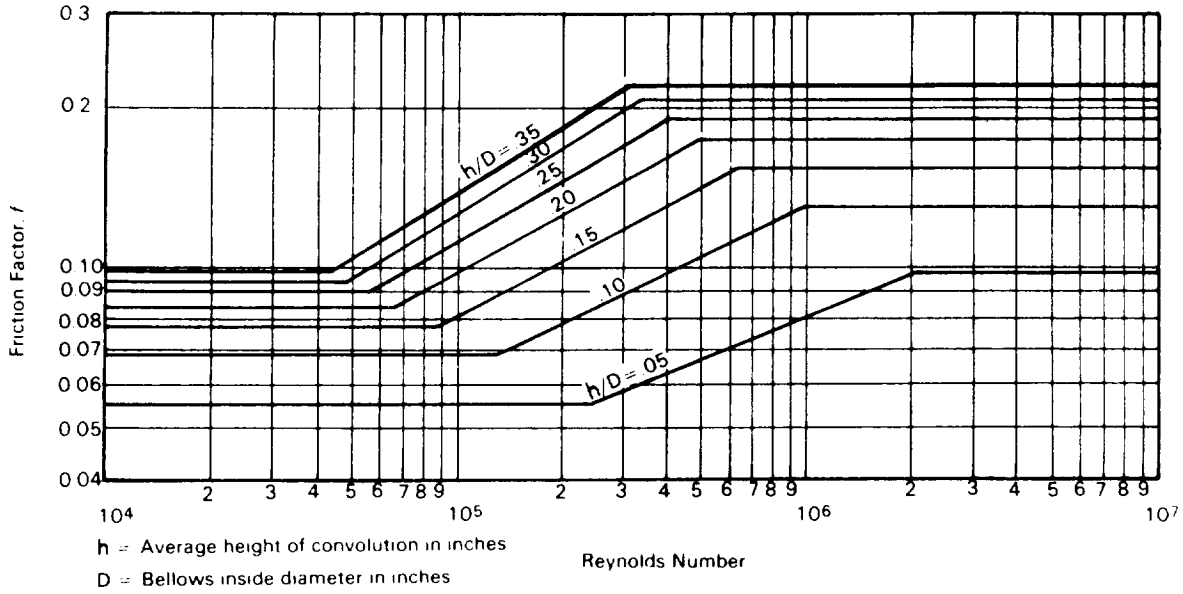

Figure 114. Bellows Friction Factor Correlation From Reference [12]

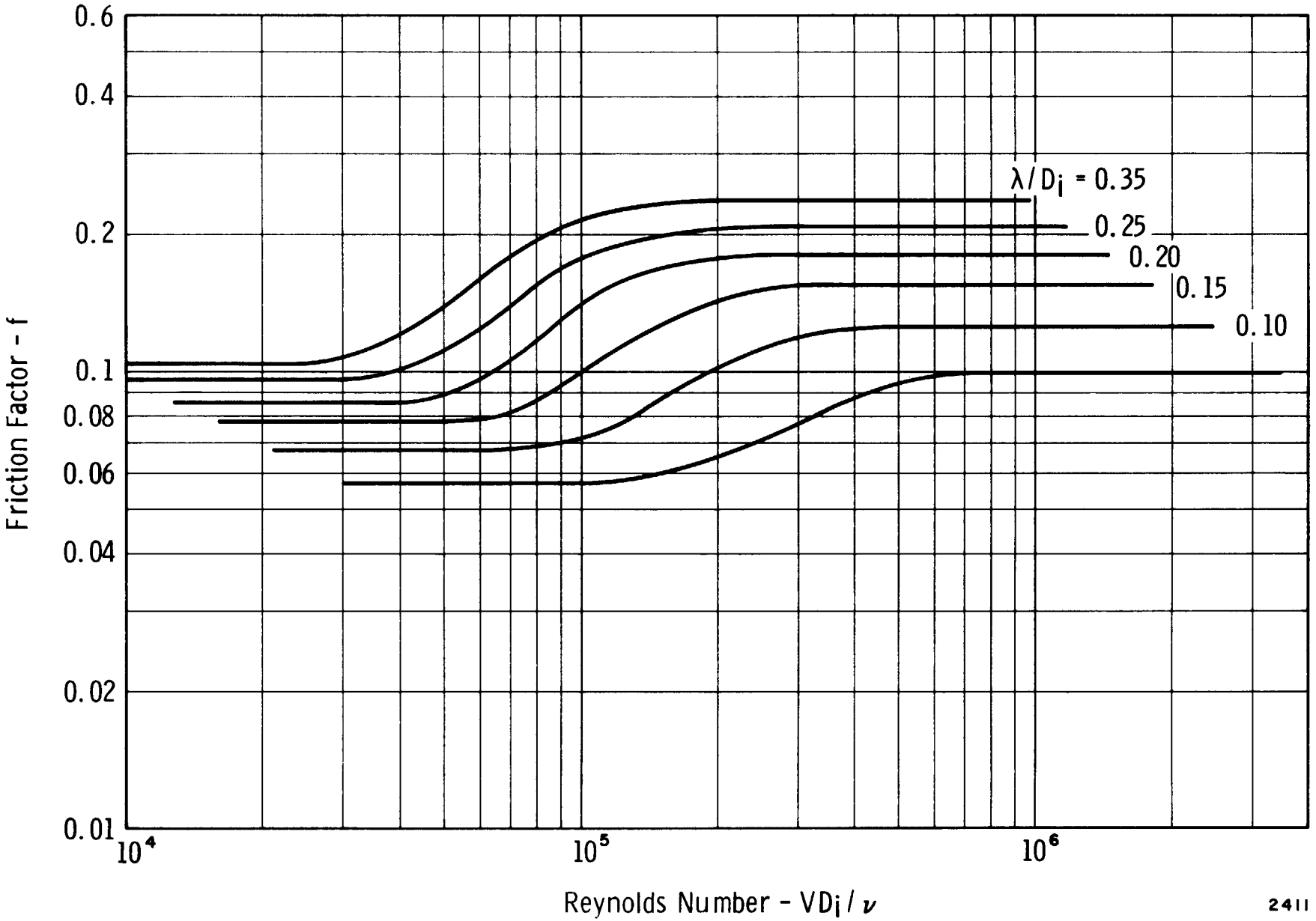

Figure 115. Bellow Friction Factor Correlation From Reference [13]

and Cleveland correlation (Figure 114 and Reference 28) is the ratio of convolute height to bellows internal diameter. The parameter used in the Riley correlation (Figure 115 and Reference 26) is the ratio of convolute pitch to internal diameter. Both correlations can only be valid at the same time for a series of bellows having convolutions with exactly similar geometry; i.e., the ratio of convolute height to pitch, etc., remains constant for all bellows of the series. Therefore, one or both cannot be completely valid for all bellows, in general.

To get a better insight into bellows pressure loss as a function of geometry, and to attempt to clear up the discrepancy of correlation methods noted above, a series of experiments were conducted with some selected bellows, and with a special convoluted test model. The special test model had provision for changing the convolution geometry so that the effect of geometry on pressure loss could be determined in a controlled manner. Figure 116 shows some pressure drop data obtained with this model. Figure 117 shows friction factor data reduced from the pressure drop data of Figure 116. All of the data in Figures 116 and 117, except one case, were for simulated convolutions with identical depths (or heights). Comparison of the data for this condition (curves 1, 2, 3 and 4) show a distinct variation in the friction factor. This data tends to invalidate the correlation given in Figure 114 since it shows a variation in f for constant values of h/D_i (the ratio of convolute depth to internal diameter). Similarly, a comparison of curves 1 and 2 in Figure 117 shows some variation in f for bellows having the same value of λ/D_i (the ratio of pitch to internal diameter). This tends to invalidate the correlation given in Figure 115. Thus, we can conclude that neither of the correlations given in Figures 114 and 115 is entirely or generally valid. Further detailed evaluation of these two correlation methods has been performed by comparison with more of our experimental data and that of other investigators. We have concluded that:

(1) The friction factor f is almost entirely independent of h/D_i (the ratio of convolute height to internal diameter); therefore, the correlation given by Daniels and Cleveland (Figure 114 and Reference 28) has no meaning for bellows of general geometry and is invalid.

(2) The correlation given by Riley (Figure 115 and Reference 26 is roughly valid for all bellows. However, the Riley-type correlation could be improved by making it a three-parameter correlation, with the three parameters being λ/D_i, λ/σ and the fluid density.

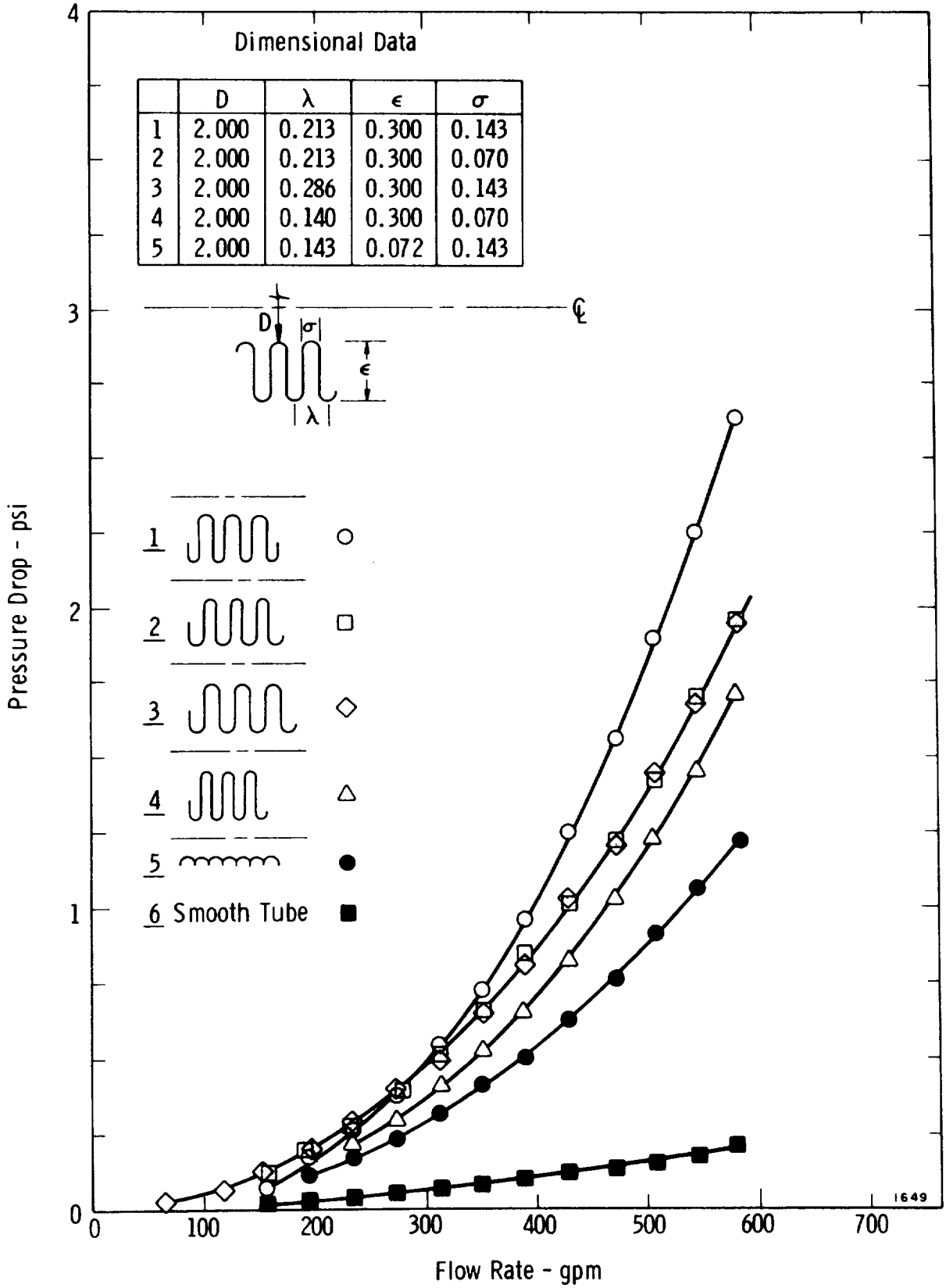

Figure 116. Pressure Drop As A Function Of Flow Rate For Five Bellows Test Geometries

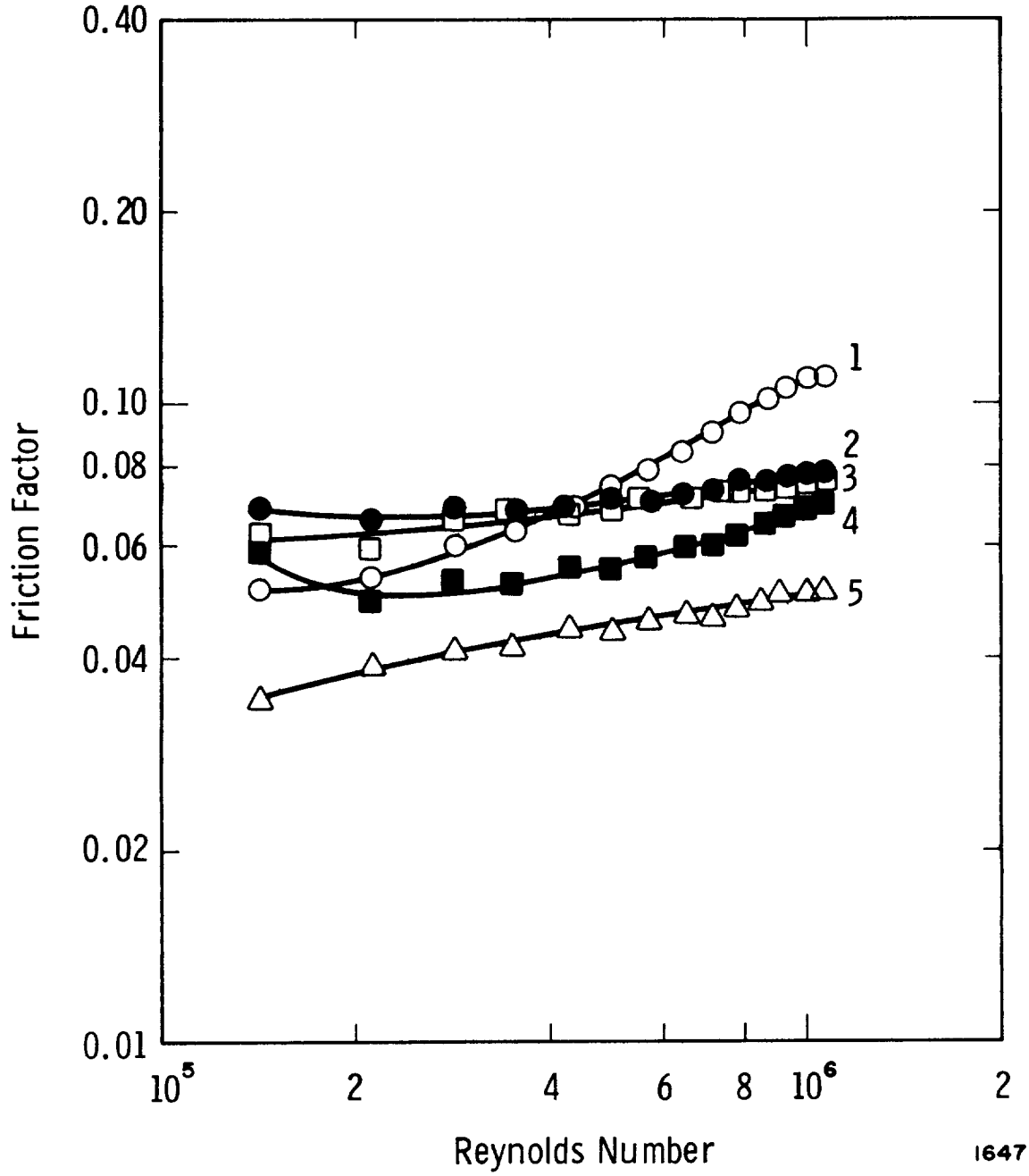

Figure 117. Friction Factor for Data from Figure 4 for the Five Test Geometries

We recommend that the Riley correlation be used for pressure loss estimate purposes with the user aware of the fact that this method generally overpredicts pressure loss for liquids and underpredicts for gases. Also, the Riley correlation tends to overpredict for bellows with "open" convolution designs ($\lambda/\sigma > 2.0$), and underpredicts for bellows with "closed"convolution designs ($\lambda/\sigma < 2.0$).

In very general and rough terms, the trends of "good" and "bad" convolutions configurations are illustrated in Figure 118. It is interesting to note that the "bad" designs correspond to those geometries which exhibit the more severe flow-induced vibration tendencies.

VII.3 Low Pressure Loss Bellows Configurations

As discussed in Chapter VI, a conical liner can be effective in suppressing flow-induced vibrations but can lead to a significant increase in the pressure loss if the required contraction is too great. For bellows not required to angulate, a cone liner can reduce the pressure loss if it is properly designed. Therefore, new ways were sought to reduce losses which might be useful for bellows required to angulate.

Several specific configurations have been tested. A sketch of one configuration is shown in Figure 119. This design employs a rigid skirt, but not one of conventional design. Rather than neck down the skirt or liner section, the convoluted section is made slightly larger (on the order of 10%) and the skirt is kept the same diameter as the duct. The ratio of skirt diameter to bellows diameter is, of course, dictated by angulation requirements. Just downstream of the bellows a converging section guides the fluid into the downstream duct. Figure 120shows pressure loss as a function of flow rate for this new design as well as for a conventional skirt design, and unskirted bellows and a smooth wall section of tubing. Notice that the conventional cone liner model coupling has roughly twice the pressure drop of the unskirted bellows while the new configuration had about one-half the pressure loss of the bare bellows.

Another type of liner which appears to have merit is a screen or wire cloth liner. Because of its flexibility, a cylinder of wire cloth can be fitted directly against the inside of the bellows, allowing some angulation. One test has been performed with this type of liner and the results are shown in Figure 120.Note that a small increase in pressure loss was realized over a bare bellows. It is anticipated that use of a finer mesh wire cloth

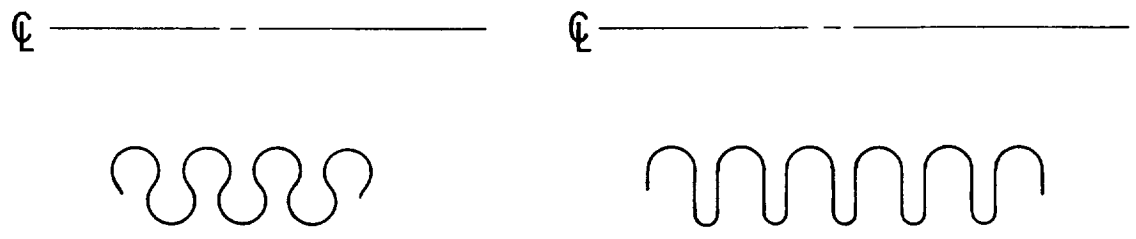

(a) Unfavorable Geometries (Large Losses)

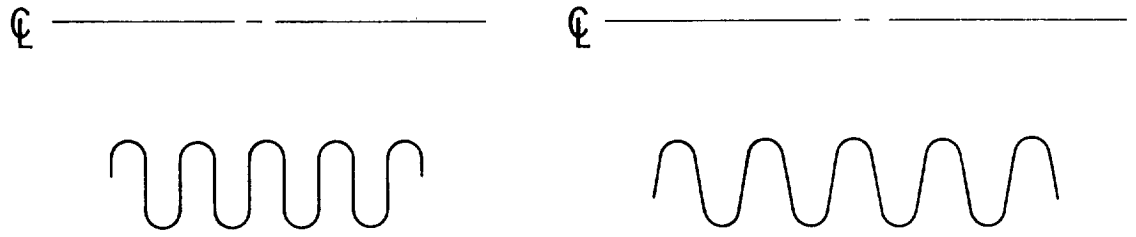

(b) Favorable Geometries (Small Losses)

1654

Figure 118. Sketch Of Bellows Convolutions Giving Unfavorable And Favorable Pressure Loss Characteristics

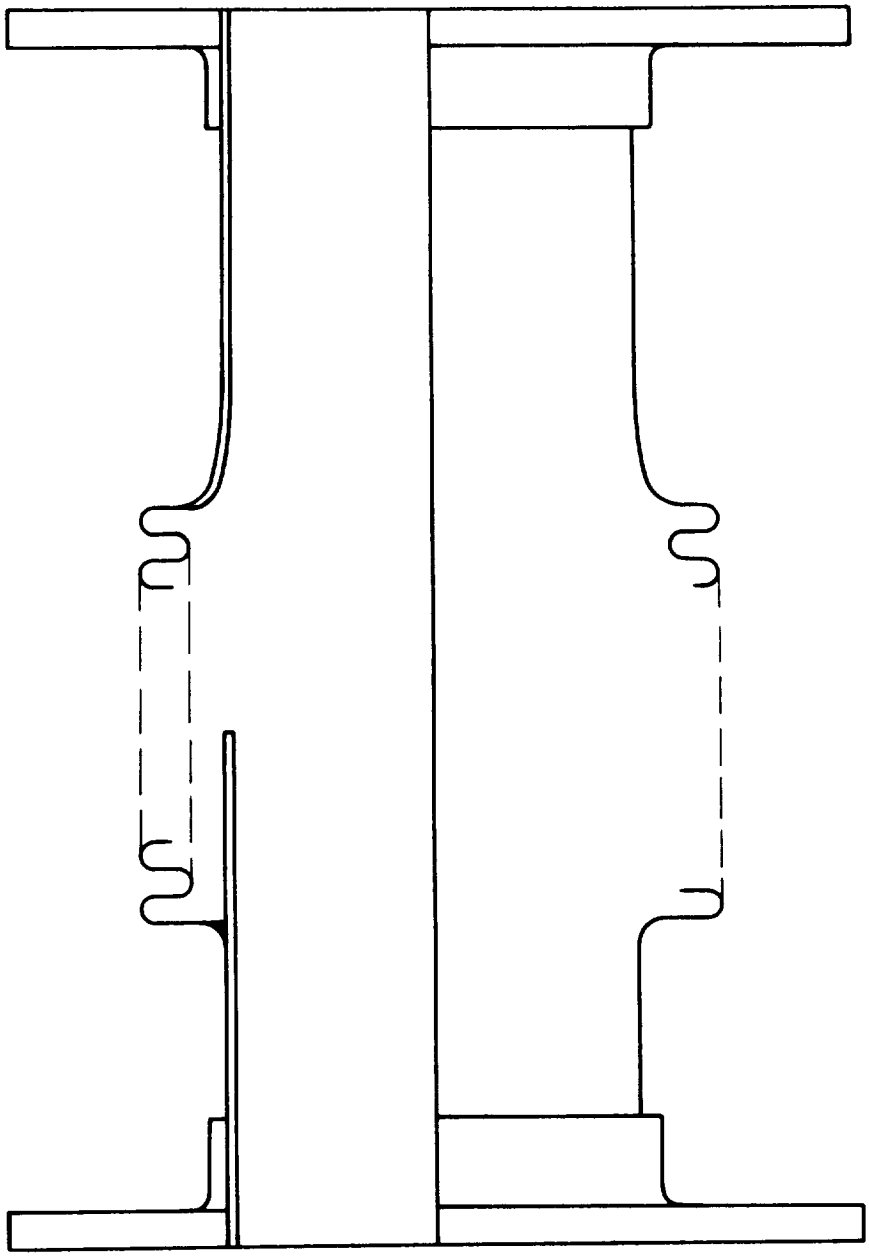

1648

Figure 119. Low Pressure Drop Coupling Design #1

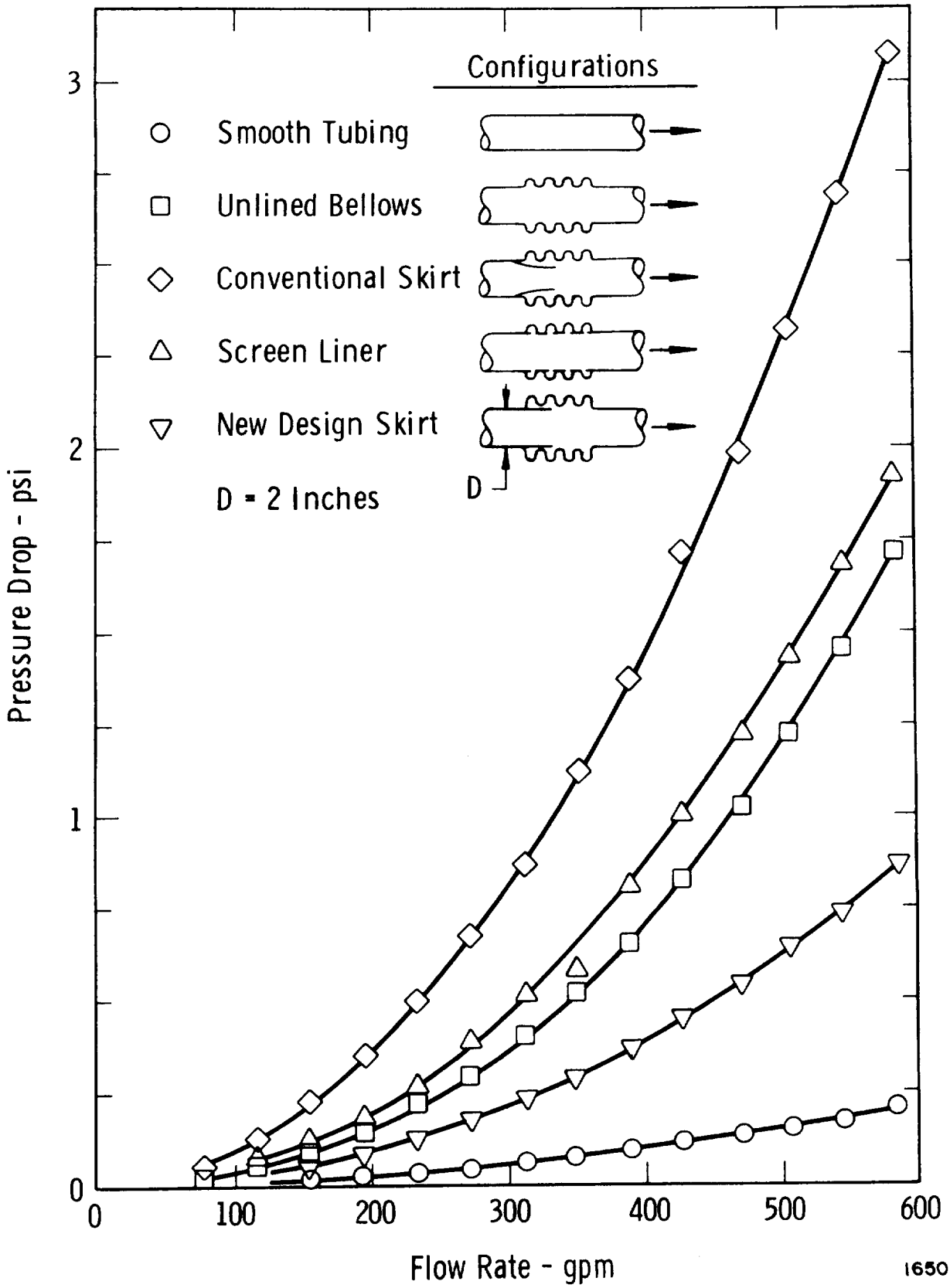

Figure 120. Pressure Loss Comparison Of Several Skirted Bellows Configurations

than used in this first test will result in an actual pressure loss reduction. Possibly of most value, however, is the fact that this type of liner suppresses flow-induced vibrations; this fact has been verified by testing. Although we experienced no problems in the laboratory, the reader will likely realize that there are potential problems with a wire cloth liner, should it break loose and be carried downstream in the duct system. Attempts to use this concept should be thoroughly verified with testing.

Two other types of liners were tried, also; a longitudinal wire screen leaf type, and a spiral wound type using either wire screen or metal shim for the liner material. Figures 121 and 122 show examples of the two types. In general, all liners suppressed flow induced bellows vibrations. For example, peak flow induced dynamic stress over the test flow range, in coupling PN 08046 was less than 150 psi with a longitudinal leaf screen liner compared with about 10,000 psi with no liner.

The pressure loss characteristics of the various liner types were quite different. The spiral wound metal shim liner (Figure 123) exhibited the best pressure loss characteristics but still needs some development work. The problem with the spiral wound metal shim liner was that for large bend angles the winding tended to be displaced too far axially, causing separation between adjacent windings. If this problem can be cured, this type of liner has good possibilities. The spiral wound screen liner (test data not shown) had higher pressure loss than the metal shim liner. Figure 124 shows test results for the longitudinal leaf screen liner. In general, the pressure loss characteristics at high flow rate are better than the unlined bellows for the straight bellows case. For large bend angles, however, the longitudinal leaf screen liner had slightly higher pressure loss than the unlined bellows at the same angle.

VII.4 Low Pressure Loss Duct Bend

Introduction

Duct elbows are known to have a large pressure loss relative to the normal friction loss in straight duct sections. The reason for these large losses can be attributed to secondary flows caused by centrifugal forces and centrifugal force gradients acting on the fluid particles in the bend.

Two experimental elbows have been constructed and tested in order to evaluate a new method of reducing pressure losses and improving velocity profiles in bends. Both elbows were built with square entrance and exit sections to simplify construction, and were identical in every

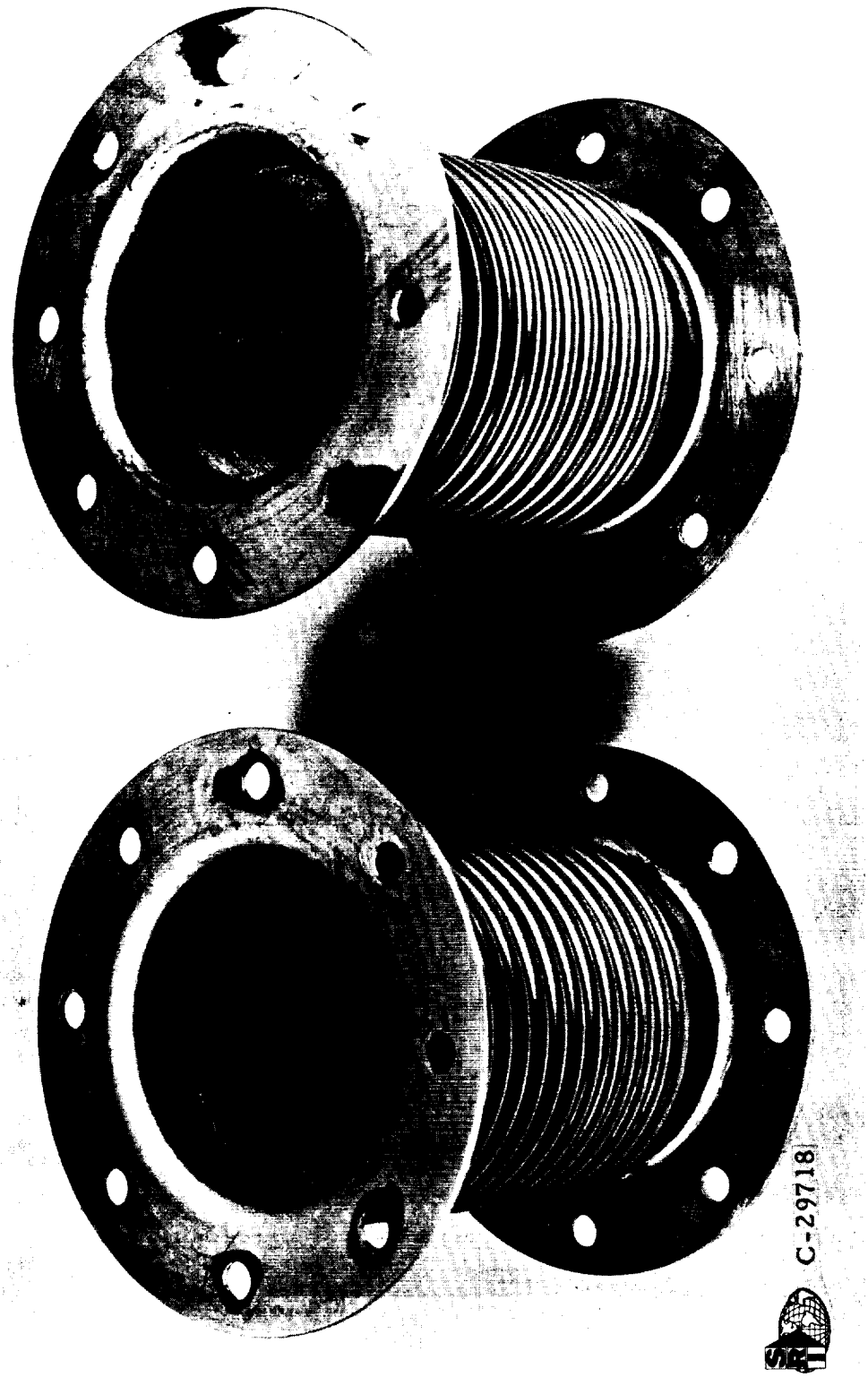

FIGURE 121. LONGITUDINAL LEAF SCREEN LINERS

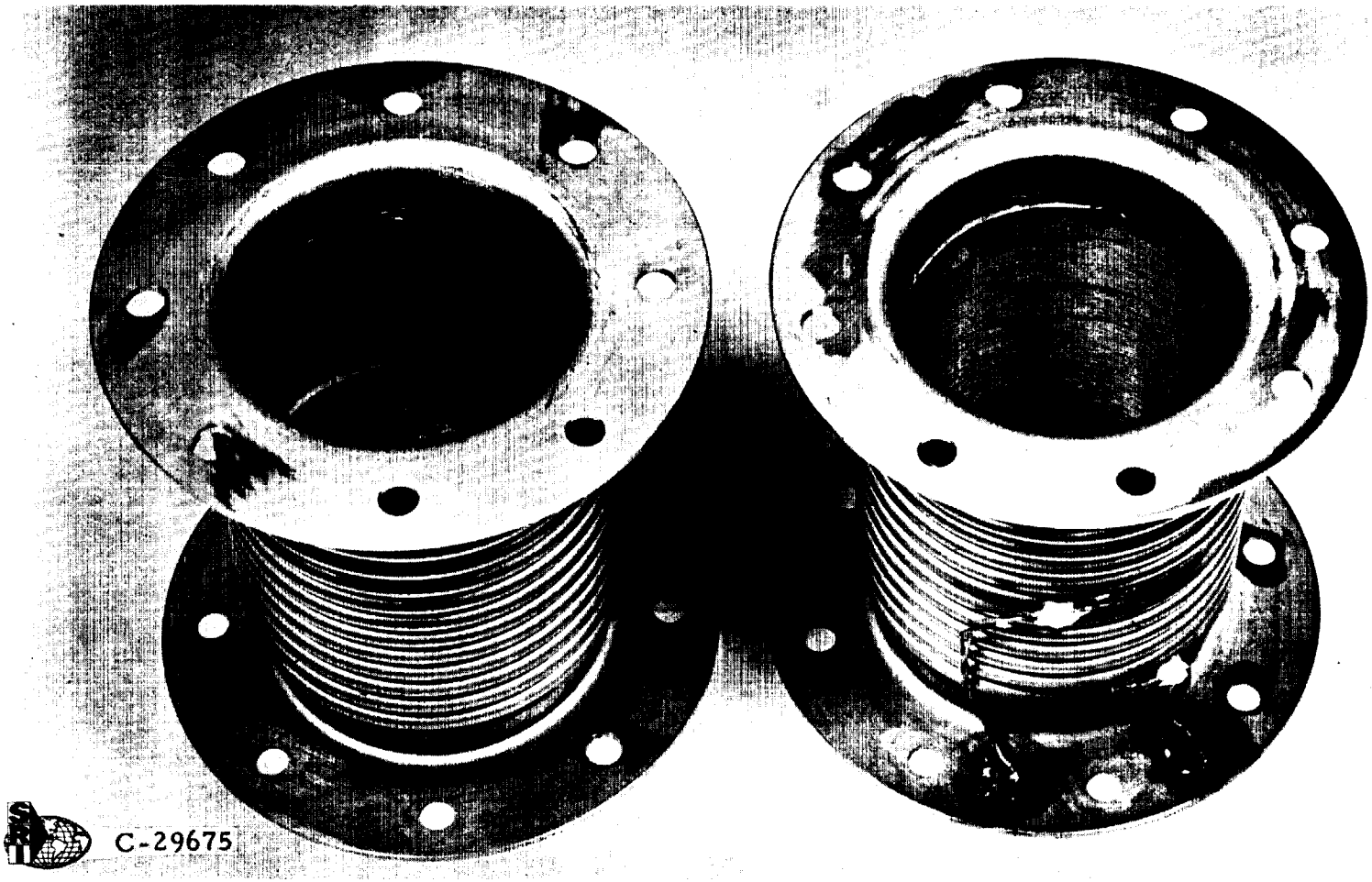

FIGURE 122. SPIRAL-WOUND LINERS (METAL SHIM ON LEFT-SCREEN ON RIGHT)

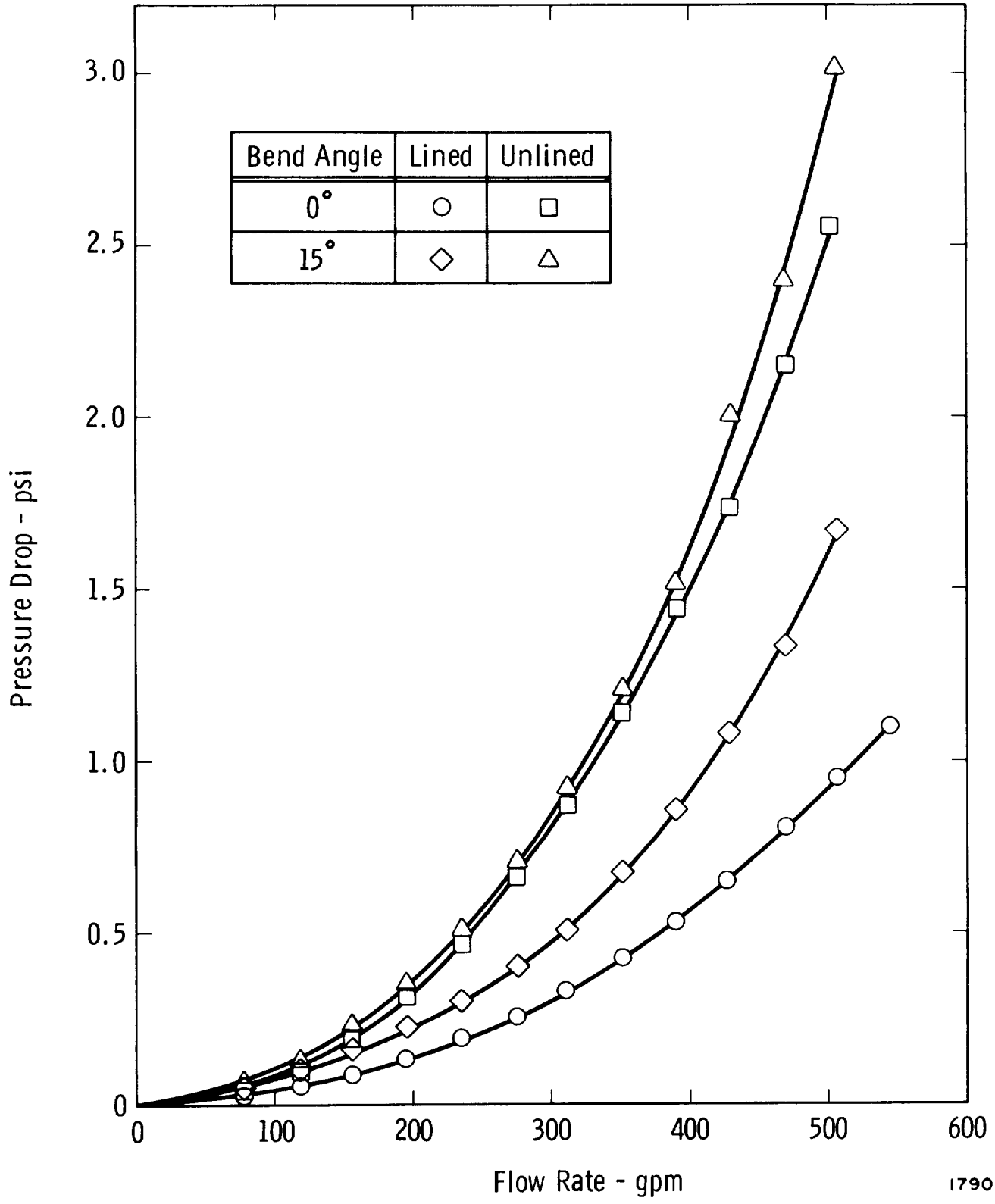

Figure 123. Pressure Loss Characteristics Of Spiral Wound Metal Shim Liner

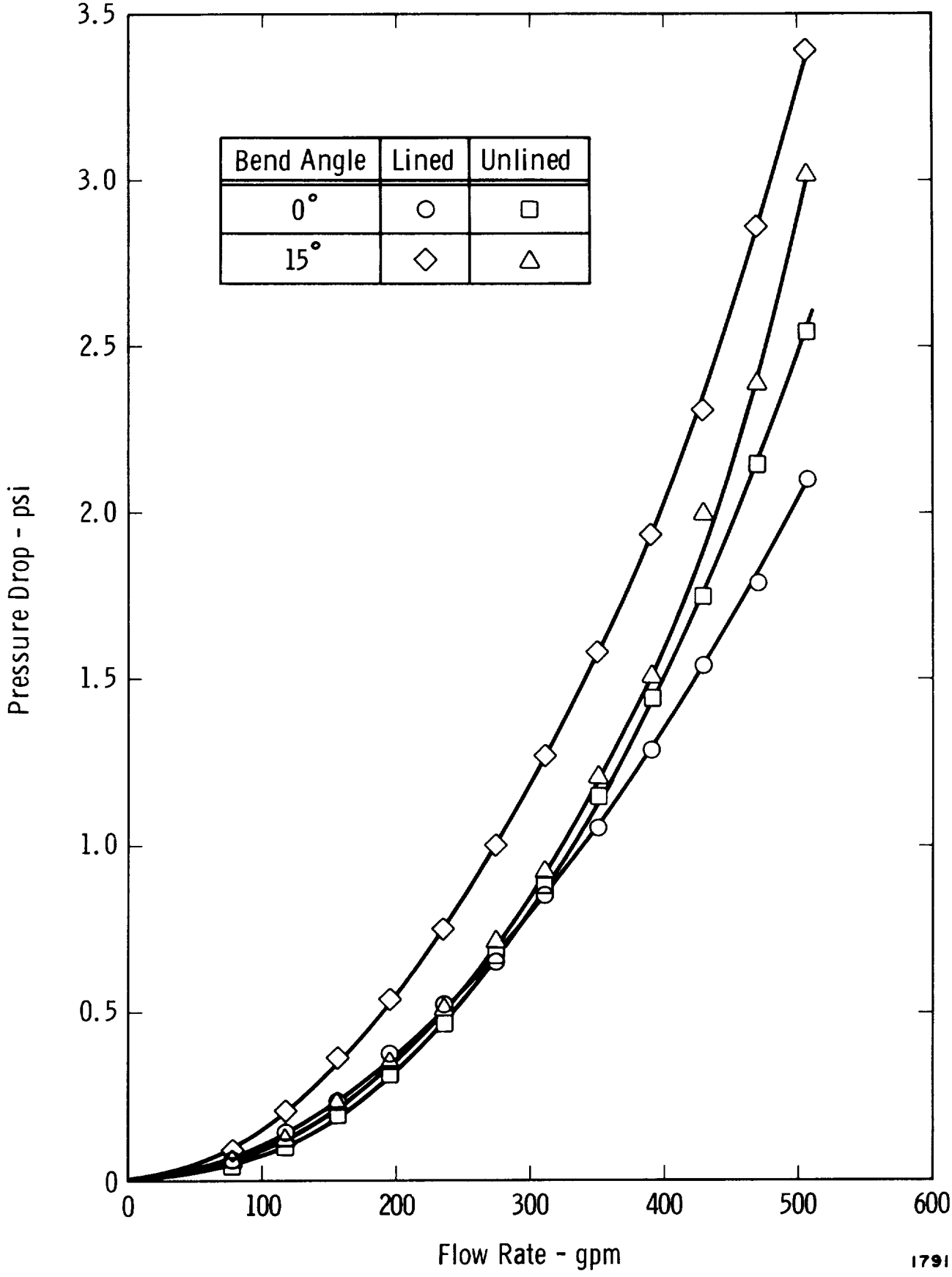

Figure 124. Pressure Loss Characteristics Of Longitudinal Leaf Screen Liner

respect, except that the cross-sectional shapes were different in the bend region. One elbow was conventional in design and had a uniform square cross section. Figure 125 illustrates the new duct design. Note that this new design has an increased area on the inside of the bend but a decreased area on the outside of the bend; the reason for this shape will be discussed below. It was found from testing that the new design had roughly 40 percent less pressure loss than the conventional design. It is anticipated that a greater reduction in loss could be achieved with more detailed changes in the cross sectional shape.

Low Loss Bend Concept

Consider Figure 126, which illustrates the flow of an ideal (no viscosity) fluid through a bend. The predicted velocity profiles immediately upstream and downstream of the bend are uniform. Typical profiles for a real fluid flowing through a bend are shown in Figure 126. Here, because of the centrifugal force gradient which exists at the start of the turn, the high energy fluid tends to migrate to the outside of the elbow while the low energy fluid goes to the inside of the elbow; such a fluid migration constitutes a secondary flow. This mixing plus the mixing which occurs downstream as the fluid develops a normal velocity profile in the downstream duct causes a pressure loss which is nominally about an order of magnitude greater than the normal friction or viscous losses in a straight duct.

If one could, by some means, effectively reduce the driving force for this secondary flow without reducing the mean fluid velocity in the channel, then the overall elbow pressure loss could be reduced. To accomplish this reduction in secondary flow it would be necessary to decelerate the fluid near the suction wall and accelerate the fluid near the pressure, or outer, wall. Once this were accomplished, there should be two results: First, the overall pressure differential across the bend should be decreased and, consequently, low energy fluid migration to the inner wall reduced. Secondly, the centrifugal force gradient should be reduced so that the migration of high energy fluid to the outer wall is suppressed.

The manner in which the duct cross-sectional shape should be changed to bring about these local accelerations and decelerations of the fluid can be estimated analytically.

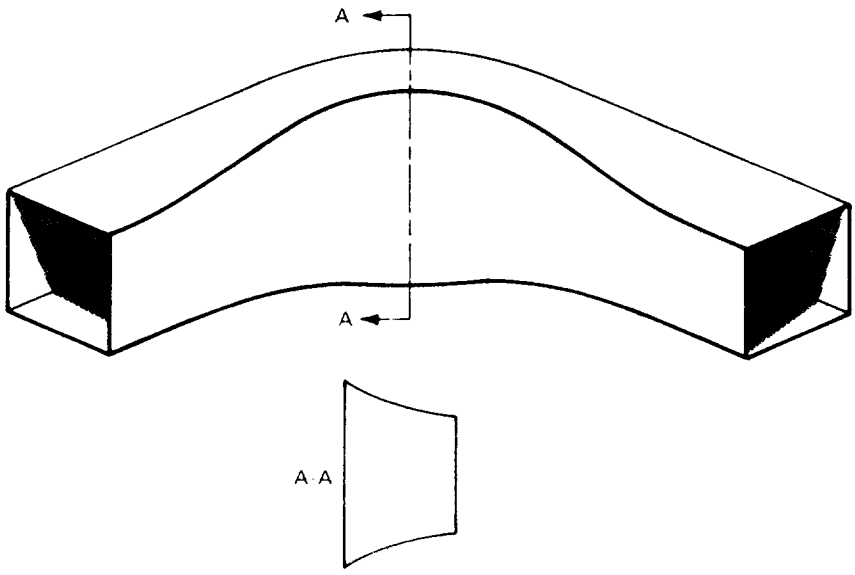

Figure 125. Illustration Of New Elbow Design

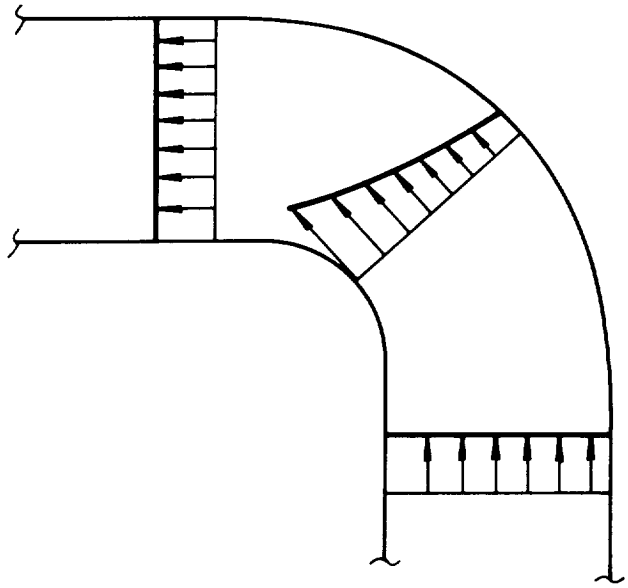

(a) Flow Of Ideal Fluid Through Bend

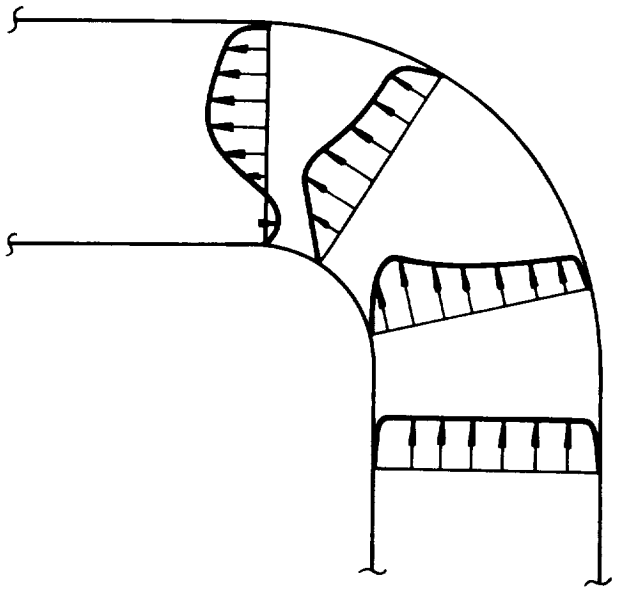

(b) Flow Of Real Fluid Through Bend

Figure 126. Ideal And Real Fluid Flow Through Bend

Neglecting viscous effects, the velocity profile at the start of a bend will tend to be of the form (see Figure 126a)

$$v(r) = \frac{k_1}{r}$$

where

$$k_1 = \frac{(r_2 - r_1)\,\overline{V}}{\ell n (r_2/r_1)}$$

Here, $v(r)$ is the local fluid velocity as a function of radius r measured from the center of curvature of the bend, r_2 is the outer wall radius, r_1 the inner wall radius and $\overline{V}$ the mean fluid velocity in the duct.

To suppress the secondary flows it has already been argued that the centrifugal force gradient should be made equal to zero (constant centrifugal force across the bend); this means that the corrected duct local velocity $v'(r)$ should be of the form

$$\frac{v'(r)^2}{r} = k_2$$

where k_2 is a constant. Therefore, the bend duct height must be corrected so that the local velocity in the bend tends to a value

$$v'(r) = (k_2 r)^{0.5}$$

or

$$v'(r) = \frac{v(r)}{C(r)} = \frac{k_1}{rC(r)}$$

The quantity $C(r)$ is a duct correction factor and has a value equal to

$$C(r) = k_1 k_2^{-0.5}\, r^{-1.5}$$

To define k_2, we will arbitrarily spcify that the corrected duct have everywhere a centrifugal force equal to the ideal centerline centrifugal force in the original duct; in other words

$$k_2 = \frac{8 k_1^{\,2}}{(r_2 + r_1)^3}$$

and, therefore

$$C(r) = 0.354 \left(\frac{r_2+r_1}{r}\right)^{1.5}$$

To correct a given duct, the height across the bend must be modified by the quantity $C(r)$. In other words, if $h(r)$ is the uncorrected duct height as a function of radius, then the corrected duct height $h'(r)$ is

$$h'(r) = C(r)\, h(r)$$

This type of correction can be applied equally well to square, rectangular, circular, etc., ducts.

Experimental Results

Two experimental elbows have been constructed and tested to verify the concept described in the foregoing. Both elbows had identical cross-sectional areas, and inner and outer wall radii; the only difference was that one elbow had a corrected cross-sectional shape in accordance with the above. Figure 125 illustrated the corrected elbow. Both test items were installed in a water flow system and overall pressure loss was monitored. On both elbows, the pressure loss was measured between two points several duct widths upstream and downstream from the bend; Figure 127 shows the resulting overall pressure loss for both test items. It is readily seen that the new design has a lower overall loss, hence, is more efficient.

Figure 128 shows plots of the cross-channel pressure envelopes for the two experimental elbows. Note the reduction in the peak pressure differential for the new design. This reduction in cross-channel pressure differential means that the driving force for the fluid migration, discussed earlier, has been reduced and, therefore, a reduction in overall pressure loss is expected.

Conclusion

The tests performed on the two elbows verified that it is possible to reduce pressure losses in duct elbows by properly designing the duct cross-section in the bend region so as to minimize secondary flows and, hence, flow profile distortion. This concept can be applied to a duct with any basic shape.

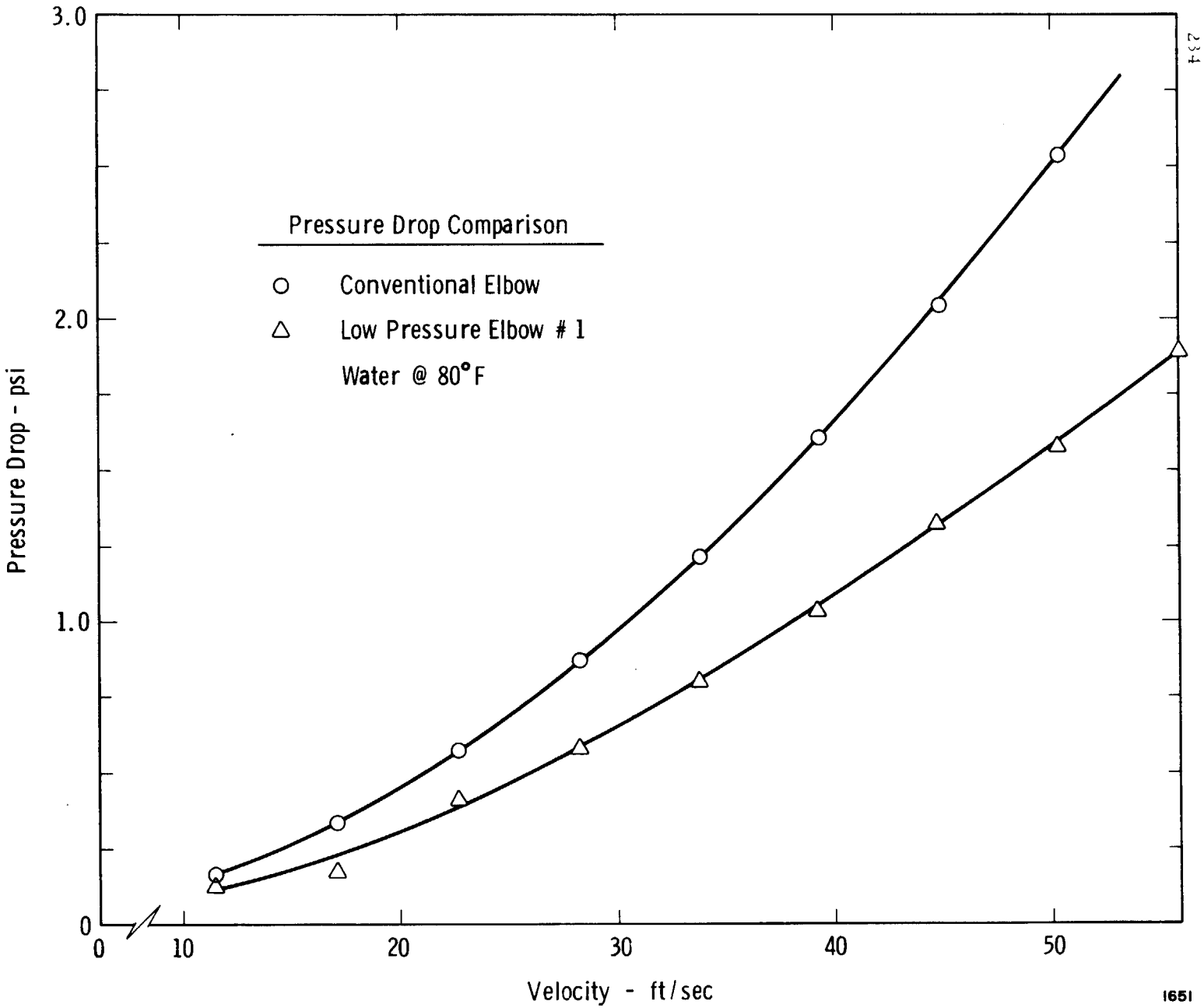

Figure 127. Comparison Of Conventional And Low Loss Bend Design # 1

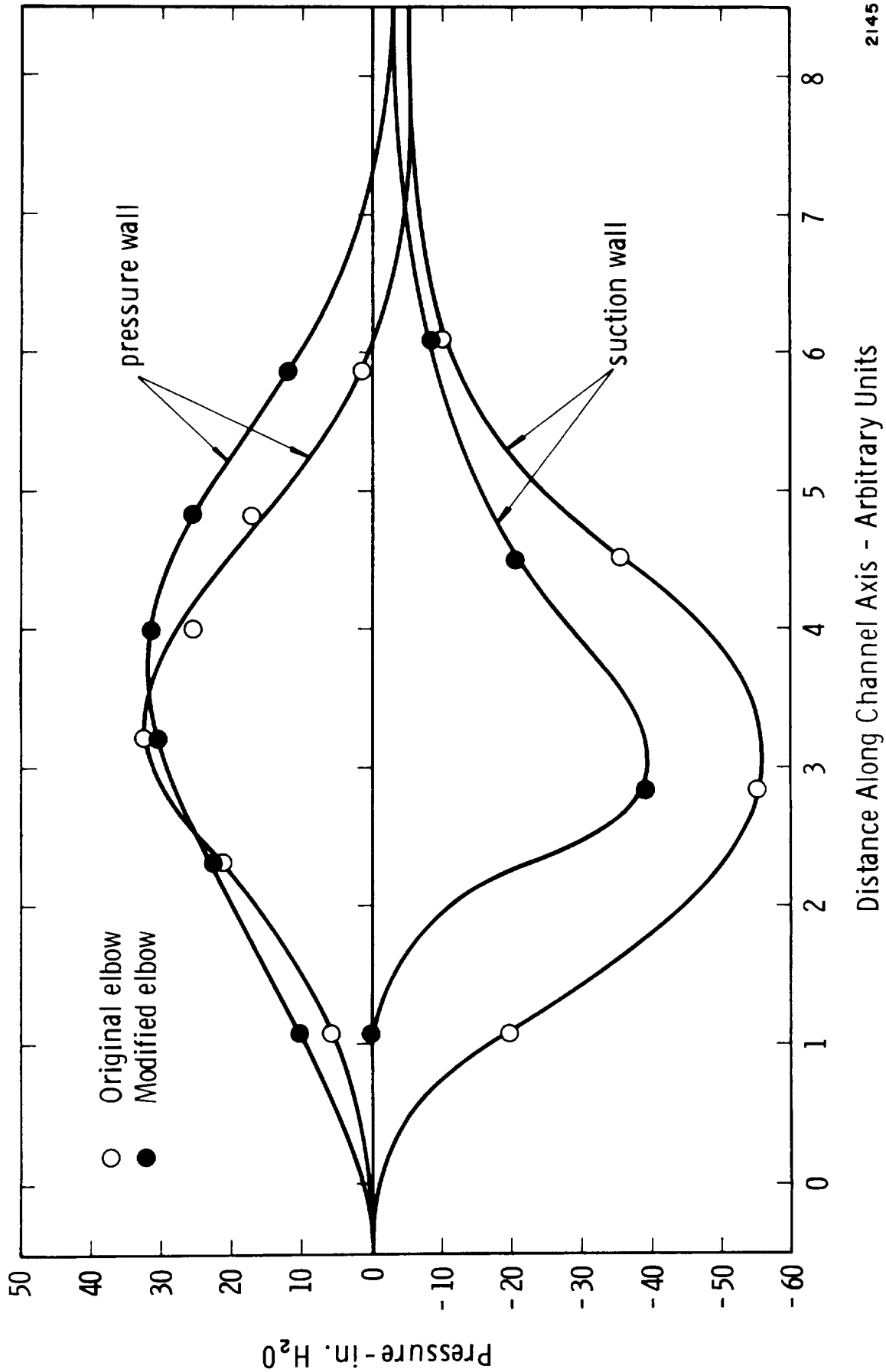

Figure 128. Cross-Channel Pressure Envelopes For Conventional And Modified Elbows

VIII. CONCLUSIONS

A number of conclusions have been derived from this study; these are listed below:

Bellows Flow-Induced Vibrations

(1) Flow-induced vibration of bellows is caused by a fluid-elastic instability; specifically it is caused by fluid vortex shedding from the bellows convolutions which couples with the convolution vibrations. In the absence of convolute motion there is no well defined large scale vortex shedding.

(2) The frequency of the vortex shedding can be related to the fluid velocity and convolute dimensions through the use of a Strouhal number given by

$$S = f_s \sigma / V$$

where f_s is the shedding frequency, V the velocity, and σ the convolute tip width. This Strouhal number appears to be a weak function of only one parameter which is λ/σ, the ratio of pitch to tip width.

(3) The fluid pressure force which is exerted on a single bellows convolute can be expressed in the form

$$F = C_F A_p (1/2\ \rho V^2)$$

where C_F is a vortex force coefficient, A_p is the height area of the convolute, ρ is fluid density, and V velocity. The data obtained for C_F from a number of bellows tests shows it to be a strong function of the parameter λ/σ.

(4) It appears that, because of a vortex reinforcement phenomena, there are "optimum" values of λ/σ which result in local minimum or maximum values of C_F. Therefore, there might be some advantage in designing the convolute geometry to give a minimum C_F value. In general, "open" convolution designs are better than "closed" designs.

(5) The response of a given bellows to flow excitation can be predicted with a method described in this report. This method has been verified by tests for bellows over a size range from 1.5 inch I. D. to 14 inches I. D.

(6) A very important factor in bellows vibrations is the value of the dynamic amplification factor Q. Test results show that Q is dependent on the bellows specific spring rate ($K_A N_c / D_m$), the internal fluid media, and the number of plies. A preliminary set of universal Q value curves has been prepared in terms of known bellows and flow parameters, and can be used for present best-estimate purposes.

(7) A special parameter, called the "Stress Indicator" has been derived and is felt to be of value in determining the relative vibration severity of various bellows. All information required to make "Stress Indicator" calculations is contained in the report.

(8) A curve giving fatigue failure information has been compiled and can be used to estimate the possibility of failure of a given bellows.

(9) Various kinds of liners can be very effective in suppressing bellows flow-induced vibrations. Care must be exercised, however, to keep from causing an increase in pressure loss because of the liner.

(10) Various kinds of external damping devices can be effected in reducing bellows vibrations. Care must be taken to ensure that damping <u>is</u> added to the bellows.

(11) Rather large errors can be expected when using existing spring rate and stress (in terms of deflection) calculation methods, largely because of an inaccurate knowledge of true convolute dimensional data.

(12) The use of an accelerometer for monitoring bellows flow-induced vibrations can give misleading results as to the most severe modes of vibration, particularly where acoustic resonances occur in the system.

Bellows and Elbow Pressure Loss

(13) Only one existing bellows pressure loss correlation method is considered valid for general bellows geometry, and this method can lead to rather large errors in certain cases.

(14) Careful attention to convolution geometry design can result in a 50 percent or more reduction in pressure loss when comparing a good design and a poor design. In general, a good design is one with small, open convolutions. Large, close pitch type convolutions generally give large losses.

(15) A bend with changes in cross section such as described in this report can result in a substantial reduction in pressure loss compared with a bend of constant geometry cross section.

REFERENCES

1. Gerlach, C. R. and Schroeder, E. C., "Study of Minimum Pressure Loss in High Velocity Duct Systems," Interim Technical Report No. 1, Contract NAS8-21133, Southwest Research Institute, July 1969.

2. Gerlach, C. R., Bass, R. L., III, Holster, J. L. and Schroeder, E. C., "Flow-Induced Vibration of Bellows With Internal Cryogenic Fluid Flows," Interim Technical Report No. 2, Contract NAS8-21133, Southwest Research Institute, August 1970.

3. Toebes, G. H. and Eagleson, P. S., "Hydroelastic Vibrations of Flat Plates Related to Trailing Edge Geometry," Journal of Basic Engineering, Trans. ASME, Vol. 83, Dec. 1961, pp. 671-678.

4. Marris, A. W., "A Review of Vortex Streets, Periodic Wakes, and Induced Vibration Phenomena," Journal of Basic Engineering, Trans. ASME, Vol. 86, Sept. 1964, pp. 165-196.

5. Toebes, G. H., "Flow-Induced Structural Vibrations," Journal of Engineering Mechanics, Proceedings, ASCE, Vol. 91-EM6, 1965.

6. Toebes, G. H. and Ramamurthy, A. S., "Fluidelastic Forces on Circular Cylinders," Journal of Engineering Mechanics, Proceedings ASCE, Vol. 92-EM, 1967.

7. Protos, A., Goldschmidt, V. W. and Toebes, G. H., "Hydroelastic Forces on Bluff Cylinders," Journal of Basic Engineering, Trans. ASME, Vol. 90, Series D, No. 3, September 1968, pp. 378-386.

8. Haugen, R. L. and Dhanak, A. M., "Momentum Transfer in Turbulent Separated Flow Past a Rectangular Cavity," Journal of Applied Mechanics, Trans. ASME, Vol. 33, Sept. 1966, pp. 641-646.

9. Townes, H. W. and Sabersky, R. H., "Experiments on the Flow Over a Rough Surface," International Journal Heat Mass Transfer, Vol. 9, 1966, pp. 729-738.

10. Daniels, V. R., "Dynamic Aspects of Metal Bellows," The Shock and Vibration Bulletin, No. 35, Part 3, Jan. 1966. pp. 107-124.

11. Lytle, A. D., "Dynamics of Bellows Filled with an Incompressible Liquid," Journal of Spacecraft and Rockets, Vol. 5, No. 1, 1968, pp. 9-13.

12. Lazan, B. J., Damping of Materials and Members in Structural Mechanics, Pergamon Press, Oxford, England, 1968.

13. Daniels, C. M. and Fargo, C. G., "Fatigue Failure in Metal Bellows Due to Flow-Induced Vibrations," Technical Support Package (TSP 69-10071) for NASA Tech. Brief 69-10071.

14. Nunner, W., and Warmenbergang and Druckabfall in rauhen Rohren, VDI-Forschungsheft, p. 455, 1956.

15. Rohsenow, W. M. and Clark, J. A., Heat Transfer and Fluid Mechanics Institute, Stanford University Press, Stanford, Calif., pp. 193-207, 1951.

16. Bromley, L. A., et al., "Heat Transfer in Forced Convection Film Boiling," Industrial and Engineering Chemistry, p. 2639, 1953.

17. Strobridge, T. R., "The Thermodynamic Properties of Nitrogen from 64 to 300°K Between 0.1 and 200 Atmospheres, NBS TN 129, p. 4, January 1962.

18. Fand, R. M., "Mechanism of Interaction Between Vibrations and Heat Transfer," Journal of the Acoustical Society of America, 34, 12, p. 1887, 1962.

19. Vance, R. W., Editor, Cryogenic Technology, John Wiley and Sons, Inc., New York, 1963, p. 177.

20. Gerlach, C. R., "The Dynamics of Viscous Fluid Transmission Lines With Particular Emphasis on Higher Mode Propagation," Ph.D. thesis, Oklahoma State University, 1966.

21. Henry, R. H. and Villet, R. B., "Flow Test Program for Stage Flexible Lines," Final Report No. SD 69-97, Contract NAS7-200, North American Rockwell Space Division, March 1969.

22. Pepersack, F. J., "Pressure Losses in Flexible Metal Hose Utilized in Propulsion Fluid Systems of XSM-68B and SM-68B," Tech. Memo, Baltimore 25-10, Martin, Baltimore, 1960.

23. Bouchillon, C. N. and Corley, C. T., Jr., "Study of Pressure Losses in Tubing and Fittings," Final Report, Contract NAS8-11297, Dept. of Mech. Engr., Mississippi State Univ., June 1966.

24. Goodloe, J. H. and Paul, H., "Friction Factors of Straight and Curved Flexible Metal Hoses as a Function of Reynolds Number," Cooling Section Memo No. 5, Guided Missile Development Group, Redstone Arsenal, Huntsville, Alabama , August 1952.

25. Neill, C. R., "Hydraulic Roughness of Corrugated Pipes," Proc. Amer. Soc. Civil Engrs., Vol. 85, HY9, pp. 35-67, 1959.

26. Riley, K. L., "Flow Losses in Flexible Hose," Ph. D. Dissertation, Louisiana State University, May 1967.

27. Daniels, C. M. and Fenton, F. R., "Determining Pressure Drop in Flexible Metal Hose," Machine Design, pp. 195-198, Oct. 13, 1960.

28. Daniels, C. M. and Cleveland, J. R., "Method of Predicting Frictional Loss in Metal Bellows and Flexible Hose," NASA Tech. Brief No. 66-10662, December 1966.

29. Hawthorne, R. C. and von Helms, H. C., "Fluid Expansion Theory Computes Flow in Corrugated Hose," Product Engineering, pp. 47-52, January 21, 1963.

30. Belcher, J. G., "Pressure Drop in Flexible Metal Hoses, Bellows, and Gimbal Joints--An Annotated Bibliography," Brown Engineering Company, Report No. ER-1174, Contract NAS8-11166, June 1964.

31. Ito, H., "Pressure Losses in Smooth Pipe Bends," Jour. Basic Engr., ASME, Series D, Vol. 82, pp. 131-143, March 1960.

32. Ito, H., "Friction Factors in Turbulent Flow in Curved Pipes," Jour. Basic Engr., Trans. ASME, Series D, Vol. 81, pp. 123-134, 1959.

33. Smith, A. J. W., "The Flow and Pressure Losses in Smooth Pipe Bends of Constant Cross Section," Jour. Royal Aero. Society, Vol. 67, pp. 437-447, July 1963.

34. Madison, R. D. and Parker, J. R., "Pressure Losses in Rectangular Elbows," Trans. ASME, Vol. 58, pp. 167-176, 1936.

35. Beij, K. H., "Pressure Losses in Fluid Flow in 90° Pipe Bends," Jour. of Research, National Bureau of Standards, Vol. 21, pp. 1-18, 1938.

36. Keulegan, G. H. and Beij, K. H., "Pressure Losses in Fluid Flow in Curved Pipes," Jour. of Research, National Bureau of Standards, Vol. 18, pp. 89-114, 1937.

37. Weske, J. R., "Investigations of the Flow in Curved Ducts at Large Reynolds Numbers," Jour. Appl. Mech., Vol. 15, Trans. ASME, Vol. 70, pp. 344-348, 1948.

38. Kamiyama, S., "Cavitation Tests in Pipe Bends," Jour. Basic Engr., Trans. ASME, Series D, Vol. 88, pp. 252-260, March 1966.

39. White, C. M., "Streamline Flow Through Curved Pipes," Proc. Roy. Soc. London, A 123, pp. 645-663, 1929.

40. Alder, M., "Stromung in gekrummten Rohren," Zeitschrift fur angewandte Mathematik und Mechanik, Vol. 14, pp. 257-275, 1934.

41. Kamiyama, S., "Theory of the Flow Through Bends with Turning Vanes," ASME Paper No. 67-FE-13.

42. Wilbur, S. W., "An Investigation of Flow in Circular and Annular 90° Bends with a Transition in Cross Section," NACA TN 3995, August 1957.

43. Stanitz, J. D. and Sheldrake, L. J., "Application of a Channel Design Method to High-Solidity Cascades and Tests of an Impulse Cascade with 90° of Turning," NACA TN 2652, March 1952.

44. Higginbotham, J. T., Wood, C. C. and Valentine, E. F., "A Study of the High-Speed Performance Characteristics of 90° Bends in Circular Ducts," NACA TN 3696, June 1956.

45. Lamb, O. P. and Holdhusen, J. S., "Investigation of Aircraft Ducting Components at High Subsonic Speeds," WADC Tech. Report 56-187, September 1956.

APPENDIX A

BELLOWS FLOW-INDUCED VIBRATION COMPUTER PROGRAM

A. 1 Governing Equations

The performance equations, which will be presented in this section, are based upon the derivations given in Reference 1 . Therefore, detailed algebraic manipulations and derivations have been eliminated for clarity. The stress indicator presented in that reference contains approximations which were necessary for rapid hand calculated estimates of the indicator. Use of a digital computer, however, permits incorporation of the exact expression, which will be noted subsequently.

Figure 1 illustrates a longitudinal cross-section of a typical bellows together with pertinent notation. The overall bellows spring rate is

$$K_A = D_m E \frac{N_p}{N_c} \left(\frac{t}{h}\right)^3 \qquad (A-1)$$

where E is the Young's modulus for bellows material and D_m is the mean bellows diameter which is defined as

$$D_m = (D_i + D_o)/2 \qquad (A-2)$$

The elemental spring rate, K, is given by

$$K = 2 N_c K_A \qquad (A-3)$$

The corresponding elemental metal mass of the bellows is

$$m_m = \pi \rho_m t N_p D_m \left[\pi a + (h - 2a)\right] \qquad (A-4)$$

where ρ_m is the metal density and the mean crown or convolute forming radius is

$$a = (\sigma - t N_p)/2 \qquad (A-5)$$

As the bellows vibrates in any one of its $2N_c - 1$ longitudinal modes, fluid is accelerated within the convolutes. The process of moving the fluid is manifested as an apparent or added mass which must be taken into account in calculating the frequencies at which a fluid-elastic instability is likely to occur. This added mass is a function of the longitudinal mode number, N.

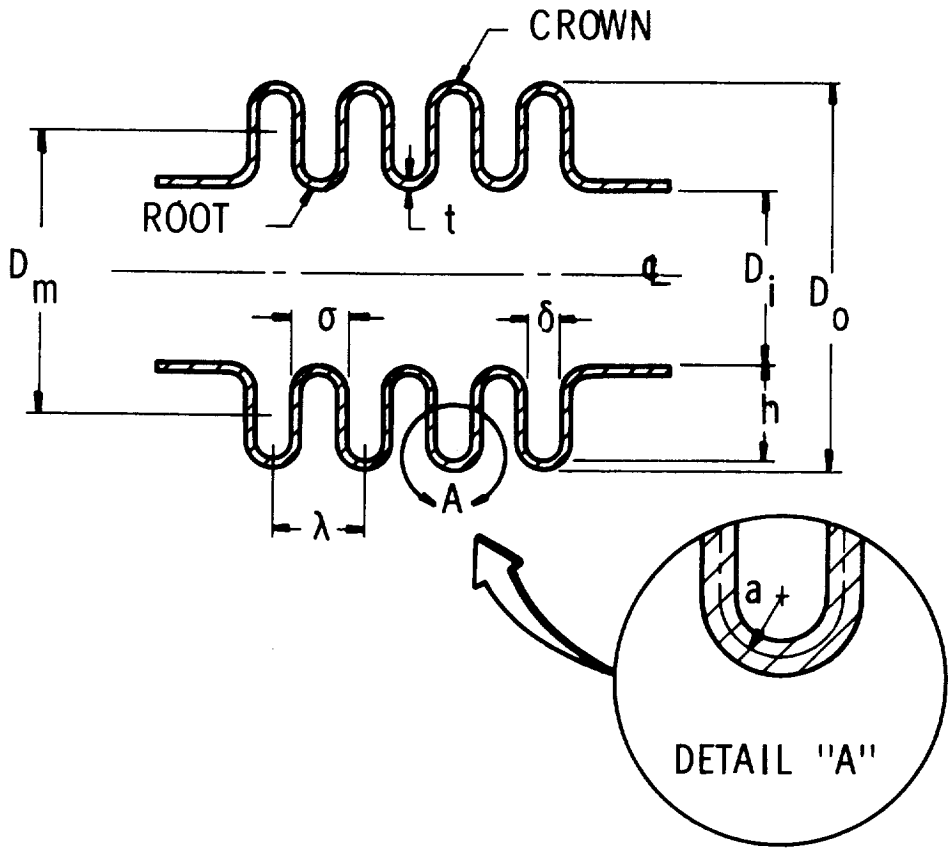

N_c = NUMBER OF CONVOLUTIONS COUNTED FROM THE OUTSIDE

N_p = NUMBER OF PLYS

D_m = MEAN BELLOWS DIAMETER

t = WALL THICKNESS (THICKNESS PER PLY IF MULTI-PLY)

λ = CONVOLUTE PITCH

σ = CONVOLUTE WIDTH

a = MEAN FORMING RADIUS

h = MEAN DISC HEIGHT

Figure 1. Bellows Nomenclature.

That is

$$m_f = m_{f1}\left(\frac{2N_c - 1 - N}{2N_c - 2}\right) + m_{f2}\left(\frac{N-1}{2N_c - 2}\right) \qquad \text{(A-6)}$$

where

$$m_{f1} = \frac{\pi \rho_f D_m h (2a - t N_p)}{2g} \qquad \text{(A-7)}$$

and

$$m_{f2} = \frac{\pi D_m \rho_f h^3}{3 g \delta} \qquad \text{(A-8)}$$

In these expressions ρ_f is the fluid density, g is the gravitational acceleration constant, and

$$\delta = \sigma - 2t N_p \qquad \text{(A-9)}$$

The mode number, N, ranges between 1 and $2N_c - 1$. A reference frequency for a particular mode number can be defined as

$$f_o(N) = \frac{1}{2\pi}\sqrt{\frac{K}{m_m + m_f}} \qquad \text{(A-10)}$$

The true modal frequency, f_N, is then obtained by multiplying the reference value by the dimensionless frequency corresponding to the desired mode number and system degree of freedom (Table 1).

It has been observed that flow excitation of a particular mode can occur over a broad range of fluid velocities, which is termed the "lock-in-range." In fact, if the modal frequencies are sufficiently close together, the lock-in ranges may overlap, thus producing nearly continuous excitation of the bellows. These lock-in ranges are estimated as follows. Extensive experimental studies have revealed that the Strouhal number provides an excellent means of correlating the vibration frequency, fluid velocity and bellows geometry as shown in Figure 2. The Strouhal number is based on convolute pitch, σ. For a bellows having a convolute pitch-to-convolute tip width ratio of λ/σ, three values of the Strouhal number are indicated. Peak bellows excitation corresponds to the curve marked $S_{\sigma_{crit}}$ from which the critical flow velocity may be calculated, i.e.,

$$V_{crit}(N) = \frac{f_N \sigma}{S_{\sigma_{crit}}} \qquad \text{(A-11)}$$

Degrees of Freedom, $2N_c - 1$	MODE NUMBER																							
	1	2	3	4	5	6	7	8	9	10	11	12	13	14	15	16	17	18	19	20	21	22	23	24	25
1	1.414																								
2	1.000	1.732																							
3	0.765	1.414	1.845																						
4	0.620	1.175	1.620	1.900																					
5	0.520	1.000	1.414	1.732	1.930																				
6	0.445	0.868	1.247	1.564	1.802	1.950																			
7	0.390	0.765	1.111	1.414	1.663	1.848	1.962																		
8	0.347	0.684	1.000	1.286	1.532	1.732	1.879	1.970																	
9	0.314	0.618	0.908	1.176	1.414	1.618	1.782	1.902	1.975																
10	0.285	0.563	0.831	1.082	1.310	1.511	1.682	1.819	1.919	1.980															
11	0.264	0.518	0.765	1.000	1.217	1.414	1.587	1.732	1.848	1.932	1.983														
12	0.245	0.479	0.709	0.929	1.136	1.326	1.497	1.646	1.771	1.870	1.942	1.985													
13	0.226	0.445	0.661	0.868	1.064	1.247	1.414	1.563	1.693	1.802	1.888	1.950	1.987												
14	0.213	0.416	0.618	0.814	1.000	1.176	1.338	1.486	1.618	1.732	1.827	1.902	1.956	1.988											
15	0.199	0.390	0.583	0.765	0.942	1.111	1.269	1.414	1.546	1.663	1.764	1.848	1.913	1.962	1.990										
16	0.185	0.367	0.547	0.722	0.891	1.052	1.205	1.347	1.478	1.596	1.700	1.790	1.864	1.923	1.965	1.991									
17	0.174	0.347	0.518	0.684	0.845	1.000	1.147	1.285	1.414	1.532	1.638	1.732	1.812	1.879	1.931	1.969	1.992								
18	0.165	0.329	0.491	0.649	0.803	0.952	1.093	1.228	1.354	1.471	1.578	1.674	1.758	1.831	1.891	1.938	1.972	1.993							
19	0.157	0.313	0.467	0.618	0.765	0.908	1.044	1.175	1.298	1.414	1.520	1.618	1.705	1.782	1.847	1.902	1.944	1.975	1.993						
20	0.149	0.298	0.445	0.590	0.731	0.868	1.000	1.126	1.246	1.360	1.466	1.563	1.652	1.732	1.801	1.861	1.911	1.949	1.977	1.994					
21	0.142	0.285	0.425	0.563	0.699	0.831	0.958	1.081	1.198	1.309	1.414	1.511	1.601	1.682	1.755	1.819	1.873	1.918	1.954	1.979	1.994				
22	0.136	0.272	0.407	0.540	0.670	0.797	0.920	1.039	1.153	1.262	1.365	1.461	1.551	1.633	1.708	1.775	1.834	1.884	1.925	1.958	1.981	1.995			
23	0.131	0.262	0.390	0.518	0.643	0.765	0.885	1.000	1.111	1.217	1.318	1.414	1.503	1.586	1.662	1.732	1.793	1.847	1.893	1.931	1.961	1.982	1.995		
24	0.126	0.251	0.375	0.497	0.618	0.736	0.852	0.964	1.071	1.175	1.274	1.369	1.457	1.541	1.618	1.688	1.753	1.809	1.859	1.902	1.937	1.964	1.984	1.996	
25	0.121	0.241	0.361	0.479	0.595	0.709	0.821	0.929	1.034	1.136	1.233	1.326	1.414	1.497	1.574	1.645	1.711	1.770	1.823	1.870	1.909	1.941	1.967	1.985	1.996

Table I - Dimensionless Frequencies For Bellows Mechanical Model

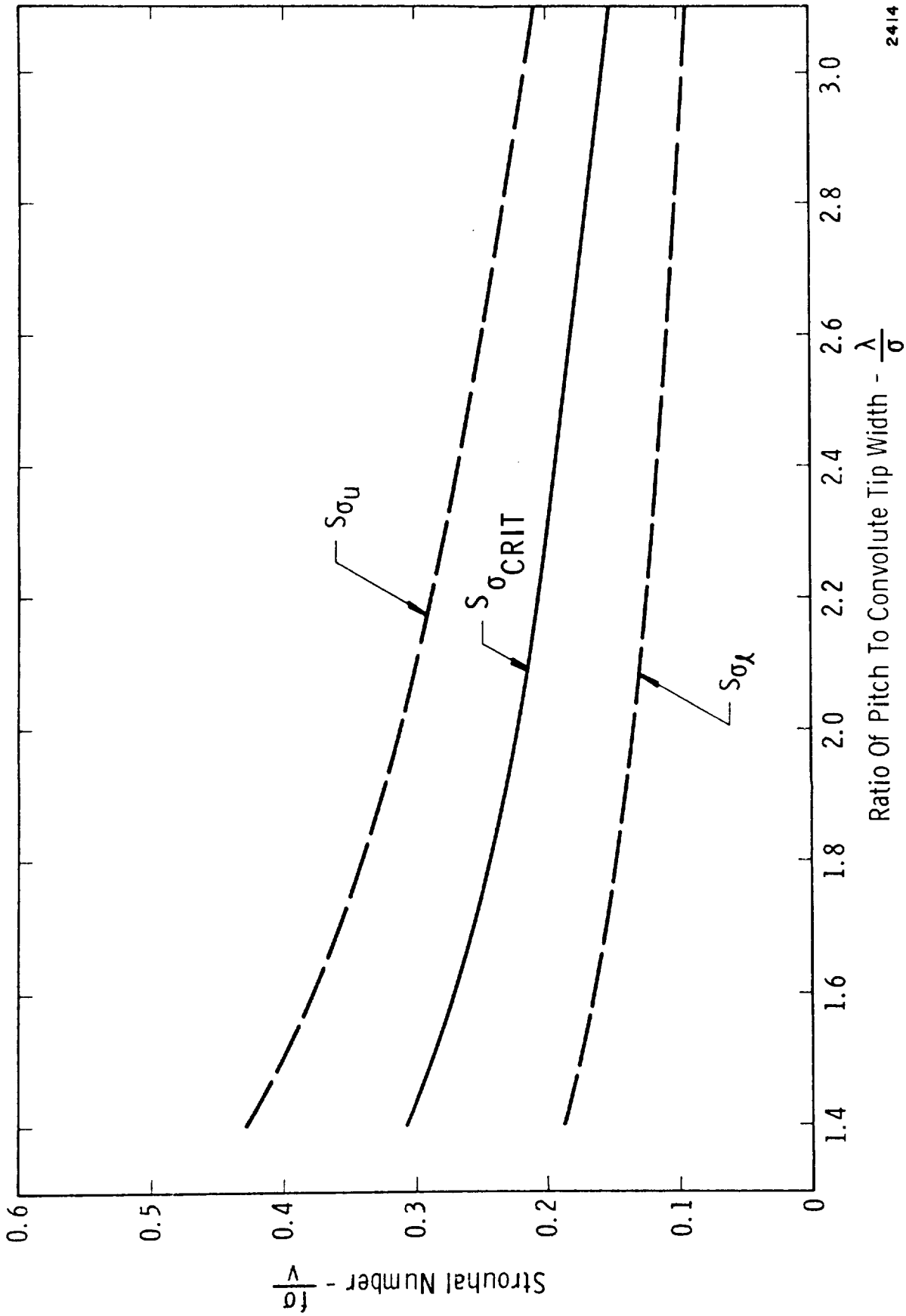

Figure 2. Composite Of All Strouhal Number Correlation Data

Similarly, the upper and lower values of velocity, which define the lock-in-range are obtained from

$$V_{upper}(N) = \frac{f_N \sigma}{S_{\sigma_\ell}} \qquad \text{(A-12)}$$

and

$$V_{lower}(N) = \frac{f_N \sigma}{S_{\sigma_u}} \qquad \text{(A-13)}$$

As mentioned earlier, the stress indicator in Reference 1 contains some approximations, which are justified when making preliminary hand calculations. However, the complete equations (no assumptions) have been included in the digital computer program. To this end, Equations a and c, page 89, Reference 1 were replaced by

$$A_p = \pi (D_i\, h + h^2) \qquad \text{(A-14)}$$

$$C_m = \frac{1}{8N} \left[\frac{N}{N_c} + \sin\left(\frac{\pi}{2} \frac{N}{N_c} \right) \right] \qquad \text{(A-15)}$$

where A_p is the projected convolute height area and C_m is the vibration mode factor. Utilizing these expressions in the derivation of the stress indicator yields

$$SI = \left[\frac{C_f C_e P_d}{N_p} \left(\frac{h}{t} \right)^2 \right] Q \left[\frac{N_c}{N} \left(\frac{D_i + h}{D_m} \right) \left(\frac{N}{N_c} + \sin \frac{\pi}{2} \frac{N}{N_c} \right) \right] \qquad \text{(A-16)}$$

where C_f = vortex force coefficient which is a function of λ/σ and is obtained from Figure 3.

C_e = elbow factor to account for above average forces exerted on bellows convolutes if an elbow located immediately upstream of the bellows.

P_d = fluid dynamic pressure

Q = dynamic amplification factor.

The first bracketed term in Equation A-16 is termed the "bellows operational parameter". This parameter is used in conjunction with the bellows specific spring rate and Table II to determine the dynamic amplification factor (Figure 4), where specific spring rate is defined as

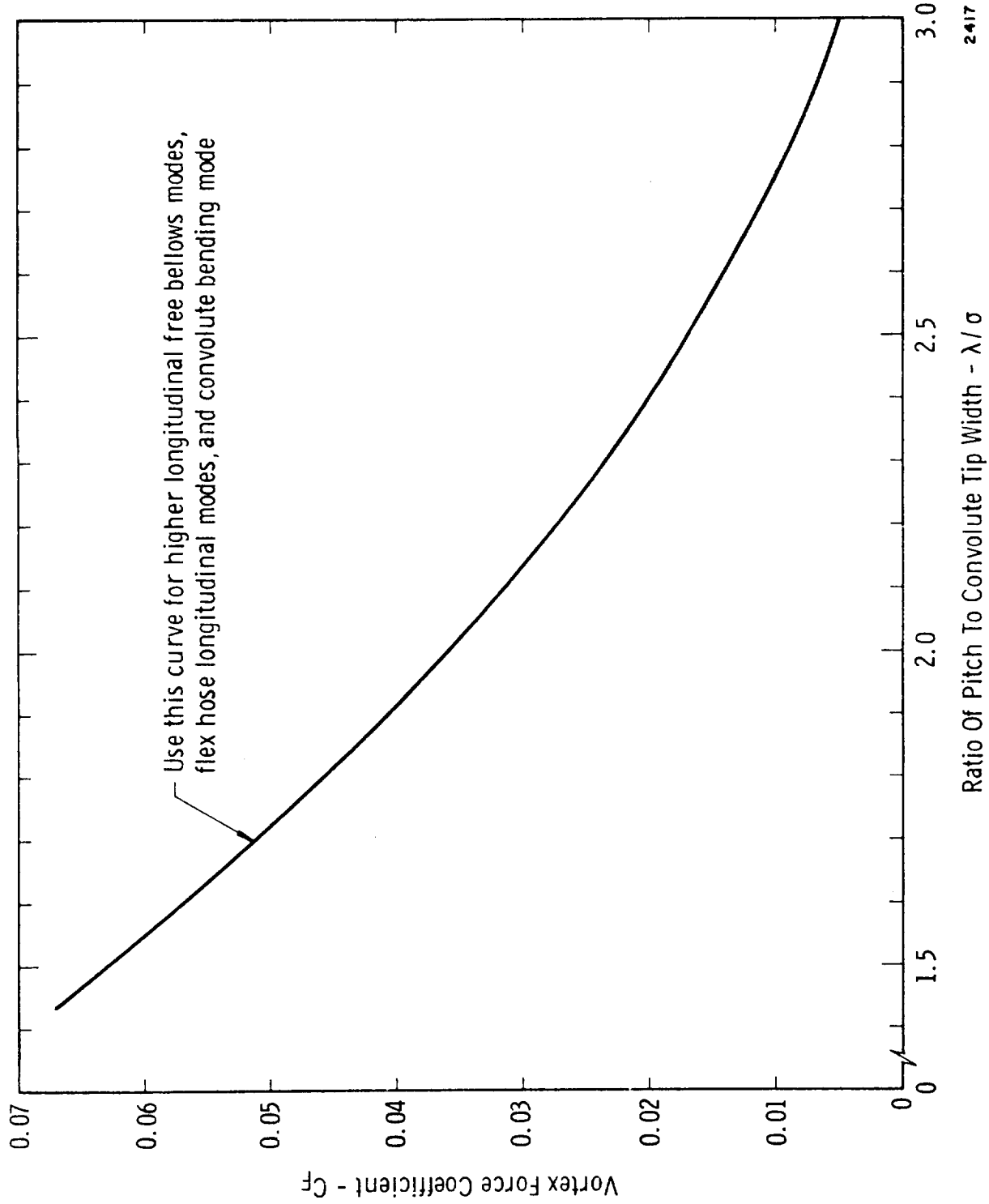

Figure 3 Summary Of Bellows Vortex Force Coefficient Experimental Data

Specific Spring Rate	Number Plies	Internal Media (see Note 1)	Curve No.
all ranges	1	low pressure gases	1
over 2000 lb/in^2	1	high pressure gases, light liquids	1
over 2000	1	water, dense liquids	2
under 2000	1	high pressure gases, light liquids	2
under 2000	1	water, dense liquids	3
over 3000	2	all	3
2000-3000	2	all pressure gases	4
under 2000	2	all pressure gases	5
2000-3000	2	all liquids	5
under 2000	2	all liquids	6
over 3000	3	all	4
2000-3000	3	all	5
under 2000	3	all pressure gases	5
under 2000	3	all liquids	6

Note 1: Low pressure gases will be defined here as being those gases below 150 psia. Light liquids will be defined as having a specific gravity of less than 0.2.

TABLE II

Applications Information for Use with Q Values
Data in Figure 4

$$SSR = \frac{K_A N_c}{D_m N_p} \qquad (A\text{-}17)$$

The computer program currently calculates the stress indicator corresponding to the critical flow velocity defined by Equation A-11.

If the internal medium is a gas, a radial acoustic resonance condition is likely to occur, wherein the acoustic pressure fluctuations couple with the vortex shedding process to produce a force amplification that is significantly larger than would be predicted by the value of Q obtained from Figure 4. Physically, these pressure fluctuations are attenuated at approximately a constant rate for all vortex shedding frequencies less than the radial acoustic resonance or cutoff frequency. In the vicinity of the cutoff frequency the increased amplification must be taken into account since it results in much higher bellows stress levels. To this end, the first mode radial acoustic resonant frequency is obtained from Figure 5 for a particular bellows geometry. This cutoff frequency is then compared with the predicted longitudinal modal frequencies. The predicted Q value from Figure 4 is modified by a suitable constant for all longitudinal frequencies that exceed the cutoff frequency. In other words, this adjustment of Q states that the radial acoustic resonance is capable of coupling with higher longitudinal modes not just at the condition where the frequencies coincide. Figure 5 is valid for convolute pitch-to-tip width ratios of 1.4 to 2.0. These values correspond to total convolute thickness of 0.3 σ and 0.0 σ (theoretical zero wall thickness). In addition, Figure 5 is valid for fluid damping numbers, D_N, of the order of 10^{-6} where $D_m = \nu / r_i c_o$, ν = fluid kinematic viscosity and c_o = isentropic speed of sound.

A.2 Equivalence of Theoretical and Computer Program Variables

This section is intended to establish the correspondence between the analysis variables presented in the previous section and the computer coded variables. Internally generated variables as well as curve fit coefficients will be discussed in subsequent sections.

Analysis	Computer	Comment
N_c	NC	Number of bellows convolutes
N_p	NPLY	Number of plys
σ	SIGMA	Convolute width
λ	LAMBDA	Distance between adjacent convolute crowns

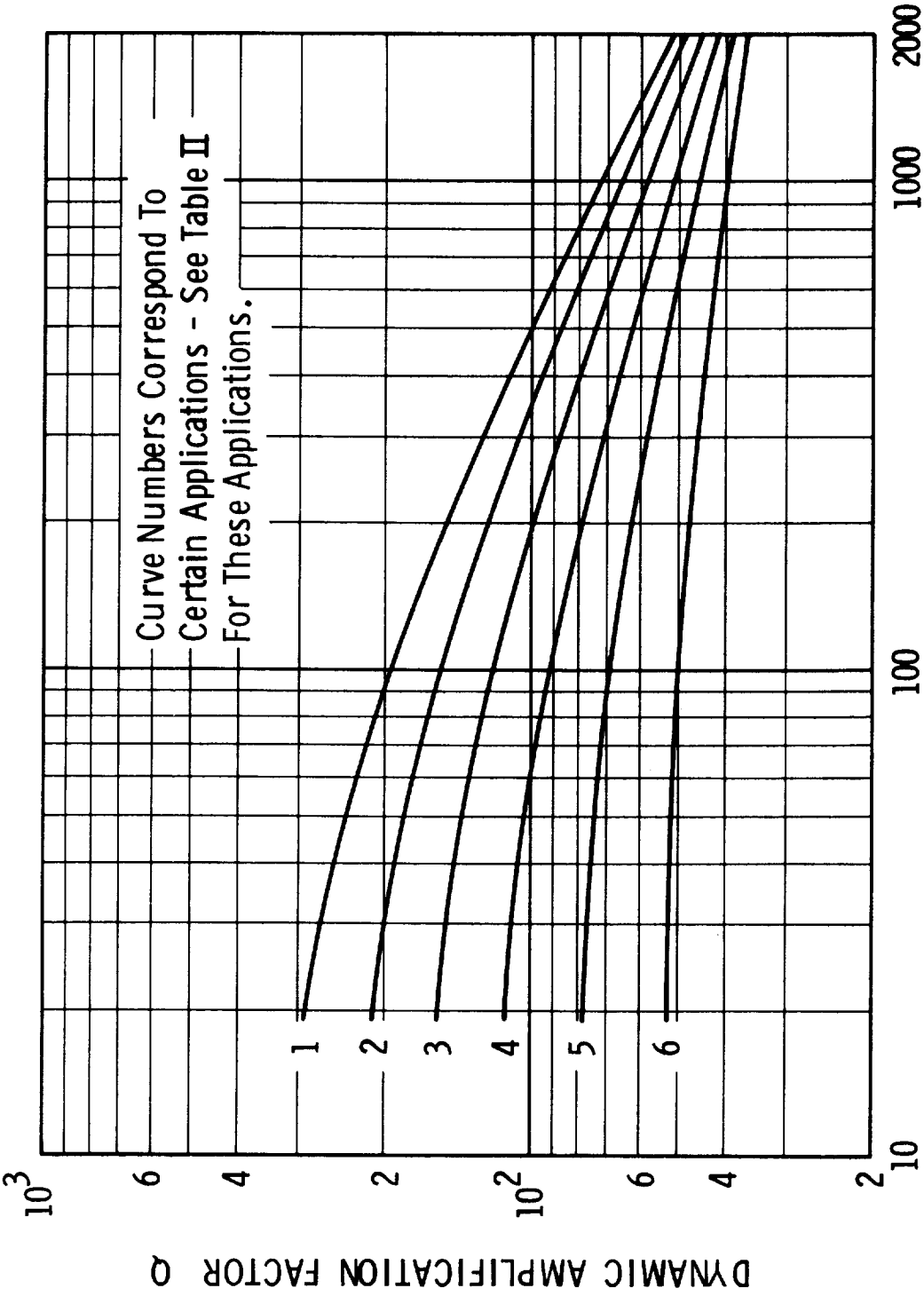

Figure 4 Dynamic Amplification Factors For Various Bellows Applications

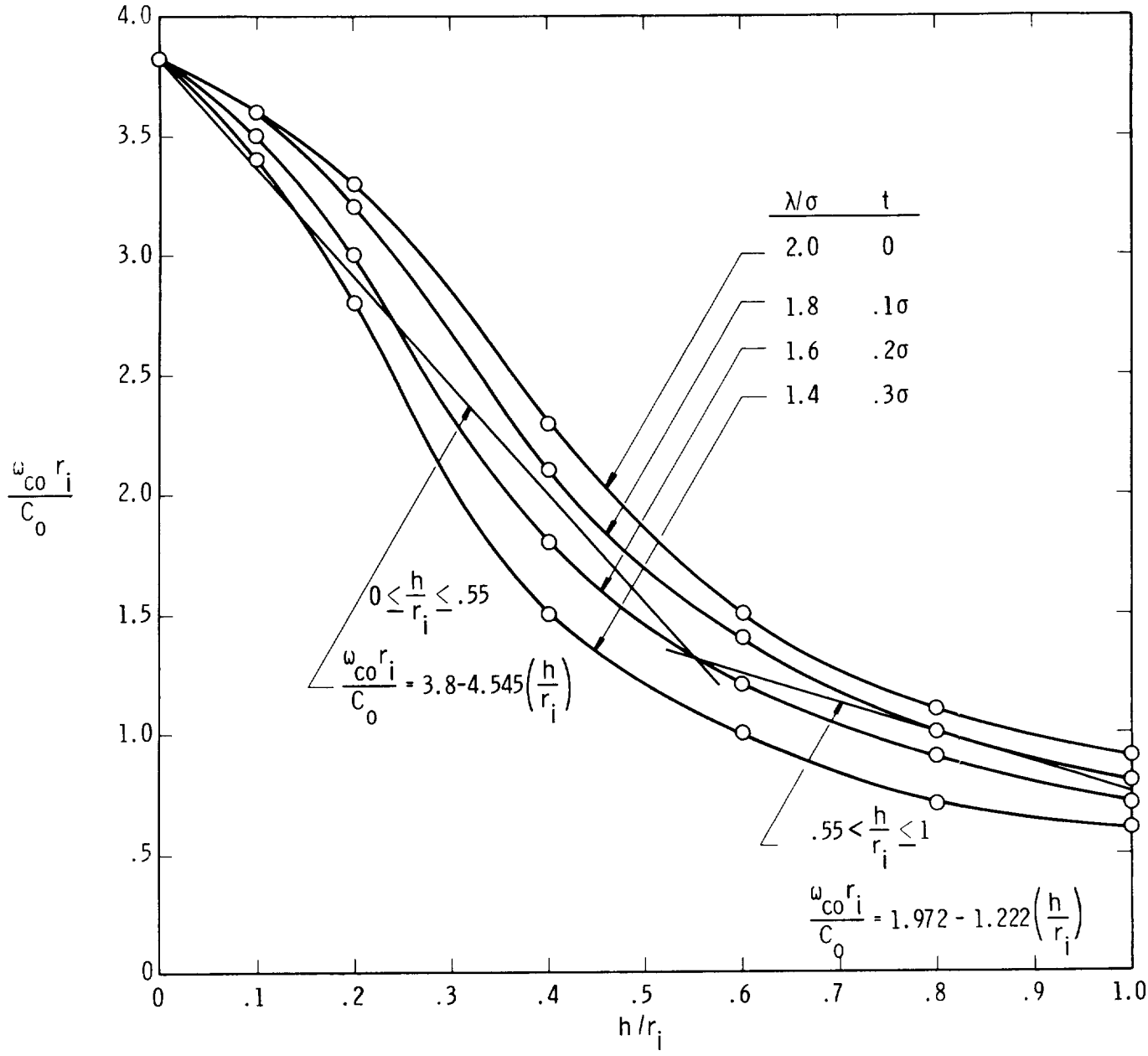

Figure 5. Bellows Cut-Off Frequency For First Mode Radial Acoustic Resonance

Analysis	Computer	Comment
h	H	Mean convolute disc height
t	T	Thickness per convolute ply
D_i	DI	Bellows inside diameter
D_o	DO	Bellows outside diameter
E	E	Young's modulus of bellows material
ρ_M	RHOM	Bellows material density
K_a	KA	Overall bellows spring rate
C_e	CE	Elbow loss factor
ρ_f	RHOF	Fluid density
D_m	DMEAN	Mean bellows diameter
K	K	Elemental spring rate
a	A	Mean convolute forming radius
m_m	MMETAL	Elemental metal mass
m_{f1}	MFLUID1	Apparent fluid mass at low mode numbers
m_{f2}	MFLUID2	Apparent fluid mass at higher mode numbers
m_f	MFLUID	Apparent fluid mass
δ	DELTA	Internal convolute width
S_{σ_ℓ}	STLO	Strouhal number defining the lower and upper bounds on lock-in-range
S_{σ_u}	STUP	
$S_{\sigma_{crit}}$	STCRIT	Strouhal number for severe excitation

Analysis	Computer	Comment
V(N) lower	V(MODE, 1)	Lower velocity bound on lock-in-range
V(N) crit	V(MODE, 2)	Flow velocity for maximum excitation
V(N) upper	V(MODE, 3)	Upper velocity bound on lock-in-range
C_f	CF	Vortex force coefficient
SSR	SSR	Specific spring rate
Q	Q	Dynamic amplification factor
SI	SI	Stress indicator
$\omega_{co} r_i / C_o$	FNCO	Frequency number for first mode radial acoustic resonance
ω_{co}	FREQCO	Angular cutoff frequency for first mode radial acoustic resonance
C_o	CO	Isentropic speed of sound
γ	GAMMA	Ratio of gas specific heats

A.3 Curve Fit Requirements

When predicting the performance of complex systems it is frequently necessary to describe experimentally observed relationships between two or more variables through the use of empirical expressions, i.e., curve fits. In predicting bellows flow-induced vibrations it was necessary to curve fit the data shown in Figures 2, 3 and 4. To this end, all data in these figures was fitted to a hyperbolic equation of the form

$$y = \frac{k}{x - a} + b + d\,x \qquad \text{(A-18)}$$

where k, a, b and d are the coefficients to be determined. Coordinate pairs are input to the fitting routine, and the resulting equations are solved

simultaneously for the unknown coefficients. A listing of the curve fit routine is included in the next section. Note that there is an option for either a four- or eight-point fit. It was necessary to use an eight-point fit only for the curves labeled 1, 2 and 3 in Figure 4 (Q-surface).

The curve fit coefficients for Figures 2, 3 and 4 are summarized below in computer floating point format.

```
STUPK   =    2.5352226E-01
STUPA   =    4.0487805E-01
STUPB   =    2.2229595E-01
STUPD   =   -3.4329268E-02

STLOK   =    1.1870422E-01
STLOA   =    4.6569343E-01
STLOB   =    7.3139166E-02
STLOD   =   -7.9927007E-03

STCRITK =    4.3502697E-01
STCRITA =   -6.1870504E-02
STCRITB =    3.7269292E-03
STCRITD =    4.0647482E-03

QK(1)   =    4.0873881E+04
QA(1)   =   -1.4052553E+02
QB(1)   =    3.7419734E+01
QD(1)   =   -2.2574946E-03

QK(2)   =    3.3980471E+04
QA(2)   =   -1.7498692E+02
QB(2)   =    3.8783556E+01
QD(2)   =   -2.7034275E-03

QK(3)   =    2.0081991E+04
QA(3)   =   -1.4917770E+02
QB(3)   =    4.5393842 E+01
QD(3)   =   -4.8689382E-03

QK(4)   =    9.8799884E+03
QA(4)   =   -1.2489887E+02
QB(4)   =    4.9950596E+01
QD(4)   =   -6.8001116E-03

QK(5)   =    7.8264710E+03
QA(5)   =   -2.0682049E+02
QB(5)   =    4.3576094E+01
QD(5)   =   -4.0612929E-03
```

QK(6)	=	2.3506969E+04
QA(6)	=	-8.4432071E+02
QB(6)	=	2.4773333E+01
QD(6)	=	1.4810690E-03

A.4 Computer Program Structure and Listing

The computer programs listed in this section were written in Fortran IV language for the CDC-6500 computer. In the form presented here, the programs must be compiled each time they are submitted to the computer; however, multiple runs can be accomplished at each submittal. The user of this program may find it more convenient to compile and store the program on tape, thus necessitating minor program modifications.

Two program listings are contained in this section.

1) Bellows performance program and

2) Curve fitting routine (CURFIT).

The latter program, which was used to obtain the coefficients listed in the previous section, is self explanatory. The source deck for the performance program consists of a main program in which the majority of the calculations are performed and two subroutines: CURVE, which is called from the main program and contains the logic for selecting the appropriate curve on the Q-surface (Figure 4) and ACOURES, which evaluates the first mode cutoff or acoustic resonance frequency as a function of bellows geometry.

The execution structure of the program consists of the following items in the order presented.

1) Program control cards - number and type of these cards varies with the user facility.

2) Main program designated Program Bellow.

3) Subroutine CURVE

4) Subroutine ACOURES

5) End of record (EOR) card; multi-punch 7-8-9 in column 1.

6) Data package containing one or more runs.

7) End of file (EOF) card; multi-punch 6-7-8-9 in column 1.

```
      PROGRAM BELLOW(INPUT,OUTPUT,TAPE60=INPUT)
C     THIS PROGRAM GENERATES A THEORETICAL PREDICTION OF THE NATURAL
C      FREQUENCIES FOR A GIVEN BELLOWS INCLUDING THE FLUID FLOW
C      VELOCITIES WHICH PRODUCE FLOW-INDUCED VIBRATIONS(EXCITATION) OF
C      THE BELLOWS NATURAL LONGITUDINAL MODES.
C * * * * * * * * * * * * * * * * * * * * * * * * * * * * * * * * * * *
C  INPUT
C     JFLAG = 1(CALCULATE KA), 2(USE EXPERIMENTALLY DETERMINED KA). KA
C       IS THE OVERALL BELLOWS SPRING RATE, LB/IN
C     NFLUID = 1(GAS), 2(LIQUID)
C     NDEG = NUMBER OF BELLOWS LONGITUDINAL DEGREES OF FREEDOM, 2*NC-1
C     JMAX = NUMBER OF CURVES NECESSARY TO DESCRIBE Q SURFACE
C     NC = NUMBER OF BELLOWS CONVOLUTES
C     NPLY = NUMBER OF PLYS IN THE BELLOWS CONVOLUTES
C     SIGMA = CONVOLUTE WIDTH, IN.
C     LAMBDA = DISTANCE BETWEEN ADJACENT CONVOLUTE CROWNS, IN.
C     H = MEAN DISC HEIGHT, IN.
C     T = THICKNESS PER CONVOLUTE PLY, IN.
C     DI = BELLOWS INSIDE DIAMETER, IN.
C     DO = BELLOWS OUTSIDE DIAMETER, IN.
C     E = YOUNG'S MODULUS OF THE BELLOWS MATERIAL, LB/SQ IN.
C     RHOM = WEIGHT DENSITY OF THE BELLOWS MATERIAL, LB/CU IN.
C     CE = DIMENSIONLESS ELBOW FACTOR
C     IF NFLUID = 1(GAS), THE PERFECT GAS EQUATION OF STATE IS USED FOR
C       CALCULATING GAS DENSITY AT THE STATE DEFINED BY P AND TEMP.
C       IT IS ASSUMED THAT THE GAS PROPERTIES ARE KNOWN AT A REFERENCE
C       STATE DEFINED BY RHOFREF, PREF, AND TREF.
C       P = GAS PRESSURE, PSIG
C       TEMP = GAS TEMPERATURE, DEG. F.
C       PREF AND TREF = REFERENCE GAS STATE, PSIA AND DEG. F.
C       RHOFREF = GAS DENSITY AT REFERENCE STATE, LB/CU FT.
C       GAMMA = RATIO OF SPECIFIC HEATS FOR GAS
C     IF NFLUID = 2(LIQUID), THE LIQUID DENSITY MUST BE KNOWN APRIORI AT
C       THE LIQUID STATE(P AND TEMP)
C       P = LIQUID PRESSURE, PSIG
C       TEMP = LIQUID TEMPERATURE, DEG. F.
C       RHOF = LIQUID DENSITY AT P AND TEMP, LB/CU FT.
C     STUPK,STUPA,STUPB,STUPD = CURVE FIT COEFFICIENTS FOR UPPER BOUND
C       ON STROUHAL NUMBER VS. LAMBDA/SIGMA
C     STLOK,STLOA,STLOB,STLOD = SAME AS ABOVE EXCEPT LOWER BOUND
C     STCRITK,STCRITA,STCRITB,STCRITD = SAME AS ABOVE EXCEPT FOR OPTIMUM
C       OR CRITICAL STROUHAL NUMBER FOR BELLOWS EXCITATION
C     CFK,CFA,CFB,CFD = CURVE FIT COEFFICIENTS FOR VORTEX FORCE
C       COEFFICIENT
C     QK(J),QA(J),QB(J),QD(J) = CURVE FIT COEFFICIENTS FOR THE DYNAMIC
C        AMPLIFICATION FACTOR(Q) SURFACE
C     DIMFREQ(J) = ONE DIMENSIONAL ARRAY OF DIMENSIONLESS NATURAL
C       FREQUENCIES AS A FUNCTION OF MODE NUMBER FOR NDEG BELLOWS
C       LONGITUDINAL DEGREES OF FREEDOM
C * * * * * * * * * * * * * * * * * * * * * * * * * * * * * * * * * * *
      DIMENSION DIMFREQ(25),FREQ(25),V(25,3),SI(25)
      DIMENSION QK(6),QA(6),QB(6),QD(6)
      COMMON NPLY,SSR,NFLUID,P,RHOF,JCURVE,BOP,Q
      REAL NC,NPLY,LAMBDA,MFLUID1,MFLUID2,MFLUID,MMETAL,KA,K,MASS
C * * * * * * * * * * * * * * * * * * * * * * * * * * * * * * * * * * *
    1 READ 1000
      IF(EOF,60)5,10
    5 STOP
   10 READ 1030,JFLAG,NFLUID,NDEG,JMAX
      READ 1010,NC,NPLY,SIGMA,LAMBDA,H,T
      READ 1010,DI,DO,E,RHOM,KA,CE
      GO TO (11,12),NFLUID
```

```
   11 READ 1010,P,TEMP,PREF,TREF,RHOFREF,GAMMA
      GO TO 13
   12 READ 1010,P,TEMP,RHOF
   13 READ 1080,STUPK,STUPA,STUPB,STUPD
      READ 1080,STLOK,STLOA,STLOB,STLOD
      READ 1080,STCRITK,STCRITA,STCRITB,STCRITD
      READ 1080,CFK,CFA,CFB,CFD
      READ 1080,(QK(J),QA(J),QB(J),QD(J),J=1,JMAX)
   15 READ 1020,(DIMFREQ(M),M=1,NDEG)
C * * CALCULATION OF NATURAL FREQUENCIES AND EXCITATION VELOCITIES * * *
   25 PI=3.1415927
      G=32.174049
      DMEAN=(DI+DO)/2.
      GO TO (30,35),JFLAG
   30 KA=DMEAN*E*(NPLY/NC)*(T/H)**3
   35 K=2.*NC*KA*12.
      A=(SIGMA-T*NPLY)/2.
      MMETAL=PI*RHOM*T*NPLY*DMEAN*(PI*A+H-2.*A)/G
      GO TO (36,37),NFLUID
   36 RHOF=RHOFREF*(P+14.7)*((TREF+460.)/(TEMP+460.))/(PREF*1728.)
      GO TO 38
   37 RHOF=RHOF/1728.
   38 MFLUID1=PI*RHOF*DMEAN*H*(2.*A-T*NPLY)/(2.*G)
      DELTA=SIGMA-2.*T*NPLY
      MFLUID2=PI*RHOF*DMEAN*(H**3)/(3.*G*DELTA)
      X=LAMBDA/SIGMA
      STLO=STLOK/(X-STLOA)+STLOB+STLOD*X
      STUP=STUPK/(X-STUPA)+STUPB+STUPD*X
      STCRIT=STCRITK/(X-STCRITA)+STCRITB+STCRITD*X
      AMODE=1.0
      DO 60 MODE=1,NDEG
      MFLUID=(MFLUID1*(2.*NC-1.-AMODE)+MFLUID2*(AMODE-1.))/(2.*NC-2.)
      MASS=MFLUID+MMETAL
      FREQ(MODE)=SQRT(K/MASS)*DIMFREQ(MODE)/(2.*PI)
      DO 55 J=1,3
      GO TO(40,45,50),J
   40 V(MODE,J)=FREQ(MODE)*SIGMA/(STUP*12.)
      GO TO 55
   45 V(MODE,J)=FREQ(MODE)*SIGMA/(STCRIT*12.)
      GO TO 55
   50 V(MODE,J)=FREQ(MODE)*SIGMA/(STLO*12.)
   55 CONTINUE
   60 AMODE=AMODE+1.
C * * * * * * * * * * * * * * * * * * * * * * * * * * * * * * * * * * * *
C     THEORETICAL STRESS INDICATOR FOR CRITICAL STROUHAL NUMBER
      CF=CFK/(X-CFA)+CFB+CFD*X
      SSR=KA*NC/(DMEAN*NPLY)
      CALL CURVE
      IF(NFLUID.EQ.1) 65,70
   65 RI=DI/2.
      HRI=H/RI
      CO=SQRT(GAMMA*(P+14.7)*G/(RHOF*12.))
      CALL ACOURES(HRI,RI,CO,FREQCO,QADJUST)
   70 AMODE=1.0
      DO 200 MODE=1,NDEG
      BOP=CF*CE*RHOF*(V(MODE,2)**2)*((H/T)**2)*12./(2.*NPLY*G)
      Q=QK(JCURVE)/(BOP-QA(JCURVE))+QB(JCURVE)+BOP*QD(JCURVE)
      IF(NFLUID.EQ.1)75,80
   75 IF(FREQ(MODE).GE.FREQCO) Q=Q*QADJUST
   80 SI(MODE)=BOP*Q*(NC/AMODE)*((DI+H)/DMEAN)*(AMODE/NC+SIN(PI*AMODE/(2
     1.*NC)))
      AMODE=AMODE+1.
```

```
  200 CONTINUE
      PRINT 1000
      PRINT 1040,SIGMA,LAMBDA,H,T,DI,DO,NC,NPLY,E,KA,RHOM,P,TEMP,RHOF,NF
     1LUID
      PRINT 1050
      PRINT 1060
      DO 210 MODE=1,NDEG
  210 PRINT 1070,MODE,SI(MODE),FREQ(MODE),V(MODE,1),V(MODE,2),V(MODE,3)
      IF(NFLUID.EQ.1)215,1
  215 PRINT 1090,FREQCO,QADJUST
      GO TO 1
 1000 FORMAT(80H1
     1                              )
 1010 FORMAT(6E12.6)
 1020 FORMAT(10F7.3)
 1030 FORMAT(5I3)
 1040 FORMAT(1H0,29X,18HBELLOWS PARAMETERS/
     $        1H0,18X,26HSIGMA(CONVOLUTE WIDTH, IN),11X,F6.3,/
     $            19X,27HLAMBDA(CONVOLUTE PITCH, IN),10X,F6.3,/
     $            19X,23HH(MEAN DISC HEIGHT, IN),14X,F6.3,/
     $            19X,30HT(CONVOLUTE THICKNESS/PLY, IN),7X,F6.3,/
     $            19X,23HDI(INSIDE DIAMETER, IN),14X,F6.3,/
     $            19X,24HDO(OUTSIDE DIAMETER, IN),13X,F6.3,/
     $            19X,24HNC(NUMBER OF CONVOLUTES),12X,F7.3,/
     $            19X,21HNPLY(NUMBER OF PLIES),15X,F7.3,/
     $            19X,28HE(YOUNG'S MODULUS, LB/SQ.IN),4X,E11.4,/
     $            19X,30HKA(OVERALL SPRING RATE, LB/IN),6X,F7.3,/
     $            19X,32HRHOM(MATERIAL DENSITY, LB/CU.IN),4X,F7.3,/
     $        1H0,30X,16HFLUID PARAMETERS/
     $        1H0,18X,17HP(PRESSURE, PSIG),19X,F7.3,/
     $            19X,24HTEMP(TEMPERATURE, DEG F),12X,F7.3,/
     $            19X,29HRHOF(FLUID DENSITY, LB/CU.IN),3X,E11.4,/
     $            19X,23HNFLUID(1=GAS, 2=LIQUID),19X,I1,/
     $        1H0,23X,31HTHEORETICAL BELLOWS PERFORMANCE)
 1050 FORMAT(1H0,79HMODE NO.  STRESS INDICATOR  NATURAL FREQUENCY      F
     $LOW EXCITATION RANGE,FT/SEC,/
     $            36X,2HHZ,14X,5HLOWER,5X,8HCRITICAL,4X,5HUPPER)
 1060 FORMAT(1H0)
 1070 FORMAT(3X,I2,8X,E11.4,9X,F9.3,5X,3F11.3)
 1080 FORMAT(4E14.8)
 1090 FORMAT(///,3X,46HFIRST MODE RADIAL ACOUSTIC RESONANT FREQUENCY=,F9
     1.3,8HQADJUST=,F5.2)
      GO TO 1
      END
      SUBROUTINE CURVE
      DIMENSION DIMFREQ(25),FREQ(25),V(25,3),SI(25)
      DIMENSION QK(6),QA(6),QB(6),QD(6)
      COMMON NPLY,SSR,NFLUID,P,RHOF,JCURVE,BOP,Q
      REAL NC,NPLY,LAMBDA,MFLUID1,MFLUID2,MFLUID,MMETAL,KA,K
      IF(NPLY.EQ.1.)180,10
   10 IF(NPLY.EQ.2.)90,20
   20 IF(SSR.GT.3000.)30,40
   30 JCURVE=4
      RETURN
   40 IF(2000..LE.SSR.AND.SSR.LE.3000.)50,60
   50 JCURVE=5
      RETURN
   60 IF(SSR.LT.2000..AND.NFLUID.EQ.1)70,80
   70 JCURVE=5
      RETURN
   80 JCURVE=6
      RETURN
```

```
   90 IF(SSR.GT.3000.)100,110
  100 JCURVE=3
      RETURN
  110 IF(NFLUID.EQ.1)120,150
  120 IF(2000..LE.SSR.AND.SSR.LE.3000.)130,140
  130 JCURVE=4
      RETURN
  140 JCURVE=5
      RETURN
  150 IF(2000..LE.SSR.AND.SSR.LE.3000.)160,170
  160 JCURVE=5
      RETURN
  170 JCURVE=6
      RETURN
  180 IF(NFLUID.EQ.1.AND.P.LT.150.)190,200
  190 JCURVE=1
      RETURN
  200 IF(SSR.GT.2000.)210,260
  210 GO TO (220,230),NFLUID
  220 JCURVE=1
      RETURN
  230 SPGRAV=RHOF/(62.4/1728.)
      IF(SPGRAV.LT.0.2)240,250
  240 JCURVE=1
      RETURN
  250 JCURVE=2
      RETURN
  260 GO TO (270,280),NFLUID
  270 JCURVE=2
      RETURN
  280 SPGRAV=RHOF/(62.4/1728.)
      IF(SPGRAV.LT.0.2)290,300
  290 JCURVE=2
      RETURN
  300 JCURVE=3
      RETURN
      END
      SUBROUTINE ACOURES(X,Y,Z,FREQCO,QADJUST)
      PI=3.1415927
      HRI=X
      RI=Y
      CO=Z
      IF(HRI.LE.0.55) GO TO 20
   10 FNCO=1.972-1.222*HRI
      GO TO 30
   20 FNCO=3.8-4.545*HRI
   30 FREQCO=12.*FNCO*CO/(2.*PI*RI)
      QADJUST=5.
      RETURN
      END
```

```
      PROGRAM CURFIT(INPUT,OUTPUT,TAPE60=INPUT)
C     HARD CURVE FITTING ROUTINE
C     N=1 ----- ACCEPTS ONLY FOUR X-Y PAIRS AS INPUT
C     N=0 ----- ACCEPTS EIGHT X-Y PAIRS AS INPUT
C     IF EIGHT X-Y PAIRS ARE USED, THE FIRST TWO X-Y PAIRS
C     (I.E.,X1-Y1 AND X2-Y2) MUST BE THE TWO END POINTS ON THE CURVE
C     BEING FITTED
      DIMENSION X(8),Y(8),YC(8)
  100 READ 90 , N
      IF (EOF,60)999,109
  109 CONTINUE
   90 FORMAT(I2)
      READ 106,X(1),Y(1),X(2),Y(2),X(3),Y(3),X(4),Y(4)
      IF (N.EQ. 1) GO TO 110
  105 READ 106,X(5),Y(5),X(6),Y(6),X(7),Y(7),X(8),Y(8)
  106 FORMAT(8F10.4)
  110 READ 111,XI,DELX,XF
  111 FORMAT(3F6.3)
      X1=X(1)
      X2=X(2)
      Y1=Y(1)
      Y2=Y(2)
      IF( N.LT. 1) GO TO 120
      X3=X(3)
      Y3=Y(3)
      X4=X(4)
      Y4=Y(4)
      GO TO 125
  120 ILOOP=1
      ERR=0.
      DO 420 I=3,7
      X3=X(I)
      Y3=Y(I)
      L=I+1
      DO 420 J=L,8
      X4=X(J)
      Y4=Y(J)
  125 R12=1./(X1-X2)
      R13=1./(X1-X3)
      R14=1./(X1-X4)
      ALPHA=X1*Y1*(R12-R13)-X2*Y2*R12+X3*Y3*R13
      BETA=X1*Y1*(R12-R14)-X2*Y2*R12+X4*Y4*R14
      GAMMA=(Y1-Y2)*R12-(Y1-Y3)*R13
      DELTA=(Y1-Y2)*R12-(Y1-Y4)*R14
      EPSIL=X2-X3
      ZETA=X2-X4
      AT=(BETA/ZETA-ALPHA/EPSIL)/(DELTA/ZETA-GAMMA/EPSIL)
      DT=(ALPHA-AT*GAMMA)/EPSIL
      BT=(X1*Y1-X2*Y2-AT*(Y1-Y2)-DT*(X1*X1-X2*X2-AT*(X1-X2)))*R12
      AKT=X1*Y1-AT*Y1-BT*X1+AT*BT-DT*X1*X1+AT*DT*X1
      ERRT=0.
      IF(N.EQ. 1) GO TO 455
  355 IF (AT-X1)390,390,360
  360 IF (X2-AT)390,390,420
  390 DO 400 K=3,8
      YC(K)=AKT/(X(K)-AT)+BT+DT*X(K)
  400 ERRT=ERRT+ABS(YC(K)-Y(K))
      GO TO (405,410) ,ILOOP
  405 ILOOP=2
      GO TO 415
  410 IF(ERRT-ERR)415,420,420
  415 A=AT
```

```
      B=BT
      D=DT
      AK=AKT
      ERR=ERRT
  420 CONTINUE
  425 PRINT 430,AK,A,B,D
  430 FORMAT(1H1,4E20.8)
      YY=XI
  435 YY=AK/(XX-A)+B+D*XX
  440 PRINT 445,XX,YY
  445 FORMAT(2E20.8)
  450 XX=XX+DELX
      IF(XX-XF)435,435,100
  455 A=A1
      B=B1
      D=DT
      AK=AKT
      GO TO 425
  999 CONTINUE
      STOP
      END
```

A. 5 Data Input Package

Instructions for preparation of a data input package are located at the beginning of the PROGRAM BELLOW listing. An experienced programmer will have no difficulty in constructing the input, but for the inexperienced user the following supplementary remarks may be useful.

Input Card 1

This card is an identification card on which the user can place information that will aid in identifying and classifying the run. Any alpha-numeric characters can be placed in columns 2 through 80. Column 1 must either contain a 1 for printer carriage control or be left blank.

Input Card 2, Word 4

JMAX is the number of individual curves necessary to describe the Q-surface (Figure 4). As shown in that figure JMAX = 6. If future data indicate that more than six curves are necessary, then the dimension statement pertaining to Q must be altered accordingly.

Input Card 4, Word 5

KA may be left blank if JFLAG = 1

Input Group 10

The curve fit coefficients for the Q-surface are read in at a rate of four words per card, i.e., QK (1), QA (1), QB (1), QD (1) are punched on Card 1 of Group 10; QK (2), QA(2), QB(2), QD(2) are on Card 2 of this group. Reading continues per this format until JMAX sets of coefficients have been read in.

Input Group 11

To input this group the user first calculates the number of bellows longitudinal degrees of freedom: 2NC-1. Using Table I, locate the row corresponding to the calculated degrees of freedom. This is the row that must be read into the program as DIMFREQ(M). Read-in is accomplished at a rate of seven words per card, and the reading progresses sequentially from the lowest mode number to the highest, e.g., if 2NC -1 = 15, then

DIMFREQ(1) = 0. 199

.

.

.

DIMFREQ(15) = 1.99

A.6 Example Problem

Listed below is an input data deck constructed in accordance with the instructions presented at the beginning of PROGRAM BELLOW. The notations that appear in columns 73 through 80 serve to identify the data group in each card. Following this listing is the corresponding computer output. The output is grouped into three sections. The first group summarizes the pertinent bellows input parameters. For this example, only the overall spring rate, KA, was generated by internal combustion. The next group summarizes the fluid parameters. The next group contains the predicted longitudinal bellows performance. Bellows lock-in-range for a particular mode of vibration is defined by the upper and lower flow velocities. Stress indicator was calculated based on the critical flow velocity for each mode. Note, that for this particular bellows configuration, the lock-in-ranges for successive modes overlap, which indicates a more or less continuous spectrum of excitation velocities. Note also that all performance variables at a mode number of 17 are less than the corresponding quantities at the previous mode number. Physically this behavior is accounted for by the fact that the apparent fluid mass is increasing at a faster rate than the dimensionless frequency numbers in Table I for this 17 degree-of-freedom bellows.

```
1BELLOWS PROGRAM CHECKOUT. BELLOWS NO. 106 WITH WATER AT 70F AND 30 PSIG
  1   2 17   6
 +.900000+01 +.100000+01 +.950000-01 +.240000+00 +.160000+00 +.600000-02      NC
 +.198000+01 +.232000+01 +.280000+08 +.280000+00 +.000000+00 +.100000+01      DI
 +.300000+02 +.700000+02 +.622800+02                                          P
 +.25352226+00 +.40487805+00 +.22229595+00 -.34329268-01                     STUP
 +.11870422+00 +.46569343+00 +.73139166-01 -.79927007-02                     STLO
 +.43502697+00 -.61870504-01 +.37269292-02 +.40647482-02                    STCRIT
 -.19458000+03 +.25500000+02 -.74460000+01 -.39900000+00                      CF
 +.40873881+05 -.14052553+03 +.37419734+02 -.22574946-02                    Q(J=1)
 +.33980471+05 -.17498692+03 +.38783556+02 -.27034275-02                    Q(J=2)
 +.20081991+05 -.14917770+03 +.45393842+02 -.48689382-02                    Q(J=3)
 +.98799884+04 -.12489887+03 +.49950596+02 -.68001116-02                    Q(J=4)
 +.78264710+04 -.20682049+03 +.43576094+02 -.40612929-02                    Q(J=5)
 +.23506969+05 -.84432071+03 +.24773333+02 +.14810690-02                    Q(J=6)
   .174   .347   .518   .684   .845  1.000  1.147  1.285  1.414  1.532  DIM 1-10
  1.638  1.732  1.812  1.879  1.931  1.969  1.992                        DIM11-17
```

INPUT DATA DECK

BELLOWS PROGRAM CHECKOUT. BELLOWS NO. 106 WITH WATER AT 70F AND 30 PSIG

BELLOWS PARAMETERS

SIGMA(CONVOLUTE WIDTH, IN)	.095
LAMBDA(CONVOLUTE PITCH, IN)	.240
H(MEAN DISC HEIGHT, IN)	.160
T(CONVOLUTE THICKNESS/PLY, IN)	.006
DI(INSIDE DIAMETER, IN)	1.980
DO(OUTSIDE DIAMETER, IN)	2.320
NC(NUMBER OF CONVOLUTES)	9.000
NPLY(NUMBER OF PLIES)	1.000
E(YOUNG'S MODULUS, LB/SQ.IN)	2.8000E+07
KA(OVERALL SPRING RATE, LB/IN)	352.734
RHOM(MATERIAL DENSITY, LB/CU.IN)	.280

FLUID PARAMETERS

P(PRESSURE, PSIG)	30.000
TEMP(TEMPERATURE, DEG F)	70.000
RHOF(FLUID DENSITY, LB/CU.IN)	3.6042E-02
NFLUID(1=GAS, 2=LIQUID)	2

THEORETICAL BELLOWS PERFORMANCE

MODE NO.	STRESS INDICATOR	NATURAL FREQUENCY HZ	FLOW EXCITATION RANGE, FT/SEC LOWER	CRITICAL	UPPER
1	2.3438E+04	684.829	21.255	29.776	49.040
2	6.0467E+04	1340.985	41.620	58.306	96.027
3	9.7592E+04	1966.825	61.044	85.517	140.844
4	1.3419E+05	2553.256	79.245	111.015	182.838
5	1.6809E+05	3102.709	96.298	134.905	222.184
6	1.9666E+05	3613.754	112.159	157.125	258.780
7	2.1746E+05	4081.412	126.674	177.458	292.268
8	2.2950E+05	4504.429	139.803	195.851	322.561
9	2.3307E+05	4885.006	151.615	212.398	349.814
10	2.2909E+05	5218.341	161.960	226.892	373.683
11	2.1929E+05	5503.189	170.801	239.277	394.081
12	2.0566E+05	5741.630	178.201	249.644	411.156
13	1.9009E+05	5929.034	184.018	257.792	424.576
14	1.7412E+05	6070.644	188.413	263.949	434.717
15	1.5891E+05	6161.823	191.243	267.914	441.246
16	1.4506E+05	6207.572	192.663	269.903	444.522
17	1.3286E+05	6206.382	192.626	269.851	444.437

APPENDIX B

DESCRIPTION OF TEST BELLOWS

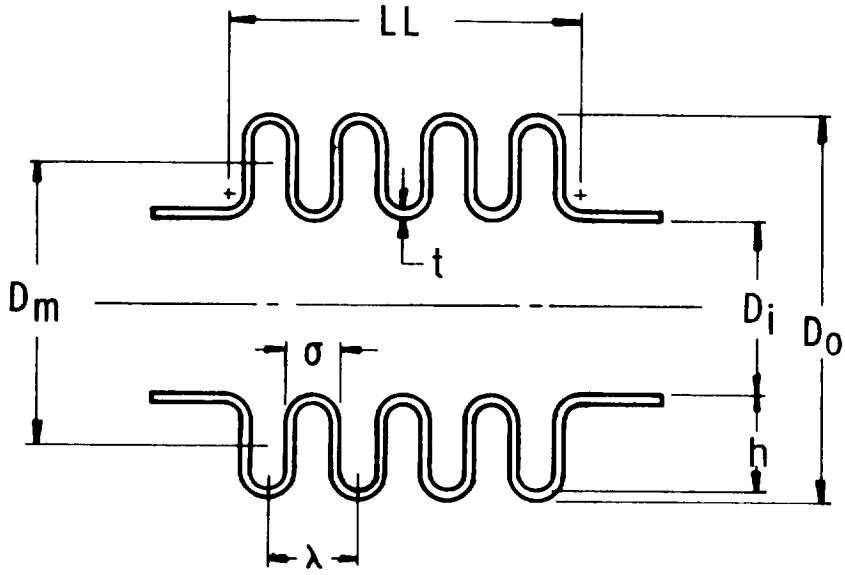

N_c = Number of convolutions counted from the outside.

N_p = Number of plys

Bellows Number	D_i	D_o	D_m	LL	N_c	N_p	h	λ	σ	t
#101, 102, 105, 112	1.49	2.22	1.85	1.80	7	1	.35	.26	.125	.013
#103, 104, 110, 114	1.46	2.03	1.74	1.77	8	1	.27	.22	.144	.013
P/N-08047, #106	1.98	2.32	2.16	2.15	9	1	.16	.24	.095	.006
P/N-08049, #107	1.97	2.33	2.15	2.15	9	2	.17	.24	.140	.006
P/N-08051, #108	2.00	2.34	2.17	2.15	9	3	.15	.24	.140	.006
P/N-08052, #113	1.99	2.45	2.22	2.41	14	1	.22	.17	.090	.013

Note: These dimensions are for geometric description only. Actual dimensions for a particular bellows may vary somewhat from these representative dimensions.

DIMENSIONAL DATA FOR TEST BELLOWS CITED

APPENDIX C

HEAT TRANSFER COMPUTER PROGRAM

Heat Transfer Program Listing

```
      PROGRAM  2-PHT(INPUT,OUTPUT)                                  Read: Flow Velocity, Bellows Inside and Outside Diameter
    1 READ 2,V,DI,DO,SIG,ENC,TS,FF,FLW,Z,FKF                        Convolute Width, Number of Convolutes, Stream Temp,
    2 FORMAT(1F4.4)                                                 Bellows Friction Factor, Wall Thickness and Frost Conductivity
      DD=(DI+DO)/2.                                               — Mean Diameter
      FLL=1.4*ENC*((DO-DI)/2.)+(2.*ENC-1.)*SIG                    — Wall Equivalent length
      AW=(3.14*DD*FLL)/144.0                                      — Wall area
      FKW=8.9                                                     — Wall Conductivity
      AA1=4.28*FLL*FKW/12.0
      AA2=4.28*FLL*FKF/12.0
      RR=DD/2.
      R3=(ALOG((RR+FLW)/RR))/AA1                                  — Wall Resistance
      DN=5.4                                                      — LN2 Density
      VISN=3.2E-06                                                — LN2 Viscosity
      CPN=.475                                                    — LN2 Specific Heat
      FKN=.079                                                    — LN2 Thermal Conductivity
      RE=(DN*V*DI)/(12*32.2*VISN)                                 — Flow Reynolds No.
      FO=.15                                                      — Smooth Pipe Friction Factor
      FPR=(VISN*CPN/FKN)*3600*32.2                                — Prandtl No.
      FPR=(FF/FO)*FPR                                             — Modified Prandtl No.
      A=1.5/(FPR**.167)
      B=FPR-1.5
      FNU=(.023*(RE**.75)*FPR)/(1.0+(A/(RE **.125)) * B)          — Nusselt No.
      FHI=(FKN*FNU*12.0)/DD                                       — Inside Convection Coefficient
      R4=1.0/(FHI*AW)                                             — Inside Resistance
      PRINT 36,FHI,   R3,R4
   36 FORMAT(30X,F10.4,2F10.6)
      A1=0.527 05
      A2=-305.07339
      A3=.16441101
      A4=-.00313*92
      A5=2.9d571 3E-05
      A6=-1.423645*E-07
      A7=2.73752 2E-10
      CAVO=0.0                                                    —┐Cavitation Number Range at
      CAVO=1.5                                                    —┘Zero Strain
      CAVM=1.0                                                    —┐Cavitation Number Range
      CAVM=3.0                                                    —┘at Maximum Strain
      DP=(5.4*V**2)/(64.4*144.)                                   — Dynamic Pressure
      FLF=0.0                                                     — Initial Frost Thickness
    5 TO=-247.0                                                   — Initial Environmental Temp
    7 FHO=2.0                                                     — Initial Outside Convection Coefficient
    3 R1=1.0/(FHO*AW)
      R1=R1*(RR/(RR+FLW+FLF))                                     — Outside Resistance
      R2=(ALOG((RR+FLW+FLF)/(RR+FLW)))/AA2                        — Frost Resistance
      R=R1+R2+R3+R4                                               — Total Resistance
      Q=(TO-TS)/R                                                 — Heat Transfer
      TF=TO-Q*R1                                                  — Outside Frost Temp
      TWI=TS+Q*R4                                                 — Inside Wall Temp
      TR=TWI+459.6
      TK=TR/1.8
      ATM=A1+A2/TK+A3*TK+A4*TK**2+A5*TK**3+A6*TK**4+A7*TK**5
      FPV=14.696*(10.0**ATM)                                      — Vapor Pressure at TWI
      FP01=FPV+CAVO1*DP                                           —┐Pressure Range at
      FP02=FPV+CAVO2*DP                                           —┘Zero Strain
      FPM1=FPV+CAVM1*DP                                           —┐Pressure Range at
      FPM2=FPV+CAVM2*DP                                           —┘Maximum Strain
      PRINT4.,TO,TS,FHO,R1,R2,R,Q,TF,TWI,FPV,FP01,FP02,FPM1,FPM2
   40 FORMAT(2F10.2,4F10.6,3F13.6,3F6.2)
      FHO=FHO+0.5                                                 — Change Outside Convection Coefficient
      IF(FHO-20.0)3,3,4
    4 TO=TO+10.0                                                  — Change Environmental Temperature
      IF(TO-300.0)7,7,8
    8 FLF=FLF+.05                                                 — Change Frost Thickness
      IF(FLF-0.5)5,5,9
    9 IF(Z-1.11)6,6
    6 CONTINUE
      STOP
      END
```

APPENDIX D

S-II LOX PRE-PRESSURIZATION FLEX HOSE STUDY

Introduction

Tests of the S-II LOX pre-pressurization hose were conducted at SwRI in support of the North American effort discussed in Reference 21.

Three hoses from the pre-pressurization system line were tested; part numbers of these items are listed below:

PN-ME271-0017-0094 (1 Solar and 1 Anaconda tested)
PN-ME271-0017-0093 (1 Anaconda tested)

Table I shows North American, Space Division, data of the reported nitrogen flow conditions throughout the pre-pressurization system. These values were assumed to be "stage rated conditions" for these hoses. The tests of these hoses consisted of further detailed sweep tests for various system pressures and hose mounting conditions, plus dwell tests at stage rated conditions. Nitrogen was used for all testing since it had been earlier established that this created a more severe condition than the pre-launch helium flow.

Results of Detailed Sweep Tests

Detailed sweep tests were conducted on both the Solar and Anaconda 0094 hoses. These tests provided dynamic convolute strain data as a function of internal flow velocity and pressure. Strain was monitored with two gages on each hose; one was mounted near the upstream end and the other near the downstream end of the hose. Tests were conducted to determine the effect of measurement location. Also, some tests were conducted to determine the effect of axially stretching the hose to provide additional "fixity" of the convolute tips. Results of these tests are given in Figures 1 through 5, and several significant observations are outlined below:

(1) From Figure 1 it may be seen that the strain at the downstream measurement point is considerably higher than that at the upstream point. The reason for this is apparently because of the difference in velocity at the two points caused by the rather large pressure loss, hence density change, along the hose. This trend is consistent for both hoses and probably explains, at least in part, why the Solar hose on the stage failed near the downstream end. It also indicates that any future monitoring tests of flex hose with high velocity gas flows should employ strain gages mounted near the downstream end.

(2) Comparison of Figures 3 and 4 indicates that the Anaconda hose is possibly more sensitive to pressure in the high velocity region above about 450 fps, since the strain levels increase more drastically as the pressure increases than with the Solar hose. This is probably caused by the double braid on the Anaconda which tends to provide less fixity at low pressure than with the Solar.

(3) From Figure 4 note that the strain is increasing very quickly with velocity in the vicinity of the rated 480 fps point. In fact, the strain at 150 psia and 510 fps is actually considerably higher than at 177 psia and about 480 fps. As noted later, the dwell tests were biased toward a higher velocity to be conservative since actual stage conditions are not precisely known.

A sweep test was also conducted on the 0093 hose, but because of the much less severe operational conditions (see Table I) no significant acoustic resonance was encountered, hence the dynamic strain levels were low. The system pressure was nominally 300 psia for this sweep, and the velocity was varied up to about 300 fps; this corresponds to the worst condition for the 0093 hoses shown in Table I (see Stations 7 and 8). The highest strain level observed during these tests was about 75 s (peak to peak).

Dwell Tests

Dwell tests were conducted on the Anaconda 0094 and 0093 hoses. The objective of these tests was to verify that the hoses could withstand two life cycles at rated flow and pressure without a failure. The time for each cycle was 195 minutes.

The first dwell test was conducted with the 0094 hose. A total dwell time of 195 minutes was accumulated in segments of about 20 to 30 minutes; the limiting factor here was a gradual heatup of the loop blower lube system. Between each dwell segment the system was run at a very low velocity to allow the blower to cool. Data monitored periodically throughout the test included pressure and temperature immediately downstream of the hose, temperature and pressure at the flow measurement orifice, convolute dynamic strain, and on occasion, acceleration at the end of the hose. Flow velocity was closely maintained between 480 and 500 fps throughout the test. Pressure varied from about 160 to 170 psia, and these conditions produced a dynamic strain level slightly higher than that observed at the rated condition of 470 fps at 187 psia. We are confident that the dwell was conducted at conditions which were as severe as those which might be encountered on the stage if the data in Table I is representative. Throughout the dwell test, the hose was enclosed in a plastic bag so that a leak could be detected shortly after it was initiated.

The peak strain level observed on this first dwell test was in the 1000 to 1200 s range, and was consistent with time as the test progressed. We were unable to monitor strain for the entire test because of failure of both gages, however, previous test results had definitely shown that the results were repeatable over a long time for a given velocity and pressure. Following this first dwell test, the hose was pressure tested to verify that no leaks had developed.

Two dwell cycles were conducted on the 0093 hose following the initial 0094 hose dwell to allow time for repair of the strain gages on the later hose. Each cycle was continuous for 195 minutes with no periodic cooling required. The dynamic strain level stayed relatively constant at from 50 to 75 s. No failure occurred.

The final dwell of the 0094 resulted in no failure of that hose and, as in the first dwell test, the strain gages failed before the test was concluded.

One significant observation of the 0094 tests was the continual generation of a "red powder". This powder appeared to be caused by some fretting action between the vibrating convolutes and the braid covering. The generation of this powder was more pronounced near the downstream end of the hose than near the upstream end. Recall that the dynamic strain was greater at the downstream end. We feel certain that when the braid is removed from this hose, score marks will be evident where the braid contacts the convolutes. These contact points are likely where this "red powder" is generated.

Conclusions

Both hoses withstood two dwell cycles of 195 minutes each at the respective rated flow conditions. The strain levels observed with the 0093 hose were too low to ever induce a failure. The dynamic strain for the 0094 was, however, of a significant level and could, we believe, eventually cause a failure at the rated conditions. A contributing factor could be the possible fretting action between the vibrating convolutes and the braid. Should velocities higher than 480 to 500 fps occur, a failure could well be realized in one 195 minute cycle.

We concluded that the 0094 hose (Anaconda) was "borderline adequate" for the job so long as the rated conditions (Table I) are not exceeded. It was recommended that the hose be replaced, however, prior to launch, or following the nitrogen operational cycle.

LOX TANK PRE-PRESSURIZATION SYSTEM

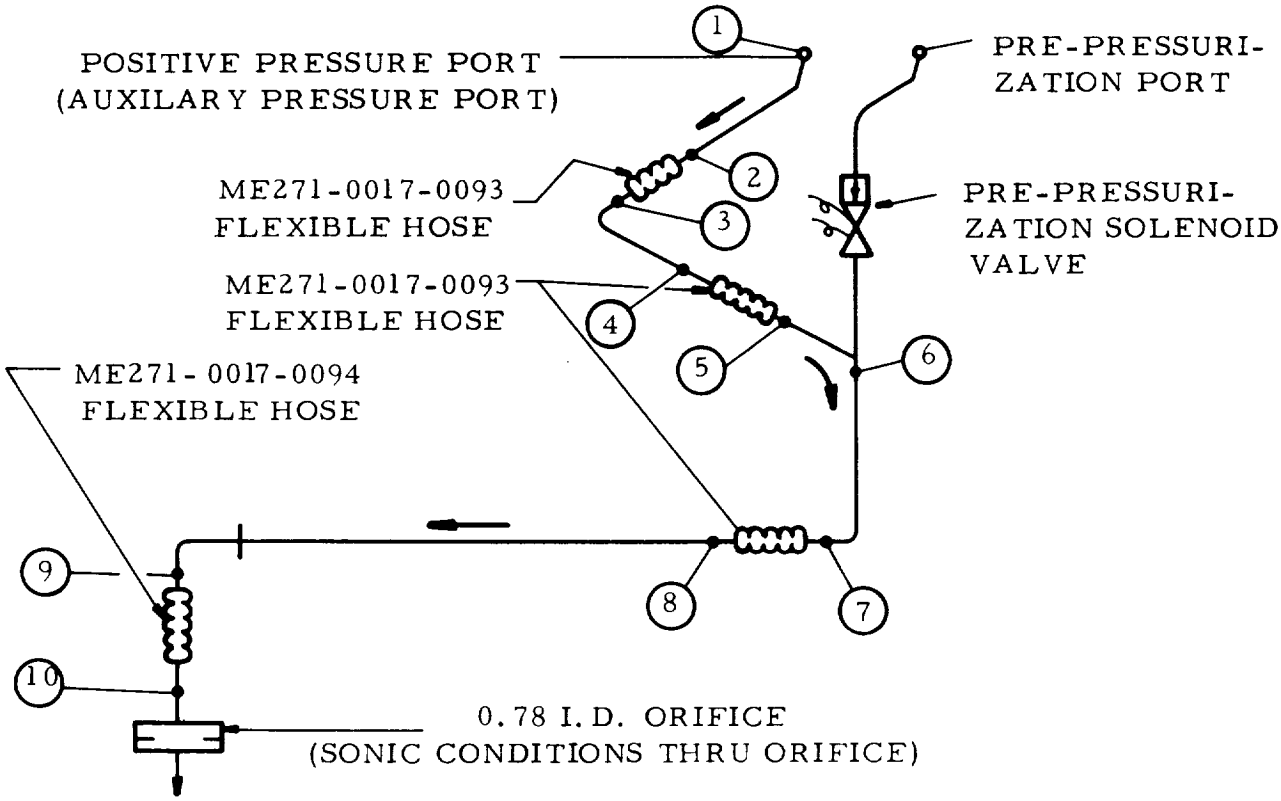

Station	GN_2 Gas Temperature = 75°F		Static Pressure psia
	M Mach No.	Velocity ft/sec	
1	.203	234	375
2	.204	235	373
3	.208	239	366
4	.210	243	362
5	.215	248	354
6	.222	255	343
7	.248	285	307
8	.255	293	298
9	.344	396	258
10	.407	470	187

M = Mach number dimensionless
P = GN_2 Static pressure, psia
V = GN_2 velocity, ft/sec
N/A = Not Applicable
a = Acoustic Velocity, ft/sec

VELOCITIES AND PRESSURES ARE BASED ON LINE I.D. = 0.93 INCHES

TABLE I. NITROGEN GAS FLOW DATA FOR 0093 and 0094 HOSES
(from North American Briefing Report dated 27 May 1970)

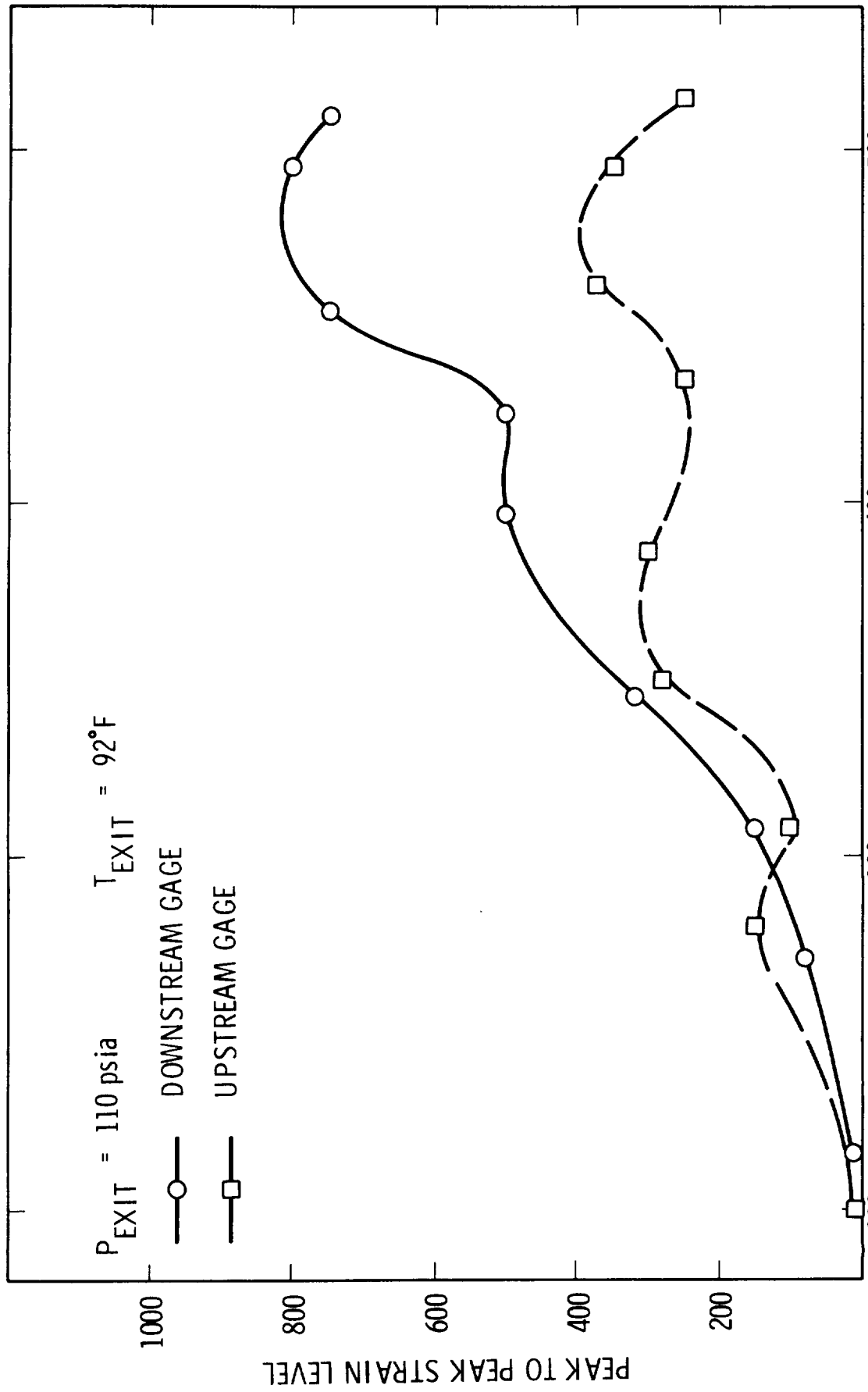

Figure 1. Solar Hose - Comparison of Upstream and Downstream Gages

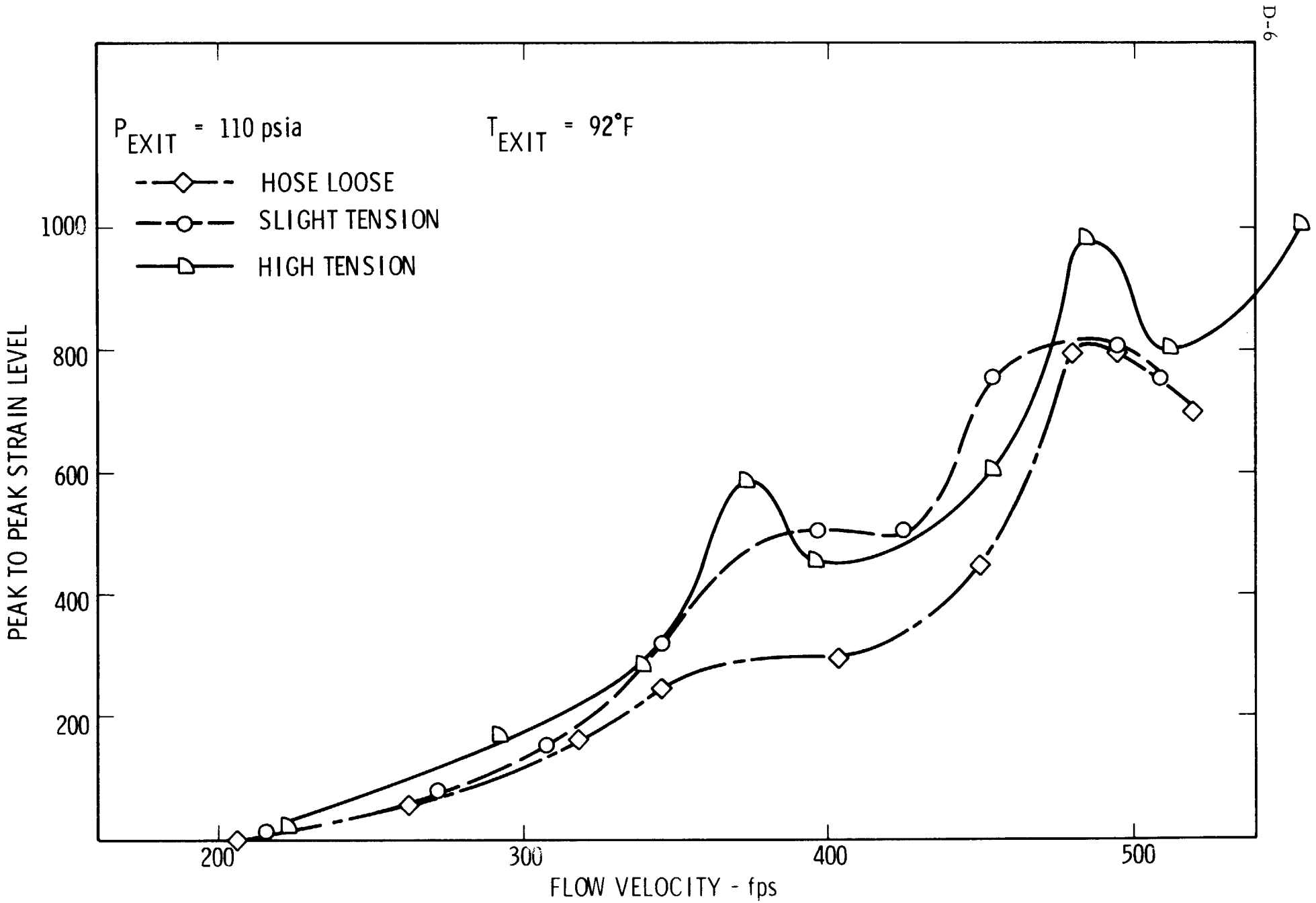

Figure 2. Solar Hose - Effect of Tension

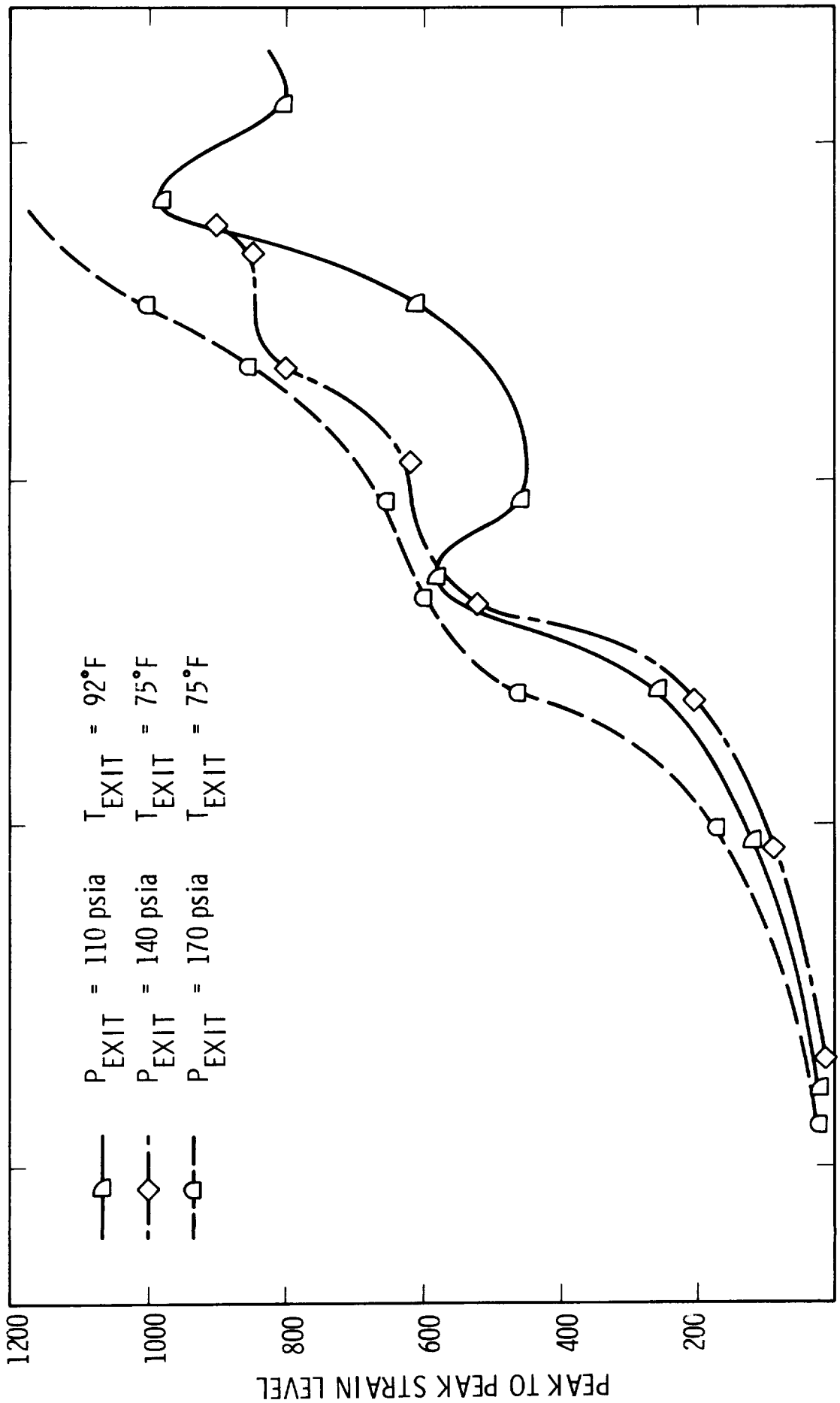

Figure 3. Solar Hose - Effect of Pressure

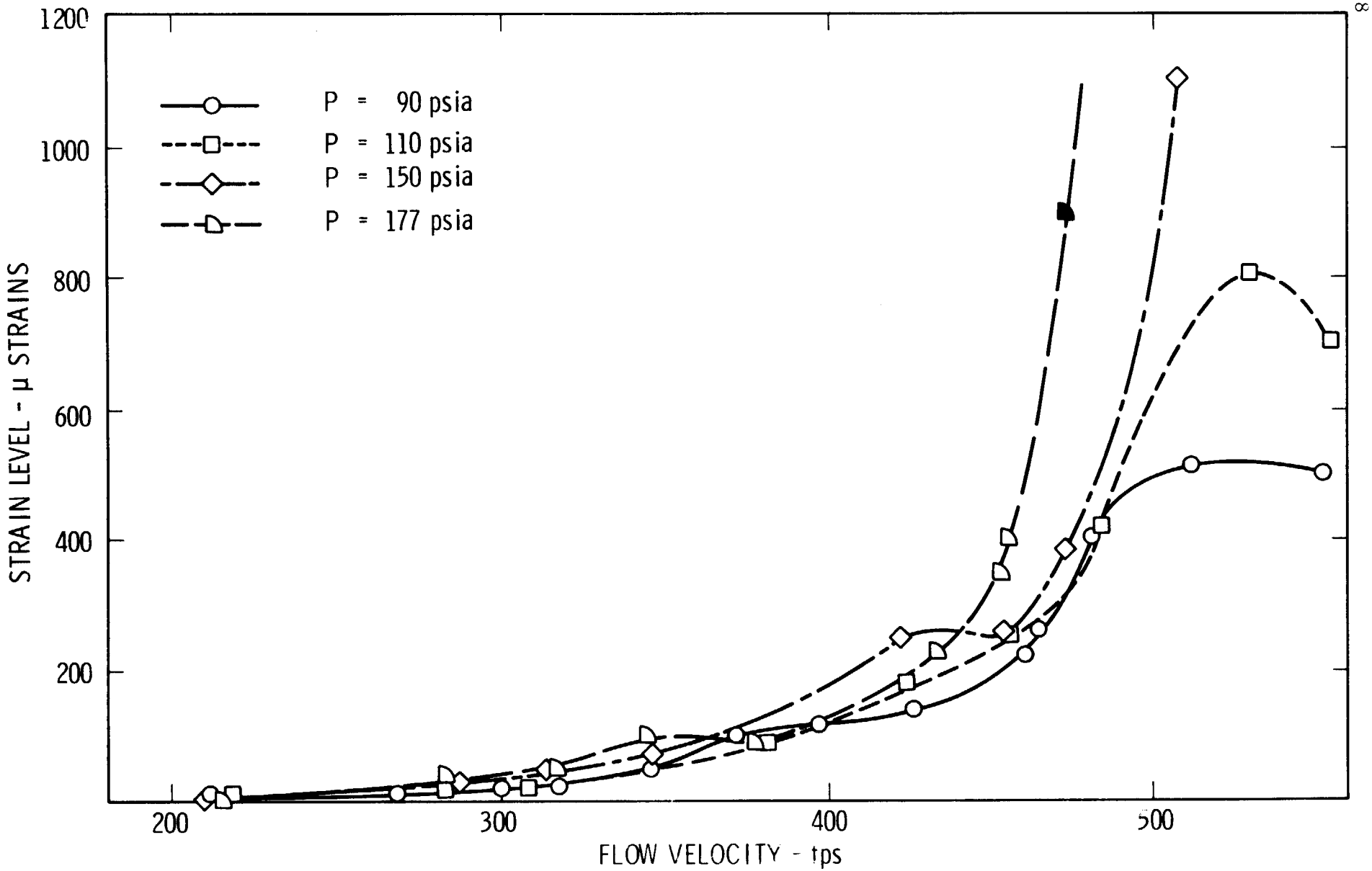

Figure 4. Anaconda Flex Hose "Loose" - Downstream Strain Gage - Effect of Pressure

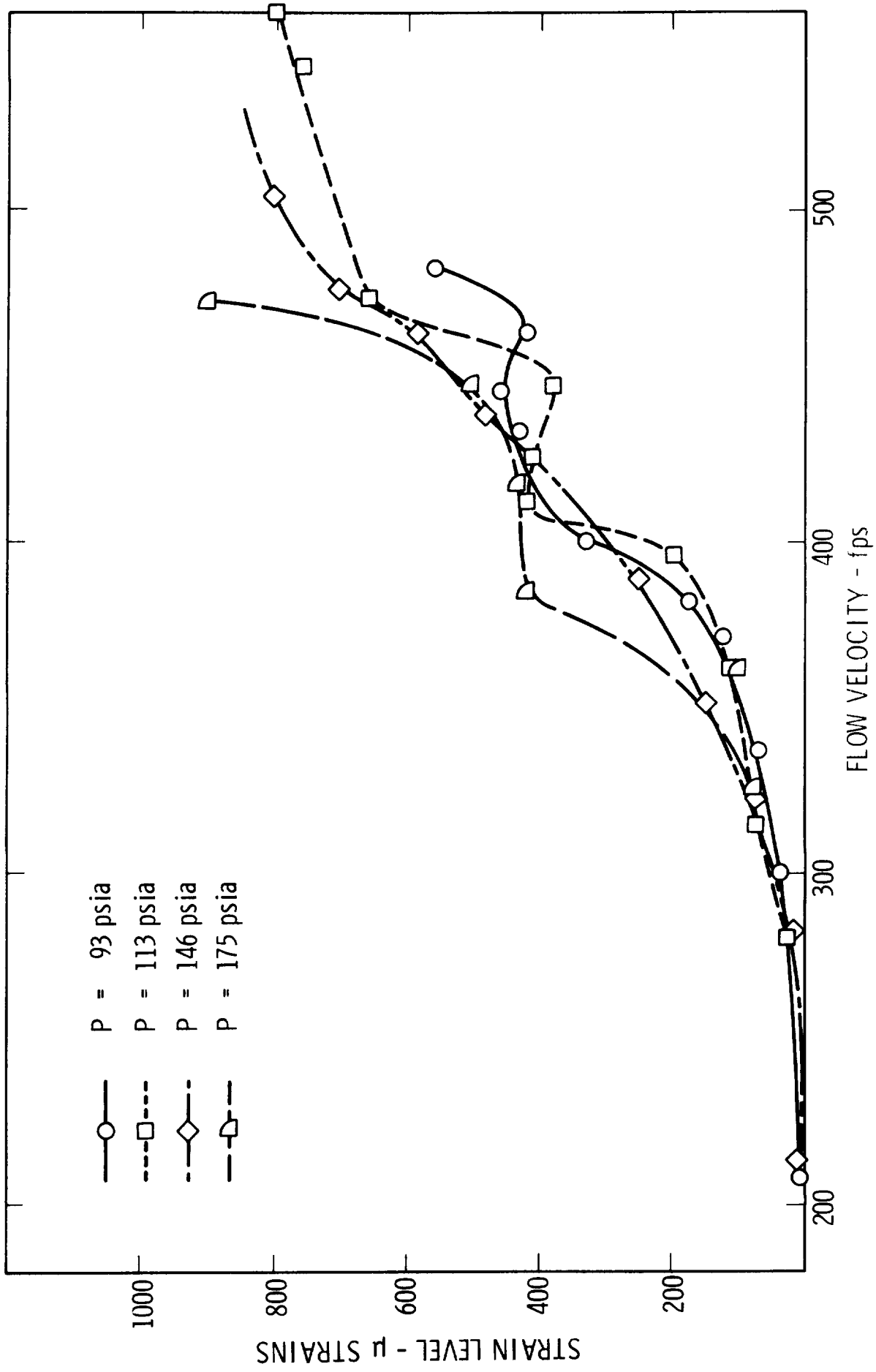

Figure 5. Anaconda Flex Hose "Tight" - Downstream Strain Gage

APPENDIX E

DATA COMPILED FOR PRESSURE LOSSES IN BELLOWS AND BENDS

E. 1 DATA COMPILED ON PRESSURE LOSSES IN BELLOWS

A considerable amount of data has been compiled on pressure losses in both straight flexible hose sections and curved flexible sections. This information was obtained from References [22-29]. In gathering this information we were aided considerably by the list of references given in a bibliography compiled by Belcher [30], and the reported results of studies recently completed at Mississippi State University [23] and Louisiana State University [26] on pressure losses in flexible hose. All significant data and other information compiled for straight section flexible hose is given in Section E. 2 while that data compiled for curved section flexible hose is presented in Section E. 3. Also given is the convolute dimensional information for those cases where it was available. In some instances, it will be noted, we have taken the liberty of simply reproducing the original data for the purpose of this report. Note also that the data includes both water and air as test fluids. From an examination of this data the following preliminary observations have been made:

(1) Test results for which the convolution geometry remained similar while the hose diameter changed show the Reynolds number* $V\lambda/\nu$, which is based on convolute spacing, to be a good parameter for correlating the data from the standpoint of the location of the critical Reynolds number, that is the point where the friction factor begins to rise.

---

* It will be noted that, since there is geometric similarity, a Reynolds number based on any convolute characteristic dimension will do, i.e., $\frac{V\sigma}{\nu}$ or $\frac{V\epsilon}{\nu}$ also.

This is demonstrated in Figure E-1 which is a replot of Figure E-5 but with the abscissa being $V\lambda/\nu$ rather than VD/ν. The data from References [25, 26] (Figures E-7 thru E-27) also display this trend. For each of these sets of data there is geometric similarity in the convolute design. When, however, there is not geometric similarity as for the data of Reference [1] Figures E-1 thru E-4) then convolute geometry must enter the picture more strongly. Preliminary results show the parameter

$$R_e \quad \frac{\sigma}{d} \quad \frac{\epsilon}{\lambda}$$

may be useful.

(2) From Pepersack's data which is really the only data available comparing convolute geometry, the following trend is noted; for both the air and water data, the Dunbar-Kapple hose has <u>lower</u> f values than the others at high Reynolds numbers (above about $R_e = 10^5$) but tends to have <u>higher</u> f values at low Reynolds numbers. Since high Reynolds number flows are of major importance, the Dunbar-Kapple design appears better than the other two. The sketch below shows the convolute geometry for the three types of hose; the highest pressure loss seems to occur for the tear-drop design. Note that one other characteristic of the Dunbar-Kapple hose is that the Reynolds number at which the friction factor begins to rise is typically higher than for the other hoses.

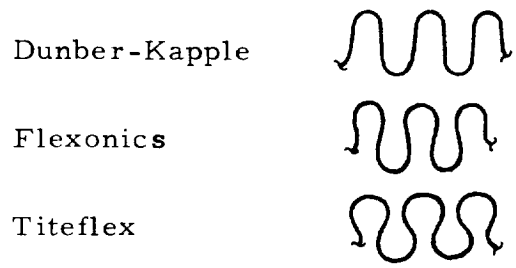

Comparison of Convolute Geometry for the Three Hose Types Tested by Pepersack [22].

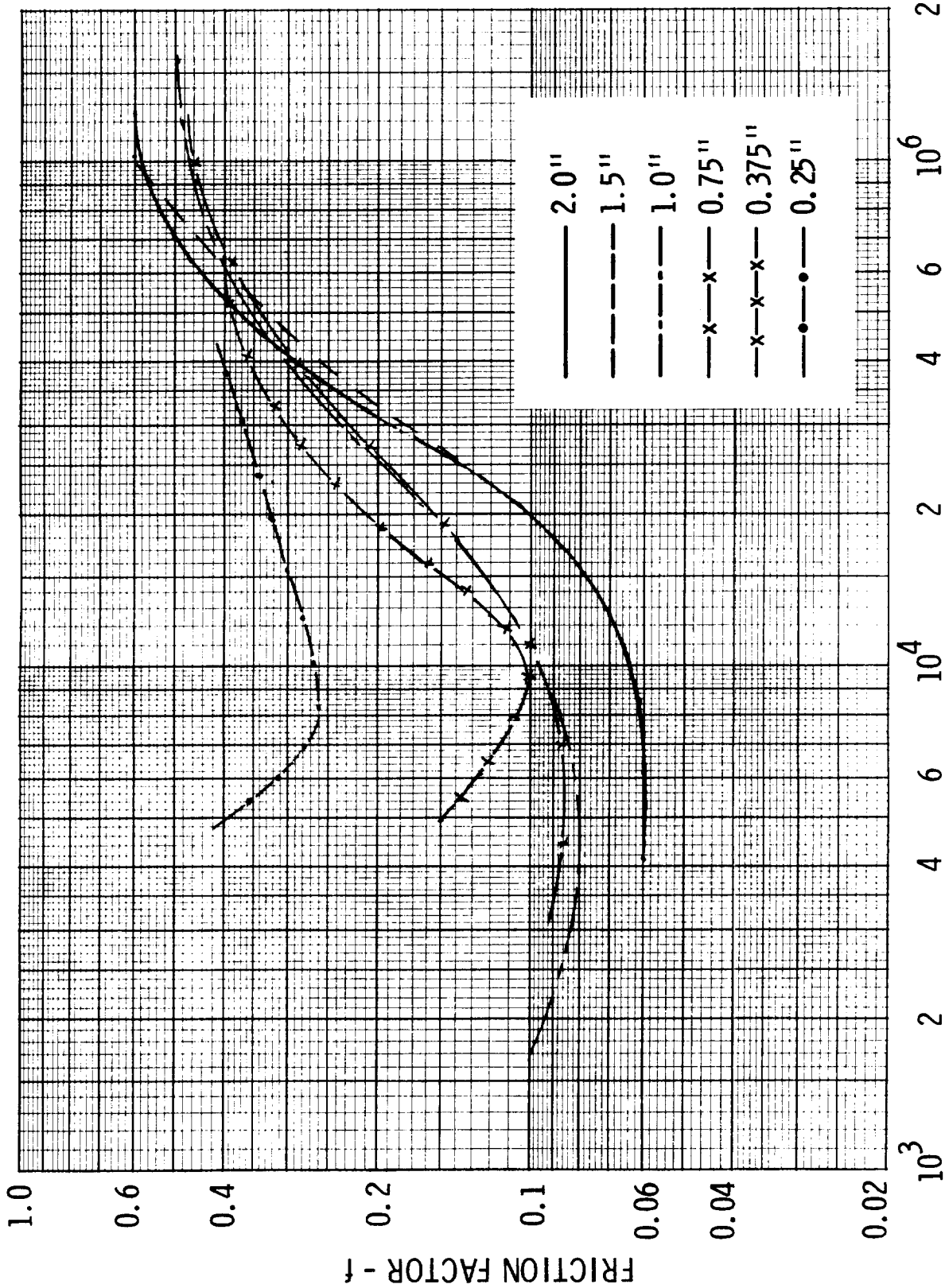

Figure E.1. Plot of Data from Figure A-5 as a Function of $V\lambda/\nu$

(3) Based on the discussions (1) and (2) above, and on further examination of the data given in Section E. 2, it has been concluded that the universal prediction methods suggested in References [26, 28] (Figures E-28, E-29 and E-30) are not accurate for all types of hoses.

E.2 PRESSURE LOSS DATA FOR STRAIGHT SECTION FLEXIBLE HOSE

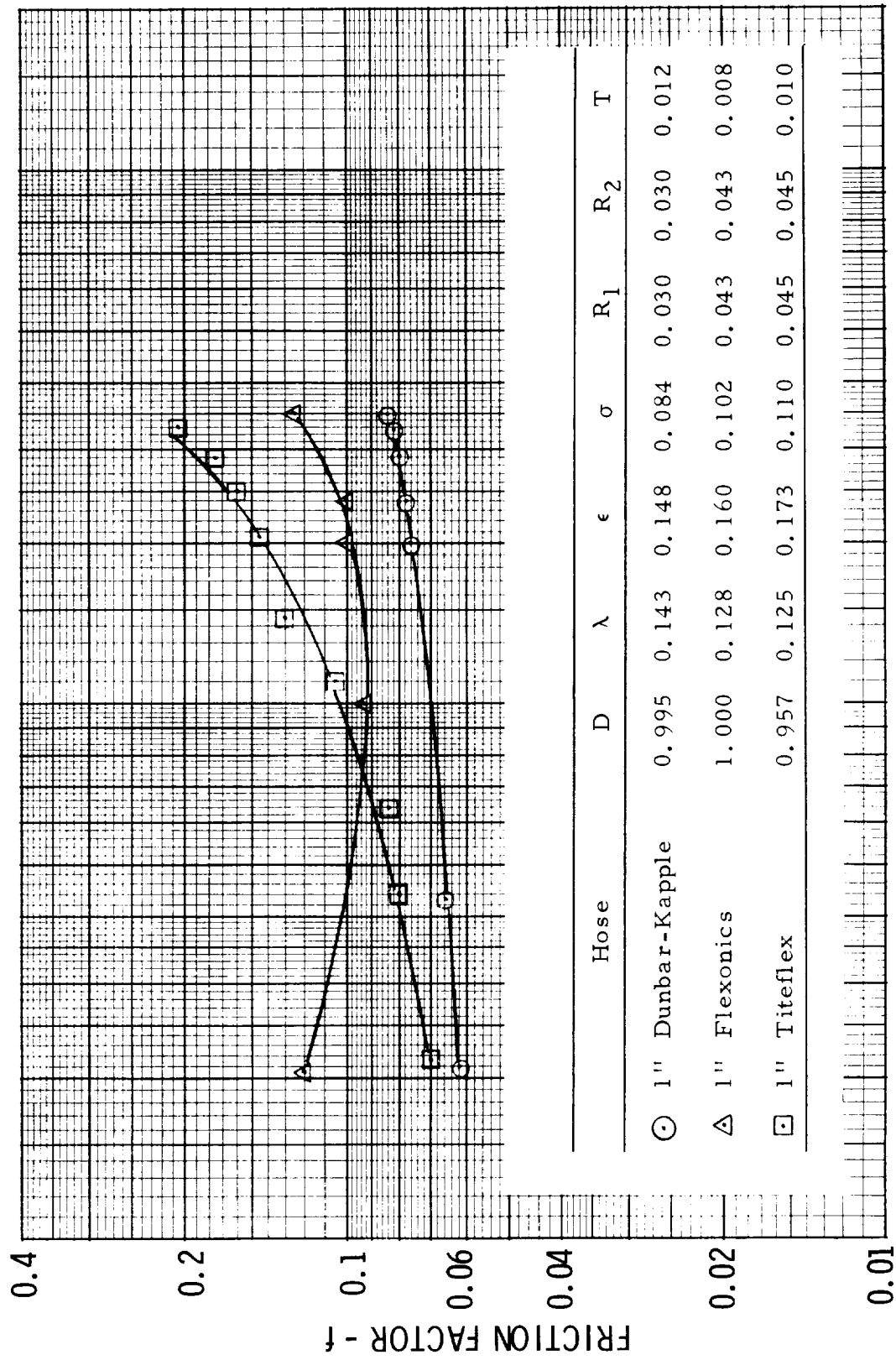

Figure E-2. Reference (22), Water

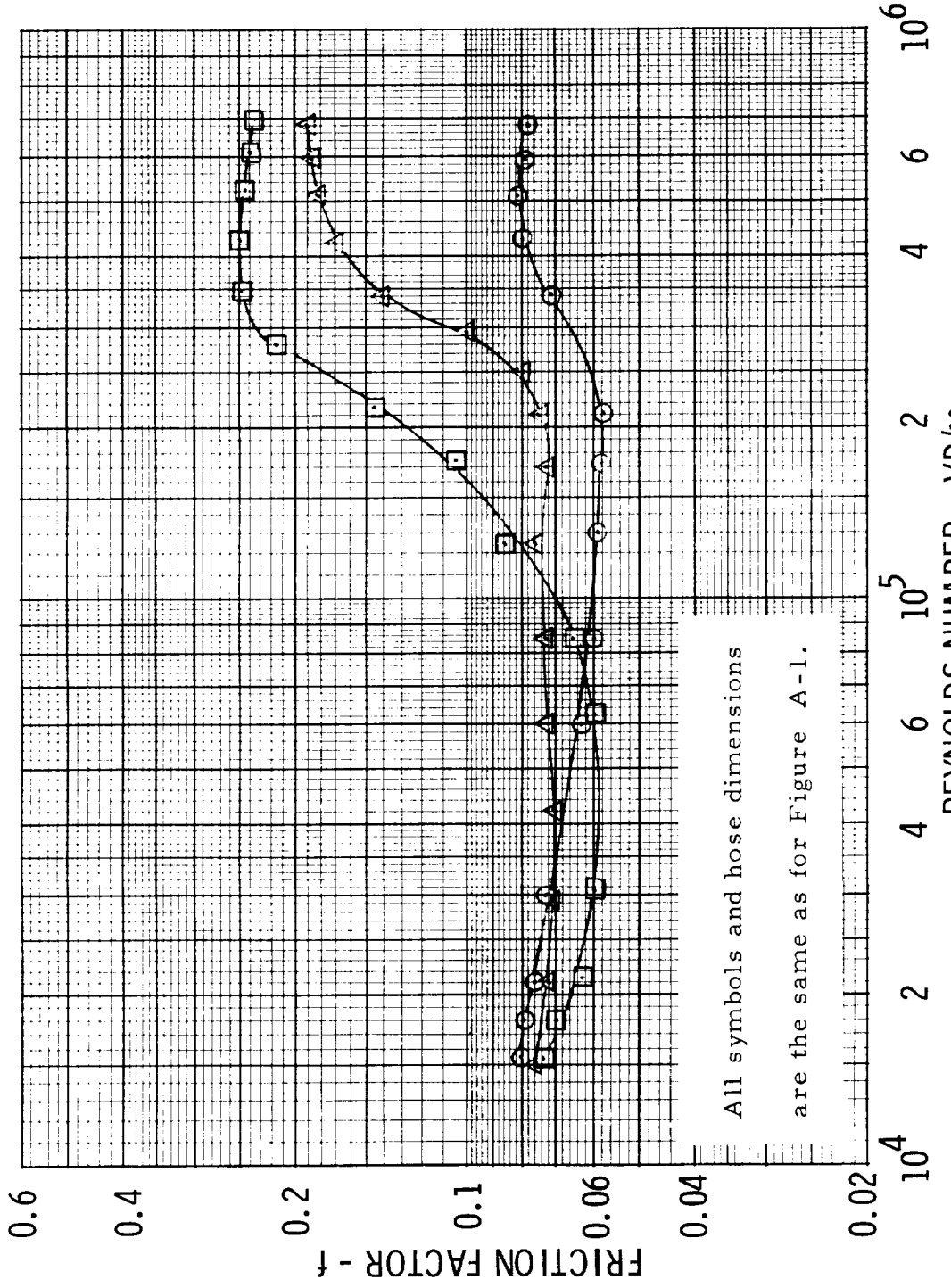

Figure E-3. Reference (22), Air

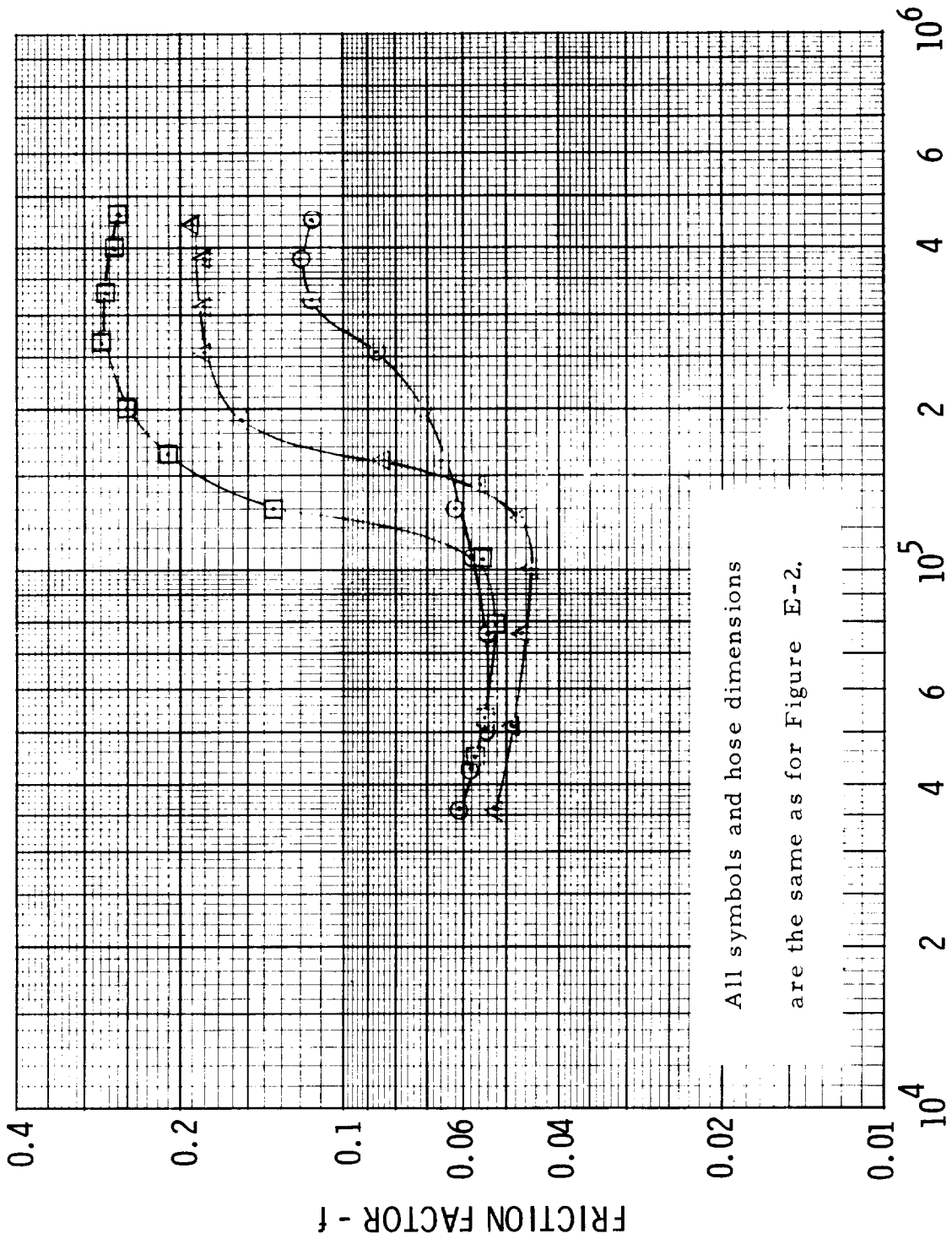

Figure E-4. Reference (22), Air

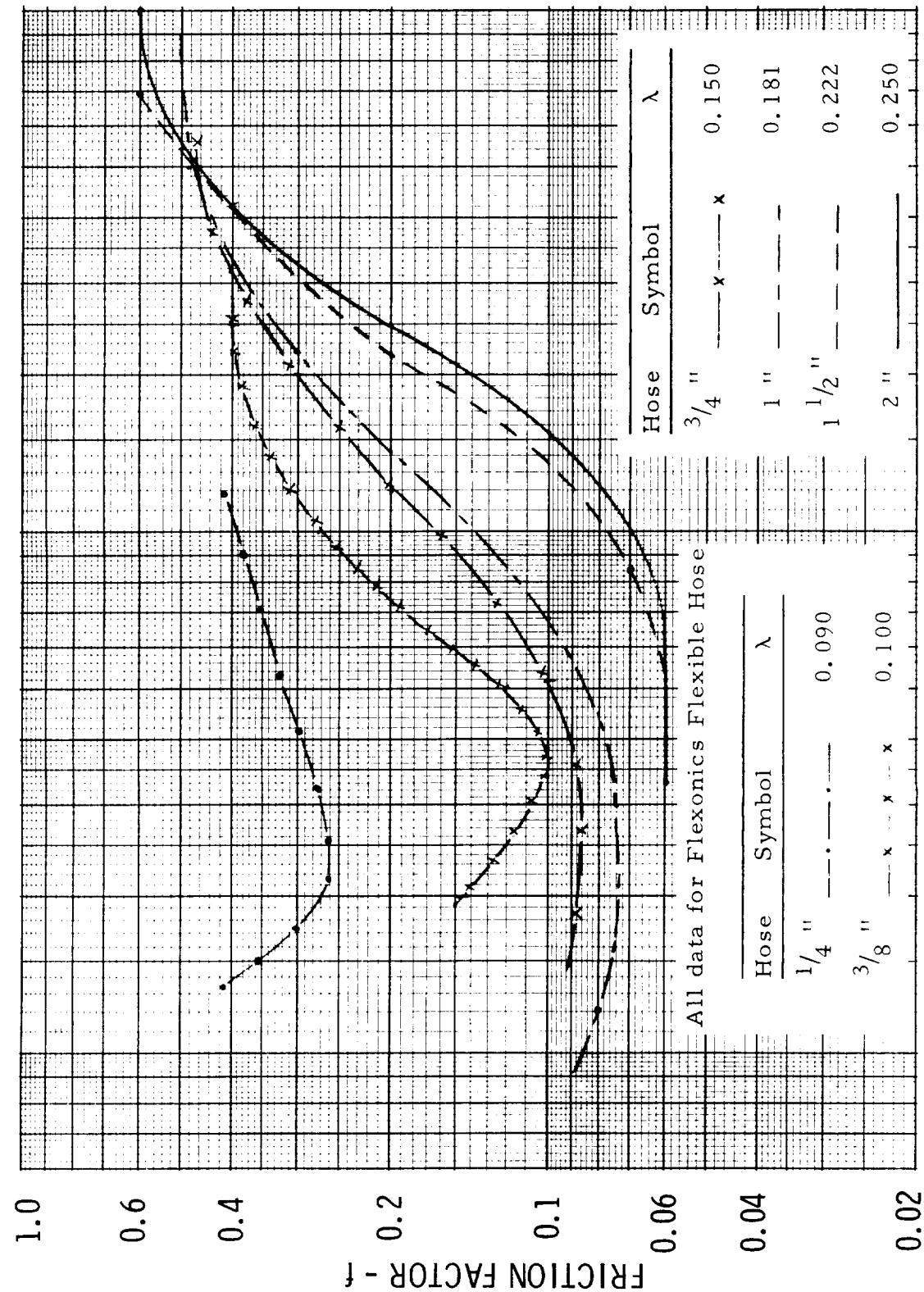

Figure E-5. Reference (23), Air

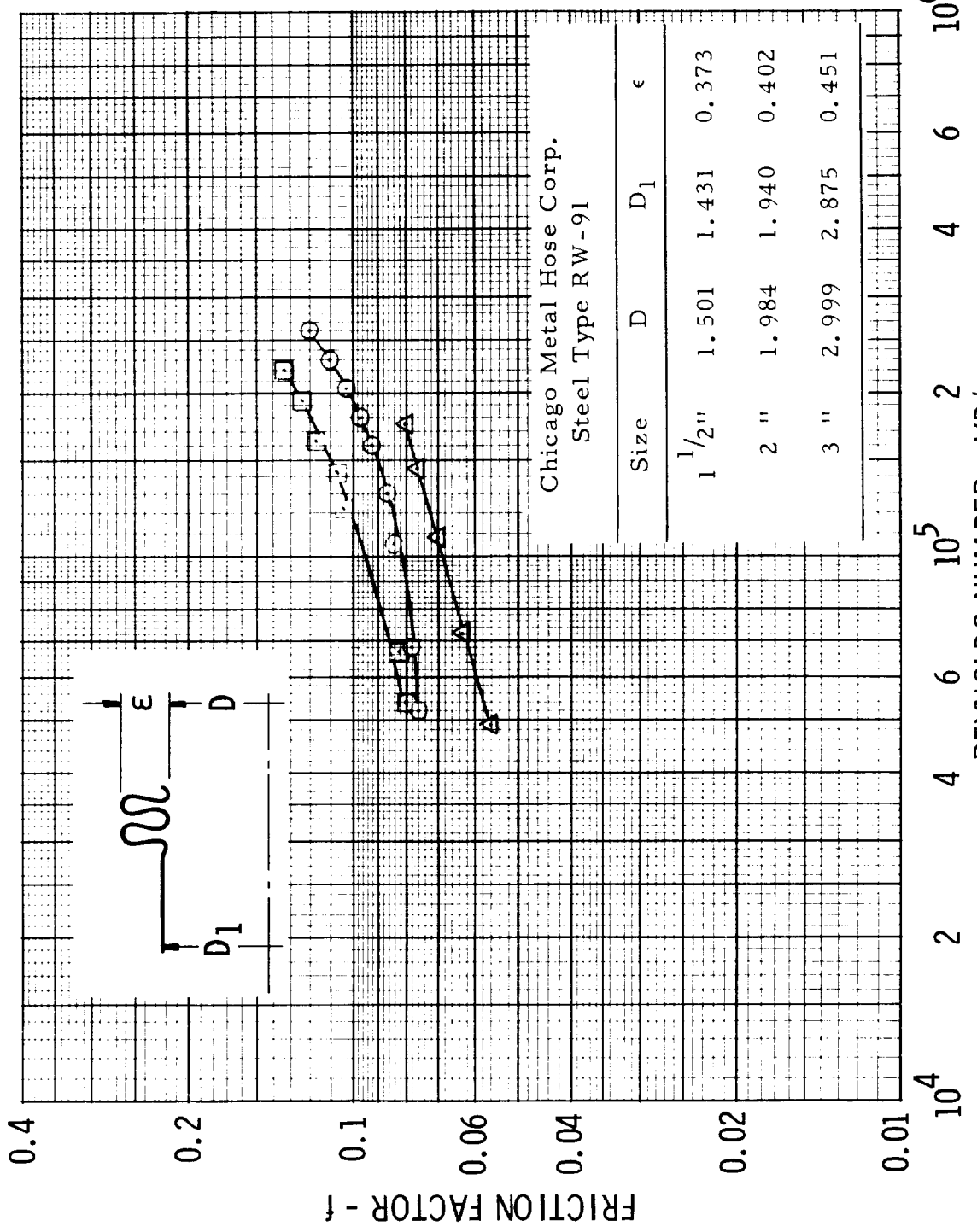

Figure E-6. Reference (24), Air

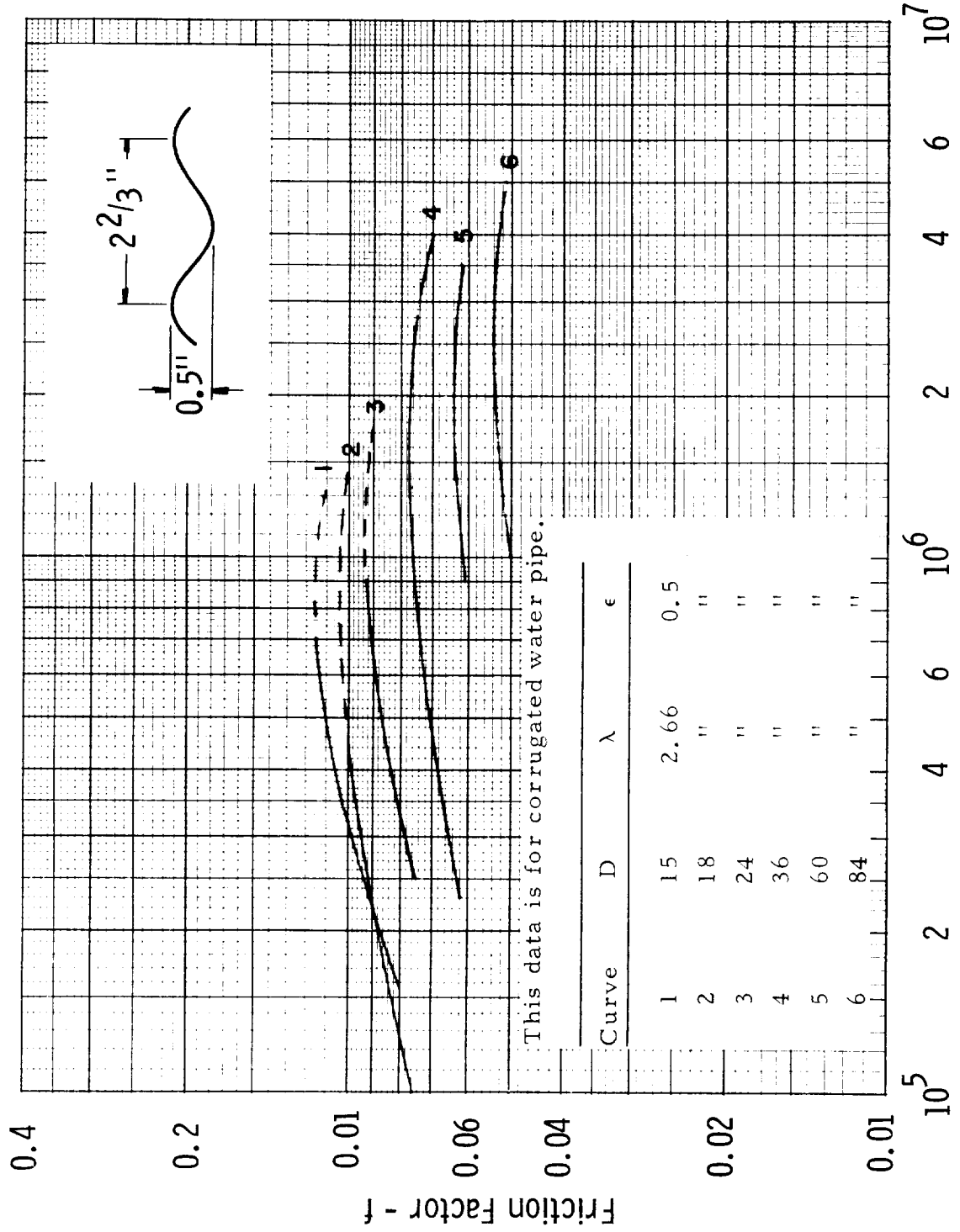

Figure E-7. Reference (25), Water

Figures E-8 thru E-29, Reference [26], Water and Air

Note: The friction factors given in these figures are Fanning friction factors and are therefore 1/4 as large as the Darcy-Weisbach friction factors given in the other figures. Thus

Fanning friction factor, $f' =$

(1/4) x Darcy-Weisbach friction factor, f.

Hose Dimensions

Hose		D	λ	ϵ	σ
		Annular Hose			
NASA	11	0.551	0.125	0.156	0.0781
"	21	0.771	0.156	0.1875	0.0937
"	31	0.0102	0.181	0.219	0.1094
"	41	1.266	0.1875	0.234	0.125
"	51	1.483	0.219	0.250	0.125
"	61	2.046	0.250	0.297	0.172
"	71	2.565	0.3125	0.344	0.1875
"	81	2.990	0.375	0.422	0.1875
"	32	1.012	0.203	0.219	0.109
"	42	1.255	0.219	0.219	0.109
		Helical Hose			
NASH	2	0.768	0.1875	0.1875	0.09375
"	3	1.061	0.250	0.250	0.1094
"	4	1.299	0.250	0.250	0.125
"	5	1.560	0.3125	0.3125	0.133
"	6	2.081	0.344	0.344	0.156
"	7	2.573	0.375	0.391	0.172

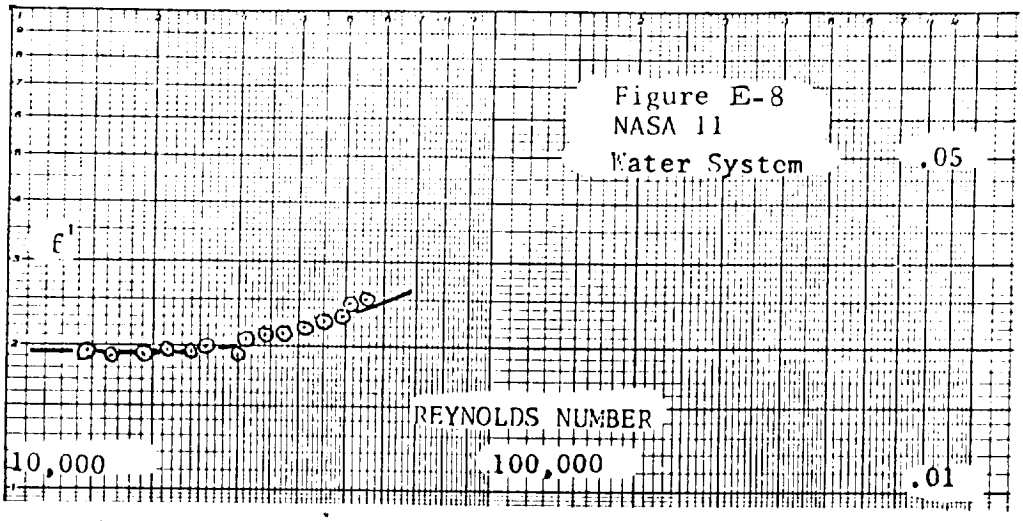
Figure E-8
NASA 11
Water System
.05
f'
REYNOLDS NUMBER
10,000
100,000
.01

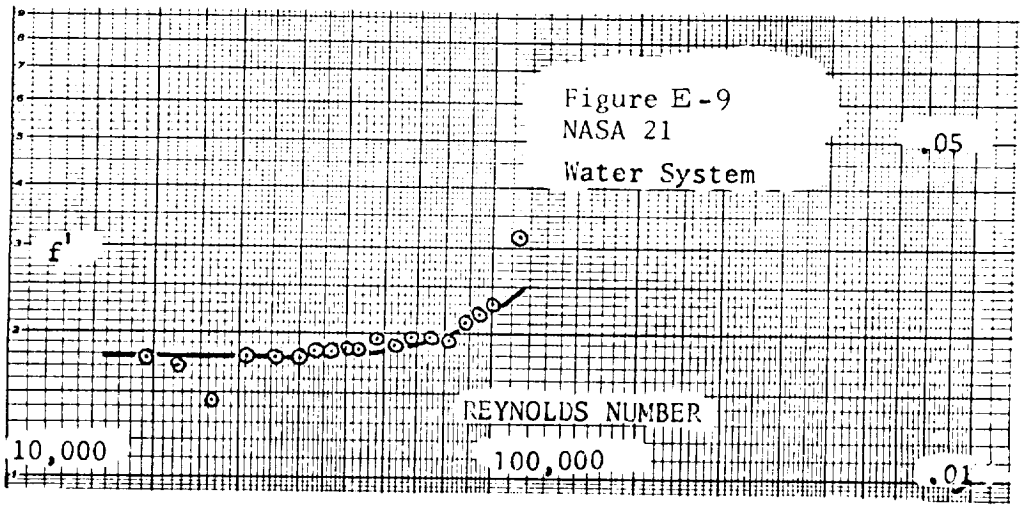
Figure E-9
NASA 21
Water System
.05
f'
REYNOLDS NUMBER
10,000
100,000
.01

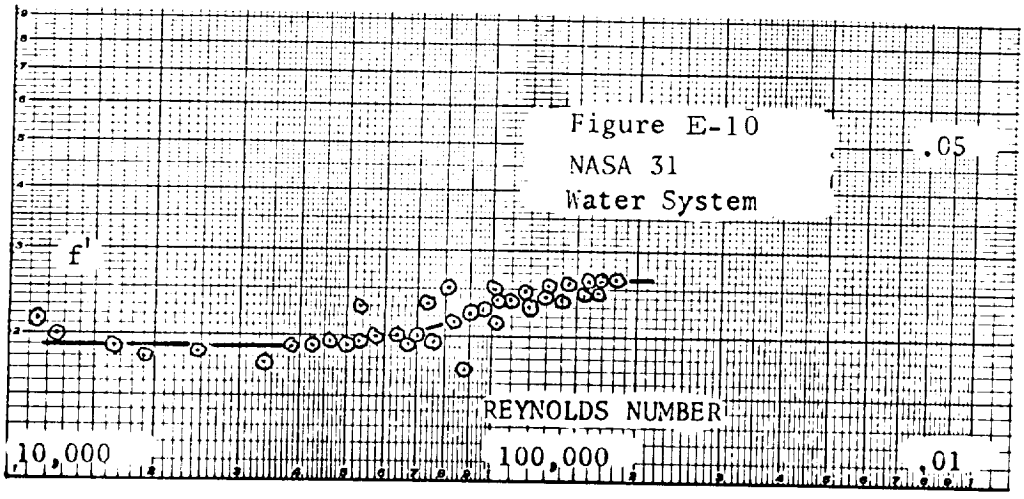
Figure E-10
NASA 31
Water System
.05
f'
REYNOLDS NUMBER
10,000
100,000
.01

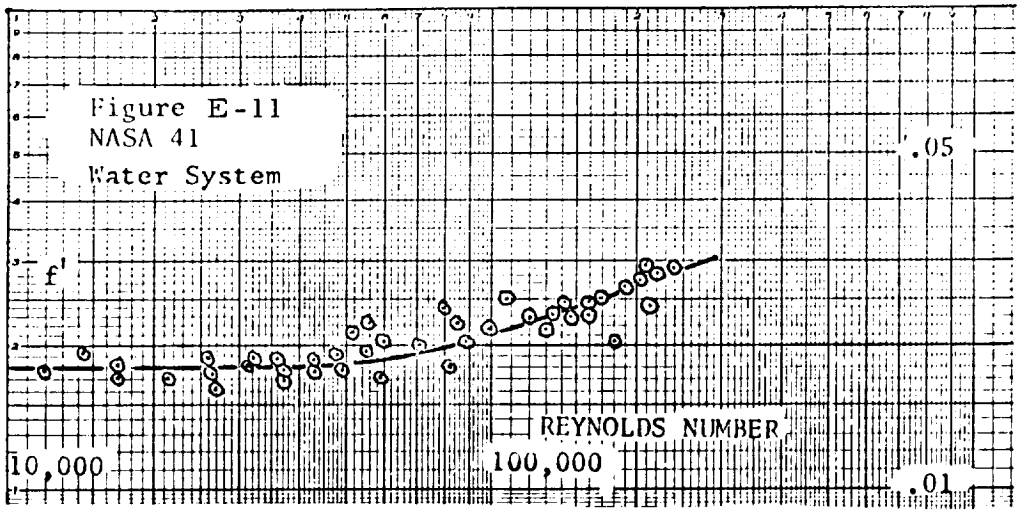
Figure E-11
NASA 41
Water System
f'
.05
REYNOLDS NUMBER
10,000
100,000
.01

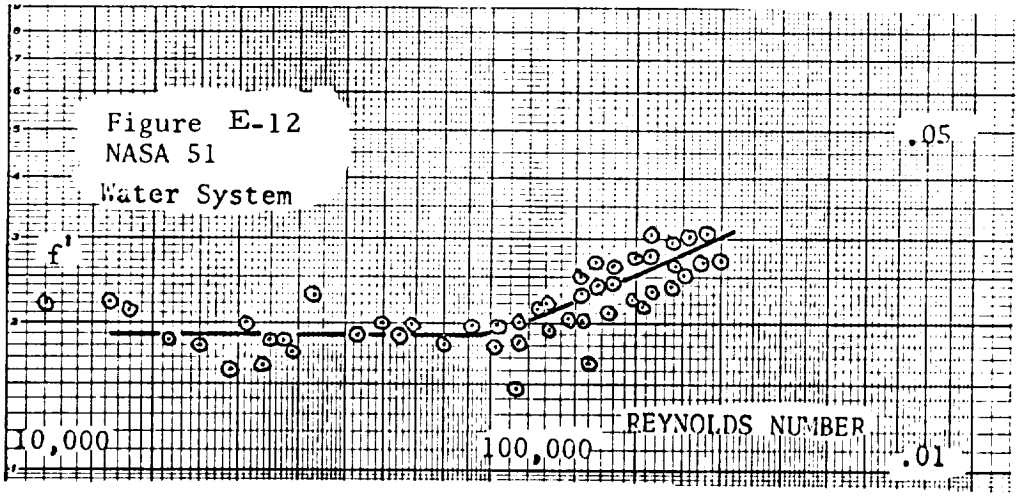
Figure E-12
NASA 51
Water System
f'
.05
REYNOLDS NUMBER
10,000
100,000
.01

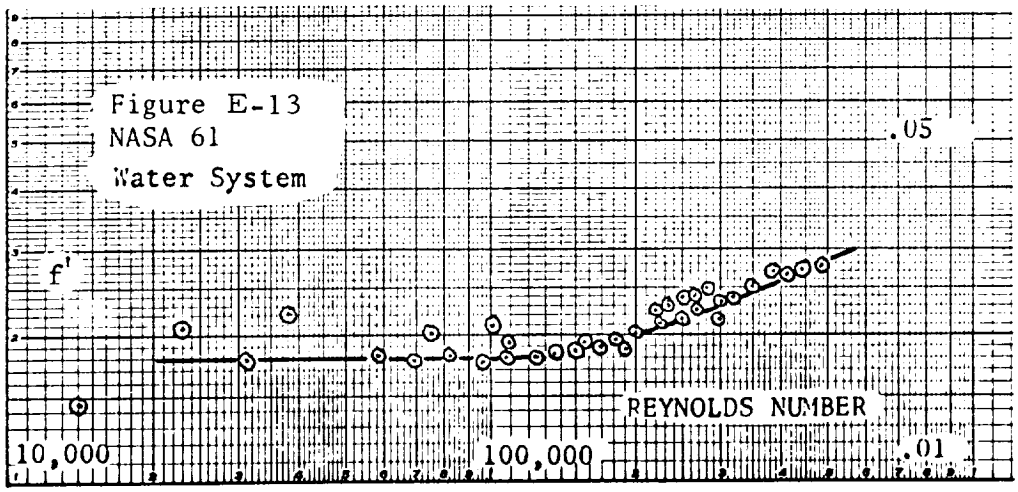
Figure E-13
NASA 61
Water System
f'
.05
REYNOLDS NUMBER
10,000
100,000
.01

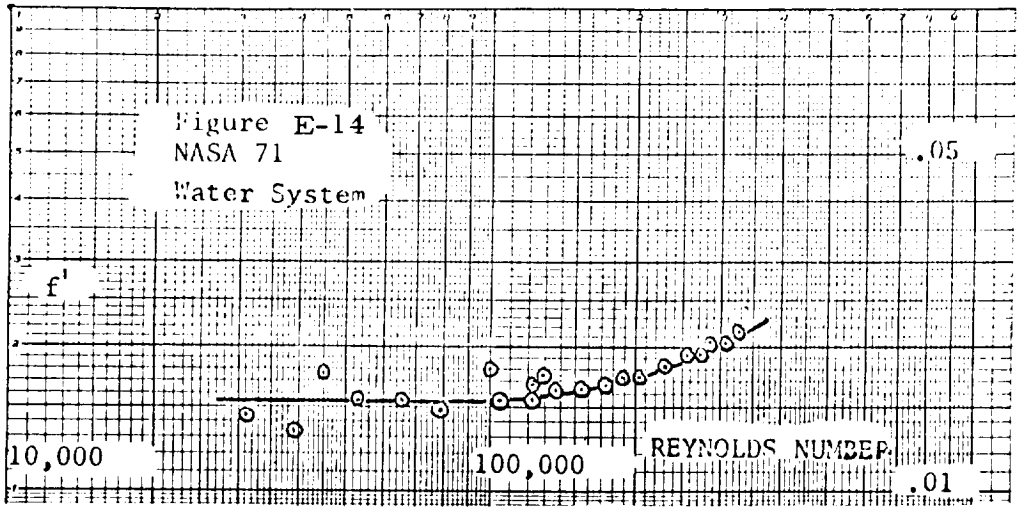
Figure E-14
NASA 71
Water System
.05
f'
10,000
100,000
REYNOLDS NUMBER
.01

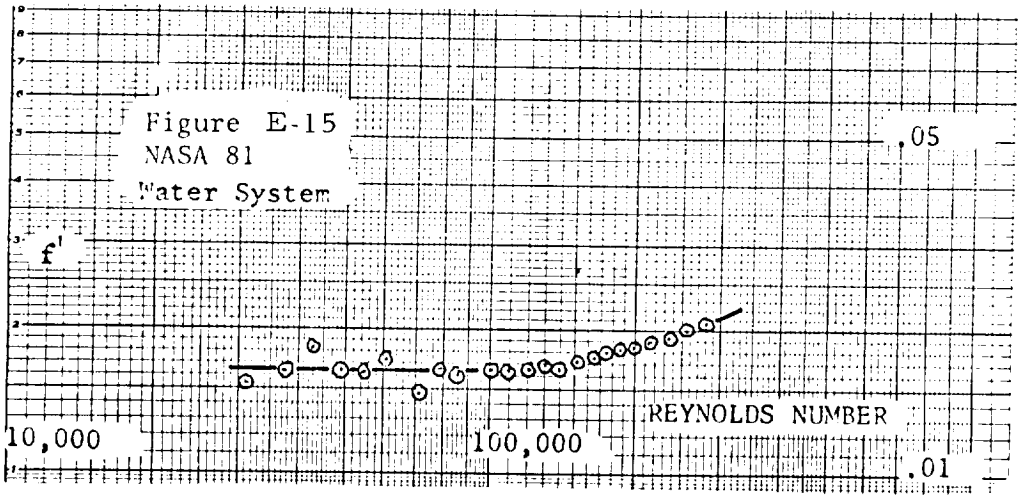
Figure E-15
NASA 81
Water System
.05
f'
10,000
100,000
REYNOLDS NUMBER
.01

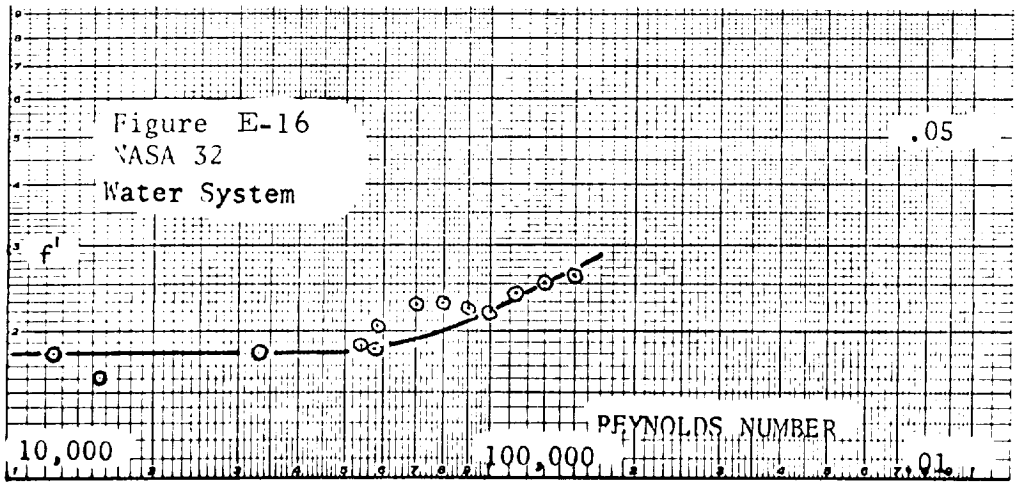
Figure E-16
NASA 32
Water System
.05
f'
10,000
100,000
REYNOLDS NUMBER
.01

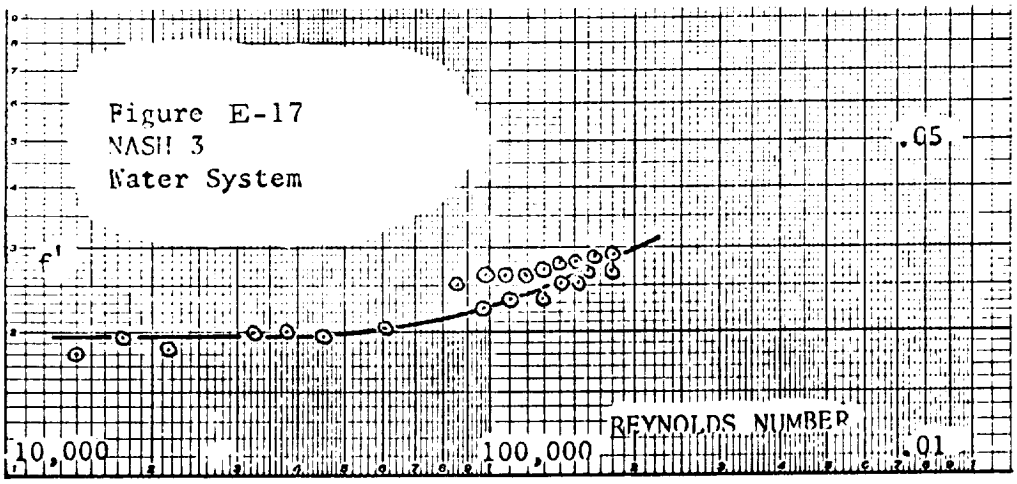
Figure E-17
NASH 3
Water System
f'
.05
.01
REYNOLDS NUMBER
10,000
100,000

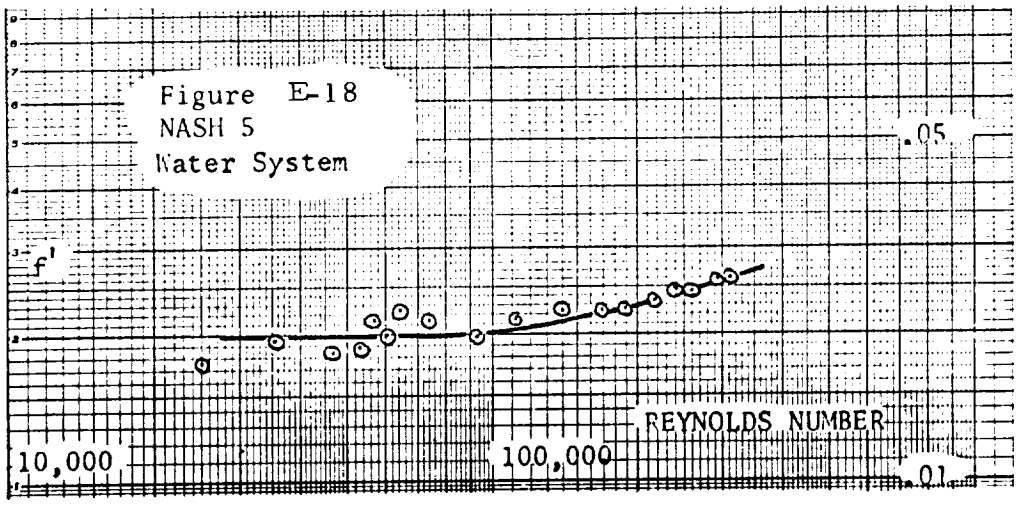
Figure E-18
NASH 5
Water System
f'
.05
.01
REYNOLDS NUMBER
10,000
100,000

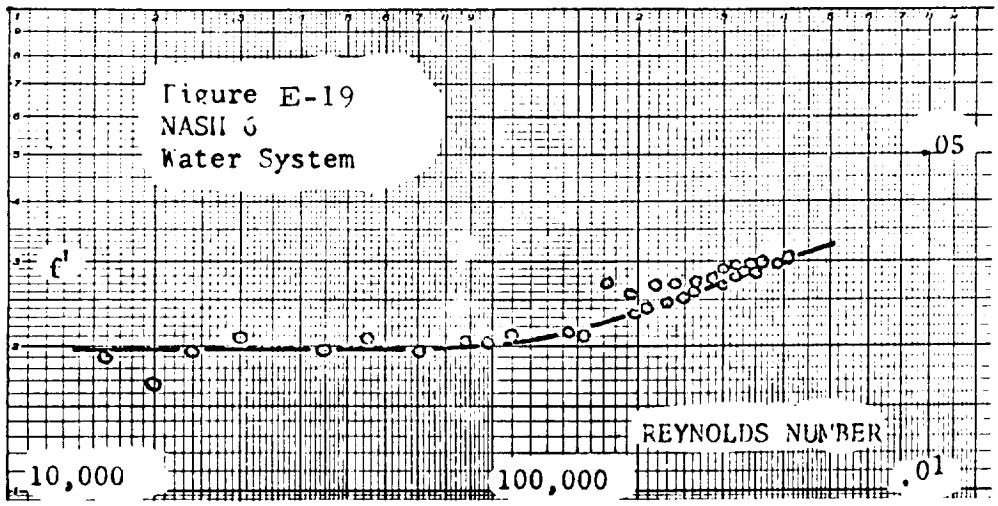
Figure E-19
NASH 6
Water System
.05
f'
REYNOLDS NUMBER
10,000
100,000
.01

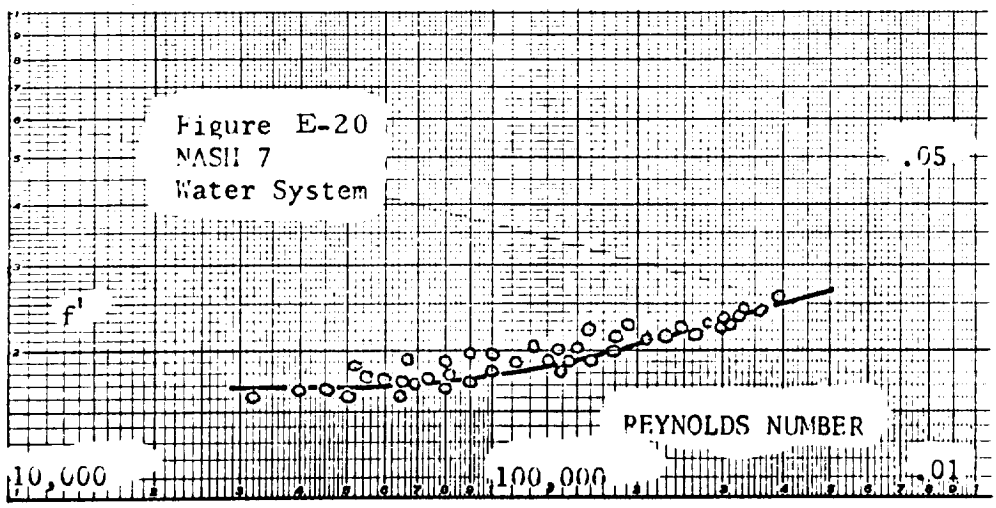
Figure E-20
NASH 7
Water System
.05
f'
REYNOLDS NUMBER
10,000
100,000
.01

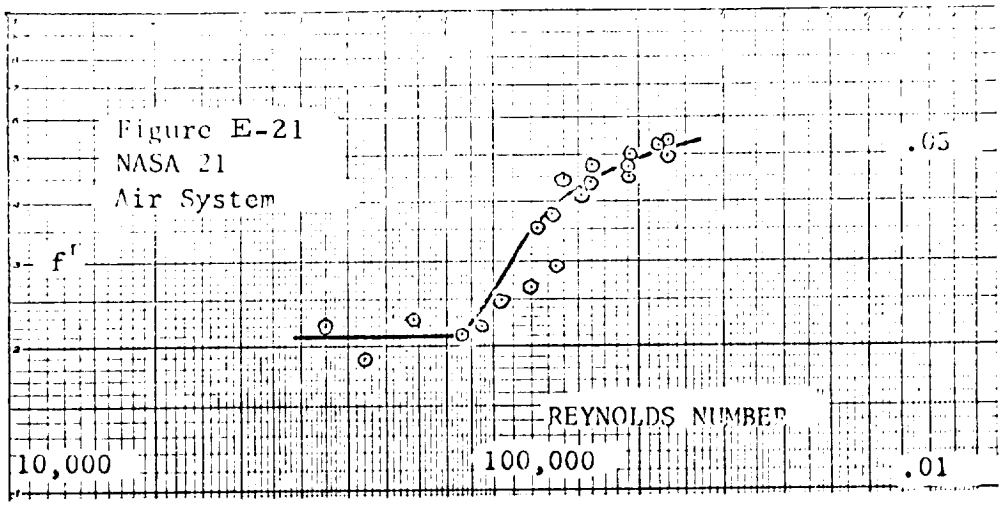
Figure E-21
NASA 21
Air System
f'
.05
REYNOLDS NUMBER
10,000
100,000
.01

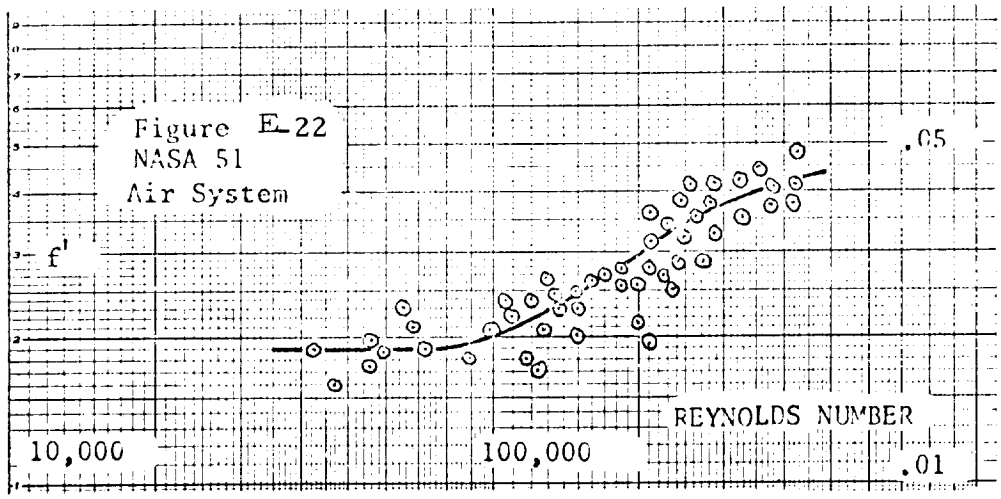
Figure E-22
NASA 51
Air System
f'
.05
REYNOLDS NUMBER
10,000
100,000
.01

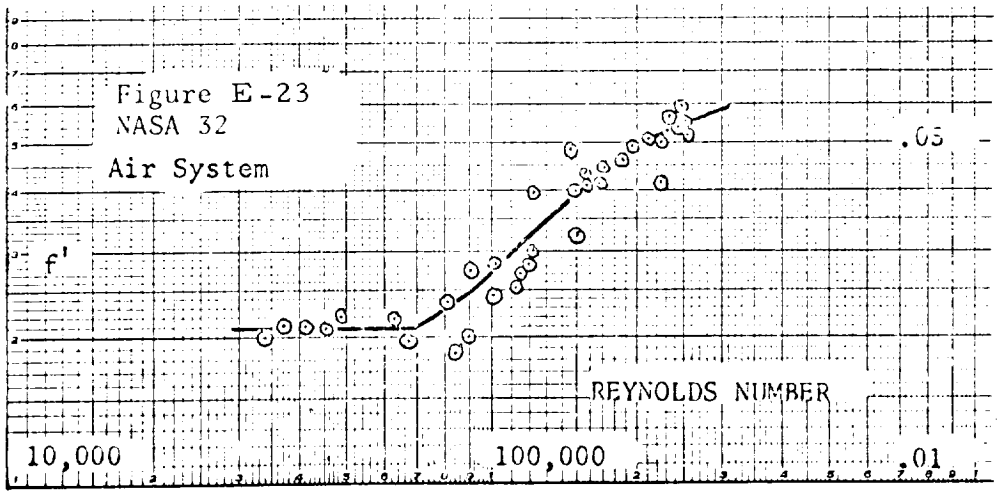
Figure E-23
NASA 32
Air System
f'
.05
REYNOLDS NUMBER
10,000
100,000
.01

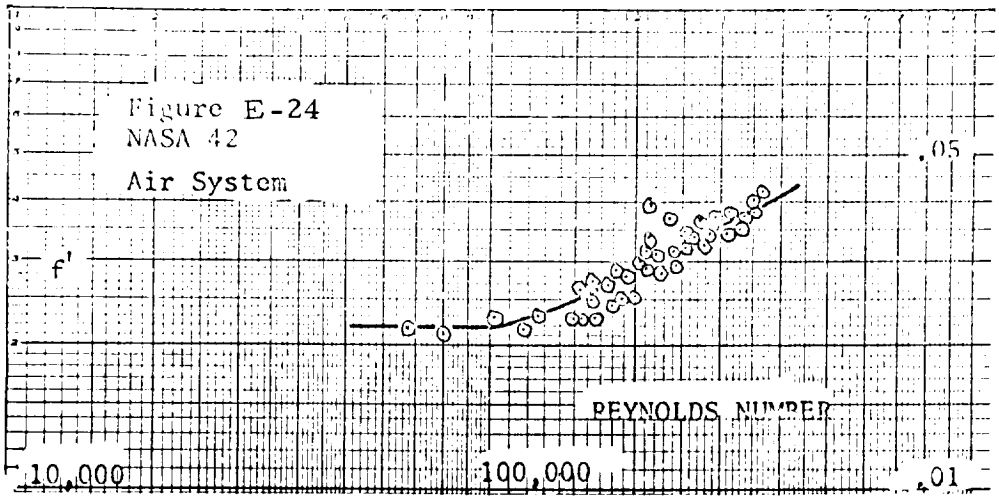
Figure E-24
NASA 42
Air System
f'
.05
REYNOLDS NUMBER
10,000
100,000
.01

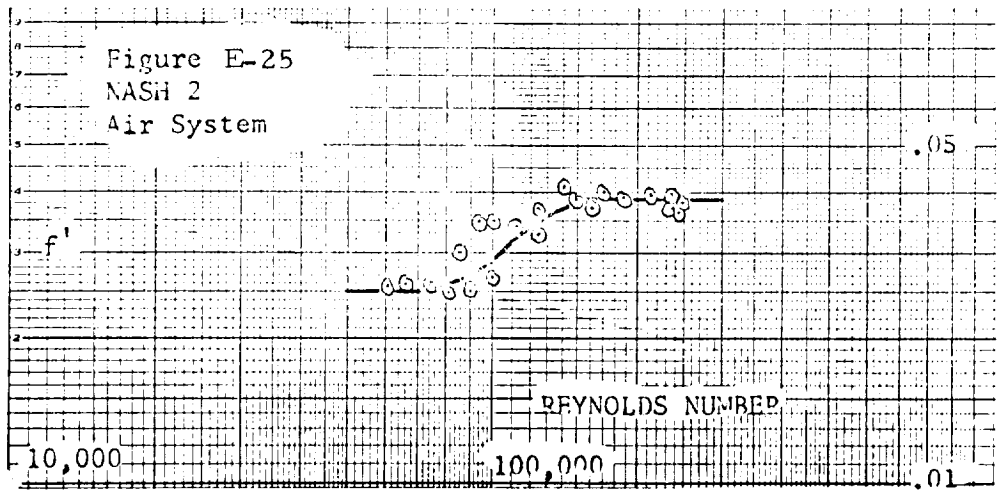
Figure E-25
NASH 2
Air System
f'
.05
REYNOLDS NUMBER
10,000
100,000
.01

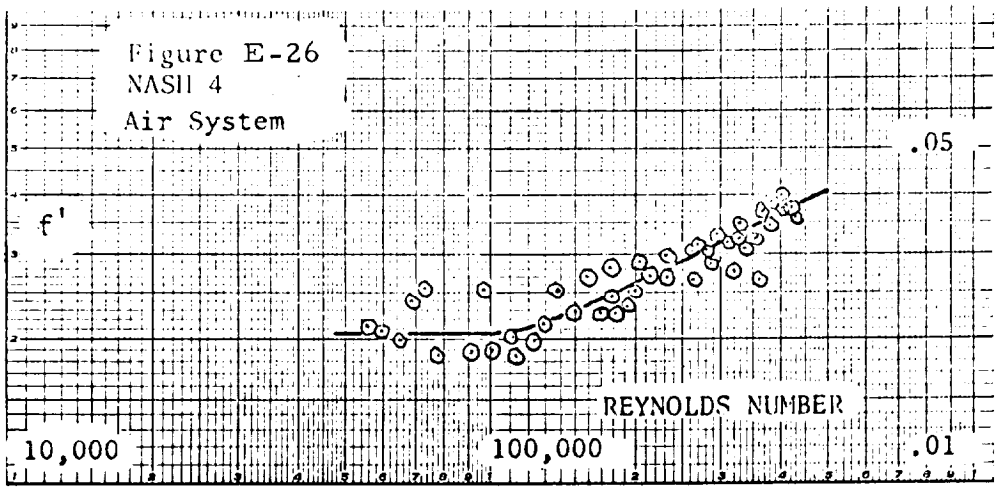
Figure E-26
NASH 4
Air System
.05
f'
REYNOLDS NUMBER
10,000
100,000
.01

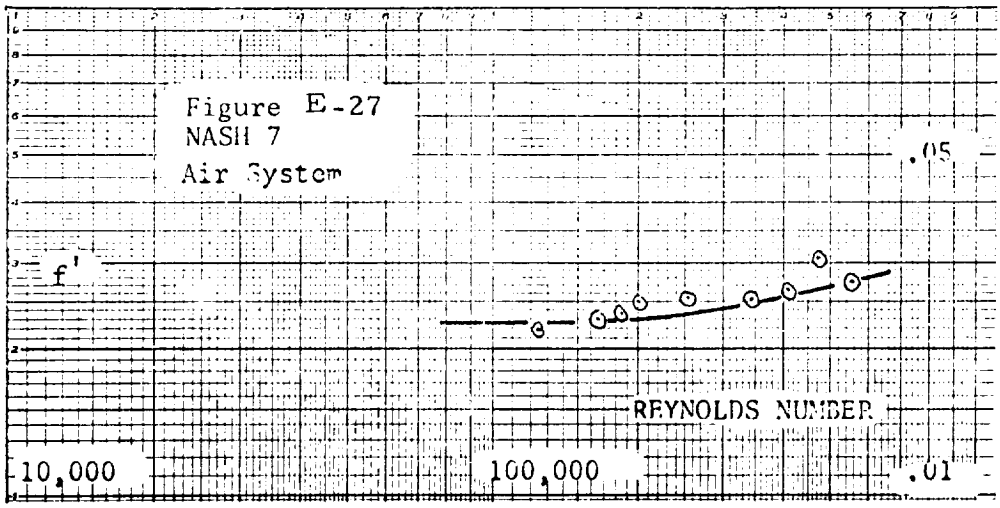
Figure E-27
NASH 7
Air System
.05
f'
REYNOLDS NUMBER
10,000
100,000
.01

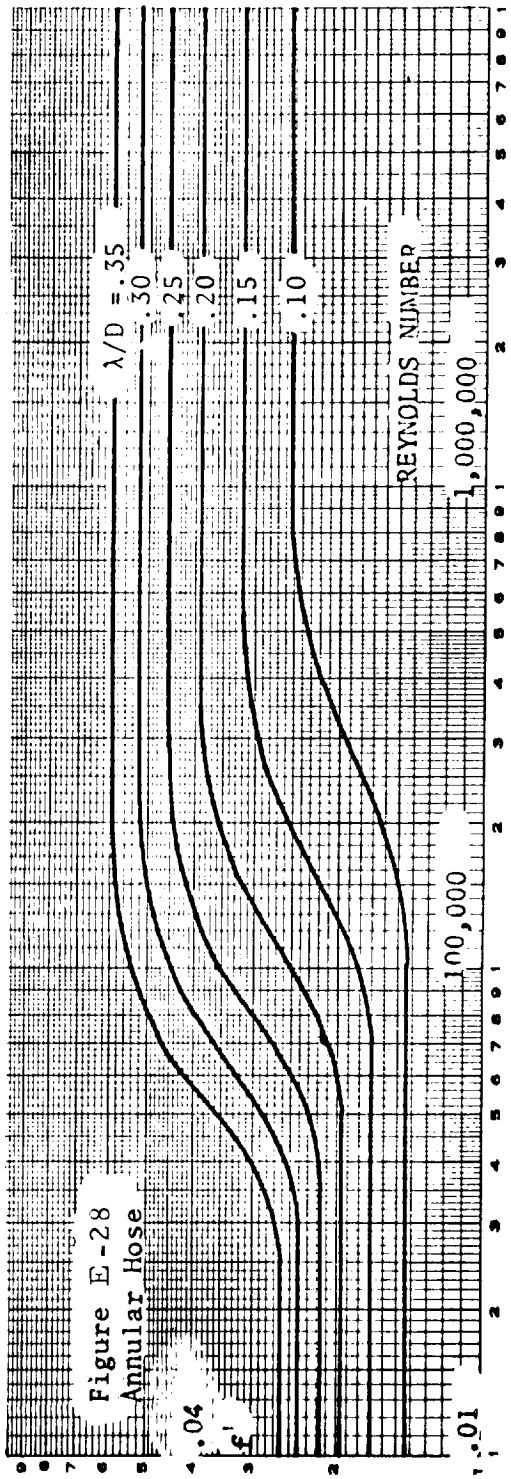

Figure E-28
Annular Hose

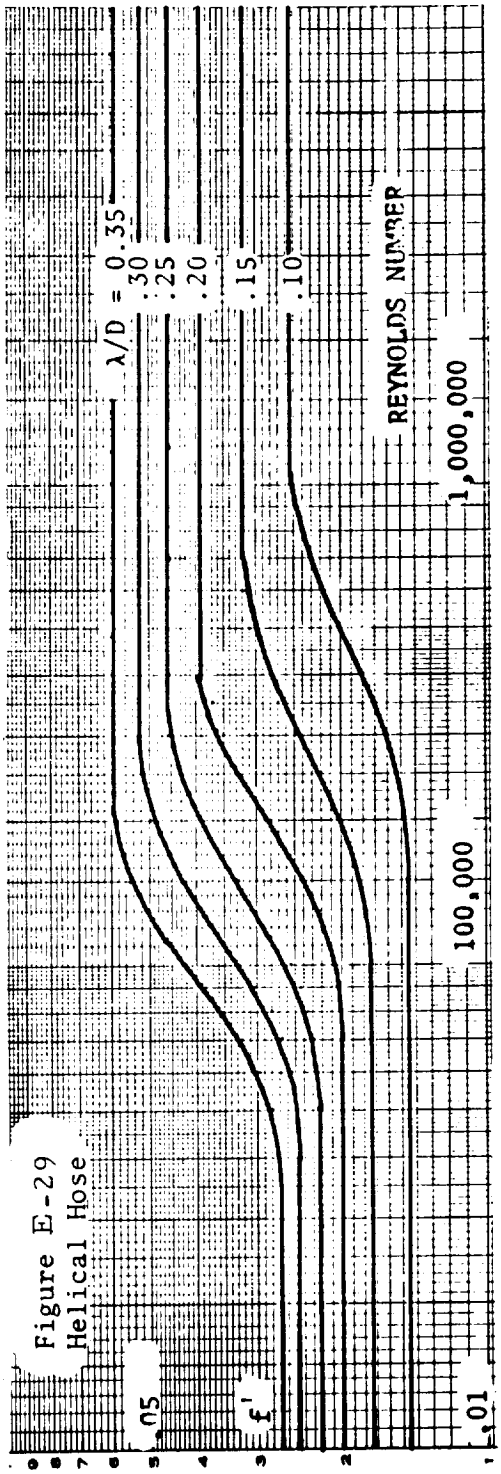

Figure E-29
Helical Hose

E. 3 PRESSURE LOSS DATA FOR CURVED SECTION FLEXIBLE HOSE

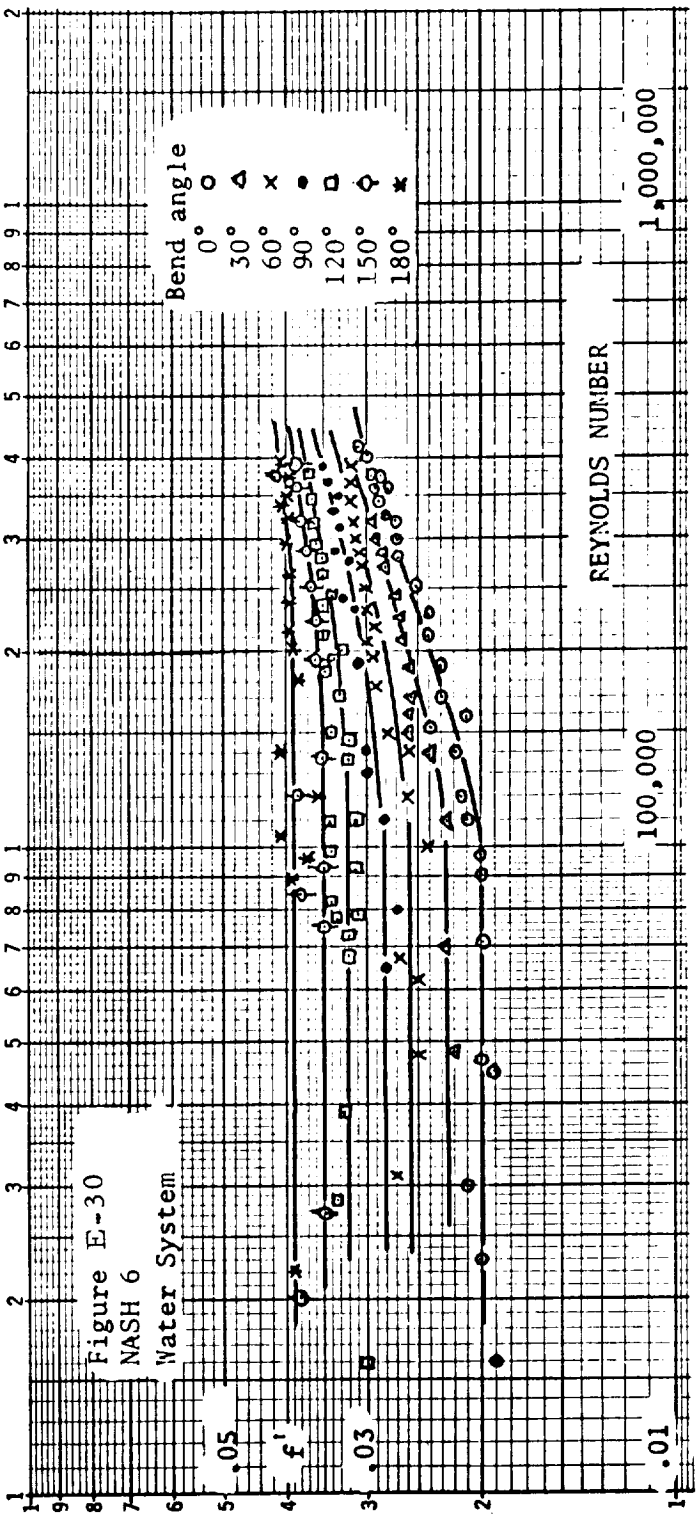

From Reference [26]. See Page E12 for hose dimensions.

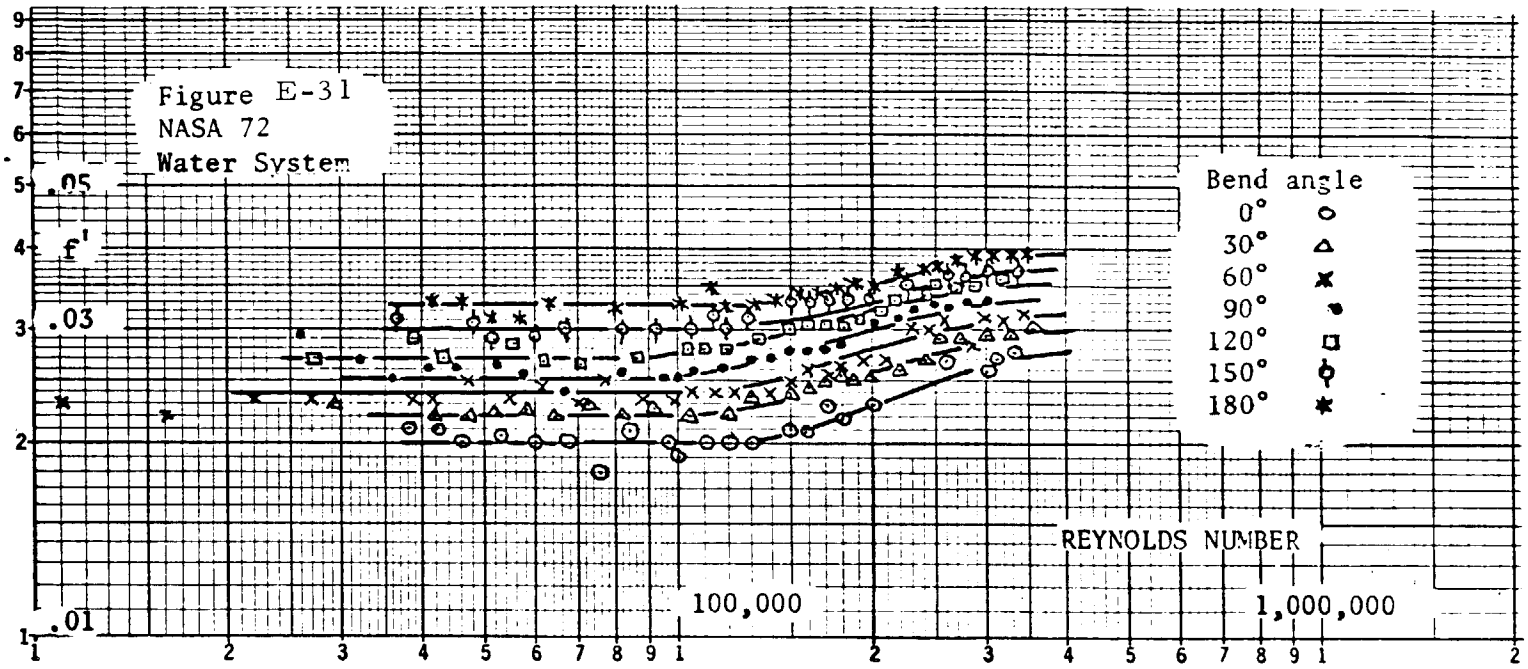

From Reference [26]. See Page E12 for hose dimensions.

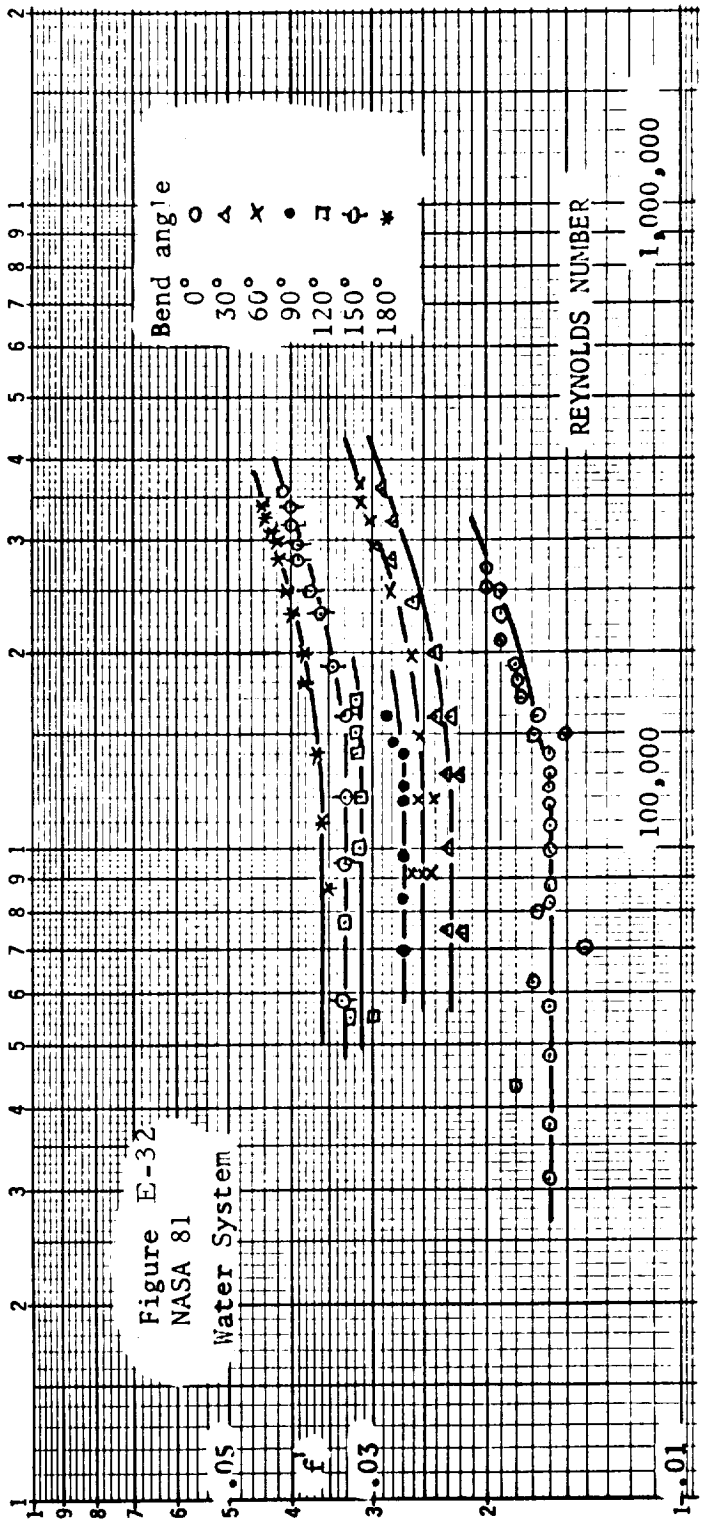

From Reference [26]. See Page E12 for hose dimensions

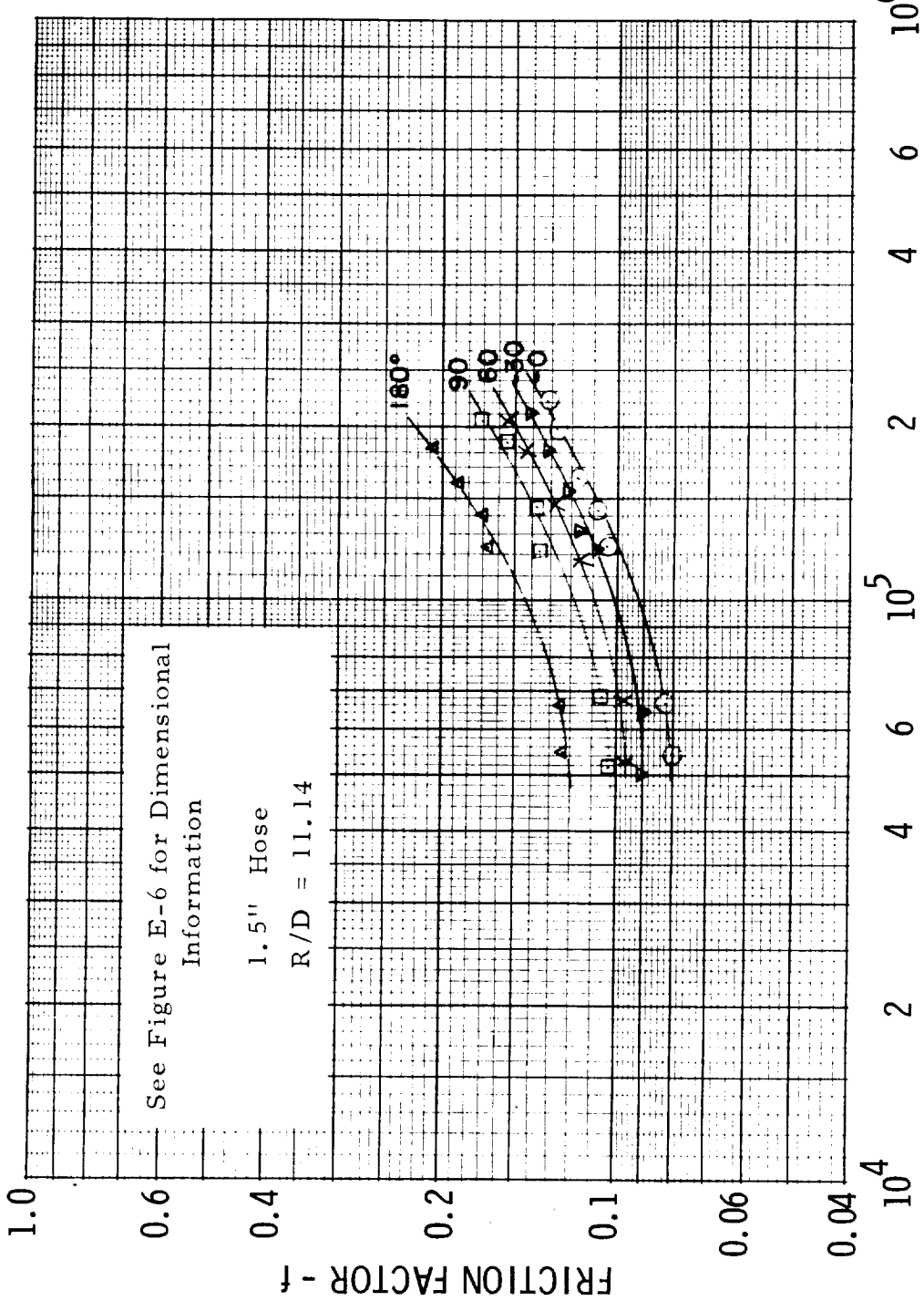

Figure E-33. Reference (24), Air

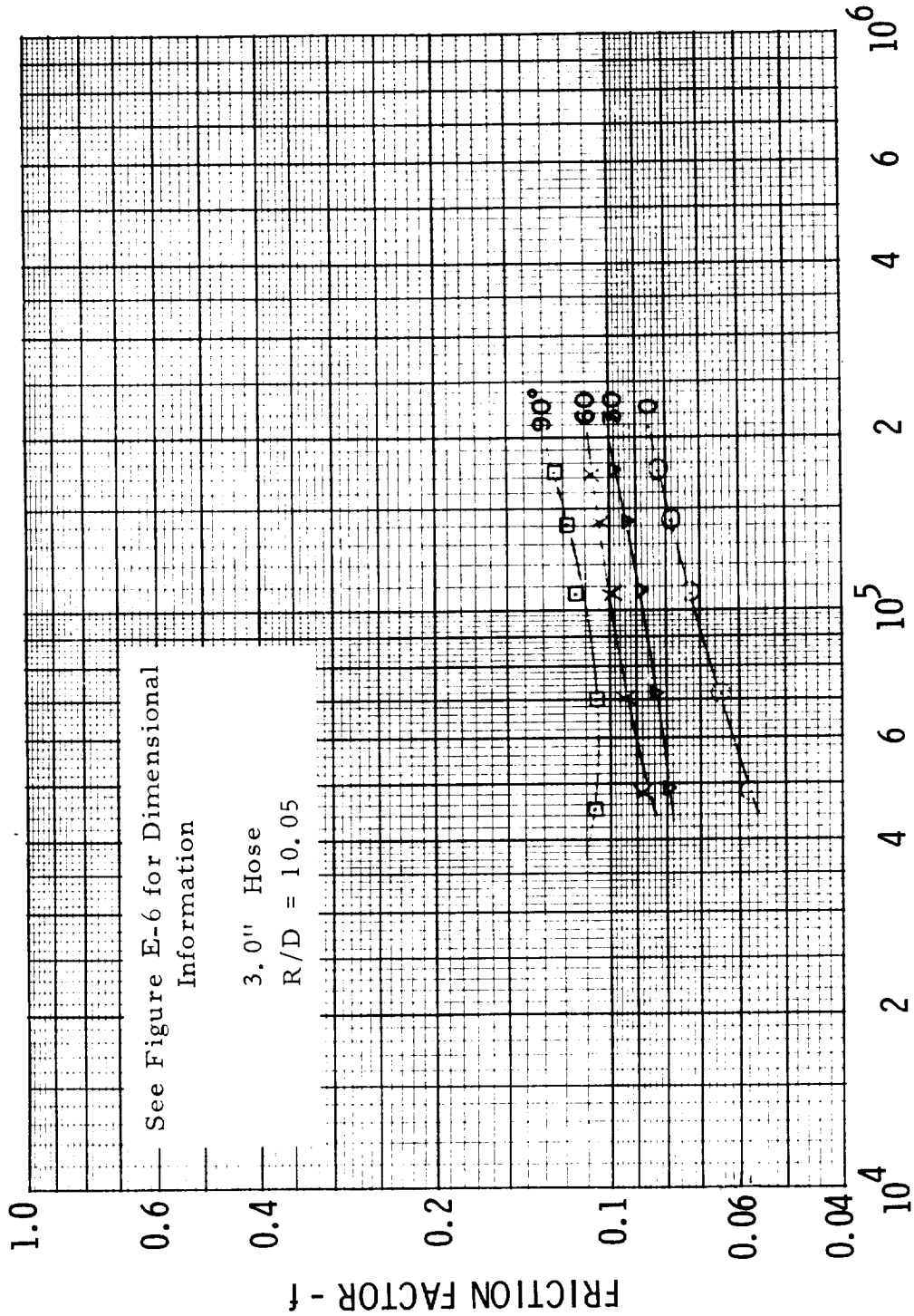

Figure E-34. Reference (24), Air

E.4 DATA COMPILED ON PRESSURE LOSSES IN BENDS

Several sources of information on pressure losses resulting from bends have been collected and reviewed [31-45]. As it turns out, the majority of the data available for bends of circular cross section have been compiled by Ito [31]. Also, Ito has developed what appears to be a valid correlation equation. Figure E-35, taken from Reference [31] shows Ito's correlation of available data. For this figure

R_e ≡ Reynolds number based on pipe diameter

(r/R) ≡ Pipe radius to center line radius ratio for bend

k_t ≡ Total bend loss coefficient, $\Delta p / 1/2\ \rho V^2$

θ ≡ Deflection angle of Bend, radians

Y ≡ Defined by $Y^3 e^Y = Re\,(R/r)^{1/2}$

The following observations have been made, based on the information contained in References [31-45].

(1) Pressure losses in bends with circular cross-section can be reliably predicted by Ito's method.

(2) The use of well designed splitter vanes or an impulse cascade can reduce pressure losses in bends considerably. For example, Stanitz and Sheldrake [13] report on a 90^o turning impulse cascade with a loss coefficient, using air, of 0.035. This should be compared with a loss coefficient of 0.1 or more for a typical 90^o bend. Probably of equal importance is the improvement in downstream velocity profiles (not as distorted) when splitters or a cascade is used.

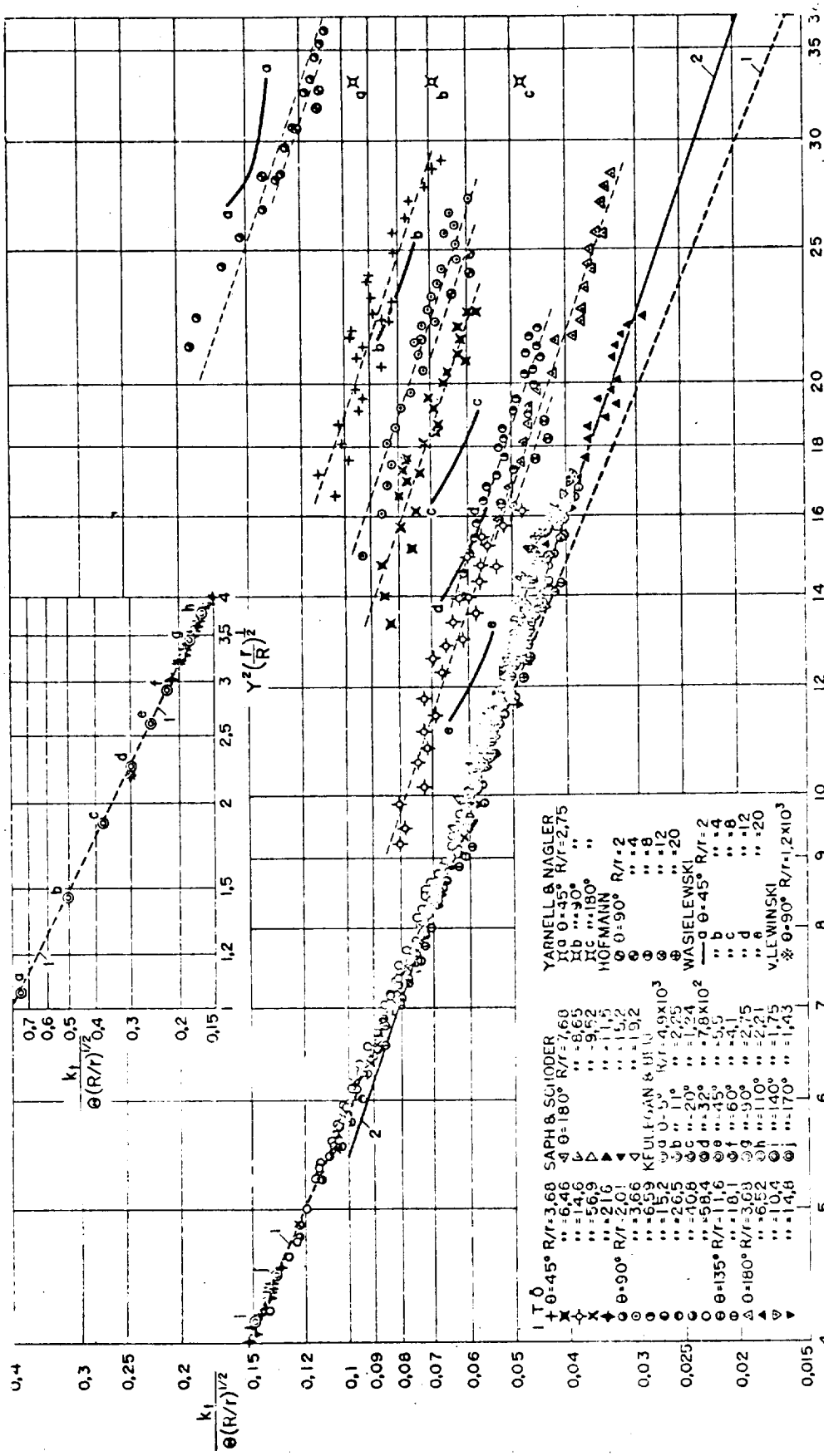

Figure E-35. Correlation of Circular Tube Bend Pressure Loss Data from Ito [32].